CARDIFF UNIVERSITY

SCHOOL OF ENGINEERING

Thesis Titled:

Effects of Geometry and Gas Composition on Swirling Flows

By

Hesham Baej

Institute of Energy

Supervisors:
Prof Philip J Bowen
Dr Agustin Valera-Medina

Thesis submitted in fulfilment of the requirements for the degree of Doctor of Philosophy, 2015

LIST OF PUBLICATIONS

[1] H. Baej, A. Valera-Medina, P. Bowen, N. Syred, T. O'Doherty, and R. Marsh, "Impacts on Blowoff by a Variety of CRZs Using Various Gases for Gas Turbines," *Energy Procedia*, vol. 61, pp. 1606–1609, 2014.

[2] H. Baej, A. Valera-medina, N. Syred, R. Marsh, and P. Bowen, "Blowoff propensity , CRZs and Flow Turbulent structure using a range of Syngas compositions for Gas Turbines .pp. 1–10 2015.

[3] H Baej, A Valera-Medina, P Bowen. CFD predictions of Swirl burner aerodynamics with variable outlet configurations. 97 WEENTECH proceedings in energy Vol. 1 (2015): ISSN 2059-2353; ISBN 978-0-9932795-0-8, page 97-103

[4] J. Lewis, R. Marsh, A. Valera-medina, S. Morris,and H . Baej"The Use of CO2 to Improve Stability and Emissions of an IGCC Combustor**,"** *ASME Turbo Expo* vol. 4, p. 11, 2014.

[5] H Baej, A Valera-Medina, Nick syred, Chong C T and P Bowen. Combustion Blowoff Effects Caused by the Central Recirculation Zone Using Various Syngas Mixtures in a Tangential Swirl Burner (Journal in apply energy) submitted

[6] A. Valera-Medina H. Baej, P. E Angelis, Bowen Flow, hydrodynamics during Turbulence and Combustion Hydrodynamics during the Transient Evolution of Open Jet Flows from/to Wall Attached Jets (Journal: Flow Turbulence and Combustion)

[7] H .Baej , Y. Sevcenco, A. Crayford , M. Johnson, "Non Premexed Combustion System by Syngas Using Swirl Burner," Low Carbon Research Centre EXPO, The Castle, Margam Park 13th March, 2013.

[8] A. Valera-Medina, H. Baej, R. Marsh, J. Runyon, "Blowoff and CRZ variance under CO2 effects UK CCS Research Centre" 2014.

DECLARATION

This work has not previously been accepted in substance for any degree and is not Concurrently submitted in candidature for any degree.

Signed ……. (Hesham Baej - Candidate)

Date …...08/02/2016.....

STATEMENT 1

This thesis is being submitted in partial fulfilment of the requirements for the degree of PhD

Signed ……. (Hesham Baej - Candidate)

Date ….....08/02/2016.....

STATEMENT 2

This thesis is the result of my own work/investigation, except where otherwise stated. Other sources are acknowledged by explicit references.

Signed ……. (Hesham Baej - Candidate)

Date ….. .08/02/2016.....

STATEMENT 3

I hereby give consent for my thesis, if accepted, to be available for photocopying and for inter-library loan, and for the title and summary to be made available to outside Organisations.

Signed ……. (Hesham Baej - Candidate)

Date ….....08/02/2016.....

STATEMENT 4

I hereby give consent for my thesis, if accepted, to be available for photocopying and for inter-library loans after expiry of a bar on access previously approved by the Graduate Development Committee.

Signed ……. (Hesham Baej - Candidate)

Date ….....08/02/2016.....

ABSTRACT

Lean premixed swirl stabilised combustion is regarded as one of the most successful technologies for flame control and NOx reduction in gas turbines. Important characteristics of these flows are good mixing, flame stability through the formation of a Central Recirculation Zone, and low emissions at lean conditions as a consequence of the low operating temperature. This project presents a series of experiments and numerical simulations using commercial software (ANSYS) to determine the behaviour and impact on the blowoff process at various swirl numbers, nozzle geometries and gas compositions at same power outputs using confined and open conditions. Experiments were performed using a generic premixed swirl burner. The Central Recirculation Zone and the associated turbulent structure contained within it were obtained through CFD analyses providing details of the structures and the Damkölher Number (Da) close to blowoff limits. The results show how the strength and size of the recirculation zone are highly influenced by the blend and nozzle geometry, with a shift of Da and turbulence based on carbon-hydrogen ratio, shearing flows and Reynolds number.

The Central Recirculation Zone was also measured and correlated to the blowoff phenomenon. A trend was found between the CRZ size/strength, the different compositions of gases used and the burner nozzle. Chemical kinetic analyses were carried out using PRO-CHEMKIN to determine flame speeds and chemical properties needed for CFD calculations. Experiments were performed using Phase Locked PIV and High Speed Photography. The Central Recirculation Zone and its turbulence were measured and correlated providing details of the structure close to blowoff.

It was found that the nozzle angle has a small effect on the LBO at low flow rates using all mixtures. During the tests, the Coanda effect was observed with some geometries, thus further research was carried out regarding the transition of this phenomenon. It was found that the process occurs at a particular geometry and step size, with a shift in frequency produced by the leading structure due to the entrainment of air and strength of the latter. Stability of the flow occurs after a Coanda Vortex Breakdown (COVB) has occurred, a process similar to the one observed in the central region of the flow under regular swirling open flames. As the step size is increased, the COVB will evolve into a slower Trapped Vortex (TV).

ACKNOWLEDGMENT

First and foremost, I would like to thank ALLAH for helping me to complete this thesis.

I would like to express my deep gratitude to Doctor Agustin Valera – Medina, Professor Philp Bowen and Professor Tim O'Doherty research supervisors for their patient guidance enthusiastic encouragement and useful critiques of this research work. I would also like to thank Professor Nick Syred for his advice and assistance in keeping my progress on schedule.

I would like to thank Dr Richard March for all his support during this research and Dr Allan Mason-Jones, Dr Ceri Morris for their support of CFD during this research.

My great thanks also extended to all technicians of the laboratory and their help in offering me the facilities to complete my experiments. Special recognition to Mr Malcolm Seaborne whose technical knowledge contributed to the successful completion of this work.

I would like to thanks for my family for their patient with me during my research. Gratefully acknowledges the support of the Libyan Embassy and the Libyan Cultural and Education Bureau in London.

CONTENTS

LIST OF FIGURES

LIST OF TABLE

Nomenclature

Alphabetic Symbol

A	=	Model constant	(-)
A	=	area	(m^2)
AFR	=	Air Fuel Ratio	(-)
A_t	=	The total area of the tangential inlet	(m^2)
A_e	=	Exit area	(m^2)
c	=	Mean Reaction progress Variable	(-)
D_a	=	Damkohler number	(-)
D_e	=	The exhaust diameter	(m)
erfc	=	The complementary error function	(-)
f	=	Oscillation frequency	(1/s)
f	=	Mixture fraction	(-)
f	=	Is a conserved quantity.	
G_x	=	Axial Flux of Axial Momentum	(Kg/m.s)
G_θ	=	Axial Flux of Angular Momentum	(Kg/m.s)
g_{cr}	=	The critical rate of strain	1/s
h	=	The flow passage height	(m)
K	=	Kinetic energy of turbulence	(m^2/s^2)
L	=	The characteristic length	(m)
L_{ref}	=	The reference length	
V_{ref}	=	The reference velocity using the average velocity	
M_a	=	Mach number	
$\dot{m}$	=	Mass flow rate	(Kg/S)
n	=	Number of products	(-)
p	=	Static pressure	(p_a)
Q	=	Flow rate	(m^3/s)
Q_v	=	the volumetric flow rate	
r	=	Radius	(m)
R_e	=	Reynolds number	(-)
r_{eff}	=	The effective radius at the centre of the inlet pipe	(m)
S	=	Swirl number	(-)
$S_{h,chem}$	=	heat gains due to chemical reaction, given by	
$S_{h,rad}$	=	heat losses owing to radiation	
S_{ct}	=	turbulent Schmidt number	(-)
S_c	=	reaction progress source term	(-)
S_g	=	Geometrical Swirl number	(-)
S_L	=	Laminar Flame Speed	(m/s)
S_r	=	Strouhal number	(-)
S_{rv}	=	Strouhal number	
S_M	=	Body force	(N/m^3)
S_T	=	Turbulent flame speed	(m/s)
T	=	Time	(s)
t	=	The flow passage width between blades	(m)

T	=	Temperature	(k)
U	=	Axial velocity	(m/s)
U’	=	Fluctuating	(m/s)
V	=	The mean flow velocity	(m/s)
v	=	Velocity vector	(m/s)
W	=	Tangential Velocity	(m/s)
Y_i	=	is the mass fraction of product species *i*	
$Y_{i,eq}$	=	is the equilibrium mass fraction of product species *i.*	
Z_i	=	is the elemental mass fraction of the element *i*	(-)
Z_{ox}	=	the value of the oxidiser stream inlet	(-)

Greek symbol

τ	=	The viscous stress	(N/m^2)
τ_{ij}	=	the viscous stress component in the j-direction	(N/m^2)
μ	=	dynamic viscosity	(Ns/m^2)
μ_{str}	=	measured in turbulent non-reacting flows	
λ	=	viscosity	(m^2/s)
ρ_u	=	density of burnt mixture	(Kg/m^3)
ρ_d	=	Particle density	
d_C	=	The characteristic dimension of obstacle	(m)
d_d	=	Diameter of the particle	(m)
μ_f	=	Dynamic viscosity of the fluid	(m^2/s)
τ	=	Particle relaxation time	(s)
τ_c	=	The chemical time scale	(s)
τ_t	=	Turbulent time scale	(s)
α	=	Thermal diffusivity	(m^2/s)
l_t	=	Turbulent length scale	(m)
ϵ_{cr}	=	Turbulence dissipation rate at the critical rate of strain	
Γ_k	=	represent the effective diffusivity of *k*	(m^2/s)
Γ_ω	=	represent the effective diffusivity of **ω**	(m^2/s)
$G\,\omega$	=	represents the generation of $\boldsymbol{\omega}$	
Y_k	=	represent the dissipation of *k*	
Y_ω	=	represent the dissipation of $\boldsymbol{\omega}$	
D_ω	=	represents the cross-diffusion term	
S_k	=	user-defined source terms	
S_ω	=	user-defined source terms	

Abbreviations

$Al2_O3$	=	Aluminium oxide powder	
CFD	=	Computational Fluid Dynamics	
COJF	=	Coanda Jet Flow	
COVB	=	Coanda Vortex Breakdown to Radial Jet Flow	
CRZ	=	The central recirculation zone	

CIVB	=	Combustion induced vortex breakdown	
ERC	=	The extend recirculation zones	
FDM	=	Finite difference method	
FEM	=	Finite element method	
FVM	=	Finite volume method	
GT	=	Gas turbine	
GTRC	=	Gas turbine research centre	
HHV	=	High heating value	(Mj/kg)
LHV	=	Low heating value	(Mj/kg)
HMFR	=	High momentum flow region	
LBO	=	lean blowoff	
OJF-MS	=	Open Jet Flow-Medium Swirl	
PVC	=	Precessing vortex core	
PIV	=	Particle image velocimetry	
RZs	=	The recirculation zones	
SST	=	Shear Stress Transport	
TV	=	Trapped Vortex	
ΔY/D	=	normalized step sizes	(m)

CHAPTER1

CHAPTER 1

INTRODUCTION

1.1 Energy supply

There has been an enormous increase in the demand for energy since the middle of the last century as a result of industrial development and population growth. Consequently, the development of new and renewable sources of energy has become a matter of priority in many countries all over the world. The most multipurpose energy carrier in our modern global economy is electricity, and it is therefore primarily linked to human and economic development. In the following decades, the trend is expected to continue with large parts of the world population in developing countries planning to be connected to local or international power grids. Electricity production deserves precise attention with regards to its contribution to global greenhouse gas emissions, and must be reflected in the continuing development of low-carbon technologies for power generation [1].

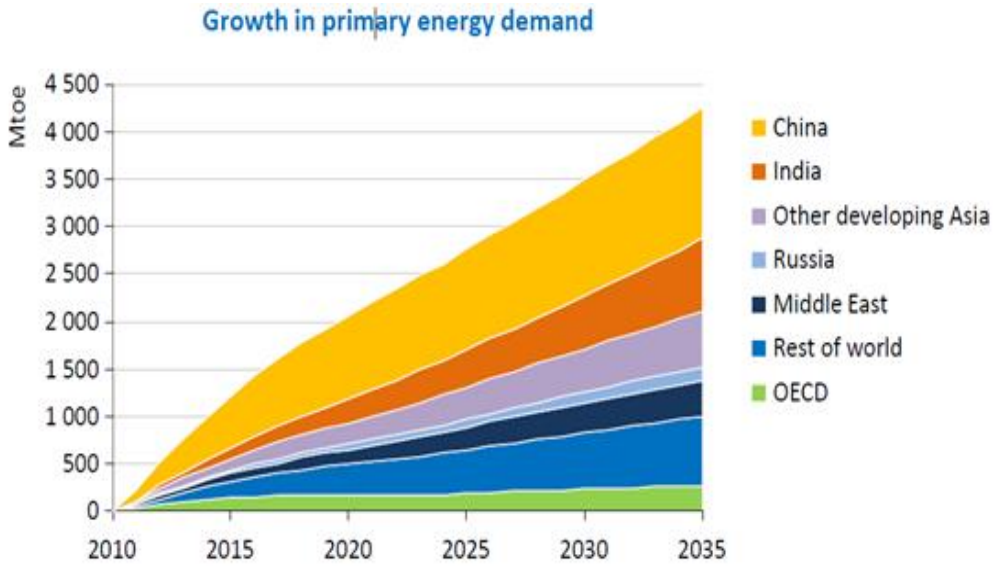

Figure 1-1: Predictions of Increasing primary energy demand [2]

The International Energy Agency (IEA) expects that energy demand will increase by one-third between 2010 and 2035 as shown in Figure 1.1, with oil increasing from 87 million barrels per day (mb/d) to 99 mb/d during that timeframe. The two biggest

drivers of that demand growth will be India and China, which the IEA expects will account for 50% of global consumption. This will create a problem for energy resources that can only be solved with better technologies [2].

1.2 Climate Change

The natural driving force behind climate change is the greenhouse effect. From the total radiation emitted by the Sun, 30 % is reflected back to the space, 50% reaches the Earth's surface, and another 20% is absorbed into the atmosphere.

Greenhouse gases such as water vapour, carbon dioxide and methane don't absorb visible sunlight. But their complex molecules interact with the infrared heat energy given off by the Earth, absorbing it by vibrating and rotating before re-emitting it in a random direction, sometimes back down towards the ground. This temporarily traps the heat in the atmosphere, warming up the Earth's surface in the process [3] . Thus, the amount of solar radiation that reaches the Earth's surface is about equal to the amount reflected, maintaining the balances of energy and sustaining life. Therefore, the environmental issues for the international community are related to keeping this balance, thus avoiding global warming. In recent years many countries have undertaken new initiatives to address climate change [3,4].

In 1994, The United National Framework on Climate Change (UNFCCC) entered into force, with the broad objective of steadying the greenhouse gas concentration levels in the atmosphere, thus preventing the dangers that anthropogenic (man-made) emissions may cause to the climate system, Figure 1.2.

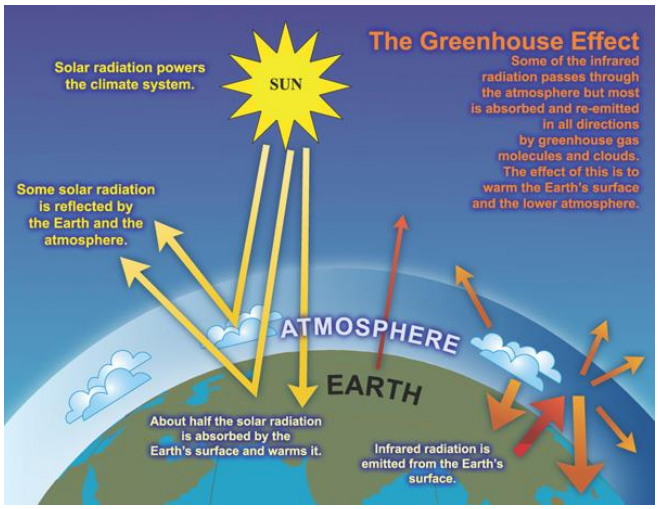

Figure 1-2:Diagram of the energy balance at the surface of the Earth [4].

The IEA publication energy technology perspectives 2010 (ETP 2010) project that, in 2050, energy-related carbon dioxide (CO_2) emissions will be twice 2007 levels in the absence of new energy policies or emissions controls. However, ETP 2010 also demonstrates that the aggressive deployment of low carbon technologies could reduce projected 2050 emissions to 50% of 2005 levels. Achieving that goal, however, will require technologies to move rapidly from its current research and demonstration phase into a significant large scale, commercial phase of global technology deployment [6].

Although the policies are in place, the energy balance is now being altered by two key issues. First, the effect caused by greenhouse gases (GHGs) - the most well-known being carbon dioxide (CO_2), methane (CH_4), nitrous oxides (N_2O), sulphur hexafluoride (SF_6), hydrofluorocarbons (HFCs), and perfluorocarbons (PFCs)- that capture some of the energy reflected from the surface of the Earth, keeping it in our atmosphere. The increase of these gases could causes higher temperatures, with major disasters over the world such as health impacts, reduction of fertile land, and increase in hurricanes and flooding in coastal areas, Figure 1.3. Second, the effect of aerosols - miniscule particles suspended in the air - as these primarily have a cooling effect on the Earth because they reflect solar radiation back into space before reaching the atmosphere. Aerosols can be produced from processes such as the burning of biomass, diesel consumption in transportation engines, aerospace applications, etc. [6,8].

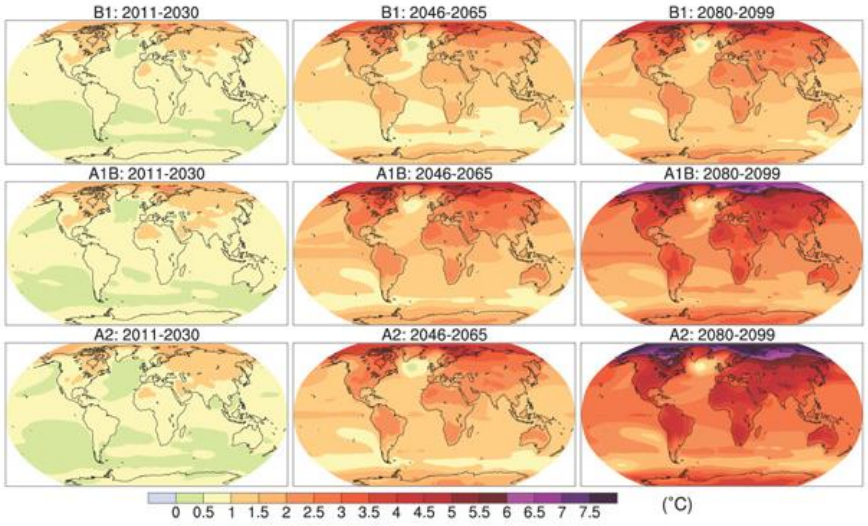

Figure 1-3: Global distribution of temperature increases in three scenarios (in rows) and three time periods (in columns) [4]

Most the fuels sourced from renewable resources, the more concerning of these gases is CO_2. It is a natural component in the breathing process. However, it is very dangerous at high concentration levels. The large quantity of carbon dioxide emissions produced from combustion of carbonaceous fuels is one of the main drivers of climate change. Carbon dioxide emissions produced from burning fossil fuels are responsible for about 87% of global warming, increasing the amount of CO_2 in the atmosphere by about 27% since the Industrial Revolution. Based on the problems caused by climate change resulting from global warming the international community has attempted to understand this phenomenon and to analyse all the scientific data over the last decades. New ideas are in place to tackle the problem. Among these ideas is the proposal of using alternative fuels such as hydrogen, methane or methanol to reduce the emissions [7].

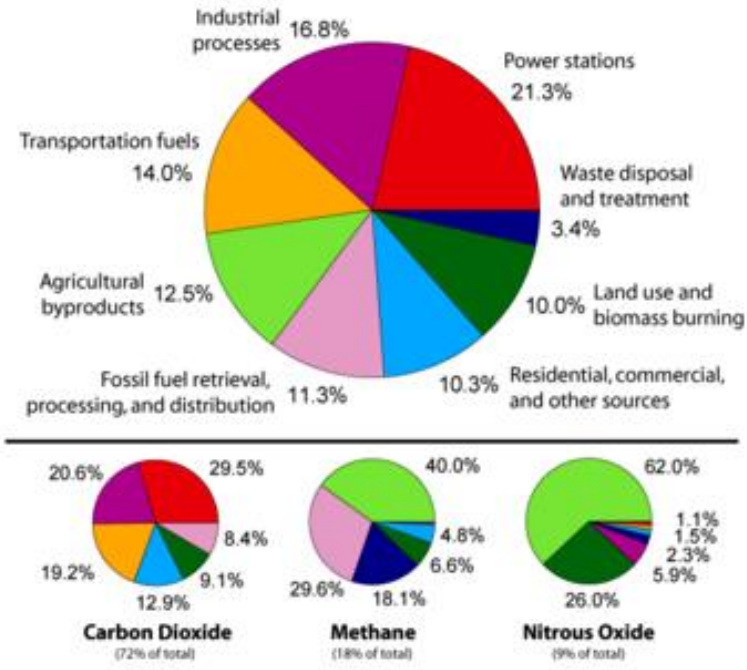

Figure 1-4:Annual greenhouse gas emissions by sector [7]

1.3 Fossil fuel demand

The Energy Information Administration (EIA), in its Annual Energy Outlook (AEO) of 2011 has published the expected energy supply, demand, and prices of the USA through 2035, serving as the basis to correlate current and future energy demands. Although some predictions tend to be toward more carbon-free fuels in the future,

the Energy Information Administration predicted an increase in the amount of fossil fuels to supply over 75% of the energy consumption in the United States by 2035. Fossil fuels are expected to decrease only 5% from 83% in 2009 to 78% in 2035. Even with such a large share of fossil fuels, and emissions of carbon dioxide-related energy still below 2005 levels in 2020, these emissions are not expected to exceed 2005 levels until 2027. Figure 1.5 shows the consumption of coal and most carbon intensive fuels, with an increase of 3% of biofuels between 2009 and 2035, and an increase of all renewables of ~14 %. However, natural gas consumption is likely to increase by 16% [9].

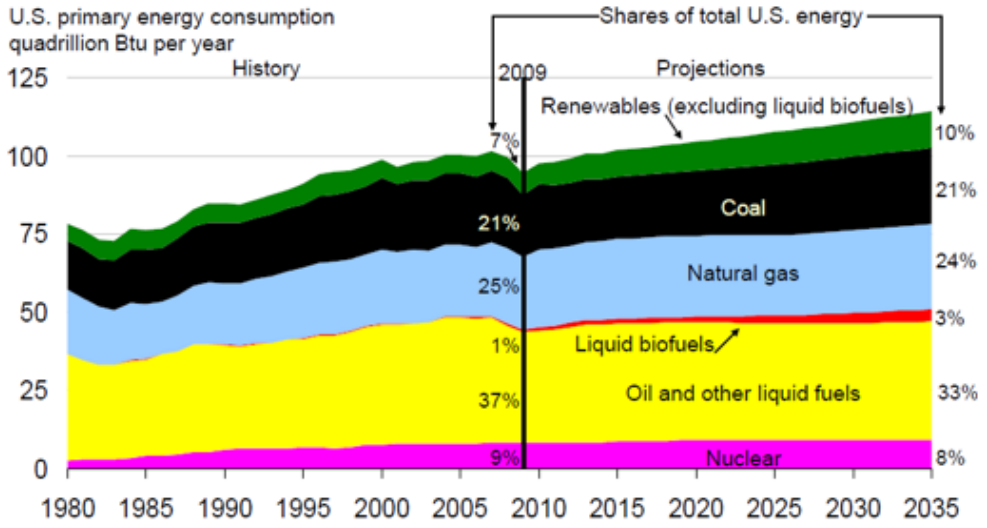

Figure 1-5:Renewables grow rapidly and fossil fuel need of U.S energy use in 2035 [9]

However, according to the last study carried out in 2010 by the Intergovernmental Panel on Climate Change (IPCC), global concerns focus on the reduction of fossil fuel consumption and harmful pollutants with their consequent increase of emissions. As the world focuses on reducing consumption of fossil fuels, the gas turbine industry has felt changes in the demands of customers pushing for the combustion of alternative fuels. Two popular options for gas turbine combustion are syngas (where the primary components are H_2 and CO) and biomass fuels where carbon dioxide emissions are greatly reduced [4].

New technologies have been raised offering reduced emissions with the combustion in gas turbine of alternative fuels [10].

1.4 The energy trilemma

As sustainability becomes a key issue in society, the environmental impacts of the energy systems of a country have come under intense scrutiny. As long as fossil fuels are an integral part of an energy system, carbon emissions to the atmosphere are inevitable. It is therefore not surprising that there has been a strong focus on greening the energy systems in many countries. Going green means to reduce the carbon emission of the energy system through means such as energy efficiency and conservation, deployment of clean or low carbon energy sources, and carbon capture and storage [11][12].

At the same time, countries around the world are increasingly concerned about energy security. The energy security has two key aspects, reliability and resilience. Reliability means users are able to access the energy services when they require them. Resilience is the ability of the system to cope with shocks and change. In the literature, energy security used to be largely about ensuring the stability of oil supplies and reducing the risk of supply disruptions. More recently, the scope of energy security has expanded because of sustained high-energy prices and the growing emphasis on environmental sustainability. The greening energy supply and systems would bring about energy security benefits such as reducing petroleum imports to fuel the economy and increasing energy productivity by using less energy to produce the same level of energy service. Indirectly, the carbon and acidic gas emissions associated with the burning of fossil fuels are reduced thereby contributing to environment protection [11,12].

However, the situation may not be as simple as it seems, as other factors, including tradeoffs, which are commonly known as the energy trilemma in energy studies, need to be considered. The energy trilemma has three competing goals: energy security, economic competitiveness, and environmental sustainability. In the Figure 1.6, presented the diagram with both intersecting and competing parts. Green initiatives such as turning to renewables could come with a hefty price tag. In electricity generation, more often than not, these technologies have not advanced to the point of grid parity, the price at which the cost of generating electricity from renewables is

competitive vis-a-vis from conventional fuels. Hence, greening energy sources may reduce economic competitiveness. While energy efficiency and conservation is generally believed to be able to help alleviate problems associated with the energy trilemma, the trade-offs and its benefits are seldom quantified and studied in a rigorous manner [11,12].

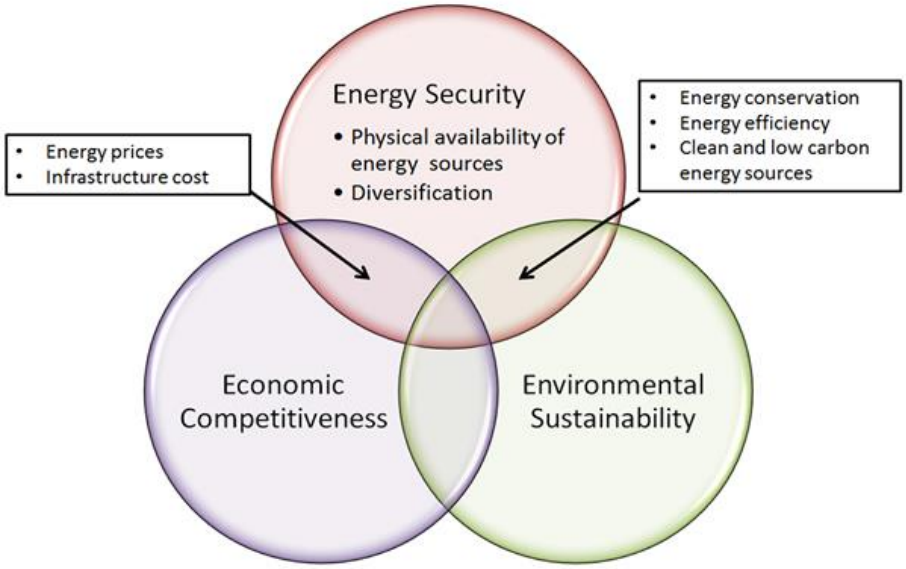

Figure 1-6: The energy trilemma[11]

1.5 Gas Turbine

Gas turbines are the mainstay of energy production nowadays. The basic mechanism of operation of gas turbines is based on three stages. The first stage admits fresh atmospheric air through a compressor that brings the flow to a higher pressure. In the second stage, energy will be added by injecting fuel that, in combination with the air, will ignite so that the combustion generates a high-temperature flow. Finally, the third stage is when the high-temperature, high-pressure gas enters a turbine. The expansion of the gas will lead to the rotation of the engine's shaft, thus driving the compressor or any devices attached to the system such as an electric generator. Also, the gases can be discharged without complete expansion, enabling them to exit at high velocity through a nozzle to produce thrust as occurs in jet engines or turbojets. Figure 1.7 shows a gas turbine for propulsion applications [10,11].

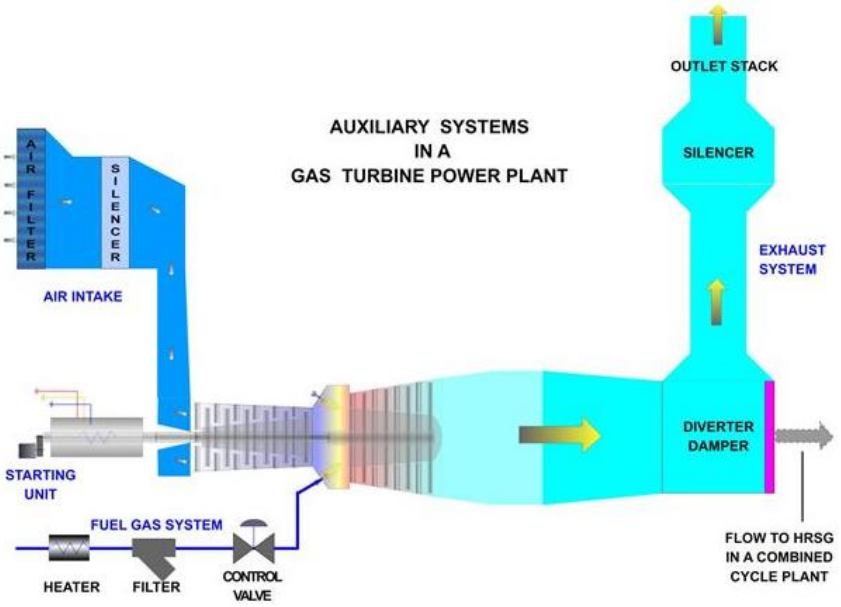

Figure 1-7:Gas Turbine [15]

1.5.1 Gas Turbine Combustors

The combustor is the part of the gas turbine where combustion takes place, as shown in Figure 1.7. Gas turbines must satisfy a wide range of requirements whose relative importance varies amongst engine types. However, the basic requirements of all combustors are as follows:

- High combustion efficiency
- Reliable and smooth ignition especially at low temperatures
- Wide stability limits
- Low pressure loss

A combustor must maintain stable combustion despite the very high air flow rates. Combustors need a more careful design at the burner and ignition system for a complete, stable combustion of the mixture of air and fuel. When the system has been stabilized, more air is fed in to complete the combustion process[11,14] This is achieved via the air admission through the secondary and tertiary zone of the burner.

1.5.1.1 Types of combustor

The combustor portion of a gas turbine engine can be of several different types: can/tubular, annular, and a combination of the two forming a can-annular combustor

Figure 1-8, 1-9 it is in this component that the compressed fuel-air mixture passes through fuel-air swirlers and a combustion reaction of the mixture takes place, creating a hot gas flow causing it to drop in density and accelerate downstream. The can type combustor typically comprises of individual, circumferentially spaced cans that contain the flame of each nozzle separately. Flow from each can is then directed through a duct and combined in an annular transition piece before it enters the first stage vane. In the annular combustor type, fuel-air nozzles are typically distributed circumferentially and introduce the mixture into a single annular chamber where combustion takes place. Flow simply exits the downstream end of the annulus into the first stage turbine, without the need for a transition piece to combine the flow. The key difference of the last type, a can-annular combustor, is that it has individual cans encompassed by an annular casing that contains the air being fed into each can. Each variation has its benefits and disadvantages, depending on the application.

In combustors for gas turbines, it is typical for the fuel-air nozzle to introduce a swirl to the mixture for several reasons. One is to enhance mixing and thus combustion, another reason is that adding swirl stabilizes the flame to prevent flame blow out and it allows for leaner fuel-air mixtures for reduced emissions. A fuel air nozzle can take on different configurations such as single to multiple annular inlets with swirling vanes on each one [16,17].

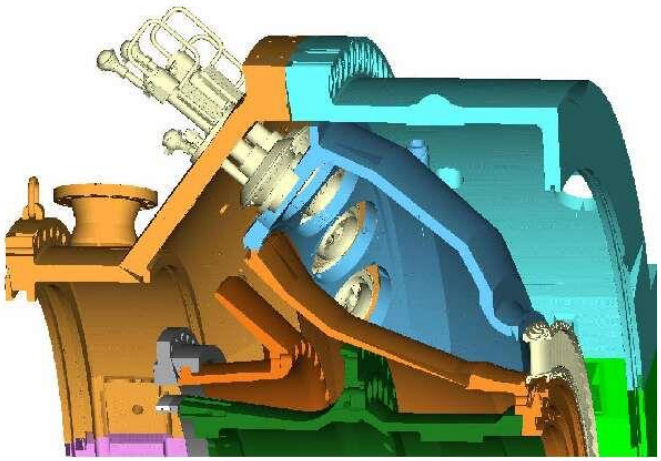

Figure 1-8: Annular Gas Turbine Combustion Chamber [19]

The advantage of the reverse flow combustor, as used in the heavy industrial gas turbine, is that this design facilitates the use of a regenerator, thereby improving overall thermal efficiency. A further distinctive design approach within the can-

annular concept is a single fuel nozzle and multi-fuel nozzles per combustion chamber. In theory, a large number of fuel nozzles provides better distribution of the fuel gas (or greater atomization of the liquid fuel particles) and more rapid and uniform burning and heat release, Figure 1.9 [20].

But the problems of equally distributing fuel to each fuel nozzle significantly limit the number of fuel nozzles employed in lean premixed combustors [8].

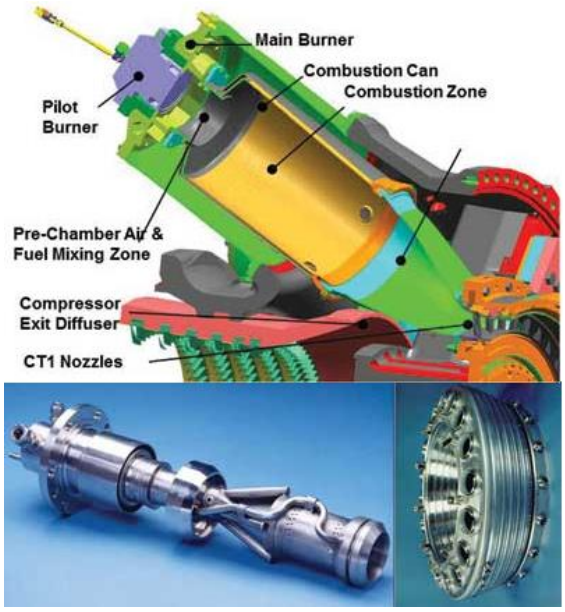

Figure 1-9: can -annular combustor [21]

1.5.1.2 Swirl Combustion

The most important technologies used in gas turbine combustors are the swirl lean premixed combustion. This provides flexibility and initial stability for the system. Swirl stabilised combustion is a widely used technique for flame stabilisation in gas turbine combustors. Lean premixed combustion enables techniques, which can be used to minimize the impact and production of NO_x. Combustion instability in lean-premixed combustion systems remains a substantial challenge for designers. Dry Low Emission (DLE) is a technology that reduces NO_x emissions that exhausts out of gas-fired turbines. The amount of NO_x produced depends on the combustion temperature, which the combustion takes place at a lower temperature the NOx emissions are reduced. Gas turbines with DLE technology were developed to achieve lower emissions without using water or steam to reduce combustion temperature (Wet Low Emission (WLE) technology).DLE results in lower NO_x emissions

because the process is run with less fuel and air, the temperature is lower and combustion takes place at a lower temperature.

1.5.2 Gas Turbine Materials

The gas turbine inlet temperature in modern industrial turbines exceeds 1300 C°, the life requirement for the highly loaded high temperature components is 25000-50000 h and efficiency requirements limit the amount of compressor air available for cooling of turbine parts. Traditionally, material technology for power generation gas turbines has followed the aircraft technology being 10-20 years behind [22].

Latest industrial gas turbines use single crystal and directionally solidified blades and vanes, rhenium-contained nickel-based super alloys, advanced metallic and ceramic coatings. The large size of industrial gas turbines shows the limits of traditional casting techniques, which have been newly developed; gas cooling casing and rediscovered liquid metal cooling processes are being extensively evaluated. Reconditioning technologies in the development of gas turbines include the rapid adaptation of aero-engine technology (sophisticated cooling techniques using single crystal air foils, and thermal fence coatings) in order to operate at the high rotor-inlet temperatures required for high efficiency generation[22].

Regarding the material of annular combustors, these consist of an inner and an outer liner, fuel injectors and an outlet to the turbine. The inner liner is made from Ni base sheet material with air plasma sprayed thermal barrier coating (TBC), to reduce metal temperatures and lowering oxidation of the metal. The TBC coating is a development area, where the long term mechanical properties must be well understood [18-20].

Development activities for the combustor are ongoing in several disciplines. In the combustion process flameless and humid air combustion are explored to reduce NOx and CO2 emissions. The increased demand for higher efficiency leads to higher firing temperatures. As a consequence, increased material temperatures in the combustor are seen, exposing the materials to creep load and oxidation.

1.5.3 Large Combustion Plant Directive

The aims of the Large Combustion Plant Directive (LCPD) are to reduce acidification, ground level ozone and particles throughout Europe by controlling emissions of nitrogen oxides (NOx), sulphur dioxide (SO2) and dust particulate matter from large combustion plants (LCPs) in power stations, petroleum refineries, steelworks and other industrial processes running on solid, liquid or gaseous fuel with a thermal capacity of 50 MW or greater. Nitrogen oxides react with volatile organic compounds in the presence of sunlight to form ozone that can adversely affect human health and ecosystems. Sulphur dioxide, nitrogen oxides and particles can travel long distances from their sources before being deposited onto land, surface water or oceans, forming ozone. These emissions contribute to pollution problems and are the principal non-domestic contributors to sulphur and nitrogen deposition in the world. Therefore, the requirements to reduce these pollutants and their impact have taken into account advanced combustion and abatement technologies [25]. Under the terms of the directive, combustion plants built after 1987 must comply with specific emissions limits. From 2007, plants built earlier than that could either opt to comply with the emissions limits, or 'opt out'. Plants which opted out have been limited to a maximum of 20,000 hours of further operation, and must close completely by the end of 2015 [26].New technologies are therefore required to allow these systems to keep running. Most of them could be retrofitted with alternative fuel technologies. However, extensive research and development is still required before stabilization can be achieved in these old plants [26].

1.6 The aim of project

The focus of this research is on the blow-off limits of the flame and how these limits can be improved using new alternative fuels. The aim of this project is to study and analyse blow-off limit characteristics of gas turbine burners with variable swirl numbers using a wide range of syngas composition fuels. Compositions of interest will be analysed numerically by CFD using commercial software (FLUENT). Comparison with experimental data for a range of different fuels under fully lean premixed combustion conditions will be carried out. The experiments will be carefully analysed to find the blow-off limits and flow interactions/turbulence during the event for several different lean premixed fuels.

The following are specific objectives

i) To study the upper limit problem of lean premixed combustion that is recognized as flame blow-off.

ii) To recognise the potential and limitations of CFD when studying the upper limit for various fuel blends.

iii) To define the stability limits for various syngas and CO_2 fuels. These limits are recognized by defining the normal combustion and blowoff limits with respect to the mixture mass flow rates at various equivalence ratios.

iv) To determine the behaviour and impact on the blowoff process at various swirl numbers, nozzle geometries and gas compositions.

v) To determine the impacts on blowoff by a variety of CRZs and various gases for gas turbines and determine how the strength and size of the recirculation zones are highly influenced by these parameters.

vi) To study various hydrodynamic effects using swirling flows and how these affect the flame. Some of the studied effects and interactions include the Coanda flow upon the High Momentum Flow Region, the Precessing Vortex Core and External Recirculation zones.

1.7 Structure of thesis

Chapter 1. *Introduction*. The current energy and environmental situation, with some insights of future trends and needs including the requirements of new environmental legislation over emissions control at Power Plant Level. The basic mechanism of operation of gas turbines with general aspects of combustion, used fuels and stabilization technologies is also mentioned.

Chapter 2. *Literature Review*. This chapter comprises the fundamental parameters of swirl flows such as the recirculation zones, shearing flow, and swirling flows with combustion, combustion principles and combustion regimes. Turbulence and hydrodynamic principles are also mentioned.

Chapter 3. *Methodology.* This chapter comprises two parts. Firstly the experimental measuring techniques used during this thesis. Special emphasis is placed on velocity

measurement with particle image velocimetry (PIV), Stereo Particle Image Velocimetry (PIV) technique and high speed photography. Secondly it describes the CFD codes used (Fluent ANSYS software) and mentions the processing analysis, basic equations and turbulence modelling.

Chapter 4. ***CFD Results***. This chapter includes the results of the CFD analysis previous to the experimental studies. The results provided guidance on which blends to use, as well as an idea of the expected results from the experimental trials. These were the foundation for the following chapter.

Chapter 5. ***Blowoff Experiments.*** This chapter consists of the isothermal and combustion experiments and the effects on blowoff using different geometries with various gas compositions. Emphasis was placed upon the blowoff.

Chapter 6. ***Hydrodynamic Effects*****.** During experiments, various hydrodynamic effects were observed. The most notorious with a particular geometry was the Coanda effect. Results on its propagation and transition from stability are reported in this chapter.

Chapter 7. ***Discussion***

Chapter 8. ***Conclusions and future work***

CHAPTER2

CHAPTER 2

LITERATURE REVIEW

2.1 Swirl flows

The introduction of swirling flows to the gas turbine engine industry has proven to be a promising way to reduce pollutant emissions. Swirling flows create internal flow recirculation zones (RZs), which entrain a portion of the hot combustion products in the gas turbine combustion chamber. These recirculation zones not only act as a heat reservoir, but also play an active role in improving the mixing and the blowoff limits. This reduces the combustor length and reduces emissions [26,27]

Swirl stabilised combustion has been used widely throughout the world, mostly in gas turbine combustors for power generation. The mechanisms and benefits of swirl stabilised combustion are well documented and depend in most instances on the formation of this central recirculation zone which recirculates heat and active chemical species to the root of the flame, increasing flame stabilisation in regions of relative low velocities where flame velocities be matched [29].

Several promising technologies are used to reduce the impact and production of nitrous oxide (NOx), with lean premixed and swirl stabilised combustion being regarded as suitable options

On the other hand, it has been found that the levels of swirl used in some combustors, coupled with the mode of fuel injection, could encourage the unwanted appearance of regular fluid dynamic instability [30]. Swirl stabilisation combustion creates coherent structures that may produce low frequency modes, which has the range of 20 – 400 Hz. These modes can couple (resonate) with the natural frequencies of the equipment, producing oscillations that can harm the system [31]. Therefore, there is considerable interest in improving these systems as they still present complex instabilities under low NOx emission conditions.

Swirling flows are defined as a flows undergoing simultaneous axial, tangential and vortex motions. This is achieved by the application of helix motion, where the swirl velocity component is initiated by the (i) swirl vanes, (ii) axial and tangential entry swirl generators, or (iii) by direct tangential entry into the chamber [32].

Intensive studies on swirling flows have been conducted with special emphasis on the three dimensional flow characteristics and the methodology for flame holding [33]. Combustor design must be improved to enable operation with lean premixed gases. However, there are instabilities that are induced by the restrained swirl stabilised combustor process. The most common of these sources is a vertical spiral structure which forms by the combined effect of swirling flow and sudden expansion of geometry [34].

When operating under lean conditions, the important characteristics to optimise are very good mixing, flame stability from the formation of the central recirculation zone, and the potential for reduction of emissions. Furthermore, the shear flow leaving the burner avoids direct contact with the high temperature flame within the combustor, leading to an increase in the durability of the equipment. These flows have been studied by many researchers over the last two decades [33,34]. It has been shown that emissions are reduced by increasing the swirl, and by producing flames stabilised by the surrounding structures. These structures include inner and outer recirculation zones with coherent structures formed as a consequence of the dynamics of the swirling mechanism [29].

2.2 Coherent Structures

Large scale coherent structures play an important role in combustion and heat release processes by controlling the mixing in non-premixed and premixed flames. The complex panorama is based on air flow rate, Reynolds number, equivalence ratio and geometries. The most important contributions to the turbulent momentum transport, and considerable mass and heat transfer, are attributed to these structures, making them a very important parameter in engineering applications. The geometry and flow

regimes are crucial parameters in the control of the flow, while the structures inherent in the flow field are an appearance of velocity change and pressure decay. However, not only complex geometries can increase the number of modes in a certain regime; they can also be increased by variation in wall surfaces and increased structures in the flow [29].

The most significant parameters the formation of these structures are Reynolds number and vortex breakdown, as these precede the initial formation of the central recirculation zone. Taking advantage of the flows is a well-known technique to increase the final efficiency of the combustion process based on a reduction in length of the flame without compromising the quality of the process and avoiding the formation of undesirable emissions. This allows the reduction of the combustor dimensions, leading to low costs and augmented efficiency [31] .

Fundamental investigation is required into the details of the recirculation zone and its potential to improve mixing. The zone's potential to influence the mixing processis coupled with stability and other parameters. It has been argued in the past that this structure is where the mixing process takes place [32]. Recent studies examining the concentrations of OH molecules in this balanced region have indicated that the stability of the flame and mixing occurs on the boundaries of this region, between it and the shearing flow [31]. Most of the previous studies focus on single swirl burners rather than concentric swirl burners, even though both concentric and single swirl burners play an increasingly important role in practical combustor design. The burner with double dual concentric swirl burners allows variation of the radial swirl distribution through control of the axial and angular momentum of the jets in two annuli of the burner. As such, even for a fixed swirl number, the comprehensive details of flow distribution can differ significantly from that of other operational conditions of the burner. Through introducing a swirling flow of the concentric annuli, it is possible to control the radial distribution of the flow and swirl to achieve very different limits of flame stability, volumetric heat release, levels of turbulence, and general characteristics of the combustion process [30].

There are many unanswered questions about these flows, particularly those involving coherent structures, their impact on the main flow, and their relationship with the recirculation zone. Valera-Medina et al.[32]detailed the impact of coherent structures on the mixing process, coupling them with acoustic and other instability modes. Despite many of the basic details about the appearance of coherent structures being described such as the essence of their movement, Precessing vortices (PVC) remain poorly understood. Previous works [32] conducted Large Eddy Simulations predicted the relationship between PVC and RZ. One problem was the lack of detailed experimental data needed to validate the results of the interaction. Hence an approach was adopted to generate basic data about these structures by using Particle Imaging Velocimetry (PIV) [32].This gave data about the interaction between RZ and PVC, with details on the form gave of their shape and dependence on non-dimensional parameters [35]. Comparing frequencies, amplitudes and number of harmonics under different conditions revealed different behaviour patterns as a function of swirl number. Analysis of different cases showed areas of operation where there was a strong disturbance. In the formation of one case, similar amplitudes were observed in the first and second harmonics. This was associated with the measurements of two PVCs, classifying other important cases as unstable, with three-dimensional reconstruction of processes using a variety of axially and tangentially planes with the help of PIV visualisation [33] .No bifurcations or major perturbations were observed with this technique. 3D holograms were created in Matlab® to show the real interaction in space of these large structures. Results refuted usually assumed to the shapes of the PVC from LES with a complex spiralling mechanism revealed [35].

2.3 Swirl Characteristics

Vortex flows result from the application of escalating the speed component of spiral movement. This is also known as the tangential or azimuthal velocity component. It flows via the use of swirl vanes, through the use of axial-plus tangential entry swirl generators or through direct access into the chamber.

Experimental studies [36] show that swirl has a large effect on the flow field, the stability, the combustion intensity, and the size of flame. The reacting flows are affected by the degree of swirl imparted to the flow. The degree of swirl number, *S*,

is a non-dimensional swirl number that defines the axial flux of swirl momentum divided by the axial flux of axial momentum. S is defined as follows:

$$S = \frac{G_\theta}{G_x d/2} \tag{2-1}$$

$$G_\theta = \int_0^\infty (\rho uw + \rho\, u'w')r^2 dr \tag{2-2}$$

$$G_x = \int_0^\infty (\rho u^2 + \rho u'^2 + (p - p_\infty r^2) dr \tag{2-3}$$

However, the above equations require knowledge of all the velocity and pressure profiles for all conditions at different swirl numbers at each point of the flow regime. This lead to a very complex calculation. Syred and Beer [27] 1974 proposed that this expression could be simplified for constant density environments, i.e. isothermal conditions, to a simple function of geometry [36,34].

$$S_g = \frac{\pi r_e r_{eff}}{A_t} \tag{2-4}$$

The geometrical swirl number, *Sg*, uses inlet conditions and ignores pressure variation effects across the flow for isothermal conditions. The density is assumed to be constant and the axial velocity can be obtained from the flow rate, *Q*, divided by the exit area, *Ae*. The angular velocity ω is taken as the inlet velocity multiplied by an effective radius r_{eff}. The geometrical swirl number is related to the inlet and outlet flow rates [38].

Under combustion conditions the geometrical swirl number is directly related to the inlet and outlet flow rates. The process is under constant pressure, so S changes according to the ratio of degrees of absolute temperature. The size of the exit volume and the axial velocity at the exit also increase with temperature[26,38].

This causes a reduction in the ratio of angular momentum to axial momentum. Thus the geometrical swirl number is reduced as a consequence of the average inlet and outlet temperatures as follows:

$$S_{gcomb} = S_{g,iso}\left[\frac{T_{inlet}}{T_{outlet}}\right] \quad 2\text{-}5$$

2.3.1 Strouhal Number

The frequency *f* of vortex shedding behind any bluff body should be completely determined by three additional kinematic variables, velocity, characteristic length (e.g.,diameter or a circular cylinder) and the kinematic viscosity of the fluid.

Since these four variable involve only two basic units, length and time, they can be arranged into a universal relation between two dimensionless groups:

$$S_{rv} = fn(R_e) \quad 2\text{-}6$$

$$S_{rV} = \frac{fL}{V} \quad 2\text{-}7$$

A dimensionless number, the Strouhal number Sr, is commonly used as a measure of the predominant shedding frequency *f*. The definition of the Strouhal number is an integral part of the fundamentals of fluid mechanics [39] is useful for analysing oscillating unsteady flows.

Strouhal number represents a measure of the ratio of inertial forces due to the instability of the flow or the local acceleration to inertial forces due to changes in velocity from one point to another in the flow field. It represents the instability of the

flow. Thus, it is a weak function of the Re number [38,39].Thus, Swirl could be correlated to the frequency of the system using the following function:

$$S_r = \frac{f D_e^3}{\mathrm{Q}} \qquad 2\text{-}8$$

Cassidy and Falvey [39,40] reported and define a Strouhel number based on the PVC frequency, D the injector diameter and Qv the volumetric flow rate. Strouhal number values obtained their study and compared with previous data as:

$$S_r = \frac{f_{pvc} D_e^3}{\mathrm{Q}_v} \qquad 2\text{-}9$$

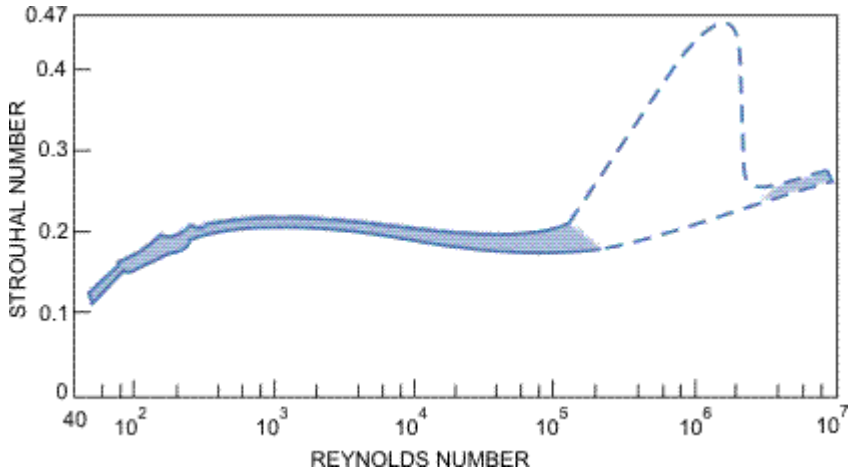

Figure 2-1: Strouhal number versus Reynolds number for circular cylinders (tubes) [42]

The variation in the Strouhal number is associated with the changes in the flow structure . From Figure 2.1 it is found that the Strouhal number is about 0.2 over a large Reynolds number interval. In the Reynolds number range $250 < \mathrm{Re_D} < 2\times10^5$ the empirical formula is sometimes recommended for estimation of the Strouhal number.

$$S_r = 0.198\left(1 - \frac{19.7}{R_{e_D}}\right) \qquad 2\text{-}10$$

At high Reynolds numbers the vortex shedding does not occur at a single distinct frequency but rather over a narrow band of frequencies [39,41].

2.3.2 Swirl mechanism

Swirl is commonly used to: (i) stabilise high combustion intensity, (ii) limit the lengths of combustion through the production of higher rates of entrainment of ambient fluid, (iii) encourage fast mixing near the nozzle exit and on the boundaries of recirculation zones, and (iv) to improve flame stability as a result of the formation of the central recirculation zone. The recirculation zones heat the active chemical species distribution to the root of the flame, thus reducing the velocity requirements for achieving flame stabilisation, which is only formed beyond a critical swirl number of 0.6. With sufficiently high Re (greater than 18000) and with swirl number greater than 0.6, large recirculation zones are produced and high levels of turbulence are present in the system. The recirculation zones occur close to the exit nozzle as shown in Figure 2.2 [26, 38].

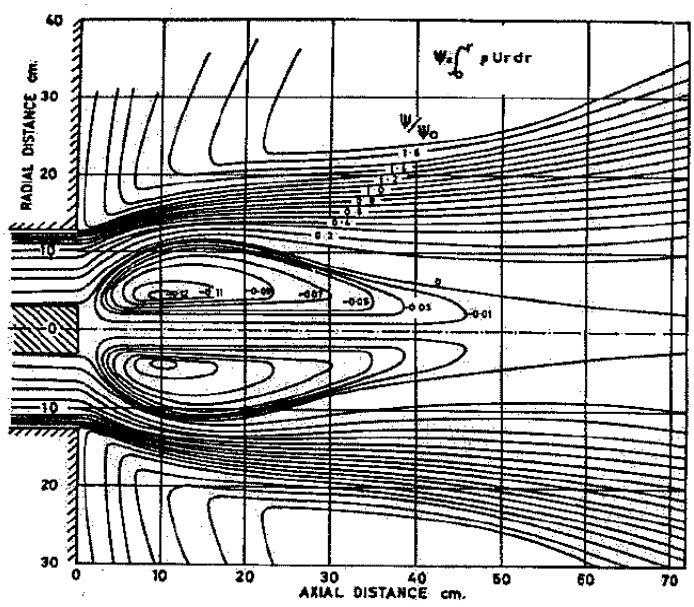

Figure 2-2:Recirculation in a swirling jet flow[36]

2.3.3 Swirl features

2.3.3.1 Vortex breakdown

Leibovich [43] describes a vortex breakdown as a change in the structure of a vortex initiated by a variation in the characteristic ratio of tangential to axial velocity components. There is evidence to show that the vortex breakdown can often be not only asymmetric, but also highly time dependent. This is the result of the forced vortex region of the flow becoming unstable and starting to precess about the axis of symmetry, thus forming the so called precessing vortex core or PVC [44].

Swirling flows undergoing vortex breakdown provide an excellent basis for flame stabilization.

On the other hand, vortex breakdown can also lead to flame flashback into the premixing section. Modern premixed combustors require a mixing tube for enhanced fuel-air mixing. The good mixing significantly reduces the emissions, but the vortex breakdown can move upstream into the mixing tube, or the swirl generator, where the high temperatures may cause severe damage [45].

2.3.3.2 The recirculation zones

The recirculation zones (RZs) incorporate a variety of flow features, for example sudden expansion, bluff bodies and combinations of domes and swirls. These are a result of flow separation. In swirling flows, these zones occur as a result of vortex breakdown and negative pressure gradients. In addition, as a result of a sudden expansion in the combustor area, external recirculation (ERZ) zones will be formed [36,37].

2.3.3.2.1 The central recirculation zone

A central recirculation zone is established in the wake of the exit burner under the influence of the swirling flow. The central recirculation zone from the vortex breakdown serves the flame stabilisation region, where it is mixed with hot products of air and fuel. The recirculation zone, generated by the flow of the vortex, is important for achieving flame stability. The pressure gradient and distribution within the combustor are the most important factors in the formation of this recirculation zone. With the flow passing through the swirl vanes, tangential velocity components

are created, further generating centrifugal force toward the outside of the combustor. A radial pressure gradient is thereby formed in order to sustain equilibrium with the centrifugal force. The flow is then known as simple radial equilibrium flow [45].

With a sufficient degree of swirl, a central recirculation zone is generated, which allows a high rate of heat release from the circulated combustible products and the igniting incoming fuel and oxidant streams. This provides a compact and stable flame, with good performance for poor quality gases. The formation of the recirculation flow zone, a form of vortex breakdown, acts as an aerodynamic blockage (a three-dimensional bluff body) which serves to stabilise the flames [46].

2.3.3.2.2 The External recirculation zone

Coghe et al. [47] gave evidence of the appearance of different recirculation zones connected to the swirl strength, which could be the effect of combustion features. In fact, the central recirculation zone is very important for mixing and flame stability, and the extend recirculation zones close to the combustion chamber walls induce entrainment of large amounts of hot burned gases into the outflowing of reactant mixture [47]. These zones also serve to attach the flame to the burner mouth.

The generation of recirculation zones can use a variety of flow features, from sudden expanse, bluff bodies and swirling flow. They are produced as a consequence of flow separation processes, except for the swirling flow that forms as a result of vortex breakdown and of gradients of negative pressure [38].

2.3.3.3 High momentum flow region (shearing flow)

Swirl flows are associated with the high momentum flow region (HMFR) and have been reported by several researchers [38,[48],[44] The central recirculation zone is displaced from the central axis and generates the high momentum flow region placed on the shear layer. This is accompanied by another spiral vortex structure defined as a precessing vortex core (PVC) as recognised by Syred and Beer[27].The PVCs enveloped and squeezed the CRZ Previous and recent work has focused on the

aerodynamic characteristics of this region, with weak emphasis on the surrounding flow. The high momentum flow region that accompanies swirling flows has attracted the attention of several groups interested in blowoff and stretching phenomena [44,49]. Figure 2.3 shows the rotating tangential velocity close to the burner outlet. There is considerable variation and negative tangential velocity near to and around the axis of symmetry. This is due to the PVC-HMFR interaction causing a high level of tangential velocity confined to a banana-shaped region near the outer wall [39].

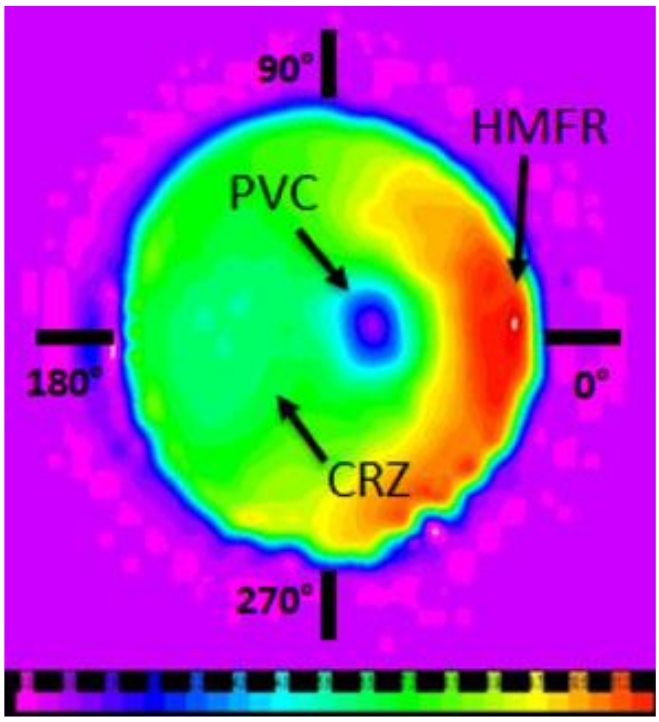

Figure 2-3: The high-momentum flow region (HMFR) [49]

2.3.3.4 Vertical Structures (PVC)

The vortex breakdown usually disrupts the flow symmetry due to inherent instability, resulting in the precession of the vortex core (PVC) of the swirling structure around the combustor axis of symmetry as shown in the figure 2.4 [50] . Vortex breakdown with CRZ and PVC has been found to be very useful for enhancing the mixing and stabilisation of flames, and is considered as a fundamental principle for stable operation of the burner[51].However, the PVC may produce undesirable vibrations and noise and can also modulate heat-release, driving thermo-acoustic oscillations.

The PVC phenomenon is clearly shown to be caused by the displacement of the centre of the vortex. This displacement, in turn, causes a squeezing of flow against the exhaust of the burner, and due to the angular momentum flux this causes a considerable increase in the tangential velocity level [51].

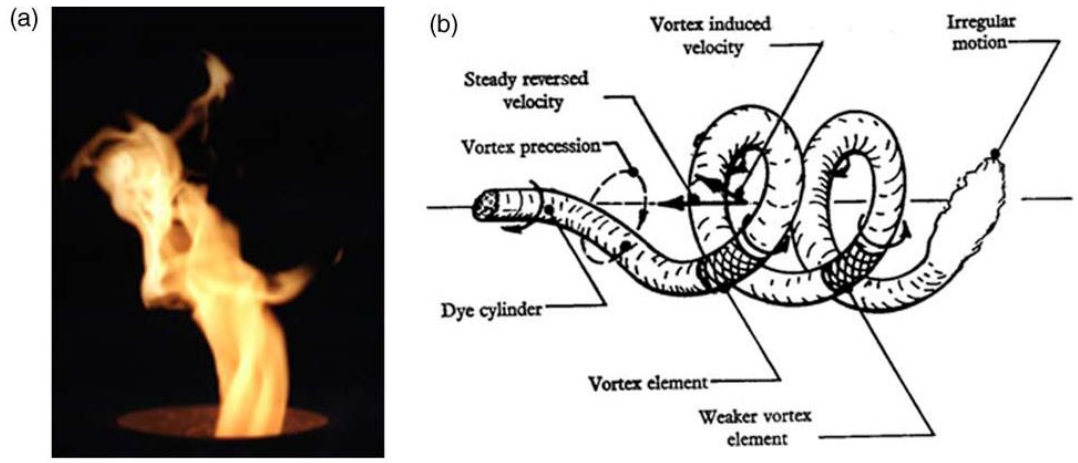

Figure 2-4:(a) Visualisation of single PVC with separate axial fuel injection into a premixed flame, swirl burner (b) visualisation of helical nature of the PVC[39]

2.3.3.5 Secondary Recirculation zones.

Further effects relate to the level of swirl, the equivalence ratio and whether or not a quarl or sudden expansion is used on the exit burner. As mentioned previously, the Central Recirculation Zone (CRZ_1) formed by an unconfined swirl burner arises due to the sudden expansion, which causes a decay in the velocity. This decay in turn generates the strong radial and axial pressure gradients that form the CRZ. Therefore, inevitably, any form of confinement will alter the size and shape of the CRZ, and will also cause the ERZ to form as the flow sticks to the confinement wall. Since the PVC is located at the boundary of CRZ, confinement has considerable effects on the flow field. The effect of the confinement will increase the frequency of PVC. This could also lead to the secondary vertical structures. The formation of a secondary PVC is undesirable as it will be become a mechanism of instability [39].

The external eddies are well known to be toroidal in nature and to increase from the sudden expansion. These eddies can be eliminated by using quarl at the burner exit.

Another set of eddies is observed to be located in between the shear flow and CRZ and reveals the initial separation of 3D coherent structures. These 3D coherent structures are formed as a consequence of the separation of CRZ into another CRZ, so called CRZ2. This second recirculation zone, CRZ2, can be formed under confined the zone is highly asymmetric and rotates with the same frequency as the high momentum crescent shaped velocity region with the rapid pressure decay conditions. This result confirmed the high importance of the pressure in the development and shape of the inner structures in such type of flows. The system showed strong second and third harmonics. Overall CRZ1 and CRZ2 increased the extent of the recirculation regionsas shown in figure 2.5 [39,33].

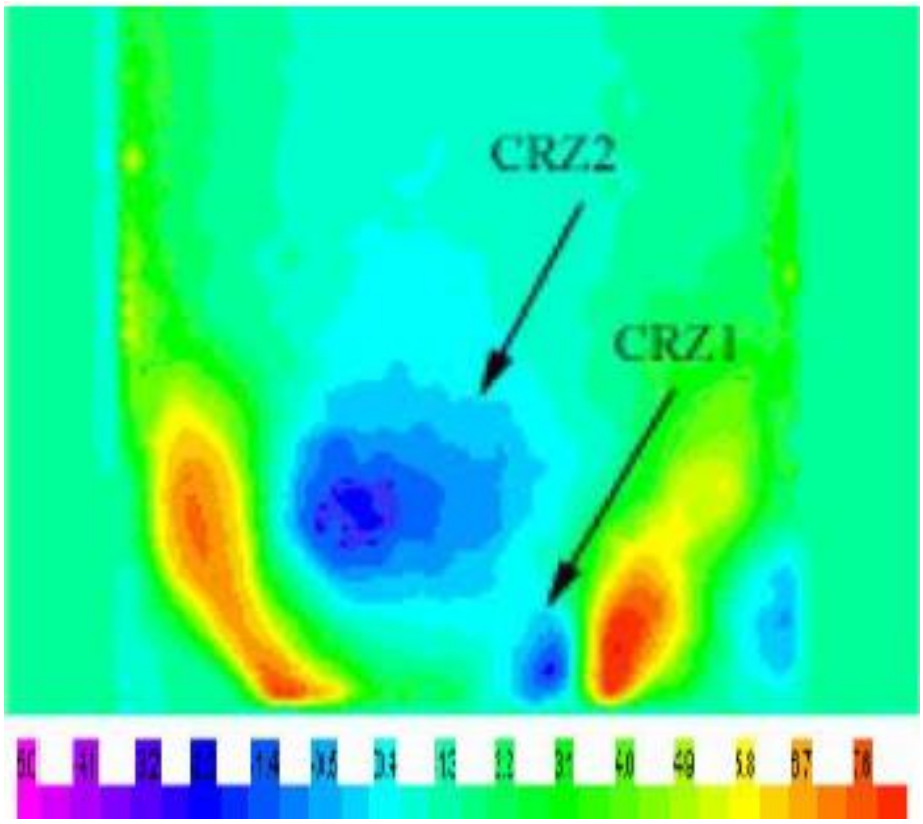

Figure 2-5: Central recirculation zones [34]

2.3.3.6 Other Hydrodynamic Effects

2.3.3.6.1 Coanda Effect Theory

A natural question is "how does the wing divert the air down?" When a moving fluid, such as air or water, comes into contact with a curved surface it will try to follow that surface. Coanda Effect a moving stream of fluid in contact with a curved surface will tend to follow the curvature of the surface rather than continue traveling in a straight line.

Same situation apply to the wing Figure 2.6. Since air behaves exactly like any fluid, Bernoulli's principle applies. Any time the wind is blowing or a fan blows air, the pressure of the moving air becomes less than it would be if the air wasn't moving .The upper surface creates an airstream, adherent to the upper curved surface, where the Coanda Effect applies also and gets more air from above in the same time, the Coanda effect speeds up the air over the upper surface, and so lowers the air pressure next to it, which in turn generates more lift in this region, creating the necessary lift forces [52].

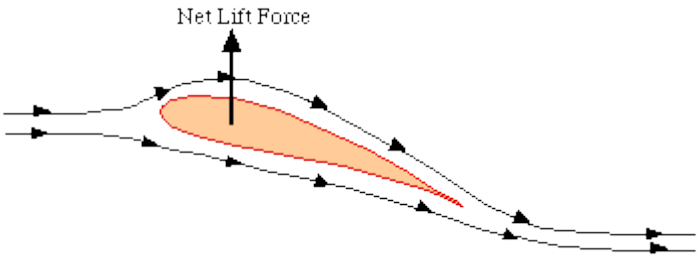

Figure 2-6: Lift according to the application of Bernoulli's Equation [52].

2.3.3.6.1.1 Bernoulli equation applications

When the Bernoulli equation is combined with the continuity equation the two can be used to find velocities and pressures at points in the flow connected by a streamline.

In the figure 2.7 is an example of using the Bernoulli equation to determine pressure and velocity at within a contracting and expanding pipe [53].

$$p_2 = p_1 + \frac{\rho}{2}(u_1^2 - u_2^2) \qquad 2\text{-}11$$

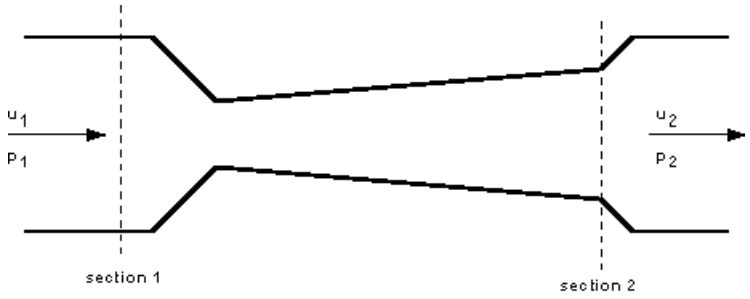

Figure 2-7: A contracting expanding pipe [53].

2.3.3.6.2 Coanda Effect

Future flexible power plants will require new and improved systems for the flexible usage of a variety of alternative fuels. However, the use of such fuels requires that the fundamental flow structures close to the burners are well understood, giving high confidence during the change of conditions in a matter of minutes, especially for multi-burner applications or flames that are not highly confined. There are well known flow structures that are essential to the stability of current burners, i.e. Central Recirculation Zone, Precessing Vortex Core, etc.[39]. However, there are some structures where the interaction with the localised flow field during transition is still poorly understood.

One of these structures is the External Recirculation Zone (ERZ) observed in Open Jet Flow-Medium Swirl (OJF-MS) flames, as shown in the Figure 2.5.Another important type of exhaust flow characteristic is the Coanda Jet Flow (COJF), which contrary to the OJF-MS pattern produced when an ERZ is formed, occurs when ejected gases from a burner attach to the flat mounting plate on which the nozzle exit is connected [53,54] .The Coanda Stabilised Flame is situated near the bottom of the combustion chamber resembling a sunflower with a large, flat flame surface, Figure 2.8 d. Vanierschot [50] showed that as a consequence of the increase in the deflection angle of the flow when decreasing the swirl, the velocity near the outlet of the nozzle increases. This causes the local pressure to decrease, deflecting the flow and

producing the Coanda effect. Nevertheless, the transition from the Coanda effect to the Swirl Stabilized Flame is still not entirely solved.

The CRZ is a product of the decaying pressure and the swirling movement of the flow ,as previously stated .Inevitably, the structure can produce complex oscillations as the high vorticity interacts with other structures (i.e. Precessing Vortex Core PVC, CRZ) whilst varied entrainment rates can encourage equivalence ratio and heat release variations[56].

The addition of a quarl to the swirl burner has shown to substantially reduce the amplitude of the oscillation by eliminating the external recirculation zone[56]. It was observed how the disappearance of the ERZ provided more stable flows close to the burner nozzle with lower values of directional intermittency. It was noticed that the Rayleigh Criterion for stratified flows could also be applied in this case, as significant levels of negative tangential velocity in the region of the ERZ and near the swirl burner existed over at least 60–70% of the oscillation cycle, thus confirming the unstable nature of this region [57].

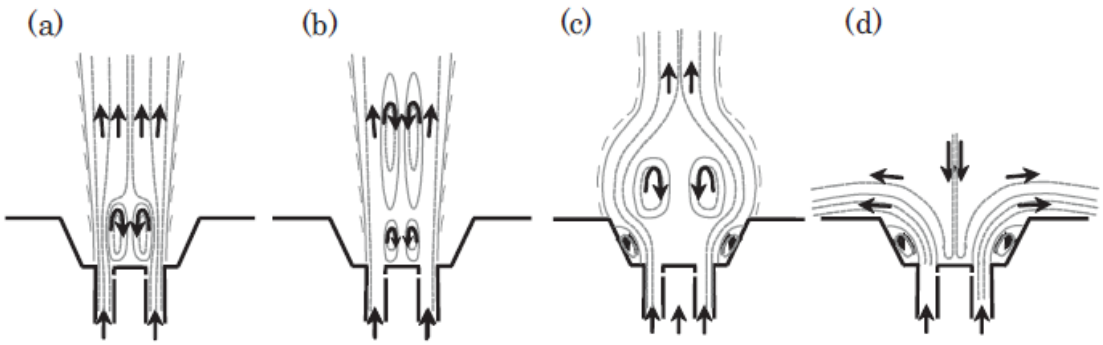

Figure 2-8: Schematic view of the different flow patterns. a) Closed Jet Flow; b) Open Jet Flow Low Swirl; c) Open Jet Flow High Swirl (OJF-HS); d) Coanda Jet Flow (COJF) [54].

On the other hand the Coanda effect was discovered early in the twentieth century. Henri Coanda deduced that the attachment was produced by a decrease in surface pressure in the separation bubble which he observed to form just downstream the

nozzle exit [58]. When a jet of fluid is passed over a curved or a strongly divergent nozzle the jet is pulled onto the curved surface as a result of the low pressure region which develops as entrainment by the jet removes gases from the region between the jet and the surface. The balance between the inward radial pressure gradient and the outward centrifugal force then holds the jet to the wall [59].

Inevitably, any form of significant confinement will affect this process and alter the size and shape of the CRZ, whilst also normally causing modifications to the ERZ that forms as the flow sticks to the external wall [39].

The substantial flow deflection offered by the Coanda principle is generally accompanied by enhanced levels of turbulence. A related, although undesirable side effect is the significant increase in associated noise levels[58,59].

Applications of the phenomenon vary from aerospace design stealth technology to burners and medicine applications [58,60,61]. In aerodynamics, it has been observed that the geometry is an important factor to the development of the effect, as observed by Wing in the 1990's with the study of angled nozzles to control the pressure [61]. Nevertheless, it is recognised that the acoustic radiation is one of the major constraints in some of these applications. This obviously detrimental side effect has meant that in many cases the potential benefits of the Coanda effect have yet to be fully realised. Turbulent Mixing Noise (TMN) is a primary high-frequency noise source when the Coanda effect is employed. Theories have been postulated for its prediction in 2D flows with good success. However, the complex nature of the flow in 3 dimensions under subsonic states is still a challenge and many of its effects are still poorly understood [63].

In contrast to subsonic jets, conditions downstream the jet can turn supersonic. Thus, discontinuities in flow properties can arise depending on the relative pressure difference between the nozzle exit and the ambient pressure. This can produce stationary shock cell structures in the mixing layer region close to the jet exit. The interaction of downstream propagating turbulent eddies with this structure generates the high frequency sound known as shock associated noise. In 3 dimensional flows, factors such as radial expansion and streamline curvature can arise complicating even more the solution of the system[60].

Some authors have studied the phenomena under isothermal conditions [64], giving ideas about the movement of the core as a manifestation of the compressing-expansive mechanism in the inner part of the structure. A modern idea stipulates that its formation comes from a series of small eddies generated by the CRZ [65]. However, the transition of different flow patterns could give a better understanding of its appearance and behaviour during this process. Thus, the transition of the ERZ to/from the Coanda effect with swirl burners could be a phenomenon that unlocks some interesting features of this and other structures, a process that still requires extensive characterization.

Vanoverberghe [54] studied the phenomena via the transition of different flame regimes in an IFRF generic swirl burner at different swirl numbers, observing that cold flows and S were to a large degree responsible for the type of flame pattern with combustion superimposed on it. Vanierschot [50] showed that as a consequence of the increase in the deflection angle of the exhaust flow when decreasing the swirl the flow near the outlet wall of the exhaust nozzle sticks and increases the velocity near the outlet of nozzle increases. This causes the local pressure to decrease, deflecting the flow and producing the Coanda effect. However, effects such as ERZ, CRZ and PVC formation and interaction with the Coanda flow have yet to be fully investigated.

Modellers have tried to predict the Coanda effect and the ERZ region for many applications. Mirkov and Rasuo [66] using in-house software and the k-ω Shear Stress Transport model accomplished the analysis of an Unmanned Aerial Vehicle (UAV) using the Coanda effect, denoting the high attachment of the upper flow and its separation at the bottom of the geometrical array, with the appearance of vortical structures similar to the ones observed with bluff bodies. Rumsey and Nishino [67] showed that with flows under 0.64 Mach number the solutions between incompressible and compressible RANS were very similar when analysing the Coanda effect on airfoils. Drangan and Stanciu [68] used the k-ε model to observe a new super circulation technique to reduce drag and improve lift in aerospace applications. Tavakoli and Hosseini [69] investigated the relation between the Swirl number and the flow pattern using different angles in an axial vaned swirler used for ventilation applications.

Although these and more advanced techniques such as LES [69,70] have been used for the study of the Coanda effect, the computational results have not shown the transient nature of the process. The transition from a vortex breakdown dominated flow to a Coanda jet has also been studied by Singh and Ramamurthi [70], who showed that the increase in swirl in sharp-edged nozzles produce a system dominated by centrifugal forces that spread the flow in the radial direction, producing the particular shape of the Coanda effect. Their results showed the appearance of vortical structures that migrated through the system. However, the computational results did not show a close correlation to the experimental values obtained by the group. For the External Recirculation Zone and PVC, extensive literature has shown its appearance just downstream the burner nozzle in power and propulsion applications [38,71,72] , but there is limited information about the transition of the structures. Thus, more work is required to quantify this process.

Thus, the fundamentals of the evolution to/from a Coanda Jet with a medium swirl device which has already passed through a vortex breakdown has never been investigated before. Therefore, swirling flows of a generic burner are studied in the present work via experimental laser and visualization techniques. The aim of the study is to observe how the transition from/to a COJF to/from a conical OJF-MS pattern takes place with different geometries, giving insights of the evolution of different structures across the flow field.

A constant swirl number of 1.05 was kept during the trials. In order to change the geometry, a flat base plate was positioned at different distances from the lip of the nozzle giving different step sizes from the tip of the nozzle to the flat surface. A nozzle angle of 45° was used in order to observe the phenomenon.

2.4 Swirl with Combustion

2.4.1 Combustion Principles

Combustion is one of the most important processes in engineering. It involves a turbulent fluid flow, chemical reaction, heat transfer, and radiation of heat from complex physical and chemical operations. Typical applications include internal combustion engines, combustion power plants, aircraft engines, gas turbines, combustion boilers, furnaces, and other combustion equipment. It is important to be

able to predict flow, temperature and resulting concentrations of species and emissions from the combustion of various designs. It is also important to improve combustion equipment and systems, particularly with current level of concern about the volume of CO_2 and other emissions and their effects on the environment [74,75].

2.4.1.1 The concept of turbulence

Despite most flows occurring in nature and engineering applications being turbulent, it is difficult to give an exact definition of turbulence. Turbulence is characterised by the random and chaotic three dimensional vorticity. Turbulence in fluid flow usually dominates the entire fluid domain and results in an increase of heat transfer, mixing and energy dissipation.

The purpose of turbulence theory is the prediction of turbulent flows and properties in various applications. Although turbulent flows have been investigated for more than a century, there is still no general solution of the problem. Consequently, the theory of turbulence is quite far from being directly solved [76] . For this reason, different turbulence models have been developed through the decades to estimate turbulence impacts on a great variety of conditions.

2.4.1.2 Turbulence Models

To understand turbulent flows it is necessary to define the characteristics of these turbulent regimes, thus allowing the prediction of the behaviour of the field of interest. In order to achieve a good prediction of certain turbulent conditions, some models can be used to describe the likely behaviour of the turbulence field [76,77].

A turbulence model is a computational procedure which closes the system with mean flow equations so that a wide variety of flow problems can be calculated [79] . For most engineering purposes it is unnecessary to resolve the details of turbulence fluctuations, so usually just a description of the effects of turbulence on the mean flow are required, and this is provided by a turbulence model.

However, there is no a general model able to solve all turbulent flow problems. A model which can describe a very good fit for solving one particular certain case may fail to solve another case. Many different techniques have been used to address different questions concerning turbulent flows.

For a turbulence model to be useful in a general purpose CFD code, it must have wide applications, good accuracy, good simplicity, and be inexpensive to run. The choice of the turbulence model will depend on considerations such as physics surrounding the flow, the level of accuracy required and the availability of computational resources considering the amount of time available for the simulation. To obtain the most appropriate choice of model for a specific application, it is necessary to understand the capabilities and limitations of various options [76,77].

The most common turbulence models are classical models. New trends and extensive research have lead to the usage of more advanced models such as large eddy simulation (LES). The classical models are based on the time-averages Reynolds equation presented as: (i) a Zero-equation model (mixing length), (ii) a One equation model (Spalart–Allmaras), (iii) a Two equation model (k-ε model and k-ω), (iv) the Reynolds stress equation model, and (v) an Algebraic stress model. These standard models use the Reynolds equations with relatively low computational cost, being widely adopted for practical engineering applications. Large Eddy Simulation (LES) is a more advanced model, directly solving time dependant flow equations for the mean flow and the largest eddies whilst modelling smaller eddies with a turbulence model. It has been observed that the largest eddies interact strongly with the mean flow and include most of the energy, and consequently this approach is suitable for modelling and predicting the main effect of turbulence [80].

2.5 Combustion Instabilities

2.5.1 Instabilities in Gas Turbines

In gas turbine the combustion flowing turbulent fuel mixture is continually accompanied by noise, whilst the noise produced from normal combustion is usually referred as core noise, which consists of two components (i) direct combustion noise that is generated by the combustion process and (ii) indirect combustion noise that is produced by the flow of hot combustion products through the exhaust nozzle and turbine[81].

Instabilities arise in combustion processes in many different ways; a detailed classification is difficult to determine as a consequence of many different phenomena

may be involved. In one approach [82] , a classification is based on the components of a system such as Gas turbines or an industrial boilers that contribute in the instability in an important method. The Substantial instabilities whether the combustion occurs within a combustion chamber, chamber instabilities, associated with the occurrence of combustion inside a chamber, and the system instabilities, which include an interaction of the processes occurring in the combustion chamber [82].

2.5.2 Thermoacoustic Instabilities

Thermoacoustic instabilities can be a problem in continuous combustion systems. Thermoacoustic instabilities take the form of large pressure oscillations typically oscillating with a frequency of several hundred Hertz. The combustion instabilities, generated by reciprocal interaction between the heat oscillations and pressure fluctuations produced by the flame in lean premixed combustion fuelled by the variety of gases, present an undesirable instability problem. In the combustion chamber acoustic waves are propagated and reflected, resulting in the generation of strong pressure oscillations that can damage the chamber. This phenomenon indicates general thermoacoustic instability, due to the coupling of heat release fluctuations and pressure waves, and is characterised by large amplitude fluctuations in natural acoustic modes [82,83] problems resulting from these instabilities include vibration and mechanical stress that may lead to structural damage and system failure. The oscillations may also cause problems to components downstream of the combustion chamber, for instance a turbine in a power plant.

The principal mechanism of acoustic oscillations is its amplification by the Rayleigh criterion. Rayleigh's criterion, which dates back to 1878, states that when the heat-release rate from the combustion process is in phase with the pressure, the system is unstable, and when the heat-release rate is out of phase with the pressure, the system becomes stable. It is established that there are always unsteady combustion process' present in a combustion system with turbulent flows, the mechanism of coupling between these heat release oscillations and perturbations in the flow and mixture is what leads to acoustic oscillations in the combustion process, as shown in Figure 2.9.

Formally, this criterion may take the form where $p1$ and $q1$ stand for pressure and heat release fluctuations, respectively, and Ω is the flow domain.

The sign of the above integral may change with the phase of the oscillation, and Equation 2.12 is often integrated over a period to characterize the stability of the system at a given frequency [41]. In the unstable case, as long as the energy added by the flame exceeds the acoustic losses at the outlet of the combustion chamber, the pressure oscillations will grow. At some point the acoustic losses will equal the 2energy added by the flame, and the system will continue to oscillate in a limit cycle (equilibrium) [83].

$$\iiint_{\Omega} p_1 q_1 d\Omega > 0 \qquad 2\text{-}12$$

2-9: Heat release and flow perturbations causing acoustic oscillations [85]

2.5.3 Flashback

The fundamental problem of all premixed-fuel combustion systems is a propensity toward flashback, which occurs when the flame travels upstream from the combustion zone into the premixing sections of the combustor. This upstream propagation of flame takes place whenever the flame speed exceeds the approach flow velocity [84].

Three main types of flashback have been identified: (i) flashback occurring in the free stream, (ii) flashback occurring through the low-velocity flow in the boundary layer along the walls of the premixing section, and (iii) flashback driven by combustion-induced vortex breakdown (CIVB) in swirl-stabilised combustors [84].

Flashback could be caused by the central recirculation zone (CRZ) which can extended back into the injector of the burner and increase the risk of flashback [86].

Flashback occurring through the low velocity flow in the boundary layer along the walls of the premixing section is associated to relevant parameters such as wall temperature, temperature distribution, boundary layer structure, turbulence properties and flame thickness [83,86].

Flames using fuel mixtures with high H2 contents were generally significantly shorter than those with mixtures with low H2 contents were. In the fuel mixture with the highest H_2 content, it was difficult to stabilize the flame, because of the occurrence of flashback [88].

The combustion induced vortex breakdown CIVB is a phenomena characterised by an upstream propagation of the flame into the combustor axis, This phenomenon is characterized by an upstream propagation of the flame on the burner axis, with propagation faster than the turbulent flame speed, against high axial velocity flow. Likelihood of this flashback increases especially when using the burner without central bluff body and with purely swirl stabilised flames [83,88].

2.5.3.1 Combustion Induced Vortex Breakdown

It has been recognized that the form of CRZ could affect the final stability system, and creation of other structures that can be push down the flame into mixing chamber, and an increased tendency to flashback. Some authors have noted how recirculation zone progresses into the mixing chamber as a combustion-induced Vortex breakdown (CIVB) (Kroner et al., 2003; Umemura and Tomita, 2001) [89,90] they are attributed the appearance of the vortex as a result of the entrance of the combustion and air , linking this phenomenon to the CRZ, which depends on the distribution of pressure downstream. Moreover, the vertical structures can be modified by geometrical factors and conditions of flow, as well as through the interaction of unburned gases and reaction zone , which complicates further its role in the occurrence of flashback and heroes. It has been recognized that this structure plays a crucial role in the propagation of the flame, especially by the impact of a similar pushing observed CRZ.

2.5.4 Blow-off phenomena

The use of new alternative fuels in the energy mix at large scales will be a reality in the near future as climate change and fossil fuel depletion in several parts of the world

are becoming more significant. The use of alternative fuels has posed new challenges for research and industrial groups that are looking for stable blends and conditions to run large industrial facilities. However, this contrasts with recent experiences of global operators who report increasing emissions and difficult combustion dynamics with even moderate variations in the fuel supply [92]. Most current gas turbines use swirl stabilised combustion, as it creates a complex flow field that anchors the flame and stabilises the combustion process [39]. The crucial feature of swirl burners is the formation of a central recirculation zone (CRZ) which extends blowoff limits by recycling heat and active chemical species to the root of the flame in the burner exit [35,86]. Thus, the CRZ is one of the mechanisms for flame stabilisation that creates a point where the local flame speed and flow velocity can match by generating an aerodynamically decelerated region [92]. However, unless strength is properly controlled, problems can arise.

Although the topic has been studied for decades, there is still uncertainty about many of the highly complex underlying processes. Many studies that have been conducted consist of large databases to improve the operability with natural gas, but there is still space for investigation on the fundamental underlying behaviour and combustion stability with alternative fuel blends [93]. There are several potential sources of blowoff, such as combustion tuned to a fuel/air ratio that is out of the flammability limits, instrumentation failure, the continuous emissions monitoring system being out of calibration, low-frequency chug dynamics, and many more [94].

As explained by Shanbhogue et al. [95], there are different theories regarding blowoff.

With some caveats noted by Shanbhogue et al. [95], there is general agreement that the blowoff process is controlled by a competition between the fluid mechanical and chemical kinetic processes, which can subsequently be defined in terms of a Damköhler number. Therefore blowoff occurs when the heat required by the combustible stream exceeds the one received from the recirculation zone. A different view is that the contact time between the combustible mixture and hot gases in the shear layer must exceed a certain chemical ignition time. This implies a direct link

between the scales of the characteristic dimension of the recirculation zone length, leading to a similar Da criterion [95].

Longwell et al. [96] suggested that blowoff occurs when it is not possible to balance the rate of entrainment of reactants into the recirculation zone, viewed as a well-stirred reactor, with the rate of burning of these gases. Since entrainment rates scale as the size of the CRZ increases and velocity of the flow is decreased, then it follows that this criterion reduces to a Damkohler (Da) number blowoff criterion, using a chemical time that is derived from the well-stirred reactor, τ_{PSR} [95]. The Damköhler number used in these assumptions is given by,

$$D_a = \frac{\tau_t}{\tau_c} \qquad 2\text{-}13$$

$$\tau_c = \frac{\alpha}{U_i^2} \qquad 2\text{-}14$$

A similar idea relates to blowoff occurring when the heat required by the combustible stream exceeds that received from the recirculation zone. This leads to the same entrainment-based fluid mechanical time scaling as above [95]. A different view is that the contact time between the combustible mixture and the hot gases in the shear layer must exceed a chemical ignition time. This leads to scaling of the characteristic dimension by the recirculation zone length, leading to a similar Da criterion [96].

Current theories are based on a flamelet based description of local extinction by excessive flame stretch [97].

The propagation of premixed flames in nonuniform flow fields causes some effects subject to various physical interactions such as strain rate and curvature, which cause change in the flame surface area. The increase in surface area of laminar flame is called flame stretch. Karlovitz 1953 conducted the study of stretched premixed flames and showed how important aerodynamic stretching on stability of flames.

The flame stretch factor K is defined as the percentage change of the flame surface area with respect to time, which is represented by the Karlovitz stretch factor. The number is defined as:

$$k_a = \frac{1}{\delta A}\frac{d(\delta A)}{dt} = \frac{1}{A}\frac{dA}{dt} \qquad 2\text{-}15$$

Stretch affects the flame speed consequently decreasing flame thickness .The reduction of flame thickness clearly changes the flame structure through its coupling effect with both thermal and mass diffusion.

The flame stretch concept could be applied to understand physical processes related to laminar flame studies in the area of flame stabilization, laminar flame speed determination and flammability limits [98].

Flame stretching instigates blowoff through the initiation of holes in the flame, that are healed by the same flame creating stretching in areas that otherwise would have been unaffected. The flame will extinguish when the flame stretch rate exceeds a critical value, κ_{ext} [92]. Higher flow velocities result in flame extinction occurring at higher values of κ_{ext}. Some sources of flame stretch are the flame curvature, unsteadiness in the flame and the flow, and hydrodynamic strain [99]. It is also recognised that this mechanism is not the one that causes the final blowoff, as it is clear from data that the flame can withstand some extinction. Therefore, it is considered that the "critical extinction level" must be somehow influenced by the entrainment of reactants, the cooling of regions and the change in size of the CRZ, thus confirming some relation between the phenomenon of blowoff and the existence of the CRZ [34]. A fair question would be to know to what extent blowoff is influenced by the strength and shape of the central recirculation zone [34].

In order to predict the event, some researchers [99,100] have developed various empirical correlations. DeZubay [100] derived a correlation for predicting the extinction equivalence ratio based on the bulk velocity and pressure. Lefebvre and Ballal [102] presented a general equation for determining the extinction equivalence ratio in terms of the mass flow rate. However, these equations were very specific to

the geometries investigated at the time. A more general equation proposed by Radhakrishnan et al. has provided better results for a series of conditions on a particular swirl burner [100,102]. Assuming that combustion occurs in the small scale structures of turbulence, extinction will occur when the time needed for the flame to propagate from one Kolmogorov-scale vortex to a neighbouring one exceeds the lifetime of the large eddies. However, this has also only been probed in conventional gases. Yamaguchi et al. [58] investigated the blowoff in a premixed propane-air flame stabilised by cylindrical rod bluff bodies. They concluded that a local extinction of the excessively stretched weak eddy flames at the end of the recirculation zone triggers the blowoff of the flame. DeZubay [100] correlated the fuel/air ratio at blowoff with the velocity, pressure and diameter of the bluff body. Zukoski and Marble [104] presented a criterion based on a characteristic chemical and residence time being equal, using the length of the CRZ as the characteristic length. Thus, the coherent structure seems to be a major contributor in generating blowoff events.

Regarding the central recirculation zone, the use of different configurations has demonstrated that the shape and strength of the CRZ can change drastically depending on these alterations [86,104] Valera-Medina et al. [36] have observed how the changing the angular of the combustor nozzle can produce different central recirculation zones under the same injection conditions. For example, stronger recirculation has been observed using different angled nozzles. Normalised CRZ velocities were calculated from PIV measurements and it was observed that the use of a 45° angled nozzle produced a negative velocity around 80 % stronger than that observed using a 90° nozzle. This velocity increment was accompanied by a reduction in size of around 11%, as the CRZ was compressed by an increased pressure as a consequence of the sudden expansion at the nozzle exit. However, it was clear that the width of both structures was almost the same, as the shearing flow coming from the nozzle maintained the high axial moment produced by the sudden constriction upstream of the nozzle mouth. This stretched the CRZ with a similar angle for both geometries.

Methane experiments carried out by Kariuki et al. [105,106] showed that when conditions were close to blowoff, the phenomenon was followed by the entrainment of fresh reactants from the downstream end of the recirculation zone, and fragmentation of the downstream flame parts. Just before the blowoff event, reaction fronts were observed inside the CRZ. This led to progressive fragmentation occurring, resulting in a shorter flame brush. The argument is that because the residence time in the wake region exceeds the shear layer residence time, the flame in the CRZ should be extinguished after that in the shear layer [101]. However, as observed by Valera-Medina et al. [43,104] the strength of the recirculation zone increases under isothermal conditions or close to final blowoff, with a very complex flow field [49].

There is a clear difference between the blowoff mechanisms in diffusion type swirling flames and premixed/partially premixed swirling flames. With diffusion flames the fuel is usually injected into the system somewhere near the axis and forms fuel rich regions in and around the CRZ which greatly aid flame stability, but do not give the low levels of emissions which can be found with premixed flames. Conversely, premixed swirling flames initially have a uniform distribution of fuel in the air; thus the CRZ region is not favoured by a high fuel concentration and the system generally has reduced blowoff limits compared to diffusion flames, though emissions can be much reduced. Conditions in and around the CRZ are much more critical to stability than the diffusion flames, as the now relatively dilute reactants in the CRZ are influenced in two opposing directions by the recirculation of heat and active chemical species from the downstream flow [108].

Positive effects arise from the addition of heat and active chemical species, whilst negative effects arise due to the dilution of the reactants by recycled burnt/partially burnt gases. Syred et al. [89] showed that for three different specific designs of premixed swirl burner (with specified geometries and swirl numbers ranging from 0.8 to 4.0) that blowoff was solely a function of the inlet swirl velocity, and not the swirl number. This surprising conclusion indicated that despite the variation in CRZ size, shape and recirculated mass flow arising from swirl number changes, the crucial area when considering blowoff is the initial shear layer around the base of the CRZ.

Here, over the swirl number range 0.8 to 4.0, the tentative conclusion is that the initial section/base of the CRZ and its associated annular shear layers are similar. Blowoff appears to be governed by the balance between total forward velocity in the annular shear layer and the turbulent flame speed (a function of the square root of turbulent kinetic energy and the Damkohler Number).

2.6 Alternative Fuels

2.6.1 Introduction

Premixed flame stabilisation in high intensity combustion is an important topic of study for the high efficiency and low emission operation of gas turbine combustors and industrial furnaces. Current lean premixing (LPM) combustion technologies focus on burning very lean fuel, either alternative or conventional. However, the wide range of fuels presents a problem in terms of variation of heating values, laminar flame speeds ,density, specific heat, chemical reactivity and thermal diffusivity. Process and refinery gases, gasified coal and petcoke are just a few examples. The biggest challenge to the fuel-flexibility of most combustors is the large differences between natural gas and the proposed replacement fuels. Moreover, gas turbines must meet the current emissions regulations, which often mean running very near lean blowoff. However, blowoff continues to be a phenomenon that is difficult to predict across reactor types and fuel compositions. To describe the lean blowoff behaviour of the combustors under various fuel compositions, correlations have to be determined and simplified models developed. This will help to further implementation of fuel flexible technologies [109].

Fuel independence has been a major driver for development in combustion systems during the last few decades, with the aim to find a technology capable of achieving high fuel flexibility for power generation. Swirl combustion is widely used as it forms coherent structures previously discussed [39]. These flows can produce other vortical structures capable of producing benefits such as improving mixing, or cause detriments by coupling with natural acoustic modes to give high levels of pressure fluctuation [35,28,104,107].

Important contributions to turbulence, mass and heat transfer are attributed to large coherent structures, making them a very important parameter in engineering applications [29]. Geometry and flow regimes are also fundamental parameters in the control of such flows since the structures inherent to the field are a manifestation of pressure decay and velocity changes. However, not only complex geometries but variation in wall surfaces can increase the number of modes in certain regimes, augmenting these complex interactions between structures inside the flow [31,109,110].

Details about the Central Recirculation Zone (CRZ) and its mixing potential have been investigated but the studies leave out some details regarding its effects on the mixing process, stability and coupling with other structures specially when using alternative fuels. It is known that OH concentrations in this region reach a formation-decay balance, indicating that the flame stabilization and mixing occur on the boundaries of this region between the CRZ and the shearing flow [38,31,111]. Highly hydrogenated blends show complex stabilization patterns, due to different temperature distributions and effects on swirl number [39]. High hydrogen content fuels alter the combustion swirl number which can considerably affect the size, shape and recirculated mass flowrate in the CRZ [111,112]. Addition of CO_2 in the fuel blend lead to changes in viscosity and density, also radiative heat transfer; these factors impact on the size of the CRZ [113].

Turbulence is also an important parameter in blowoff limits. The continuous efforts by Peters [74] resulted in a theory of turbulent premixed flames that has become generally accepted in the combustion research community. Experimental observations (e.g. Schlieren photography, laser sheet imaging techniques, etc.) have revealed that, in general, the structure of a turbulent premixed flame is to be seen as superimposed instantaneous contours of convoluted reaction zones. The appearance of the reaction zone depends heavily on the governing turbulent structures and the chemical properties of the flow. Thus, the fuel compositions produced from alternatives result in many different chemical properties in terms of thermal diffusivity, density, laminar flame speed, high heating value and low heating value. This will affect the turbulent behaviour.

The experiments conducted by Lieuwen et al. [114] to investigate the impact of fuel composition on the operability of lean premixed gas turbine combustors have focused on H_2/CH_4 flames. It was shown that small additions of H_2 substantially enhance a mixture's resistance to extinction or blowoff. For example, fundamental studies show that the extinction strain rate of methane flames is doubled with the addition of 10% H_2. Similarly, CO/CH_4 flames showed a variance in their extinction strain rate. Experiments were also conducted using N_2, H_2O and CO_2. It was concluded that the flame speeds in mixtures with CO_2 dilution are lower than those in mixtures diluted with chemically inert species that have the same specific heat as CO_2. The CO_2 dilution can lead to lower laminar flame speeds and lower flame temperatures due to radiative losses from the flame, which can also impact emissions [114]. Correlations of the turbulent flame speed were obtained in the form of $S_T=S_L \bullet f(u')$. (S_T turbulent flame speed, S_L laminar flame speed and $f(u')$ a function of turbulent level). One of the main factor influencing changes in turbulent flame speed due varying fuel composition is laminar flame speed. In particular, it was shown that as the turbulence intensity increases, the turbulent flame speed initially increases. The main factor governing the turbulent flame speed is the laminar flame speed with the change in composition. However, turbulence intensity and laminar flame speed alone do not capture many important characteristics of the turbulent flame speed. One must also consider the effects of flame instabilities and flame stretch. This effect is strongly dependent on thermal diffusivity and mass diffusivity and Lewis number [114]. Lewis number (Le) is a dimensionless number defined as the ratio of thermal diffusivity to mass diffusivity. It is used to characterize fluid flows where there is simultaneous heat and mass transfer by convection.

The Lewis number is defined as,

$$L_e = \frac{\alpha}{D} \qquad 2\text{-}16$$

A Lewis number <1 indicates that mass transfer is greater than heat transfer. This means heat transfer is the rate-determining step. When the Lewis Number >1, heat

transfer is greater than mass transfer and the system becomes mass transfer dependent.

Lee et al. [115] investigated the combustion performance of synthetic gas composed of hydrogen, carbon monoxide, nitrogen, carbon dioxide and steam, evaluating the dilution effect of the last three gases. It was observed that NOx decreased as the amount of dilutents was increased. Nitrogen, carbon dioxide and/or steam are applicable to a syngas turbine to control NOx emissions while ensuring reliable operation; thus blowoff could be avoided with careful control of these gases[115]. Strakey et al. [116] studied the effects of hydrogen addition on flame extinction in a lean-premixed swirl-stabilised combustor operating on natural gas and air. Different equivalence ratios and pressures from 1 to 8 atmospheres were used. Hydrogen concentration in the fuel was changed from 0 to 80 %. It was observed that increasing the hydrogen concentration in the fuel reduced the equivalence ratio before blowoff from 0.46 to 0.30.

Schefer et al.[117] conducted experiments on the combustion characteristics of a premixed, swirl-stabilised flame to determine the effects of enriching methane with hydrogen under fuel-lean conditions. Hydrogen addition resulted in a significant change in the flame structure, indicated by a shorter and more robust flame. However, the studies have not shown any clear correlation between blowoff processes and the strength of CRZ and its related coherent structures. Changing the fuel composition in modern low-emission gas turbine combustors from natural gas to hydrogen-containing mixtures has been reported to severely disrupt their operation. Blowoff, flashback, and auto-ignition have been observed when using alternative fuels such as hydrogen–methane mixtures or synthesis gas in modern gas turbines [88]. Flashback and auto-ignition pose a particularly high risk for hydrogen-containing fuel mixtures, due to the fast chemical reaction rates and high flame speed of hydrogen in air. Flashback occurs when the flame propagates upstream from the combustion chamber into the premixing section.

The experiments were conducted by Sayad et al. [88] showed that three different mechanisms for flame propagation in the premixing tube occurred, depending on the

test conditions and they concluded the flashback occurred due to CIVB at swirl numbers ≥ 0.53 for all of the tested fuel mixtures, depending on the equivalence ratio.

In the case of flashback due to CIVB, the adiabatic flame temperature at flashback changed almost linearly with H2 mole fraction of the fuel mixture. Image processing indicated that the speed at which the flame propagated through the optical section of the premixing tube was significantly higher for flashback due to CIVB than that for flashback in the boundary layer.

Another study by Sayad et al. [118] on the influence of various syngas (CO, H_2 and CH_4) compositions on the lean blowoff (LBO) limits under various swirl numbers and conditions was performed by adding N_2 to the syngas mixture. The results showed that by increasing the swirl number the LBO equivalence ratio was reduced for a given fuel composition. Adding CH_4 to the H_2/CO shifted the LBO limit to higher equivalence ratios. Moreover, adding N_2 to the mixture somehow increased the LBO equivalence ratio. Syred et al. [89] investigated the effects of inlet and outlet configurations on blowoff and flashback with premixed combustion. They detailed the measurements of both phenomena and used the results to develop a new correlation based on the tangential inlet velocity for a range of swirl numbers and burners. The effects were attributed to the influence of the annular shearing flow leaving the burner. This flow interacts strongly with a powerful CRZ close to blowoff and for one mode of flashback by strongly influencing conditions in the outer boundary layer. The correlation has been found to be applicable to COG, methane and natural gas combustion for those particular configurations.

The CRZ is one of the mechanisms for flame stabilisation, whereby an aerodynamically decelerated region creates a point at which the local flame speed and flow velocity are matched [92] Thus, in this study, the structure of premixed swirl stabilised flames is analysed via various time, length and velocity scales including the size of the CRZ. As previously observed the blowoff phenomenon is correlated with various syngas compositions, in order to classify the flame in a combustion regime. It has been observed that there is an area of turbulence close to

the boundaries of the central recirculation zone, a region of high stability swirl flow. This region is impacted by the outlet geometry and chemical properties of the fuel mixture. The blowoff

phenomenon is still not understood, as the theoretical behaviour does not match with the real process. Therefore, the aim of this study is to measure the turbulence across a flame based on the Da number. This will indicate the comparison of reaction rate and diffusion rate, and will specify the size of the CRZ in each case.

CHAPTER3

CHAPTER 3

METHODOLOGY

3.1 Introduction

The aim of this work to investigate experimentally and numerically of lean premixed swirl combustion of $CH_4/H_2/CO$ blends was investigated experimentally and numerically to understand the impacts of these fuels on flame blowoff. An atmospheric pressure generic swirl burner was operated with ambient temperature inlet conditions using swirl number of 1. Different exhaust nozzles were used to determine the impact of the fuel blends on the Central Recirculation Zones and blowoff. Methane content in the fuel was decreased from 50% to 10% (by volume) with the remaining amount split equally between carbon monoxide and hydrogen plus blended taken with pure methane and methane blended with carbon dioxide. Chemical kinetic analyses were carried out using PRO-CHEMKIN to determine flame speeds and chemical properties needed for CFD calculations. Experiments were performed using Phase Locked PIV.

All the experimental work and CFD analyses in this research were done using the same rig but with different measuring techniques. These techniques allowed the proper correlation of results and understanding of fundamental structures during blowoff transition. Thus, this chapter is dedicated to detailing the techniques and devices using various synthetic gases.

3.2 Experimental Setup

A swirl burner constructed from stainless steel was used to examine the flame stability limits at atmospheric conditions (1bar, 293K) within Cardiff University's Gas Turbine Research Centre (GTRC) and the Cardiff University Engines Laboratory. A photograph and schematic of the generic burner and burner rig are presented in Figure 3.1, 3.2.the system consist of a single tangential inlet (a). A central diffusion fuel injector, which extends centrally through the swirl burner up to the bottom edge of the nozzle (b). It introduces premixed air and fuel into the mixing chamber (c). The swirl has four radial tangential inlets (d), which are symmetrically distributed. The swirling

unburned mixture then passes into the burner nozzle (f) where the gases pass around the flame stabilising the central recirculation zone (e).

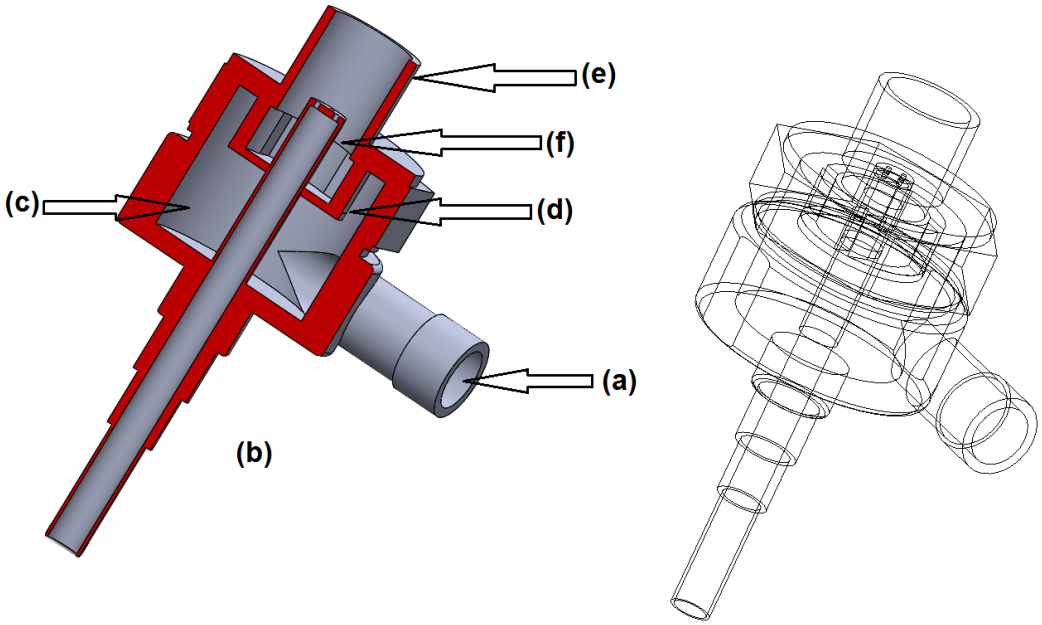

Figure 3-1: Schematic diagram and swirl burner, respectively.

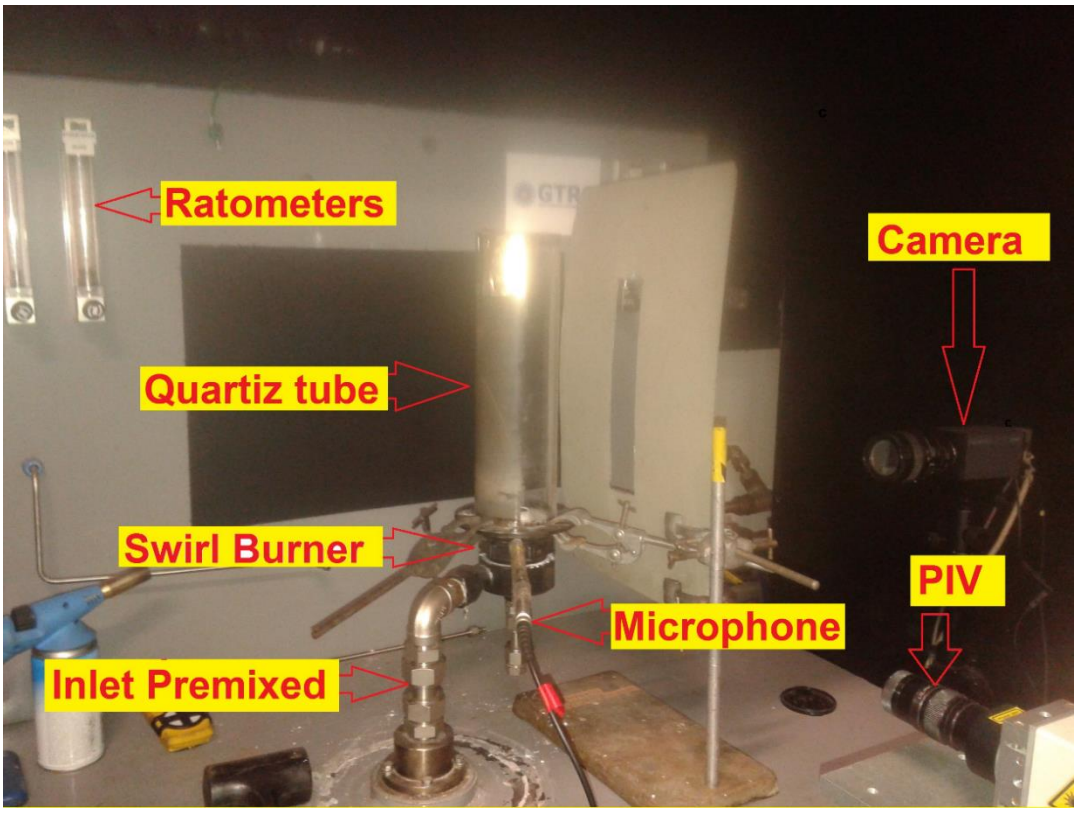

Figure 3-2: Photo of rig and burner

Figure 3.3 shows the swirlers used for the analyses. Swirl numbers from 1.0 to 1.5 were used. The schematics present the dimensions of the components at swirl numbers of 1.0 and 1.5, respectively, showing a device whose geometry emulates current industrial systems. Two swirl numbers and 4 different nozzles were used, just as in the CFD study presented in Chapter 4.

Moreover, the recirculation zone was also distorted using 30°, 45°, and 60° nozzles as shown in Figure 3.4. Confined and open conditions were tested. Confinement was achieved by quartz cylinders with diameters of 3D, where D is the external nozzle diameter (0.028m) as shown in Figure 3.5.

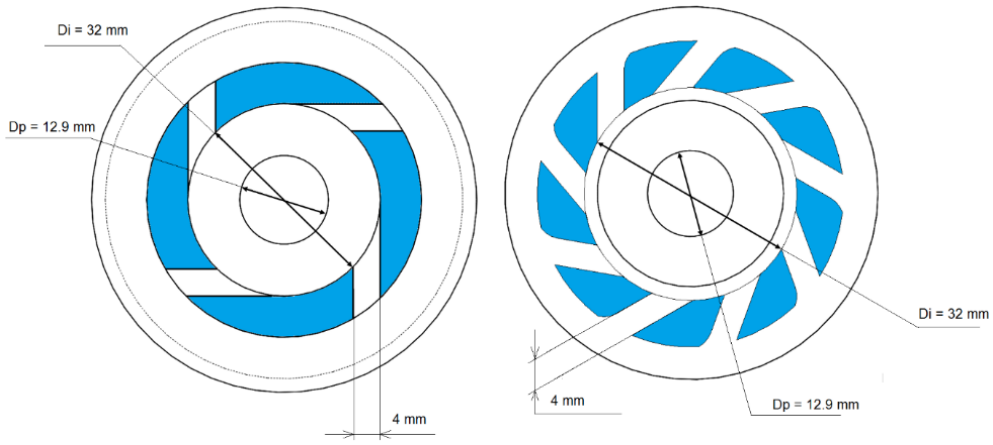

Figure 3-3: Swirl burner dimensions

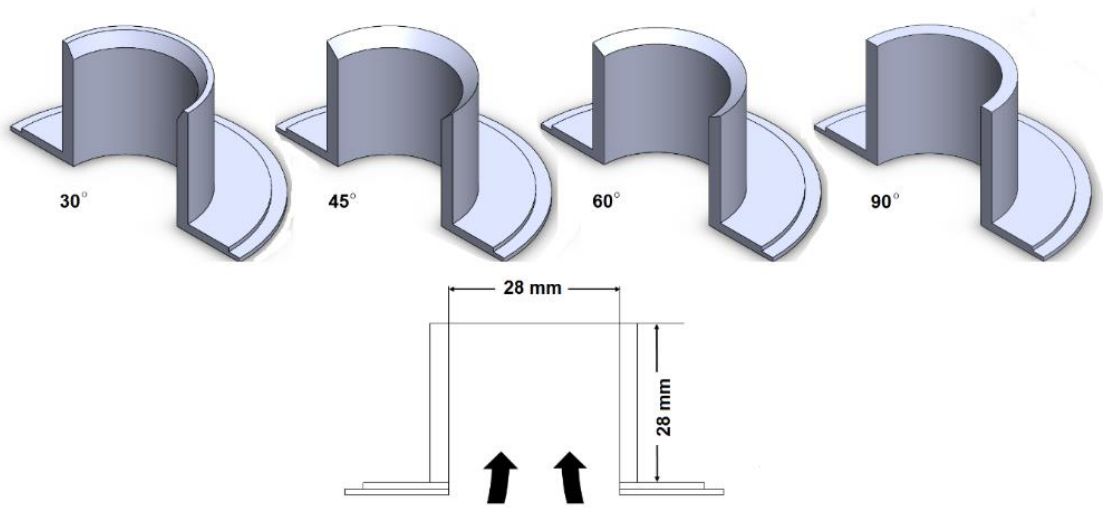

Figure 3-4: Various divergent angled nozzles.

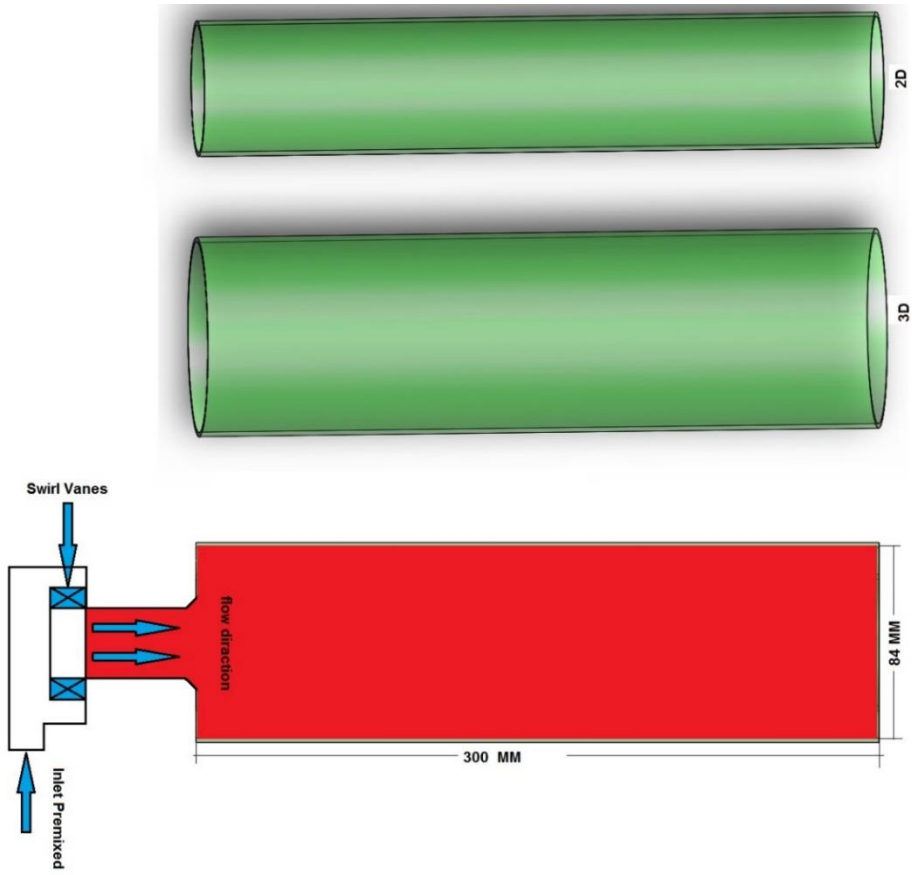

Figure 3-5: Scheme of Quartz Confinement Tube

3.2.1 Test Rig

3.2.2 Compositions

Experiments were run to define the blowoff limits and swirling frequency shift of different configurations using different gases under these conditions. The first gases used were mixtures of CO_2 and CH_4, as these gases represent a high percentage of the composition of pyrolysis/gasification syngases. The compositions are specified in Tables 3.1 and 3.2.

Table 3-1: Experiments with methane

Test	CH4 [g/s]	Air [g/s]	Total [g/s]	Φ	Φ[-]	Total [m/s]	Velocity	Power KW
T1	0.13	3.2	3.33	0.69		1.92		7.489
T2	0.15	3.5	3.65	0.77		2.11		8.32
T3	0.21	4.6	4.9	0.77		3.57		11.65
T4	0.24	5.2	5.44	0.79		4.28		13.32
T5	0.27	5.5	5.85	0.83		3.99		14.98

Table 3-2: Experiments with methane and CO_2

Test	CH4[g/s]	AIR[g/s]	CO2[g/s]	Total[g/s]	Φ[-]	Total Velocity[m/s]	Power KW
T6	0.13	2.57	0.13	2.83	0.87	1.92	7.489
T7	0.15	3.01	0.16	3.32	0.89	2.18	8.32
T8	0.21	3.93	0.21	4.35	0.91	3.26	11.65
T9	0.24	4.12	0.24	4.60	1.00	3.49	13.32
T10	0.27	4.94	0.27	5.48	0.94	3.68	14.98

Several blends were tested to determine blowoff phenomena. Pure gas and syngas compositions (by volume) used during this project are specified in Table 3.3.

As a consequence of the depletion of fossil fuels and environmental concerns about CO_2 emissions, promising technologies are being developed allowing gas turbine combustors to use alternative fuels such as synthetic gas (syngas). Syngas can be obtained from renewable sources such as biomass, or from traditional fuels, such as coal or heavy oil.

Depending upon the gasification process and the feedstock used, syngas may contain varying amounts of CO, H_2, and CH_4, as well as CO_2, N_2, H_2O, and small amounts of higher hydrocarbons [118]. Because of this variation in composition, such fuels can differ significantly from natural gas in terms of their chemical and physical properties. Therefore, firing syngas in gas turbine combustors may cause problems, such as blowout, flashback, dynamic instability, and auto-ignition. Combustion systems are generally optimised for operation within a narrow fuel specification in order to achieve legal emission levels. It is therefore important to determine combustion behaviour in the case of unconventional fuels and to extensively investigate the development of fuel-flexible combustors.

It is necessary for gas turbines fuelled with such gases to have similar reliable operation and low pollutant emissions when compared with their natural-gas-fired counterparts. Therefore, this study was carried out to investigate the impact of syngas composition on the lean blowoff (LBO) limit at different swirl number under normal conditions using a swirl burner of lean premixed combustion.

Table 3-3: Fuel Blends by Volume

FUEL	%CH_4	%H_2	%CO	%CO_2
CH_4	100	0	0	0
50%CH_4/50%CO_2	50	0	0	50
10%CH_4/45%H_2/45%CO	10	45	45	0
20%CH_4/40%H_2/40%CO	20	40	40	0
30%CH_4/35%H_2/35%CO	30	35	35	0
50%CH_4/25%H_2/25%CO	50	25	25	0

Different geometries were used to better understand Coanda effect phenomenon. Different normalized step sizes, ΔY/D, were used from 0.000 to 0.145, Figure 3.6. Nozzle angles, α, of 30°, 45°, 60° and 90° were also utilized. Outlet diameter and Swirl number were kept constant at 0.0280m and 1.05, respectively. Geometrical changes were based on the observations of Sidhu et al [55] who used a radiused exhaust nozzles leading to a flat exhaust plate on the exhaust of a vortex diode. Thus, it was expected that the aerodynamics would change considerably as the step between the flat exhaust plate and the nozzle lip was altered.

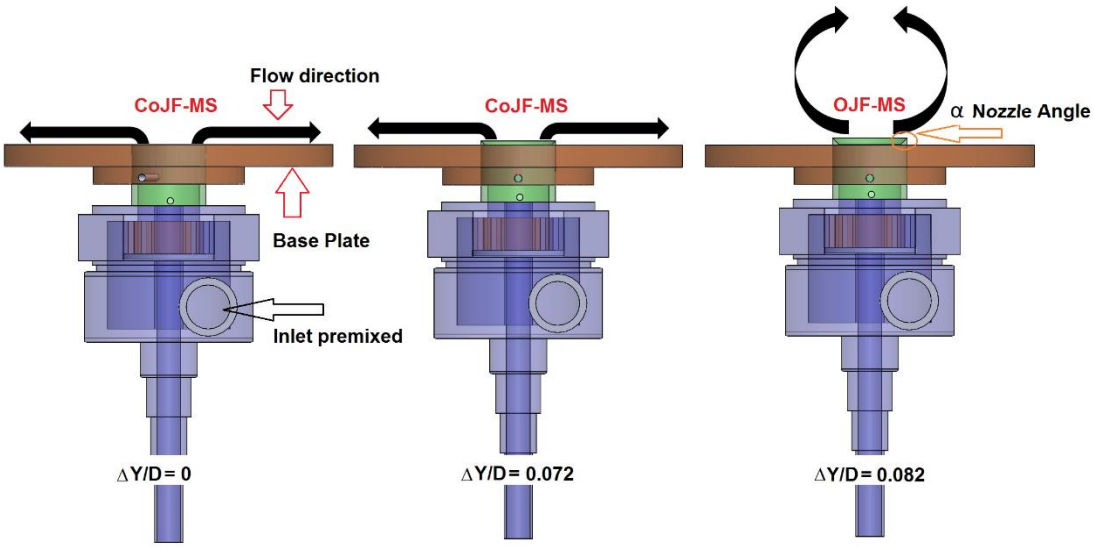

Figure 3-6: Geometrical changes at the exit nozzle. Step size, ΔY, nozzle angle, α and diameter D.

3.3 Experimental Methodology

The system was supplied with compressed air through flexible hoses, and a Coriolis meter was used to measure and control flow rate The flow rates of fuel and air into the rig are monitored by Coriolis meters with accuracies between ± 0.1 % and ± 0.2 % of total

flow rate[119] .The Micro Motion F-Series Coriolis flow and density meters are known as the preferred choice for process control applications. Many gases in the premixed rig were supplied from compressed gas cylinders and regulated via cylinder gauges from 200 to 3.0 bar. The reactants were fed through flexible hoses passing through another Coriolis meter. The air and fuel mass flow rates were measured simultaneously using the Coriolis flow meters. The maximum flow rate of the mixture in all the cases of pure methane was 5.85 g/s, and methane blended with CO_2 was 5.48 g/s. While the maximum mass flow rate of the mixture of syngas 1-4 was 1.946, and Reynolds number ranged from Re ≈ 9,000 to Re ≈ 27,000. Thus, the jets were in the fully turbulent regime.

According to Lefebvre[14], the blowoff limit can be determined in two ways: both stable combustion is established at a fixed air mass flow rate and the fuel flow rate is varied until extinction occurs, or the fuel flow rate is kept constant and the air mass flow rate is increased to the point of extinction. In the present work both methods were used.

3.4 Particle Image Velocimetry

Particle image velocimetry (PIV) is an intuitive measurement technique for measuring two or three components of velocity in a variety of flows. Particle image velocimetry measures the whole velocity field based on two images obtained shortly after one another, calculating the distance that individual particles travelled within this time. Based on the time difference and the measured displacement the velocity can be calculated [120].

3.4.1 PIV Technique

PIV is an optical measurement technique. It works by injected seeding particles into the flow field and illuminating them using a sheet of laser light. The illuminated particles inside the laser plane are recorded by cameras. The particles are registered as grey values on the image plane. Therefore, the analysis of double frames separated by a certain time step allows the estimation of the planar velocity field. The image plane is divided into small interrogation areas, and the particle displacement of each interrogation area is calculated via two-dimensional cross-correlation of the grayscale

values inside. The displacement and time step are then used to calculate the velocity vector for each interrogation area, forming a full velocity field [120].

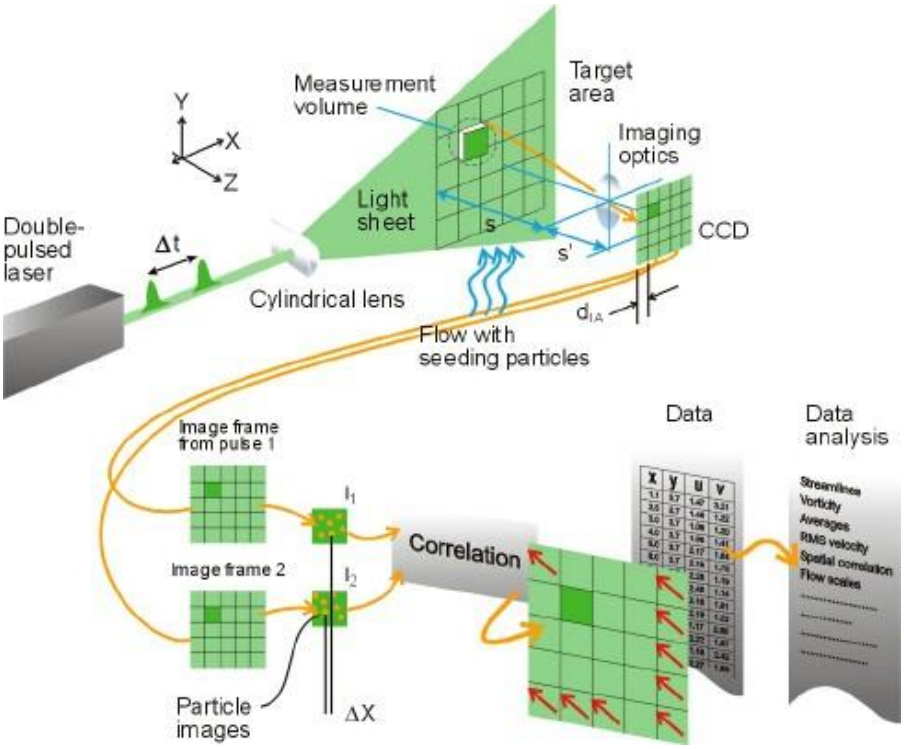

Figure 3-7: PIV Technique [121].

3.4.1.1 Seeding

Seeding is required to track particle velocities using PIV. Seeding particles should be introduced into the flow with spatial uniform distribution with sufficient and stable concentration, while minimising deposition and coagulation of particles on windows [85]. From the literature review is clear that in almost all cases a particle diameter near or below 1 μm of Aluminium oxide (Al_2O_3) has been used for seeding in gas flows, which is consistent with the requirements for particles with a high density ratio [85].

Actually, the degree to which the particles follow the flow dynamic is not perfect, and is defined by the Stokes number (Stk), a dimensionless number corresponding to the behaviour of particles suspended in a fluid flow, as defined by Equation 3.1 [118,121].

$$Stk = \frac{\tau U}{d_c} \quad 3\text{-}1$$

$$\tau = \frac{\sigma_d d_d^2}{18\mu_f} \quad 3\text{-}2$$

As much as the Stokes is smaller as the tracking particle give the butler accuracy. When STK particles larger than 1 will be separated from the flow, especially under heavy acceleration, while STK when less than 1 simplifies the particles will follow very closely. STK and less than 0.1 is compatible with an accuracy of greater than 99% [85].

A reason for the small particle size is the need for high laser pulse energy in a combustion regime, in most cases being around 100 MJ or more. Ceramic materials such as Al_2O_3, TiO_2 and ZrO_2 are favoured for seeding flames and high-temperature flows and also offer the advantage of a high refractive index, although they suffer dispersion in a gas flow. Slightly larger seeding particles were used in the combustor experiments by Anderson et al [123].

3.4.1.2 PIV Set-up

Frequency measurements were made within the shearing flow using a PCB Piezotronics 378B02 condenser microphone calibrated to frequency applications from Microsoft. The microphone is located 0.01m upstream of the nozzle outlet. The microphone sent a signal to a conditioner, which in turn resent the reconditioned signals to the BNC Model 500 plus generator. The generator sent TTL signals to the Dantec Stereo PIV system. The TTL signal triggered the firing of the dual cavity Nd: YAG Litron Laser, which had a wavelength of 532 nm, and was capable of operating at 15 Hz. Dantec Dynamics laser sheet optics (9080X0651) were used to convert the laser beam into a 1 mm thick sheet. Hi Sense MkII Cameras (model C8484-52-05CP) were used to record the images, with 1.3 MPixel resolution at 8 bits. 60 mm Nikon lenses were used to optimise the resolution over a 75x75 mm visual area, giving a resolution of 5.35 pixels per mm and a depth of view of 1.5 mm. Aluminium oxide powder (Al2O3) was used to seed the flow. It was introduced to the compressed air at

a position 2m upstream of burner inlet. After 6 minutes of running the entire system, recording was triggered at 90% of the highest peak. The repetition rate was set at 1/100 of the shearing flow frequency, which was measured via a 4 channel, 2 G/s Tektronix Oscilloscope (Figure 3.8).

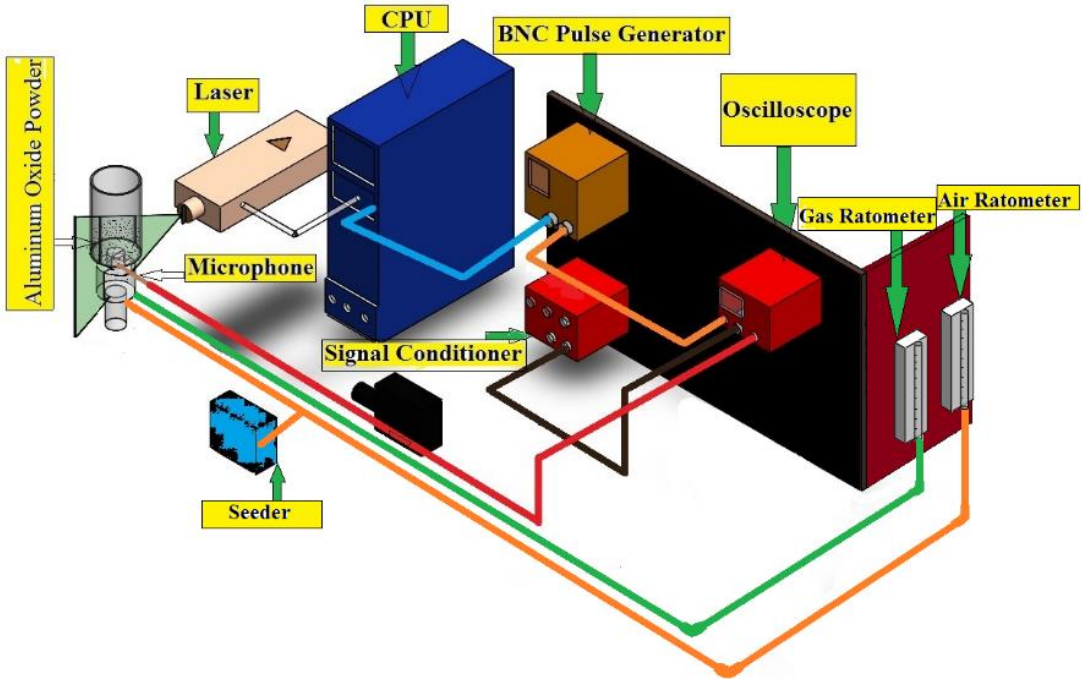

Figure 3-8: Experiment Setup

3.4.2 Image Processing

PIV image processing is based on the measurement of the small displacement of micro particles transported by the flow between two images separated by a very short time interval. The time between these two images is known, and coupled with the particle displacement the velocity of the particles can be calculated. In order to translate changes in image position to actual velocities the system must be calibrated to calculate the scale factor between the pixel position and the actual position of the field of view. Therefore, a calibration target was used to calculate the scale factor Figure 3.9. DANTEC's PIV software, Dynamic Studio, was used to recognise the position of the grid and to determine the scale factor during image processing[85].

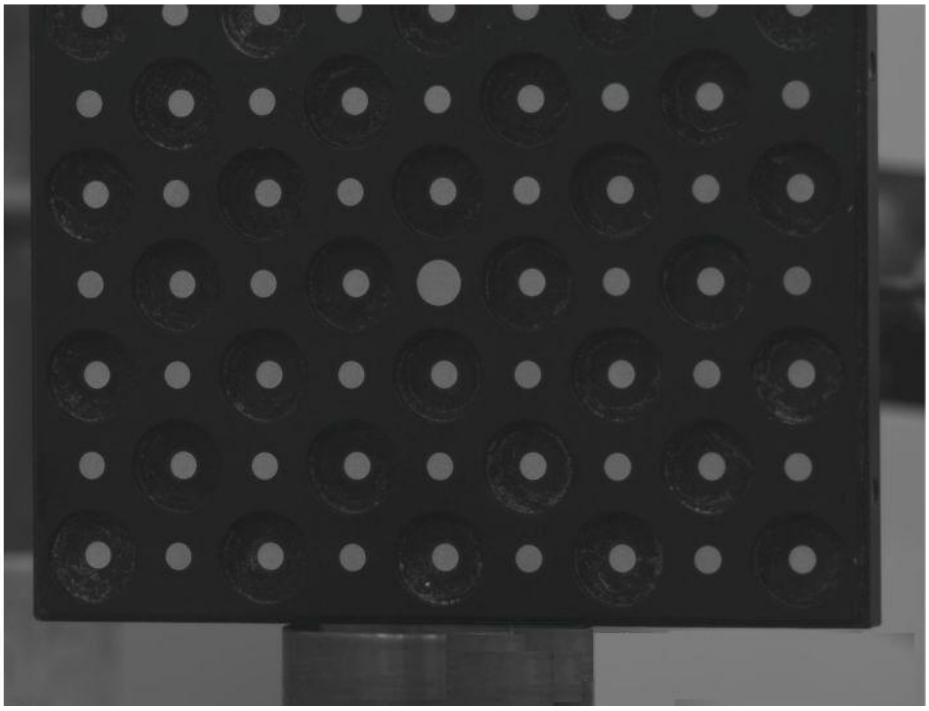

3-9: Calibration target

3.4.3 Stereo Particle Image Velocimetry (PIV)

In general, the utilisation of a single camera can only provide two velocity components (in the plane of the laser). However, the use of stereo PIV (two cameras) results in the acquisition of instantaneous 3D velocity vectors for the whole area of interest, including the through-plane component.

The stereo PIV principle is based on the stereo vision of human eye sight. Our left and right eyes see slightly different images of the things that surround us. Then, the brain compares these images and compiles them into a 3-dimensional version of the field of view. Although one eye is perfectly able to recognise relative motion, it is difficult to determine true distances or velocities. The greatest accurate determination of the out-of-plane displacement (and therefore velocity) is accomplished when there is perpendicularity between the two cameras. Figure 3.10 demonstrates how the velocity calculation is made for a three-component field analysis [84,121].

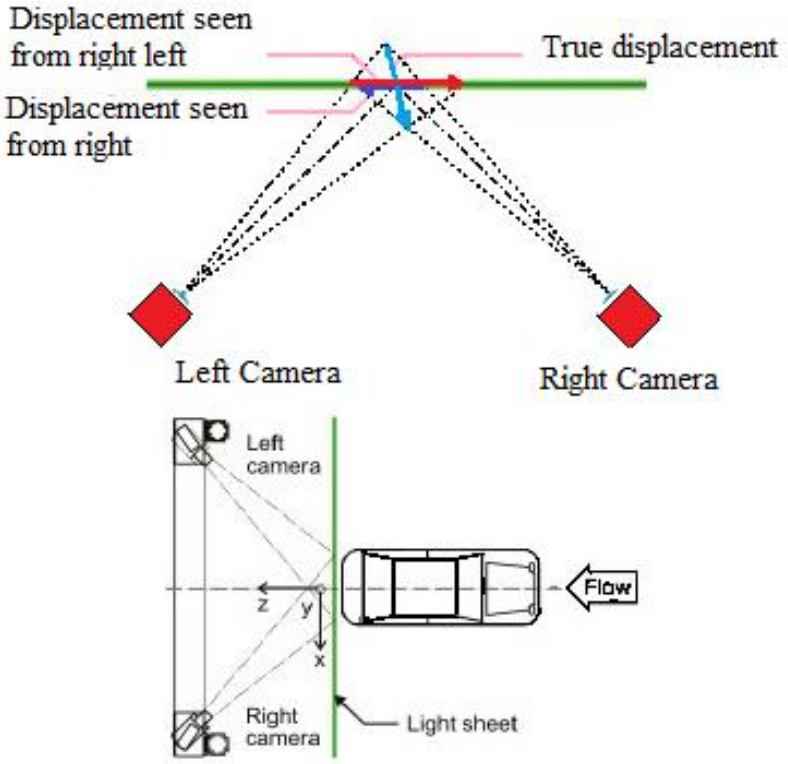

3-10:Stereo PIV concept [124].

3.4.4 High Speed Photography

The Society of Motion Picture and Television Engineers (SMPTE) (1948), defined high speed photography as any set of photographs captured at 128 frames per second or greater. High speed photography (HSP) can be considered to be the opposite of time-lapse photography [125]. The light was captured by a charge coupled device used in photron FASTCAM APX-RS high speed camera at rate 3000 fps. The configuration utilised allowed for a spatial resolution of 0.14 mm per pixel, with radial propagation rates derived via bespoke software, employing commercially available edge detection algorithms [126].

3.5 CFD Methodology

In the past decade, the use of computational fluid dynamics (CFD) has increased dramatically for predicting internal and external flow conditions.

Due to the rapidly improving high-powered super-fast computers, more efficient CFD software has been developed to provide higher accuracy and more efficient predictions

at lower computational cost. Furthermore, CFD is becoming a vital component in the design of industrial processes. Thus, CFD is used nowadays in the analysis of systems concerning fluid dynamics, heat transfer, and also associated phenomena such as chemical reactions. The technique has expanded to a wide range of industrial and non-industrial applications such as aerodynamics of aircraft, hydrodynamics of ships, power plant combustion, internal combustion engines, gas turbines, diffusers, and electronic engineering [79].

3.5.1 CFD Mechanism

CFD is structured around numerical algorithms that can tackle fluid dynamic problems and provide easy access to the solvers by applying input parameters, thus allowing a deep examination of results. All types of CFD contain three elements: (a) a pre-processor, (b) a solver, and (c) a post-processor [78 ,126].

3.5.1.1 Pre-processing

Pre-processing consists of the input of boundary conditions for a particular problem using an operator friendly interface. The interface provides a subsequent transformation of these inputs into a form suitable for the solver. The user is involved in defining the geometry of the region of interest (the computational domain), and generating a grid through the division of the domain into a number of smaller subdomains. These subdomains need to be processed into a mesh of small elements (cells) to solve differential equations by numerical methods. In fluid mechanics the concept of finite volume methods (FVM) is to divide the domain into a number of control volumes where the variable of interest is located at the centroid of the control volume. The differential form of the governing equations is then integrated over each control volume and the variation of the concerned variable between cell centroids is determined via interpolation [76].

The fluid problem is then solved by resolution of equations around or at the nodes of each cell. Accuracy depends on the number of cells in the grid. However, higher accuracy requires an increase in computational cost, leading to the need for mesh independency analyses, allowing good accuracy with lower computational costs [78, 126].

3.5.1.2 Solver

The numerical solution in CFD uses three types of method: a) spectral methods, b) finite element, and c) finite difference. The spectral methods approximate the unknown by means of a truncated Fourier series or a series of Chebyshev polynomials[78, 126] . Counter to the finite difference and finite element approaches, the approximations are not local but are valid throughout the entire computational domain. Again the unknowns are replaced in the governing equation by truncated series. From a weighted residuals concept, the constraint that leads to the algebraic equations for the coefficients of the Fourier or Chebyshev series is provided. This is similar to the finite element method by making the approximate function coincide with the exact solution at a number of grid points[78,126] .

The finite difference method (FDM) describes the unknown ϕ of the flow problem by means of point samples at the node points of a grid of co-ordinate lines[127] . Finite difference approximates derivatives of ϕ in terms of point samples of ϕ at each grid point and its immediate neighbours. The most common method is the truncated Taylor series expansion. Those derivatives appearing in the governing equations are replaced by finite differences, yielding an algebraic equation for the value of ϕ at each grid point. The finite element method (FEM) uses simple piecewise functions linear or quadratic on elements to describe the local variations of unknown flow variables ϕ [78,126].

The most versatile of discretisation techniques used in CFD is the finite volume method (FVM). The first step in FVM is to divide the domain into a number of control volumes or cells where the variable of interest is located at the centroid of the control volume. The next step is to integrate the differential form of the governing equations over each control volume. The variation of the concerned variable between cell centroid is then described by interpolating profiles between cell centroids. The subsequent equation is called the discretised or discretisation equation which expresses the conservation code of variables inside the control volume. The most convincing feature of the FVM is that the resulting solution satisfies the conservation of quantities such as mass, momentum, energy and species. These features are satisfied not only for the control volume, but also for the entire computational domain [127].

3.5.1.3 The post -processor

An enormous amount of development work has recently taken place in the post-processing field. The increase in the needs for engineering applications has led to: CFD packages that need to deal with flexible data; visualisation tools with outstanding graphics capabilities; and domain, geometry and grid displays of 2D or 3D results using velocities, particle tracking, heat transfer, transitional states, etc.[126,79].

3.5.2 Conservation laws of fluid motion

The governing equations needed for the resolution of fluid problems need to comply with the following characteristics,

The mass of fluid is conserved.

The rate of change of momentum equals the net force on a fluid particle (Newton's second law).

The rate of change in the energy is equal to the sum of the heat flux and the rate of work done on a fluid particle (the first law of thermodynamics).

3.5.2.1 Mass conservation equation in three dimensions

The mass balance for a fluid element (the continuity equation) states that the rate of increase of mass in a fluid element equals the net rate of flow of mass into that fluid element. This can be expressed mathematically by:

$$\frac{\partial \rho}{\partial t} + \frac{\partial \rho u}{\partial x} + \frac{\partial \rho v}{\partial y} + \frac{\partial \rho w}{\partial z} = 0 \qquad 3\text{-}3$$

or using vector notation:

$$\frac{\partial \rho}{\partial t} + \mathrm{div}(\rho U) = 0 \qquad 3\text{-}4$$

Equation 3.4 is the unsteady, three-dimensional mass conservation or continuity equation employed in compressible fluids. The equation consists of two sides; on the left hand side is the rate of change of density (mass per unit volume); the right hand side describes the net flow of mass out of the element across its boundaries and is called the convective term [78, 126].

3.5.2.2 Momentum equation

Newton's second law states that the rate of change of momentum of a fluid particle equals the sum of the forces acting on the particle. Applying this to a fluid passing through an infinitely small, fixed control volume, yields the following equations:

(The x-component of the momentum equation):

$$\rho\frac{\mathrm{Du}}{\mathrm{Dt}} = \frac{\partial(-\mathrm{p} + \tau_{\mathrm{xx}})}{\partial \mathrm{x}} + \frac{\partial \tau_{\mathrm{yx}}}{\partial \mathrm{y}} + \frac{\partial \tau_{\mathrm{zx}}}{\partial \mathrm{z}} + \mathrm{S_{Mx}} \qquad \text{3-5a}$$

(The y-component of the momentum equation):

$$\rho\frac{\mathrm{Dv}}{\mathrm{Dt}} = \frac{\partial \tau_{\mathrm{xy}}}{\partial \mathrm{x}} + \frac{\partial(-\mathrm{p} + \tau_{\mathrm{yy}})}{\partial \mathrm{y}} + \frac{\partial \tau_{\mathrm{zy}}}{\partial \mathrm{z}} + \mathrm{S_{My}} \qquad \text{3-5b}$$

(The z-component of the momentum equation):

$$\rho\frac{\mathrm{Dw}}{\mathrm{Dt}} = \frac{\partial \tau_{\mathrm{xz}}}{\partial \mathrm{x}} + \frac{\partial \tau_{\mathrm{yz}}}{\partial \mathrm{y}} + \frac{\partial(-\mathrm{p} + \tau_{\mathrm{zz}})}{\partial \mathrm{z}} + +\mathrm{S_{Mz}} \qquad \text{3-5c}$$

The three dimensional form of Newton's law of viscosity for compressible flow involves two constants of proportionality: stresses to linear deformations to the dynamic viscosity,$\boldsymbol{\mu}$ and the viscosity,$\boldsymbol{\lambda}$ to relate stresses to the volumetric deformation. The component of viscous stress is related to μ and λ. Replacing the values of viscous stress in the momentum equations yields the so-called Navier-Stokes equations:[78,126].

$$\rho\frac{Du}{Dt} = -\frac{\partial p}{\partial x} + div(\mu\ grad\ u) + \mathrm{S_{Mx}}$$

$$\rho\frac{Dv}{Dt} = -\frac{\partial p}{\partial y} + div(\mu\ grad\ v) + \mathrm{S_{My}} \qquad \text{3-6}$$

$$\rho\frac{Dw}{Dt} = -\frac{\partial p}{\partial z} + div(\mu\ grad\ w) + \mathrm{S_{Mz}}$$

3.5.2.3 Energy Equation

The energy equation derives from the first law of thermodynamics, which states that the rate of change in energy of a fluid particle is equal to the rate of heat addition to the fluid particle plus the rate of work done on the particle. The rate of change in energy of a fluid particle per unit volume is given by $\rho \frac{DE}{Dt}$. The total rate of work done on a fluid particle by a surface force can be expressed as[78,126] .

$$\begin{aligned}\rho \frac{\mathrm{DE}}{\mathrm{Dt}} = & -\mathrm{div}(\rho \mathrm{U}) \\ & + \left[\frac{\partial(\mathrm{u}\,\tau_{\mathrm{xx}})}{\partial \mathrm{x}} + \frac{\partial(\mathrm{u}\,\tau_{\mathrm{yx}})}{\partial \mathrm{y}} + \frac{\partial(\mathrm{u}\,\tau_{\mathrm{zx}})}{\partial \mathrm{z}} + \frac{\partial(\mathrm{v}\,\tau_{\mathrm{xy}})}{\partial \mathrm{x}}\right. \\ & + \frac{\partial(\mathrm{v}\,\tau_{\mathrm{yy}})}{\partial \mathrm{y}} + \frac{\partial(\mathrm{v}\,\tau_{\mathrm{zy}})}{\partial \mathrm{z}} + \frac{\partial(\mathrm{w}\,\tau_{\mathrm{xz}})}{\partial \mathrm{x}} + \frac{\partial(\mathrm{w}\,\tau_{\mathrm{yz}})}{\partial \mathrm{y}} \\ & \left. + \frac{\partial(\mathrm{w}\,\tau_{\mathrm{zz}})}{\partial \mathrm{z}}\right]\end{aligned} \qquad 3\text{-}7$$

The net rate of heat transfer to the fluid particle due to heat conduction across element boundaries can be written as:

$$-div\ q = div\ (K\ grad\ T) \qquad 3\text{-}8$$

If any source of energy exists with an S_E energy per unit volume per unit time, the energy equation becomes:

$$\begin{aligned}\rho \frac{\mathrm{DE}}{\mathrm{Dt}} = & -\mathrm{div}(\rho \mathrm{U}) \\ & + \left[\frac{\partial(\mathrm{u}\tau_{\mathrm{xx}})}{\partial \mathrm{x}} + \frac{\partial(\mathrm{u}\tau_{\mathrm{yx}})}{\partial \mathrm{y}} + \frac{\partial(\mathrm{u}\tau_{\mathrm{zx}})}{\partial \mathrm{z}} + \frac{\partial(\mathrm{v}\tau_{\mathrm{xy}})}{\partial \mathrm{x}} + \frac{\partial(\mathrm{v}\tau_{\mathrm{yy}})}{\partial \mathrm{y}}\right. \\ & \left. + \frac{\partial(\mathrm{v}\tau_{\mathrm{zy}})}{\partial \mathrm{z}} + \frac{\partial(\mathrm{w}\tau_{\mathrm{xz}})}{\partial \mathrm{x}} + \frac{\partial(\mathrm{w}\tau_{\mathrm{yz}})}{\partial \mathrm{y}} + \frac{\partial(\mathrm{w}\tau_{\mathrm{zz}})}{\partial \mathrm{z}}\right] \\ & + \mathrm{div}(\mathrm{k\ grad\ T}) + \mathrm{S_E}\end{aligned} \qquad 3\text{-}9$$

3.5.2.4 General Transport Equation

It is clear that there are significant commonalities between the various equations. If a general variable *f* is introduced, the conservative form of all fluid flow equations can usefully be written in the following form:

$$\frac{\partial(\rho\emptyset)}{\partial t} + \text{div}\,(\rho\emptyset\text{u}) = div(\Gamma\, grad\phi) + S_\phi \qquad 3\text{-}10$$

Equation 3.10 is the so-called transport equation of property f. It clearly highlights various transport processes: the rate of change term and the convective term in the left hand side and the diffusive term (G being the diffusion coefficient) and the source term, respectively, on the right hand side [79].

3.5.3 CFD Solver in Fluent

Fluent is a CFD solver which uses the finite volume method. This method uses nodes or grid points to replace the continuous computational domain. The discrete variables such as temperature, pressure, velocity etc. are determined by constructing algebraic equations from the integration of the governing equations of the fluid flow across the control volume. The discrete, non-linear governing equations are linearised to produce a system of equations for the dependant variable in every computational cell, in which the resultant linear system is then solved to yield an updated flow-field solution[80]. The variable of interest within the cell is then computed using the known and the unknown values from the neighbouring cells. Two numerical methods are used in Fluent: the Segregated Solver and the Coupled Solver. According to [80], the Segregated Solver is a solution algorithm in which the governing equations are solved sequentially. Numerous iterations of the solution loop are performed before a converged solution is determined since the governing equations are non-linear. The steps for the iteration are shown in Figure 3.11a. In the Coupled Solver the governing equations of continuity, momentum, energy and species transport are solved simultaneously. Again the governing equations are non-linear, so several iterations of the solution loop are performed before a converged solution is obtained. The iterative steps are shown in Figure 3.11b.

The accuracy and numerical stability of the solution is a function of the density and distribution of the grid and the interpolation schemes between the cells. According to

[80] ,convergence can be hindered by a number of factors including size and number of computational cells, overly conservative under-relaxation factors, and complex flow physics. Convergence is best judged by monitoring relevant integrated quantities such as drag or heat transfer coefficient and not necessarily the residual levels.

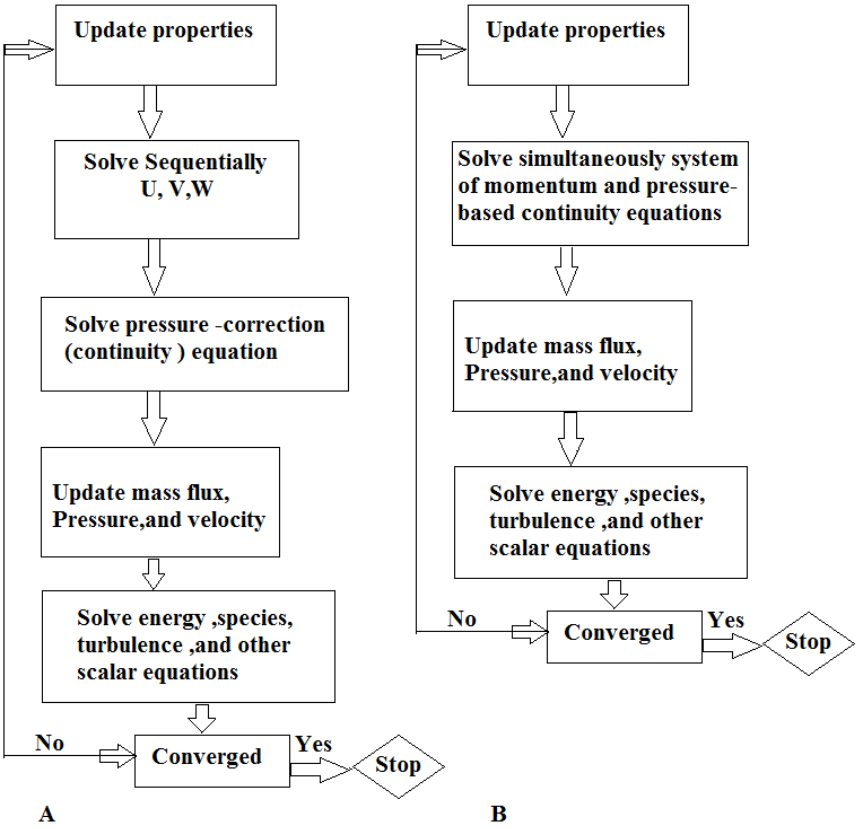

Figure 3-11:Overview of the Segregated (A) and Coupled (B) Solution Methods [80].

Four segregated types of algorithms are provided in Fluent; PISO, SIMPLE and SIMPLEC. These schemes are indicated as the pressure-based segregated algorithm. In general Steady state calculation will use SIMPLE or SIMPLEC. However PISO is recommended for transient calculations. Therefor in this research SIMPLE schemes were used for all analysis.

3.5.4 Turbulence Modelling

3.5.4.1 Modelling Turbulent Flows in Fluent

Fluent provides a large variety of models to suit the demands of individual types of problems. The optimal choice of the turbulence model depends on the required grade

of the accuracy, computational resources and physics of the problem available models in fluent are [80]:

Spalart-Allmaras model
k-$\boldsymbol{\varepsilon}$ models
- Realisable k-ε model
- Standard k-ε model
- RNG k-ε model

k-$\boldsymbol{\omega}$ models
- Standard k-$\boldsymbol{\omega}$ model
- Sear stress transport (SST) k- $\boldsymbol{\omega}$ model

$v^2 - f$ model

Reynolds stress model (RSM)

Detached eddy simulation (DES) model

Large eddy simulation (LES) model

Details of each model can be found in [78, 126,76,127].

Table 3-4: Turbulence models available in Fluent [129]

Model	Features	
Spalart-Allmaras model	One equation model	Designed especially for aerospace applications, involving wall-bounded high speed flow
Standard k- ε model	Two equation models	Robust. Suitable for primary iterations
(RNG) k- ε models	Variant of standard k- $\boldsymbol{\varepsilon}$ Has an additional term in equation	Accurate for rapidly strained and swirling flows.
Realisable k- ε model	Variant of Standard k- $\boldsymbol{\varepsilon}$ model New formulation for turbulent viscosity New transport equation for $\boldsymbol{\varepsilon}$	Accurate for spreading of both planar and rounded jets. Suggested for flows with boundary layers under strong adverse Δp, separation and recirculation.
Standard k-ω model	Solves for k-$\boldsymbol{\omega}$ $\boldsymbol{\omega}$ = Specific dissipation rate ($\boldsymbol{\varepsilon}$/k)	Recommended for low-Re Flows, for wall boundary layer, and for transitional flows
(SST) k-ω model	Variant of Standard k- $\boldsymbol{\omega}$ model Behaves like k- $\boldsymbol{\omega}$ in near wall region Behaves like standard k - $\boldsymbol{\varepsilon}$ in the free stream	More accurate and reliable for a wider class of flows, like adverse Δp in airfoils, transonic shock waves, etc.
Reynolds stress model	Five equation model Avoids isotropic formulation of turbulent viscosity	Suitable for complex 3D flows with strong swirl / rotation. Run time and memory intensive

3.5.4.2 Shear-Stress Transport (SST) k-ω model

The most suitable turbulence model for the research in this thesis is the shear-stress transport (SST) k-ω model as it is suitable for complex 3D flows with strong swirl at

low computational cost. Thus, the SST k-ω model was chosen to model all the different combustion regimes in this thesis.

The shear-stress transport (SST) k-ω model was developed by Menter [130]. The turbulent viscosity in this model is modified to account for the transport of the principal turbulent shear stress, hence its name. The shear stress transport (SST) k-ω turbulence model is a type of hybrid model, combining two models in order to better calculate flow in the near-wall region. Due to the k-ε model's unsatisfactory solving of near-wall boundary layers with adverse pressure gradients, the standard k-ε model is used to calculate flow properties only in the free-stream (turbulent) flow region far from the wall. A modified k-ε model is used near the wall by using the turbulent frequency ω as a second variable instead of using the turbulent kinetic energy dissipation term ε [129].

The advantage of the SST k-***ω*** model is the superior performance over both the standard k-ε model and standard k-***ω*** models. A cross-diffusion term is assessed into the ***ω*** equation and blending function to ensure that the model equations behave appropriately in both the near-wall and far field zones [80]. The SST k-***ω*** model has a similar form to the standard k-***ω*** model. To obtain the specific dissipation rate ***ω***, and turbulent kinetic energy k, the following transport equations are applied:

$$\frac{\partial}{\partial t}(\rho k) + \frac{\partial}{\partial x_i}(\rho k u_i) = \frac{\partial}{\partial x_i}\left(\Gamma_k \frac{\partial k}{\partial x_j} \right) + G_k - Y_k + S_k \qquad 3\text{-}11$$

And

$$\frac{\partial}{\partial t}(\rho \omega) + \frac{\partial}{\partial x_i}(\rho \omega u_i) = \frac{\partial}{\partial x_i}\left(\Gamma_\omega \frac{\partial \omega}{\partial x_j} \right) + G_\omega - Y_\omega + D_\omega + S_\omega \qquad 3\text{-}12$$

3.5.5 Combustion modelling

Vast improvements in the analysis of combustion processes through CFD have been made over recent years. Combustion processes are governed by basic transport equations for fluid flow and heat transfer, with additional models for combustion chemistry, radiative heat transfer and other important sub-processes. In addition to all

flow equations, the transport equations for the mass fraction mi of each species i must be solved. The species equation can be written by using the general transport equation [127].

$$\frac{\partial(\rho m_i)}{\partial t} + div(\rho m_i U) = div(\Gamma\ grad\ m_i) + S_i \qquad 3\text{-}13$$

The volumetric rate of generation (or destruction) of a species due to chemical reactions appears as the source (or sink) term S_i in each of the transport equations. The transport equations for the fuel and oxygen mass fraction may be written as:

$$\frac{\partial(\rho m_f)}{\partial t} + div\left(\rho m_f U\right) = div\left(\Gamma_f\ grad\ m_f\right) + S_f \qquad 3\text{-}14$$

$$\frac{\partial(\rho m_o)}{\partial t} + div(\rho m_o U) = div(\Gamma_0\ grad\ m_o) + S_o \qquad 3\text{-}15$$

Where the subscript *f* refers to fuel and *o* refers to oxidiser. Under the assumption of equal diffusivities, Γf = Γo = Γ , the species equations can be reduced to a single equation for the mixture fraction, *f:*

$$f = \frac{Z_i - Z_{i,ox}}{Z_{i,fule} - Z_{i,ox}} \qquad 3\text{-}16$$

The reaction source terms of the species equation cancel, and thus *f* is a conserved quantity. Whereas the assumption of equal diffusivities is problematic for laminar flows, it is suitable when the molecular diffusion and convection are overwhelmed by turbulent flow [80].

3.5.5.1 Non-Premixed Combustion

Unlike premixed combustion, where the reactants are mixed at the molecular level previous to burn, the fuel and oxidiser of non-premixed combustion enter the reaction zone in different streams. Examples of non-premixed combustion include furnaces, diesel internal-combustion engines and gas turbine combustion systems using a diffusion flame.

3.5.5.2 Premixed combustion modelling

In premixed combustion, fuel and oxidiser are mixed prior to ignition [131]. Combustion occurs as a flame front propagates into the unburnt reactants. However, premixed combustion is much more difficult to predict than non-premixed combustion since premixed combustion usually occurs as a thin, propagating flame that stretches and contorts as a consequence of local turbulence. The overall rate of subsonic flow propagation of the flame is determined by both the turbulent eddies and laminar flame speed. The laminar flame speed is determined by the rate that species and heat diffuse upstream into the reactants and burn. The flame front propagation is modelled by solving a transport equation for the density-weighted mean reaction progress variable, denoted by *c* [132] (Equation 3.17). Therefore, premixed combustion was used for all this thesis.

The turbulent premixed combustion model, based on work by Zimont et al.[132] [132], involves the solution of a transport equation for the reaction progress variable. The closure of this equation is based on the definition of the turbulent flame speed. The flame front propagation is again modelled by solving a transport equation for the density-weighted mean reaction progress variable, denoted by c [132]:

$$\frac{\partial}{\partial t}(\rho c) + \nabla.(\rho \vec{v} c) = \nabla.\left(\frac{\mu_t}{S_{c_t}} \nabla c\right) + \rho S_c \qquad 3\text{-}17$$

$$C = \sum_{i=1}^{n} Y_i \ / \sum_{i=1}^{n} Y_{i,eq} \qquad 3\text{-}18$$

Based on this definition, c = 0 is where the mixture is unburnt and c = 1 is where the mixture is burnt. The value of c is defined as a boundary condition for the inlet flow. The mean reaction rate in Equation 3.17 is modelled as:

$$\rho S_c = \rho_u S_T |\nabla c| \quad 3\text{-}19$$

where ρ_u is the density of burnt mixture, S_T is the turbulent flame speed, given by:

$$S_T = A\,(u')^{3/4} S_L{}^{1/2} \alpha^{-1/4} l_t^{1/4} = Au' \left(\frac{\tau_t}{\tau_c}\right)^{1/4} \quad 3\text{-}20$$

$$l_t = C_D \frac{(u')^3}{\varepsilon} \quad 3\text{-}21$$

where ε is the turbulence dissipation rate. The turbulent parameters use constant values of A = 0.52 and C_D = 0.37, as specified by Zimont et al. [132], which are suitable for most premixed flames.

Non-adiabatic premixed combustion model was used in this research, due to its consideration of heat release. The energy transport equation is solved in order to account for any heat losses or gains within the system. These losses or gains may include heat sources due to chemical reaction or radiation heat losses. The energy equation in terms of practical enthalpy, h, for fully premixed conditions is as follows:

$$\frac{\partial}{\partial t}(\rho h) + \nabla.(\rho \vec{v} h) = \nabla.\left[\frac{k + k_t}{c_p} \nabla h\right] + S_{h,chem} + S_{h,rad} \quad 3\text{-}22$$

$$S_{h.chem} = \rho S_c H_{comb} Y_{fuel} \quad 3\text{-}23$$

Therefore, turbulent premixed combustion model was used in this thesis based on work by Zimont et al. [132], which involves the solution of a transport equation for

the reaction progress variable. The closure of this equation is based on the definition of the turbulent flame speed. The flame front propagation is again modelled by solving a transport equation for the density-weighted mean reaction progress variable, denoted by c [132].

3.6 Definition of stretch factor

Premixed combustion is more difficult than non-premixed combustion because premixed combustion occurs where fuel and air are mixed prior to ignition; secondly, premixed combustion usually occurs as a reaction, which allows turbulence control the overall rate of propagation of the flame and stretch. The laminar flame speed and turbulent eddies determine of the propagation of the flame.

The flame propagation is modelled by solving transport equations (equation 3-17) for the weighted mean density reaction progress variable donated by c based on the Zimont Model [131,78].

Since industrial low emission combustor usually operate near blow-off , flame stretch had a significant effect on the mean turbulent heat release intensity. To take flame stretch into account the source term for the progress variable (ρS_c in Equation 3.17) is multiplied by a stretch factor G [132].

The stretch factor represent the likelihood that the stretching will not quench the flame if there is no stretching (G=1),the probability that the flame will be unquenched 100%

The stretch factor, G, is obtained by integrating the log-normal distribution of turbulence dissipation rate, ϵ:

$$G = erfc\{-\sqrt{\frac{1}{2\sigma}\left[Ln\left(\frac{\epsilon_{cr}}{\epsilon}\right)\right]} + \frac{\sigma}{2} \qquad 3\text{-}24$$

$$\sigma = \mu_{str} ln\left(\frac{L}{\eta}\right) \qquad 3\text{-}25$$

$$\epsilon_{cr} = 15 v g_{cr}^2 \qquad 3\text{-}26$$

If the value of the g_{cr} is set very high ($1x10^8$) that's mean no flame stretching occurs.

To considering the flame stretching effects, the critical rate of strain g_{cr} should be adjusted based on experimental data of the burner. For the numerical models, an appropriate value can be determined for a reasonable model for the critical rate of strain g_{cr} is

$$g_{cr} = \frac{BS_L^2}{\propto} \quad 3\text{-}27$$

3.7 Summary

This chapter describes both the experimental apparatus and CFD methodology, along with the methodology to operate them.

Firstly, the experimental techniques were described including the equipment used and their specifications. A generic swirl burner with radial swirl vanes was used and the flow field was analysed under both atmospheric and confinement conditions. Confinement was achieved using a pair of quartz cylinders with diameters of 2D and 3D, respectively, where D is the external nozzle diameter of 0.028m. The shear flow and high momentum flow regions were controlled by four nozzles with angles of 30°, 45°, 60° and 90°. Frequency measurements were made using a PCB Piezotronics 378B02 condenser microphone located in the middle of the nozzle outlet. Particle image velocimetry (PIV) was used to specify the velocity behaviour of the flow field. Photron high speed cameras were used to visualise the flows.

Secondly, descriptions of the Computational Fluid Dynamics (CFD) techniques and turbulence models used in this work were presented. CFD is presented as an important tool in designing combustion systems in gas turbines. The main function of CFD is to analyse fluid flows, heat transfer and combustion. Fluent ANSYS was used to analysis both the combustion and flow regimes. The CFD work was based on the Zimont model [132], using a shear-stress transport (SST) *k-ω* model as it is suitable for complex 3D flows with strong swirl. A lean premixed combustion model was used for all the experimental and numerical work in this thesis.

CHAPTER4

CHAPTER 4

COMBUSTOR MODELLING AND SIMULATION

4.1 Introduction

Swirl stabilised combustion is one of the most widely used techniques for flame stabilisation in gas turbine combustors. Lean premixed combustion systems allow the reduction of NO_x coupled with fair flame stability. The swirl mechanism produces an aerodynamic region known as the central recirculation zone (CRZ), providing a low velocity region where the flame speed matches the flow velocity, thus anchoring the flame whilst serving to recycle heat and active chemical species to the root of the former. Another beneficial feature of the CRZ is the enhancement of the mixing in and around this region. However, the mixing and stabilisation processes inside of this zone have been shown to be extremely complex [27]. The level of swirl, burner outlet configuration and combustor expansion are very important variables that define the features of the CRZ.

Therefore, in this chapter swirling flame dynamics are investigated using computational fluid dynamics (CFD) with commercial software (ANSYS). A new generic swirl burner operated under lean-premixed conditions was modelled. A variety of nozzles were analysed using several syngas blends at a constant power output. The investigation was based on recognising the size and strength of the central recirculation zones. The dimensions and turbulence of the Central Recirculation Zone were measured for correlation with experimental trials in Chapters 5 and 6. The results show how the strength and size of the recirculation zone are highly influenced by the blend, and infer that blowoff is governed by both the shear layer surrounding the Central Recirculation Zones (CRZ) and the Damkohler number (Da). Good correlation was observed using previous experimental results[48,132], thus providing more information about the impact of the CRZ and the flame turbulence intensity during the blowoff process.

The flow chart shown in Figure 4.1 summarises the work carried out, outlining the main topics discussed in the following chapter.

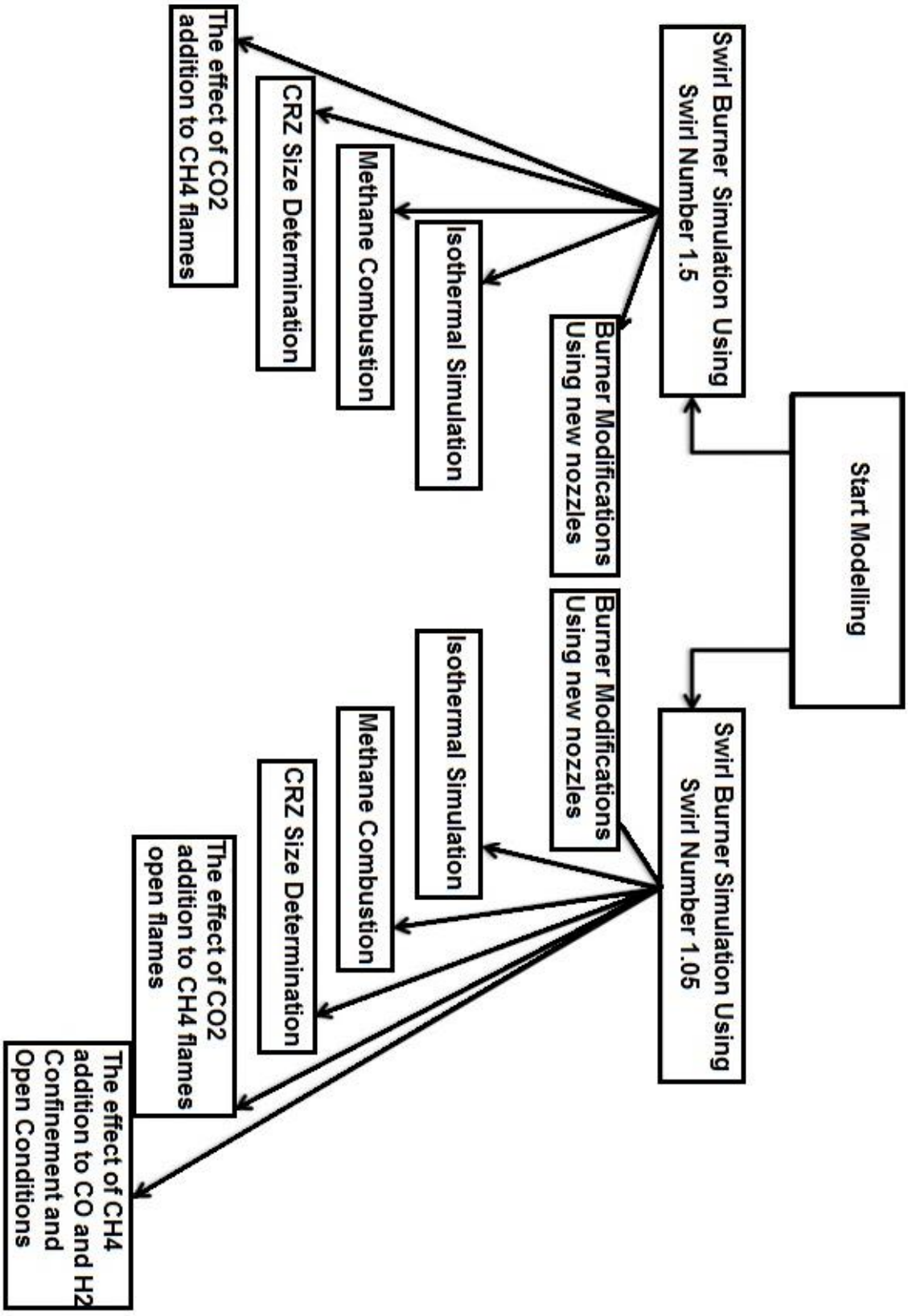

Figure 4-1: Outline of the research work

4.2 Numerical Methodology

4.2.1 Using Open Conditions

CFD modelling was used to simulate the combustion of a premixed swirl burner that uses different types of fuels. A 100 kW swirl burner was modelled to examine the flame stability limits at atmospheric inlet conditions (1 bar, 293 K). Different angled nozzles were examined (30°, 45°, 60°, 90°) at two swirl numbers of 1.05 and 1.50. A single tangential inlet (a) feeds the premixed air and fuel to an outer plenum chamber (b) which uniformly distributes the gas to the slot-type radial tangential inlets (c). Swirling unburned fuel then passes into the burner body (d), and into the burner exhaust (e) where the gases pass around the flame stabilising central recirculation zone. The central diffusion fuel injector (f) (which was not used for fuel during the course of this study) extends centrally through the combustor body to the exhaust (Figure 4.2).

CFD modelling is initially performed to simulate the combustion of methane-air without and with carbon dioxide. Laminar flame speeds were calculated for pure methane and CH_4/CO_2 blends at atmospheric pressures, at a temperature of 300 K, and at various equivalence ratios. This was done using CHEMKIN-PRO with the PREMIX code. The numerical values for the laminar flame speeds were then fed into the CFD model. Isothermal conditions with no combustion were used to calibrate the system and indicate the flow pattern, although it is well known that there are also 3D time dependant coherent structures, thus the results are of an indicative nature. During the simulation, various types of solvers were investigated and conclusions were drawn as to which were the most effective. Based on the experimental results obtained at 5.85 and 5.48 g/s total mass flow rates, the best turbulent option for the present work was found to be the κ-ω SST model [78,130].

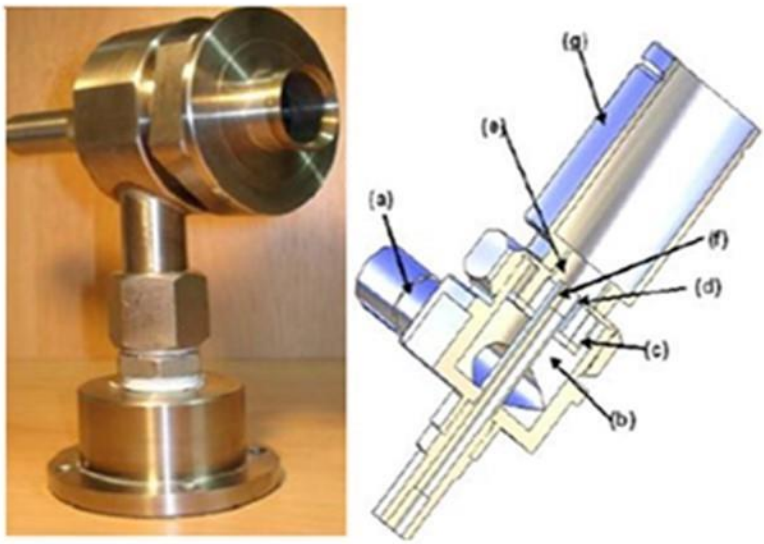

Figure 4-2: Swirl burner and schematic diagram, confinement 3D, 2D respectively

Swirl combustors and burners are usually characterised by their degree of swirl, via a swirl number (S). For this particular project, the swirl element of S = 1.05 has four tangential inlets which are symmetrically distributed, whilst the swirl element of S = 1.50 has nine tangential inlets symmetrically distributed. The swirl burner gives good flame stabilisation but produces a CRZ that extends back over the central fuel injector, allowing the flame to propagate into this region. This effect can be altered by fitting a divergent exhaust nozzle (Figure 4.3), producing a different shapes of CRZ. Figure 4.4 shows a nozzle divergence diagram, keeping the final outlet radius to the same value to maintain the swirl number.

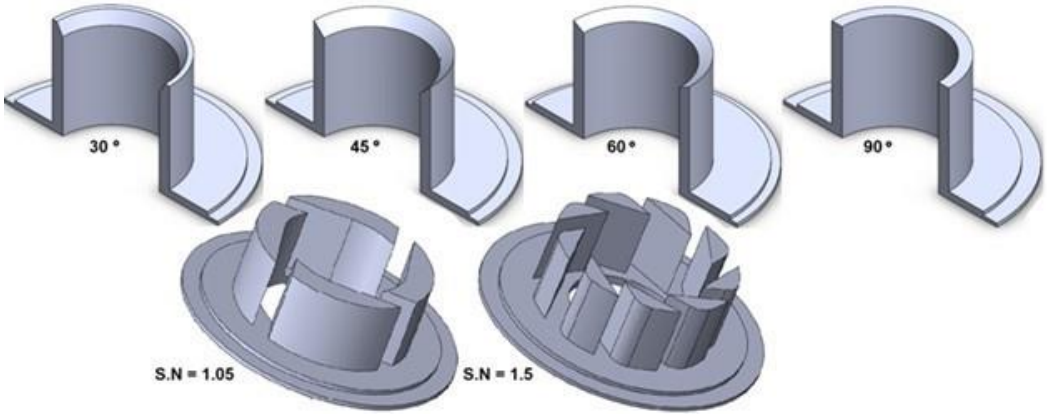

Figure 4-3: Geometrical swirl number 1.50, 1.05 and various divergent angles nozzles, respectively

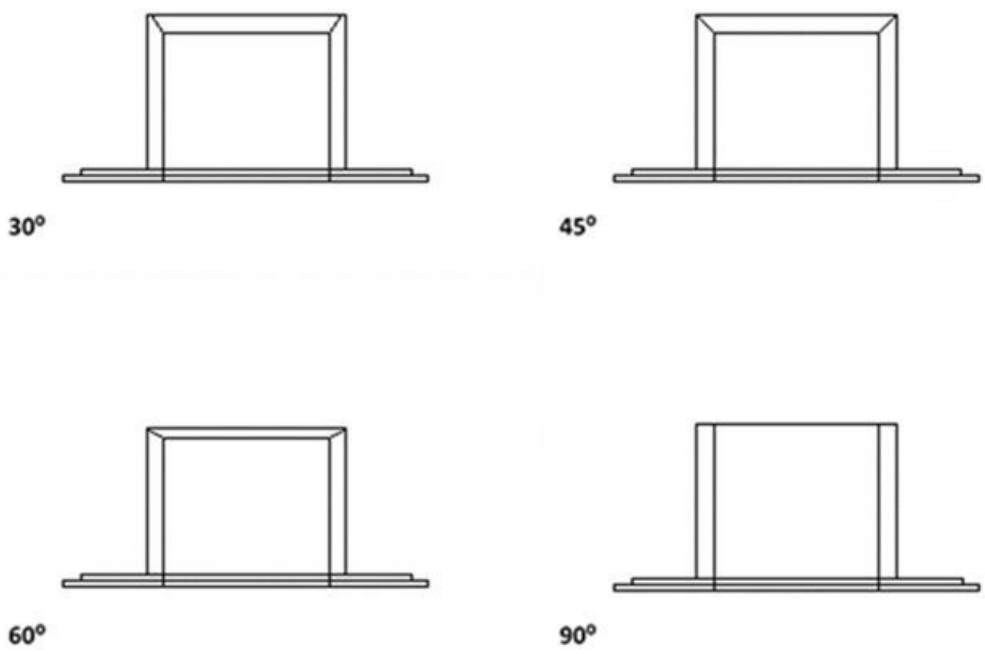

Figure 4-4: Nozzle divergence diagram

4.2.2 The swirl burner model

The first step of the CFD simulation is to prepare the model for analysis. Therefore, in order to analyse fluid flows, flow domains are split into smaller subdomains made up of geometric primitives like hexahedral and tetrahedral cells. The governing equations are then solved inside each of those subdomains. A better mesh quality (smaller cells) gives a more accurate solution, so a good quality mesh is desirable in certain areas of the geometry, for example, where the gradient of the flow field is more complex. A high quality mesh increases the accuracy of the CFD solution and improves convergence compared to that of a poorer quality mesh.

The swirl burner model considered in this researh is first modelled for an open flame condition. This model consists of three parts: a) swirl vanes, b) ignition, and c) combustion champer. The model can be seen in Figures 4.5 and 4.6.

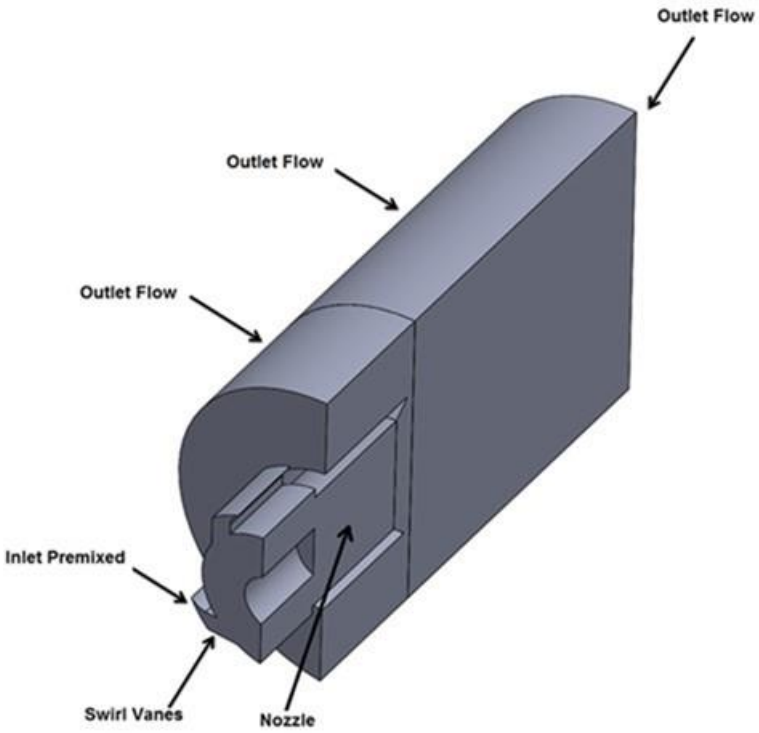

Figure 4-5: Combustor Model with a Swirl Number of 1.05

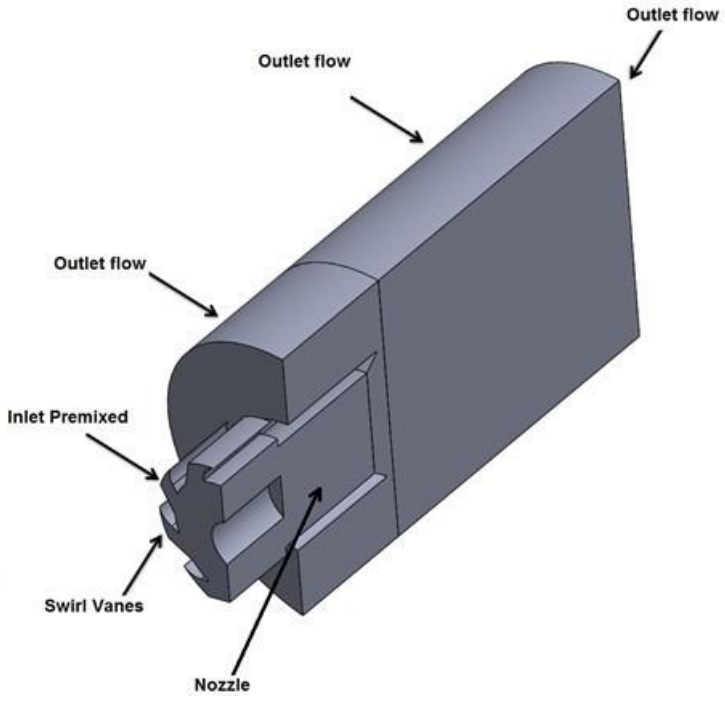

Figure 4-6: Combustor Model with a Swirl Number of 1.5

4.2.3 Mesh Construction

FLUENT 14.5 was used to perform the modelling and simulation. The pre-processor used to construct the model grid was ICEM 14.5.7. Two types of grid exist in CFD: structured and unstructured. The structured grids are usually created manually and consist of hexahedral elements. Unstructured grids are generated automatically and consist of a number of different element types, most of them being tetrahedrons. Each cell is used to define nodes where fluid properties are calculated. The solution is iterated at each node based on the values obtained from the neighbouring nodes. Thus, a higher number of elements results in a higher number of nodes and ultimately more calculations required, i.e. higher computation costs. This results in a trade-off between reduced mesh size, giving shorter computational time, and higher mesh densities required for capturing the details of the flow, with computational expenses. Manually created structured grids usually give the user better control over the generated mesh and allows denser node concentrations in parts where better resolution is required. This better control comes at a cost since making the grid usually requires significant time and work. Furthermore, structured grids tend to have a higher number of nodes compared to unstructured grids. Therefore, a mesh independency analysis must be performed so that the variation in the mesh does not affect the quality of the results and allows a reduction in computational time.

Thus, an independency analysis was carried out in this study. Three meshes were examined as shown in Figure 4.7. The 3 cases were run using boundary conditions taken from experimental studies [133]. Figure 4.7 shows each of the meshes with different node densities. Table 4.1 denotes the number of elements into which each mesh has been divided.

ICEM 14.5 was used for constructing the model mesh. A three dimensional model obtained from Solid Works was used for the simulation. The entire system can be meshed easily by a tetrahedral unstructured mesh but it leads to a higher number of elements generated, which translates to longer computational times, whilst the solution is not stable for some viscous models. A hexahedral mesh can give faster and stable solutions so it was the preferred option here.

The main problem with this model was the huge number of cells which affects the time for the solution to become converged. Roughly, the consumed time for only one run was about 4 days. Hence the volume of the cells was increased to reduce their number, via the modifications as shown in Figure 4.10. The number of cells was reduced to three stages from15,080,239 upto1,893,797 , which still gave too long a time for a converged solution. Several trials are done until the suitable mesh was constructed as shown in Figure 4.7c. The final mesh was satisfactory from both the accuracy and consumed time view points and it contains 237,374 elements which consumed about one day for the solution to be converged.

Table 4-1: number of elements

	Mesh density		Swirl number1.05	Swirl number1. 5
A	High quality	**Number of Nodes**	**152129899**	**15389368**
		Number of Elements	**15080239**	**15252503**
B	Medium quality	**Number of Nodes**	**1927468**	**1948929**
		Number of Elements	**1893797**	**1914204**
C	Low quality	**Number of Nodes**	**245724**	**249385**
		Number of Elements	**237374**	**240846**

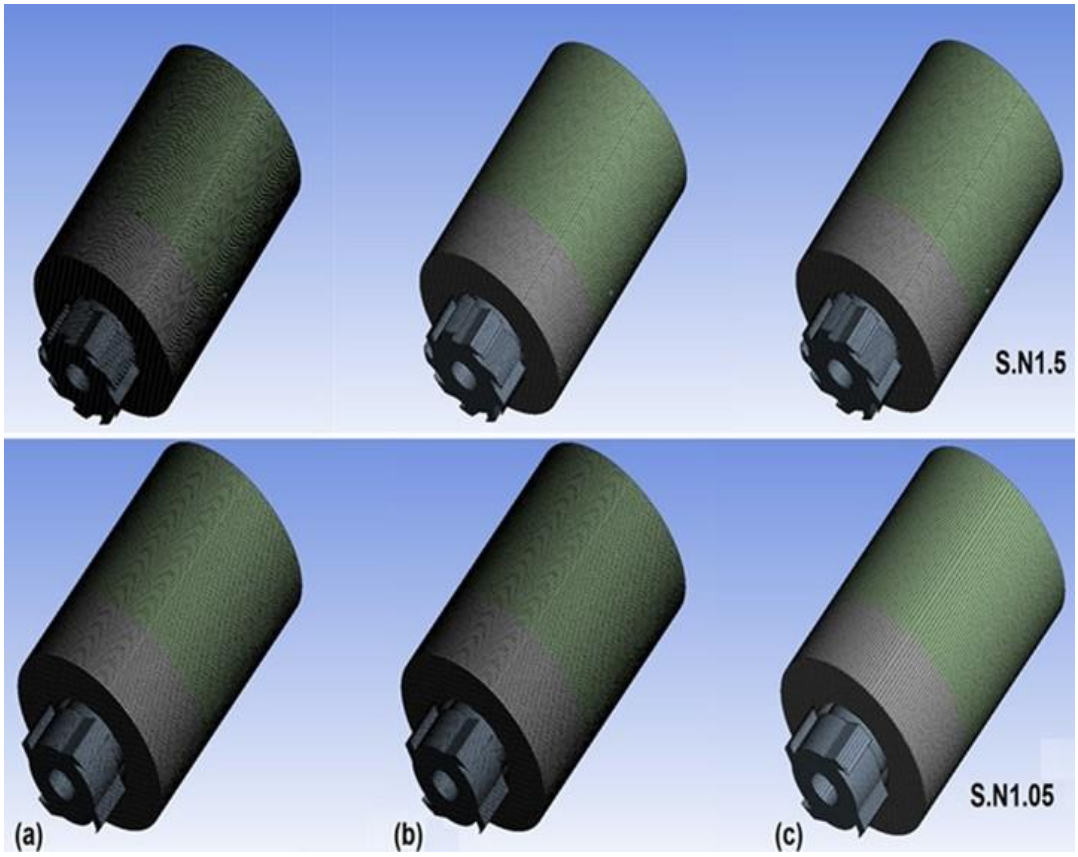

Figure 4-7: Combustor mesh distribution

4.2.4 CFD simulation of Swirl Burner and Boundary Conditions

Pure methane and methane blends with carbon dioxide were used to compare simulations with experiments obtained during previous studies [48,132].The gas composition and the operating conditions of the burner are given in Tables 4.2 and 4.3, respectively.

Table 4-2: Inlet boundary conditions of pure methane

Test	Inlet Tem	Inlet Pre	CH4 [g/s]	Air [g/s]	Total [g/s]	Φ [-]
T1	300K	1 bar	0.13	3.2	3.33	0.69
T2	300K	1 bar	0.15	3.5	3.65	0.77
T3	300K	1 bar	0.21	4.6	4.9	0.77
T4	300K	1 bar	0.24	5.2	5.44	0.79
T5	300K	1 bar	0.27	5.5	5.85	0.83

Table 4-3: Inlet boundary conditions of methane blend with CO_2

Test	Inlet Tem	Inlet Pre	CH4 [g/s]	AIR [g/s]	CO2 [g/s]	Total [g/s]	Φ [-]
T1	300K	1 bar	0.13	2.57	0.13	2.83	0.87
T2	300K	1 bar	0.15	3.01	0.16	3.32	0.89
T3	300K	1 bar	0.21	3.93	0.21	4.35	0.91
T4	300K	1 bar	0.24	4.12	0.24	4.60	1.00
T5	300K	1 bar	0.27	4.94	0.27	5.48	0.94

4.3 CFD Simulation Using Confinement Condition

4.3.1 Setup

The swirl burner considered in this part of the project was modelled using confined flame conditions. Therefore, the model consists of three parts: a) swirl vanes, b) ignition zone, and c) combustion chamber. These zones are describe only for a Swirl Number of 1.04 (Figure 4.8). Figure 4.9 shows the nozzles used, just as in the previous unconfined cases.

Comparison criteria that were considered for the selection of the best mesh (Figure 4.7) were based on axial velocity contours, turbulence intensity and Damköhler numbers located in three planes. Figure 4.10 shows these three planes, i.e. P1, P5 and P10. P2 was also compared for turbulent flame speeds, ST, and stretch factors, G.

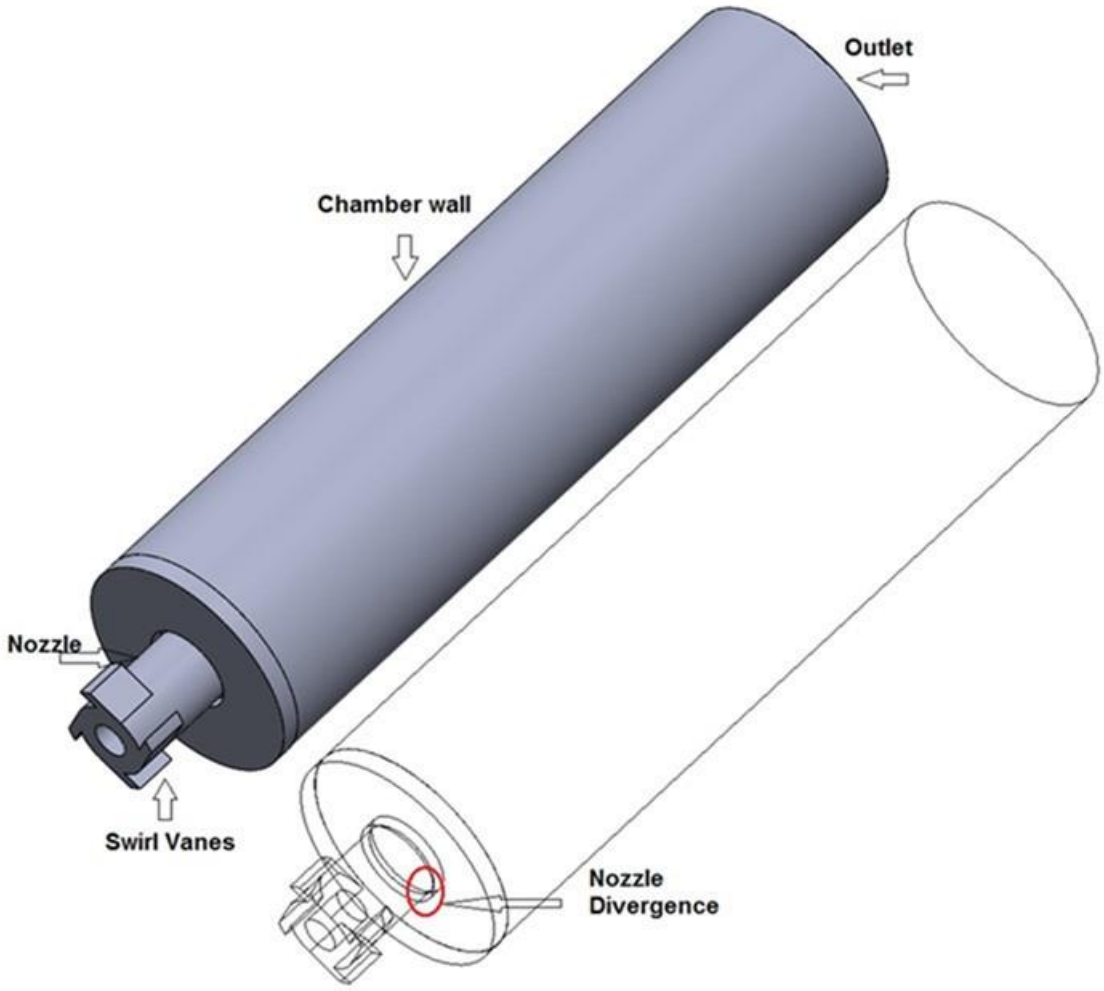

Figure 4-8: Combustor flow fields

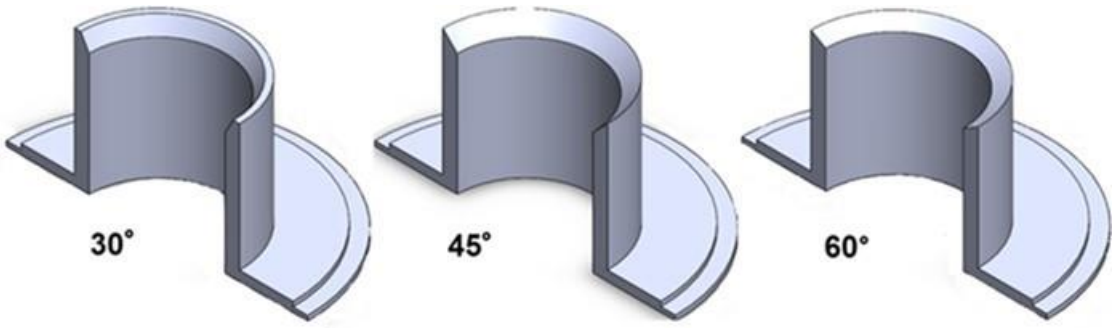

Figure 4-9: Nozzle configurations

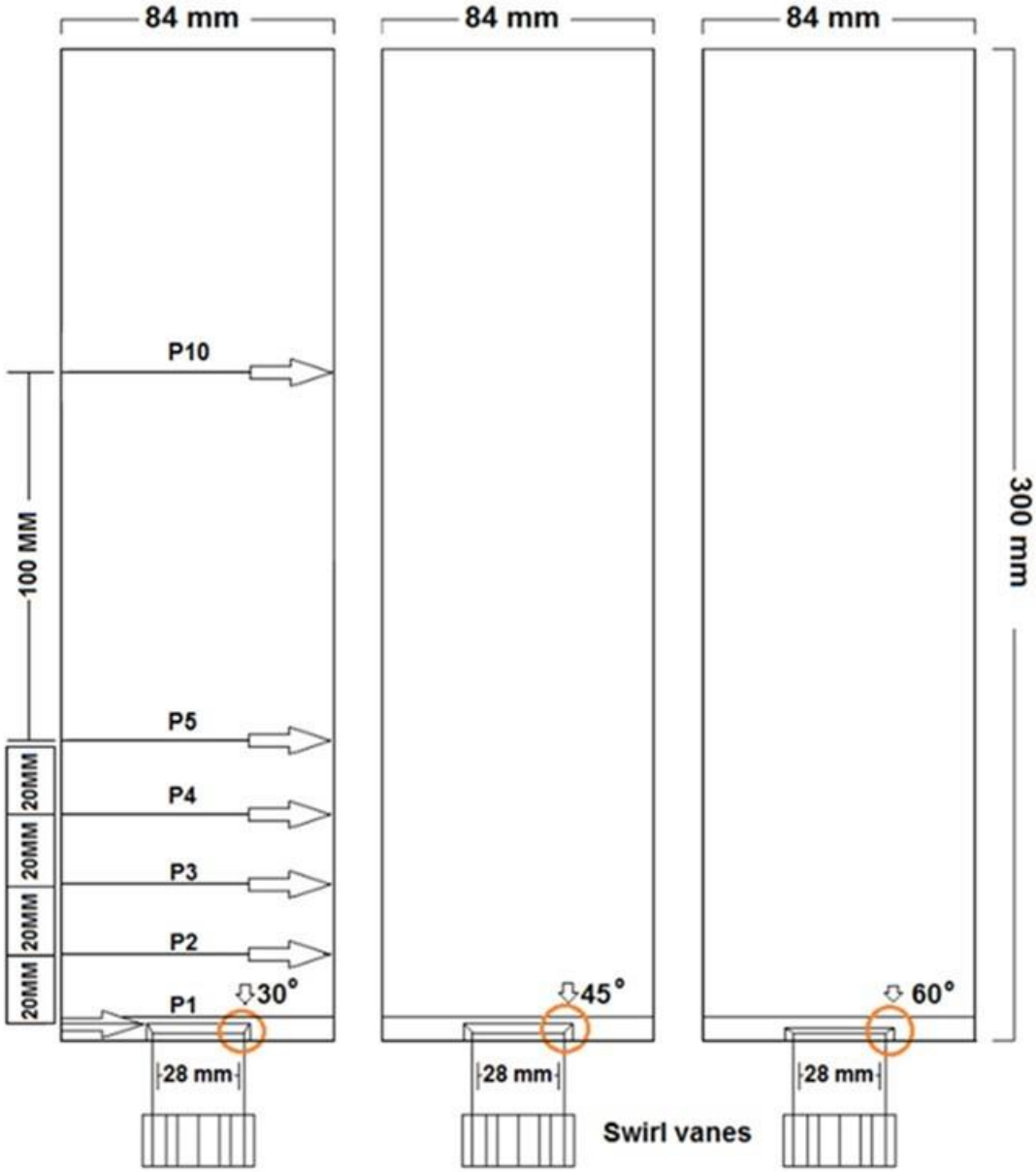

Figure 4-10: Comparison planes

4.3.2 Initial mesh size calculation

When the turbulent quantities are calculated, it is important to place the first node of the mesh within a certain range. This is necessary because the inclusion of viscosity in the equations produces high gradients in the boundary layer. In order to capture these high gradients in a numerical simulation, it is important to have a large quantity of mesh points inside of the boundary layer [134]. To obtain the initial cell size, y_{wall},

that best fits the simulation using the Navier-Stokes equations, y+ must be calculated. Based on local Reynolds numbers, skin friction correlations [133,134], and a reference boundary length of 0.3 m, Table 4.4 shows the estimated y_{wall} for y+ up to 10 units:

$$y_1^+ = \frac{\rho u_t y_{wall}}{\mu} \qquad 4\text{-}1$$

Where u_t is the friction velocity given by,

$$u_t = \sqrt{\frac{\tau_{wall}}{\rho}} = \sqrt{\frac{1}{2}\ (V_{ref})^2 C_f} \qquad 4\text{-}2$$

The wall friction coefficient is also obtained as follows,

$$C_f = \frac{0.027}{R_{e_x}^{1/7}} \qquad 4\text{-}3$$

The pre-processors used to construct the model grid were the FLUENT in-built package and ICEM 14.5.7. After independency mesh analyses, it was concluded that a medium sized mesh of 6,151,375 nodes and 6,085,618 elements would provide similar results with both pre-processors. A finer mesh was created close to the burner exit and around the fuel nozzles as shown in Figure 4.11.

4.3.3 Combustion Simulations and Boundary Conditions

Simulations were performed using all syngases in Table 4.5 under premixed conditions with FLUENT 14.5. All the CFD analyses were conducted using an output power of 7.49 kW. The energy transport equation was solved in order to account for any heat losses or gains within the system since a Non-adiabatic premixed combustion model was considered. Inlet conditions were set at a pressure of 1 bar and temperature of 300K.

Table 4-4: y wall values (m) for different y+ values.

	Lref = 0.3 m		Y+ =1	Y+ =5	Y+ =10
Gas mixture	Mass Flow (Kg/s)	Initial Vel. (m/s)	Y wall (Eq. 1)	Y wall (Eq. 1)	Y wall (Eq. 1)
SYN1-30°	0.00168	6.378	4.72E-05	0.000236	0.000472
SYN2-30°	0.00163	6.491	4.64E-05	0.000232	0.000465
SYN3-30°	0.00166	6.876	4.40E-05	0.000220	0.000441
SYN4-30°	0.00147	6.704	4.51E-05	0.000225	0.000451
SYN1-45°	0.00165	6.280	4.79E-05	0.000239	0.000479
SYN2-45°	0.00157	6.242	4.82E-05	0.000241	0.000482
SYN3-45°	0.00165	6.837	4.43E-05	0.000221	0.000443
SYN4-45°	0.00157	7.166	4.24E-05	0.000212	0.000424
SYN1-60°	0.00166	6.305	4.77E-05	0.000238	0.000478
SYN2-60°	0.00159	6.324	4.76E-05	0.000238	0.000476
SYN3-60°	0.00159	6.604	4.57E-05	0.000228	0.000458
SYN4-60°	0.00150	6.827	4.43E-05	0.000221	0.000444

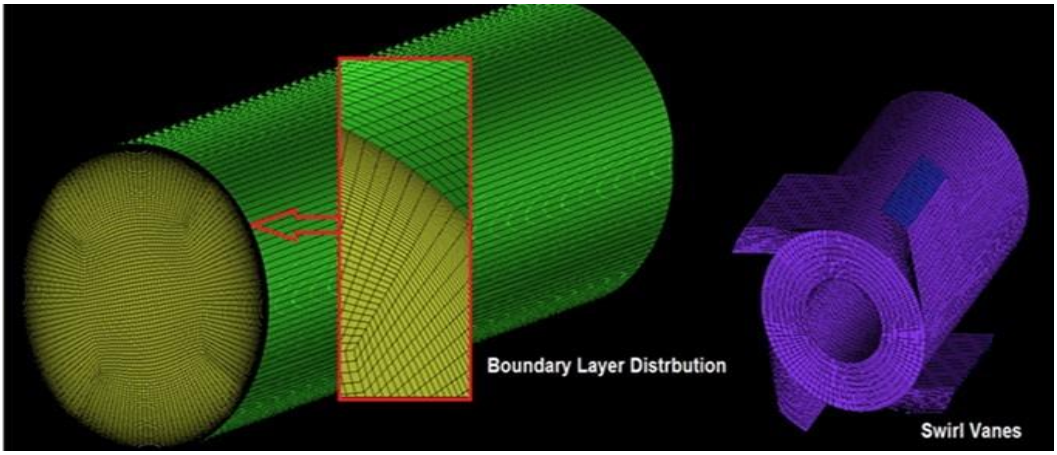

Figure 4-11: Mesh distribution of swirl burner

Table 4-5 : Syngas compositions

Gas number	*Gas compositions*
Syngas 1	10% CH_4 + 45%H_2 + 45%CO
Syngas 2	20% CH_4 + 40%H_2 + 40%CO
Syngas 3	30% CH_4 + 35%H_2 + 35%CO
Syngas 4	50% CH_4 + 25%H_2 + 25%CO
Gas 5	100% CH_4
Gas 6	50% CH_4+50% CO_2

Table 4-6 : CFD Simulations of all examined conditions.

Gas Number	Ṁ fuel [g/s]	Ṁ Air [g/s]	Nozzle angle	Total [g/s]	Φ	HHV Mj/kg	Power Output KW
Syn1	0.101	1.414	30°	1.515	0.425	73.941	7.49
Syn1	0.101	1.405	45°	1.507	0.428	73.941	7.49
Syn1	0.101	1.383	60°	1.485	0.453	73.941	7.49
Syn2	0.104	1.557	30°	1.661	0.485	71.892	7.49
Syn2	0.104	1.554	45°	1.658	0.486	71.892	7.49
Syn2	0.104	1.489	60°	1.593	0.508	71.892	7.49
Syn3	0.107	1.631	30°	1.738	0.563	69.843	7.49
Syn3	0.107	1.677	45°	1.784	0.548	69.843	7.49
Syn3	0.107	1.650	60°	1.757	0.557	69.843	7.49
Syn4	0.113	1.839	30°	1.953	0.689	65.745	7.49
Syn4	0.113	1.791	45°	1.905	0.707	65.745	7.49
Syn4	0.113	1.832	60°	1.946	0.692	65.745	7.49

4.4 Results and Discussions - Open Conditions

4.4.1 Combustion with Pure Methane

Isothermal conditions were first simulated in order to ensure mesh independency and good accuracy. Once a medium sized mesh was selected, comparison with pure methane flames was performed to observe the effects of combustion on the flow patterns. Comparison of the CFD simulations presented in Figure 4.12 (a) and (b) reveals the effects of combustion on the flow. The predicted and measured boundaries of the CRZ for isothermal flows show a longer CRZ extending up to the combustor exit, as expected. However, the use of combustion showed a reduction in both the size and the strength of the CRZ (Table 4.7).

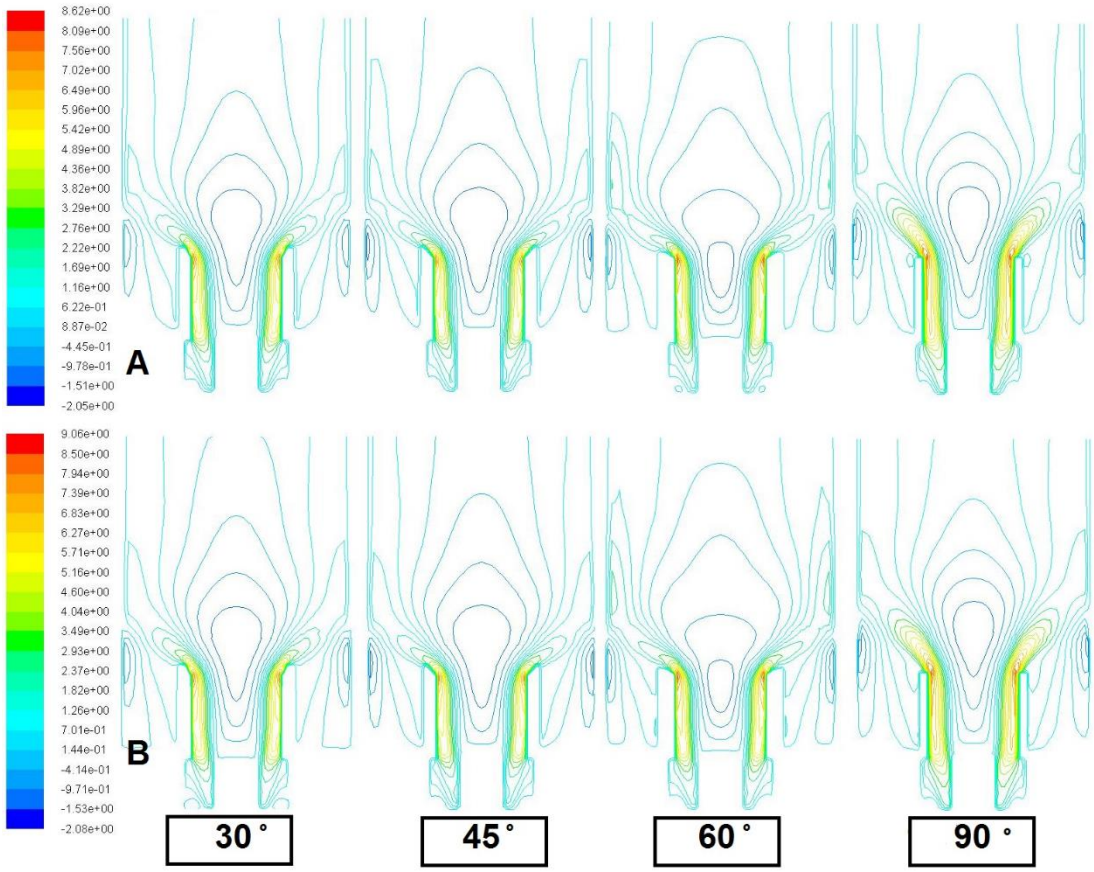

Figure 4-12: Comparison of axial velocity using different nozzles under (A) isothermal and (B) combustion conditions, with S =1.05

Table 4-7: Comparison of axial velocity using isothermal and combustion CRZ patterns using different nozzle angles.

	30^0	45^0	60^0	90^0	Conditions
Width	1.23D	1.34D	1.66D	1.19D	ISOTH
Height	2.65D	2.97D	3.41D	2.93D	ISOTH
Width	1.19D	1.34D	1.58 D	1.15D	COMBUS
Height	2.53D	2.85D	3.29D	2.89D	COMBUS

The reduction of the size and strength of the CRZ in the combusting flow is due to the decreased level of swirl in the combustor as a consequence of the increased axial velocity [39]. The measurements show that the axial velocities in the forward flow region increase significantly due to combustion-induced flow acceleration while the tangential velocities are slightly altered. Consequently, the ratio of the tangential to axial momentum fluxes decreases substantially.

To determine the flow pattern changes between the two swirl numbers analysed, comparison was made between different geometries under isothermal conditions,

specifically aiming to investigate the effect of swirl on the recirculation zone sizes (Figures 4.13 and 4.14). The results indicate that the CRZ size increased in length with higher Swirl numbers using 30° and 45° nozzle, while the 60°, and 90° nozzles produced a smaller CRZ in terms of length and width as shown in Table 4-8.

Table 4-8 : CRZ size measurement

ISO	S.N1.05	Size	S.N1.5	Size
30^0	Width	1.11D	Width	1.09D
	Higher	2.51D	Higher	2.85D
45^0	Width	1.22D	Width	1.22D
	Higher	2.77D	Higher	3.40D
60^0	Width	1.55D	Width	1.07D
	Higher	3.18D	Higher	2.88D
90^0	Width	1.14D	Width	1.07D
	Higher	2.88D	Higher	2.70D

4-13: CRZ Comparison size between Swirl Number 1.05 and 1.5

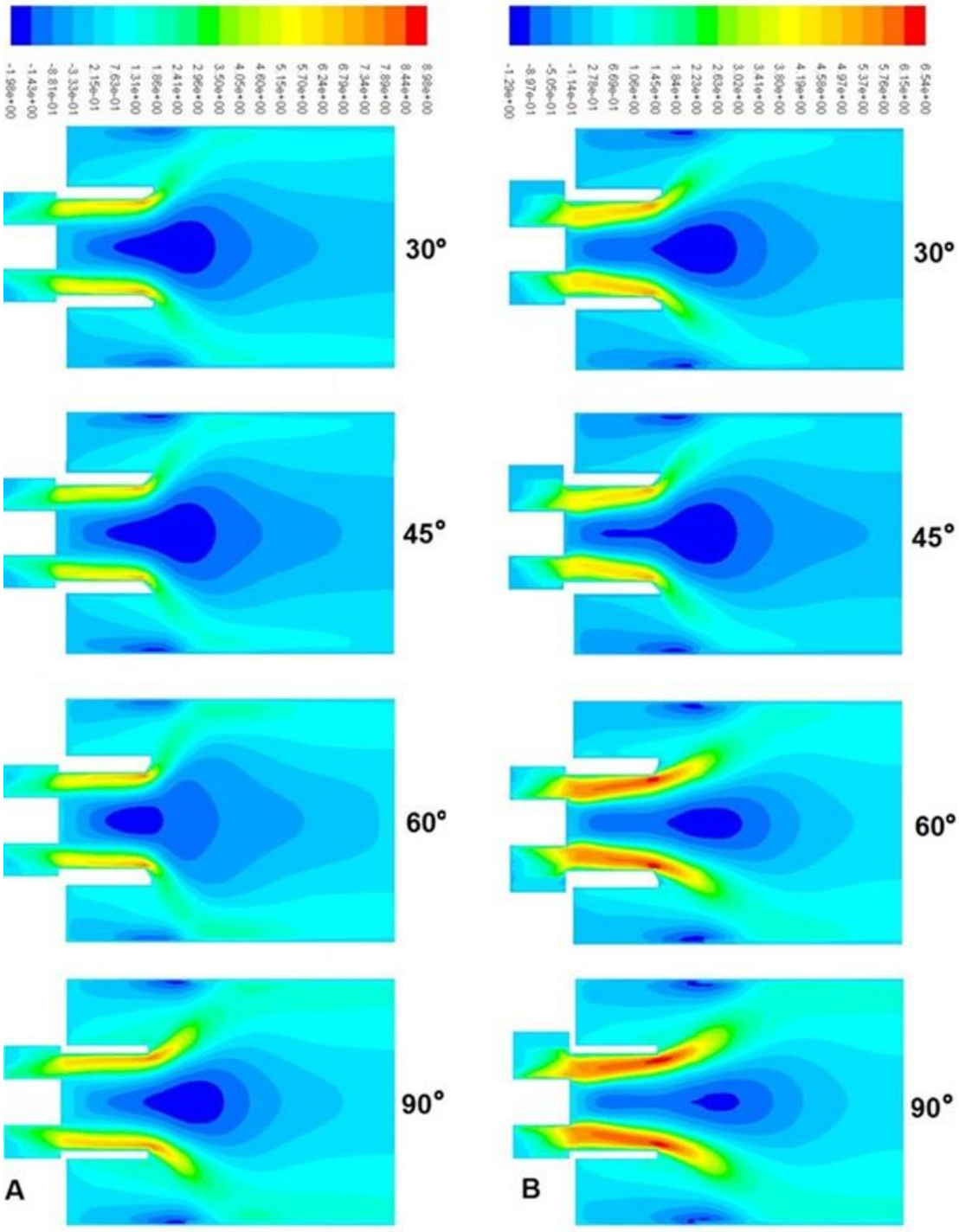

Figure 4-14: Isothermal results of axial velocity using different nozzles and swirl numbers: (A) 1.05, (B) 1.5

4.4.2 Effect of CO_2 Addition to CH4 Flames

The use of CO_2 alters the size and inner turbulence of the CRZ structure. Table 4.9, Figures 4.15, and 4.16 clearly show that turbulence intensity inside the CRZ with blends of methane and CO_2 is greater than with pure methane. Therefore, it is expected

that experimentally in chapter 5 will show a 7-10 % increase in turbulence when using carbon dioxide, and a change of around 10 % in the width and length of the CRZ (Figure 4.17). The length of the recirculation zone increases due to the reduced reaction time of the blend and the higher turbulence inside of the structure, a consequence of the addition of an inert gas such as CO_2. The results in Table 4.10 show that the combustion of pure methane and methane/carbon dioxide blends produce a slightly larger and stronger CRZ. These results were obtained by using all the nozzles with a swirl number of 1.05. The differences in turbulent intensity between combustion of pure methane and its blend with CO_2 are highlighted in Table 4.9. Following the addition of CO_2, a significant increase in turbulent intensity of more than 10 % was observed using both the 45° and the 60° nozzles. For the 30° and 90° nozzles the turbulence intensity increased by about 5 %.

As previously observed by other authors [49], these swirl flows will converge into a new structure called the High Momentum Flow Region (HMFR), which is highly correlated with the CRZ. This will increase the strength of the CRZ but reduce its dimensions, as observed in Table 4.10. The addition of CO_2 affects the velocity of the flow, the mixing and the combustion characteristics, thus generating slower profiles than with pure methane. At the same time, it seems that the dimensions of the CRZ with CO_2 are increased to a width of 1.33D and height of 2.83D. This can be compared to a width of 1.14D and a height of 2.75D when using pure methane under similar conditions (Figure 4.15). Figure 4.16 shows the progression of the CRZ and its boundaries, defined as a region of greater turbulence compared to the pure methane case. It is clear that the CRZ using CO_2 has increased in size.

On other hand, the addition of CO_2 increased the density of the mixture, which is reflected in the increasing centrifugal force. This leads to an augmenting of the dimensions of the CRZ, with increased width and height compared to that of pure methane under similar conditions, consequence of increasing of CRZ producing the reduction on average velocity resulting reduction of the turbulent intensity.

Table 4-9: Comparison of turbulent intensity of all cases for both pure methane blended with CO_2.

	TI % 30°	TI% 45°	TI %60°	TI % 90°	POWER KW
CH_4	66.6	67.4	65.3	63.5	7.49
CH_4+CO_2	71.6	76.2	74.5	69.4	7.49

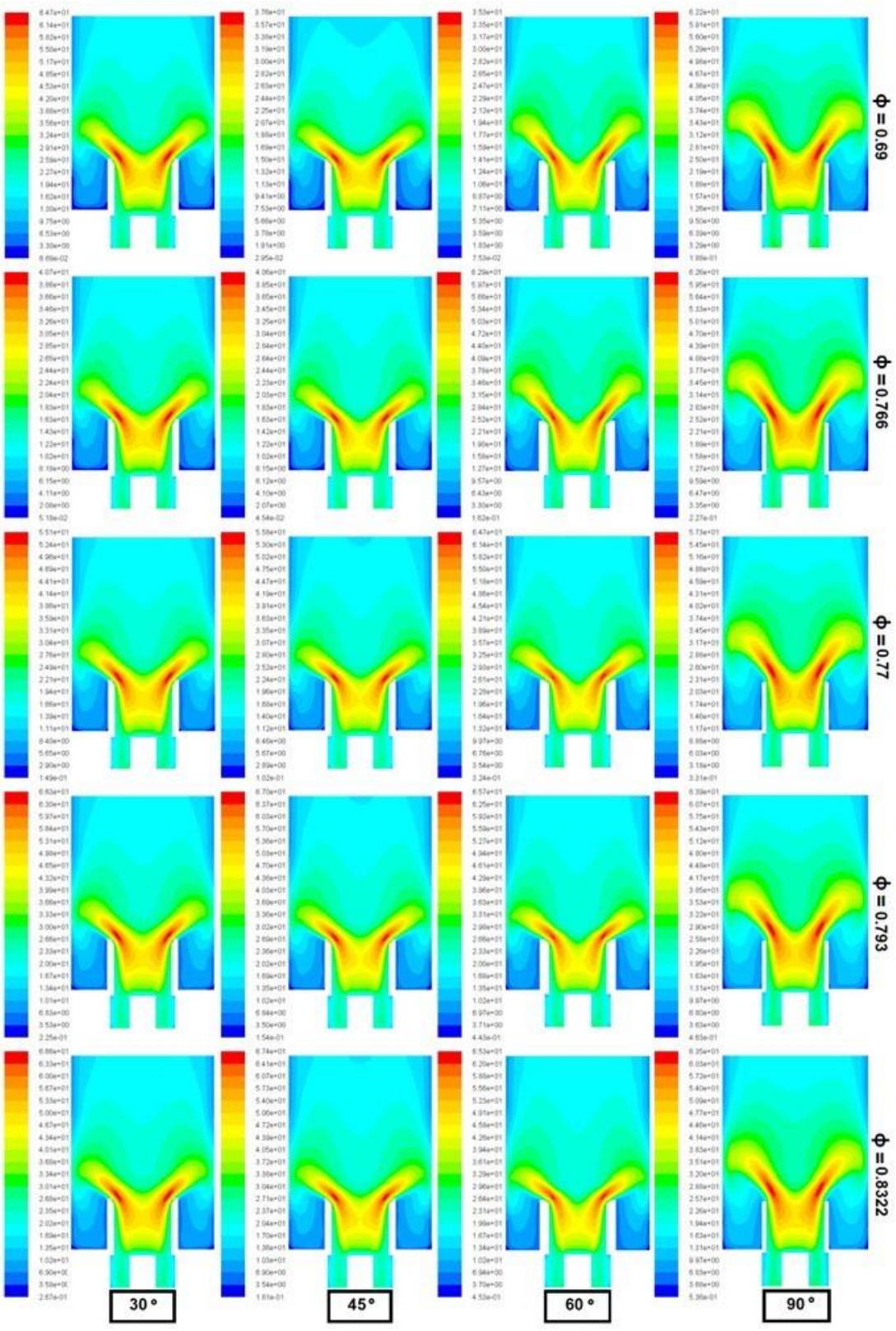

Figure 4-15: Comparisons of turbulent intensity using pure methane at different equivalence ratios with all nozzles. Swirl number of 1.05

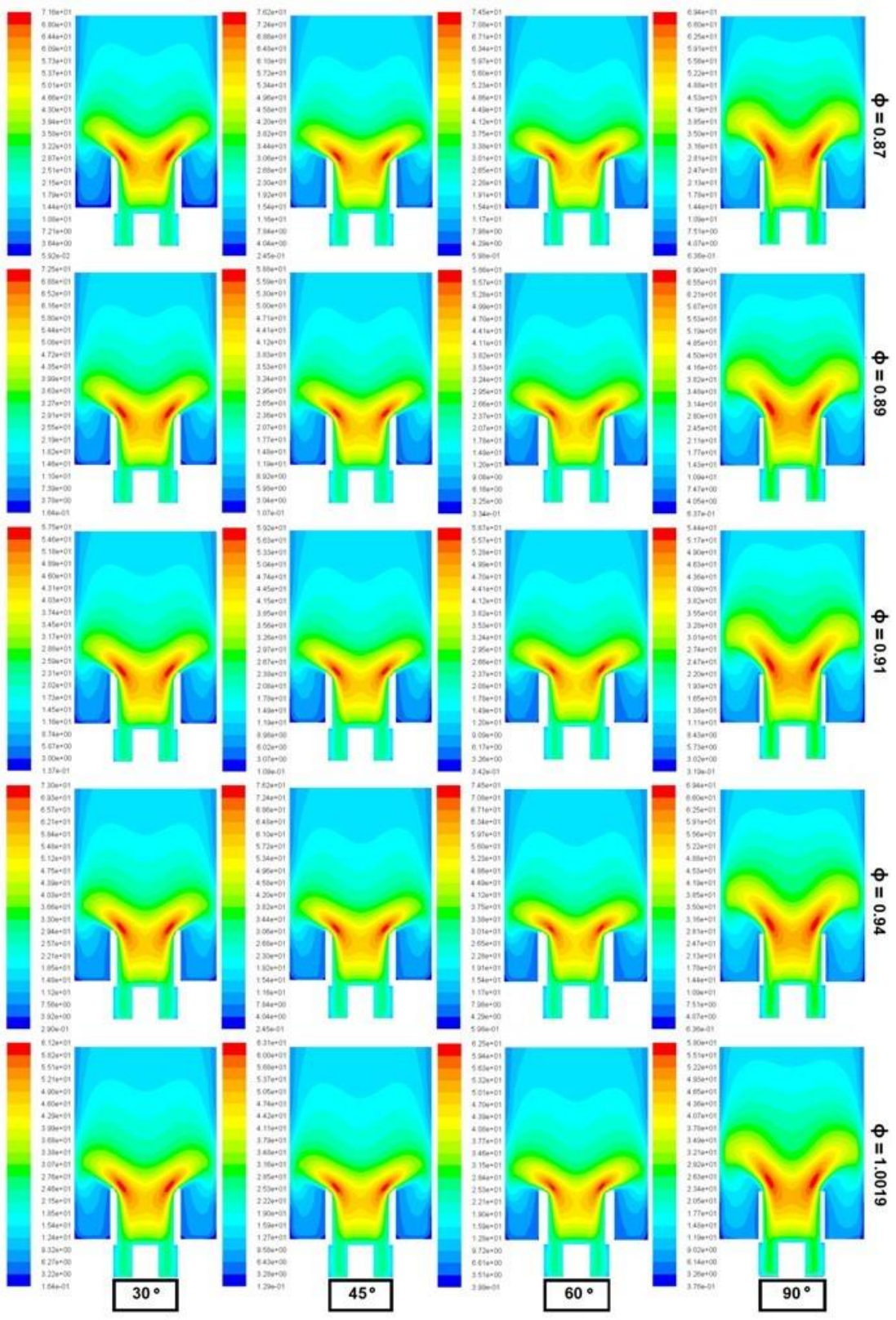

Figure 4-16: Comparisons of turbulent intensity using methane blends with CO_2 at different equivalence ratios will all nozzles. Swirl number is 1.05

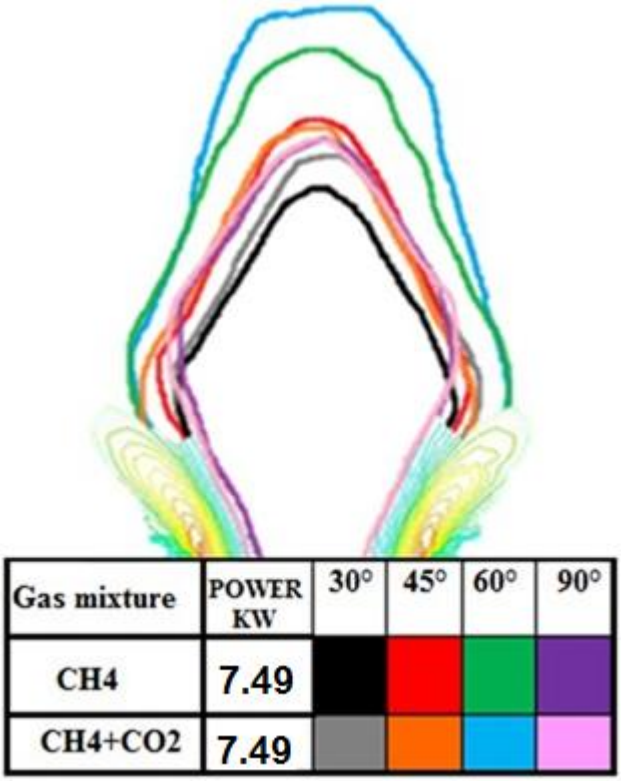

Figure 4-17: Comparison of CRZ size between pure methane and methane blended using CO_2

Table 4-10: Comparison of CRZ size for all cases. Methane data is on the left, while methane blended with CO_2 is on the right.

	Φ CH4	30^0	45^0	60^0	90^0	Φ CH4+CO2	30^0	45^0	60^0	90^0
W	0.69	1.41D	1.29D	1.49D	1.14D	0.87	1.33D	1.45D	1.49D	1.24D
H		3.46D	2.79D	3.14D	2.63D		2.83D	3.07D	3.38D	2.75D
W	0.76	1.41D	1.29D	1.49D	1.12D	0.89	1.29D	1.45D	1.57D	1.22D
H		3.54D	2.83D	3.22D	2.75D		2.75D	2.91D	3.54D	2.75D
W	0.77	1.41D	1.31D	1.57D	1.16D	0.91	1.31D	1.48D	1.57D	1.24D
H		3.54D	2.83D	3.22D	2.75D		2.75D	2.91D	3.58D	2.79D
W	0.79	1.41D	1.29D	1.25D	1.14D	0.94	1.27D	1.39D	1.57D	1.22D
H		3.62D	2.83D	3.22D	2.75D		2.73D	2.89D	3.54D	2.76D
W	0.83	1.14D	1.29D	1.61D	1.16D	1.00	1.33D	1.45D	1.33D	1.22D
H		2.75D	2.83D	3.26D	2.75D		2.75D	2.91D	3.62D	2.75D

4.4.3 The Effect of Changing Equivalence Ratio

To study the effect of different equivalence ratios on the combustion characteristics and aerodynamic behaviour of premixed combustion, further tests were carried out. Pure methane and methane blended with CO_2 both were analysed. Inlet pressure and temperature remained constant at 1 bar and 300 K, respectively. The equivalence ratio with pure methane was controlled to give values of 0.69, 0.76, 0.77, 0.79, and 0.83. Equivalence ratios with methane blended with CO_2 were also controlled to give values of 0.87, 0.89, 0.91, 0.94, and 1.00. Axial velocity contours are shown in Figures 4.18 and 4.19 for pure methane and for blends respectively. Equivalence ratio has little effect on the shape of the CRZ, but the nozzle angle does cause a noticeable effect. Figure 4.20 shows there is a considerable change in the structure of the CRZ as a consequence of the different shearing flows and pressure decays along the burner. Equivalence ratios using pure methane show great variance between cases. For example the 30° nozzle produces the largest CRZ, a condition expected as a consequence of the further expansion of the flow and likely reduction of reactions due to a less intense interaction between shearing flow and recirculatory bodies.

The combustion of methane-CO_2 blends (Figure 4.21) illustrates how the CRZ increases in size when using the 60° nozzle. This result, contrary to pure methane, was unexpected. Meanwhile, the 30° nozzle produces the smallest CRZs.

In general the addition of CO_2 affects the velocity of the flow. It would have been expected that the velocity of the flow would increase as a consequence of the combustion being closer to stoichiometric conditions. However, it was observed that the total velocity with pure methane provided faster profiles than with methane and carbon dioxide, due to the increasing of negative velocity when burning with CO_2. On other hand the addition of CO_2 increased the density of the mixture which is reflected in the increasing centrifugal force. This leads to an augmenting of the dimensions of the CRZ, with increased width and height compared to that of pure methane under similar conditions (Figure 4.21).

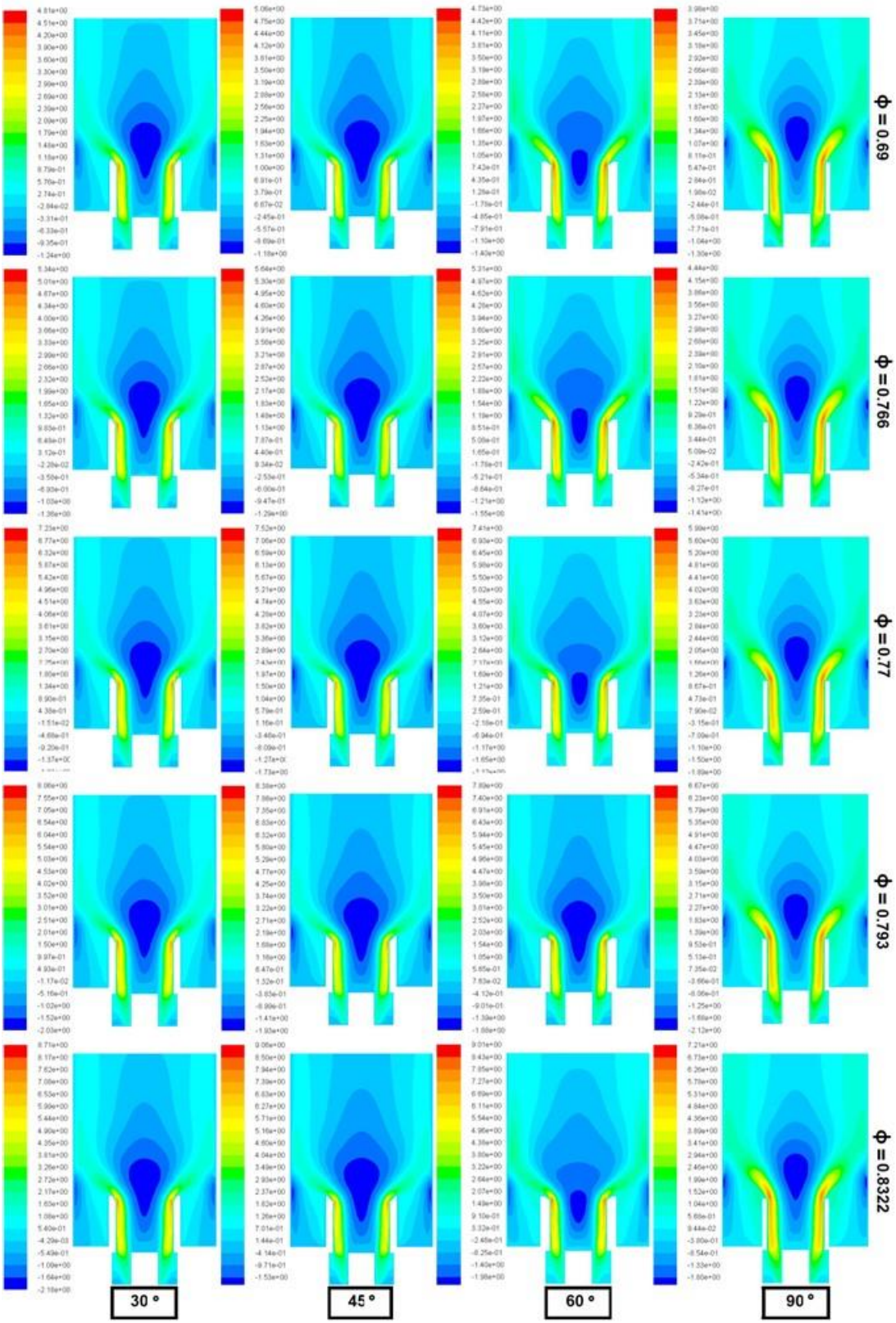

Figure 4-18: Effect of equivalence ratio on the size of the CRZ using pure methane and a Swirl Number of 1.05

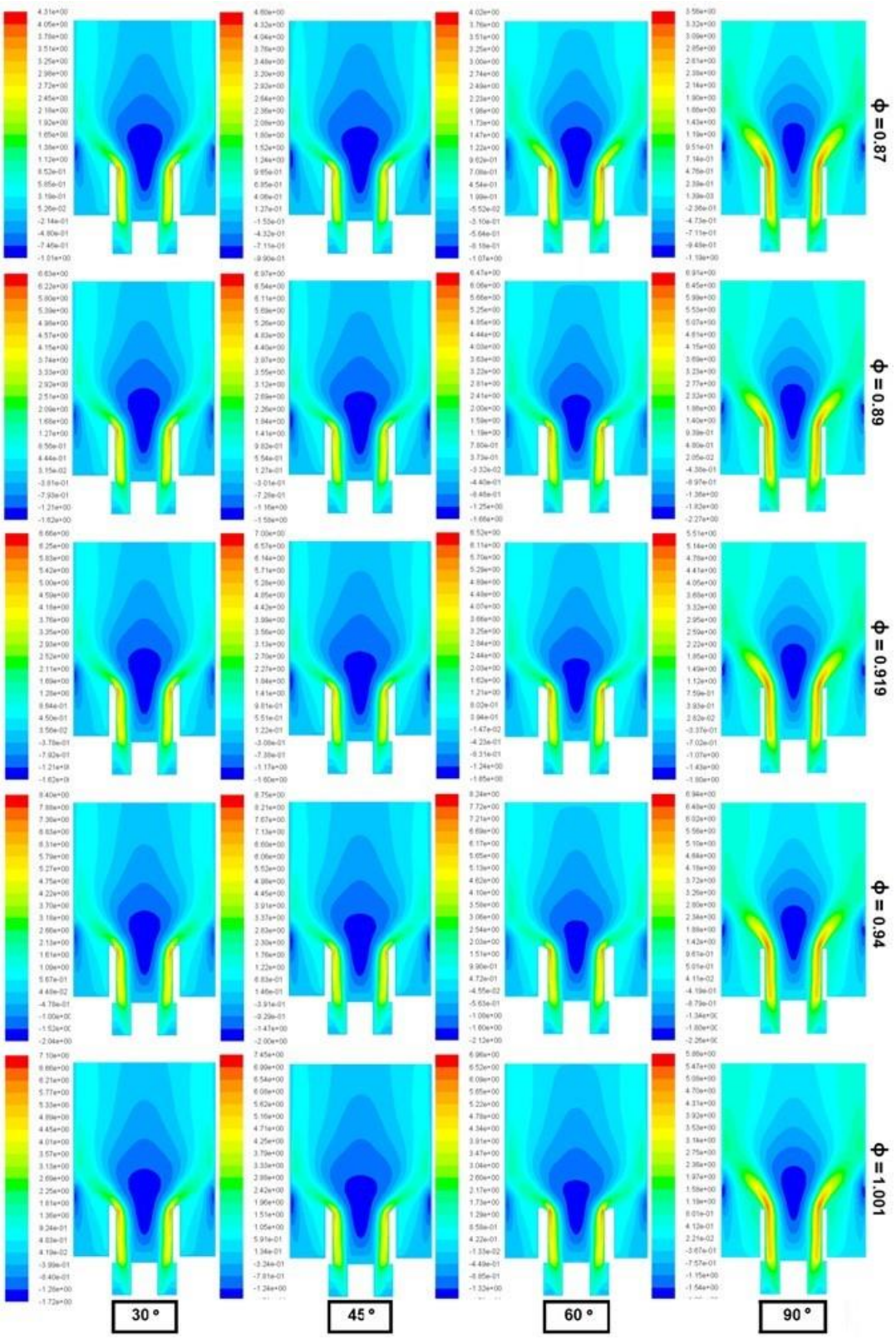

Figure 4-19: Effect of equivalence ratio on the size of the CRZ using methane blended with CO2 and a Swirl Number of 1.0

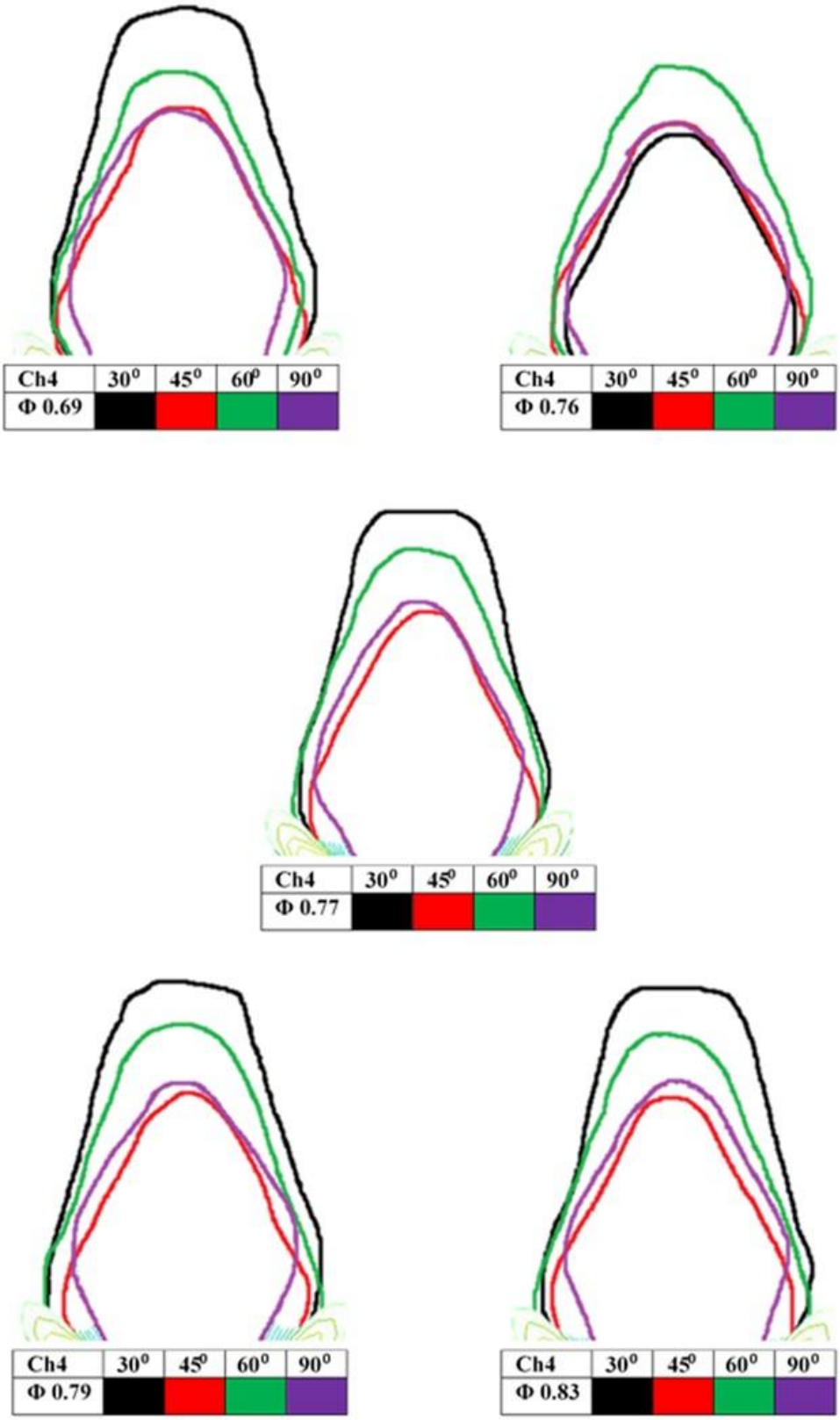

Figure 4-20: Comparison of the CRZ size at different Equivalence ratios with pure methane

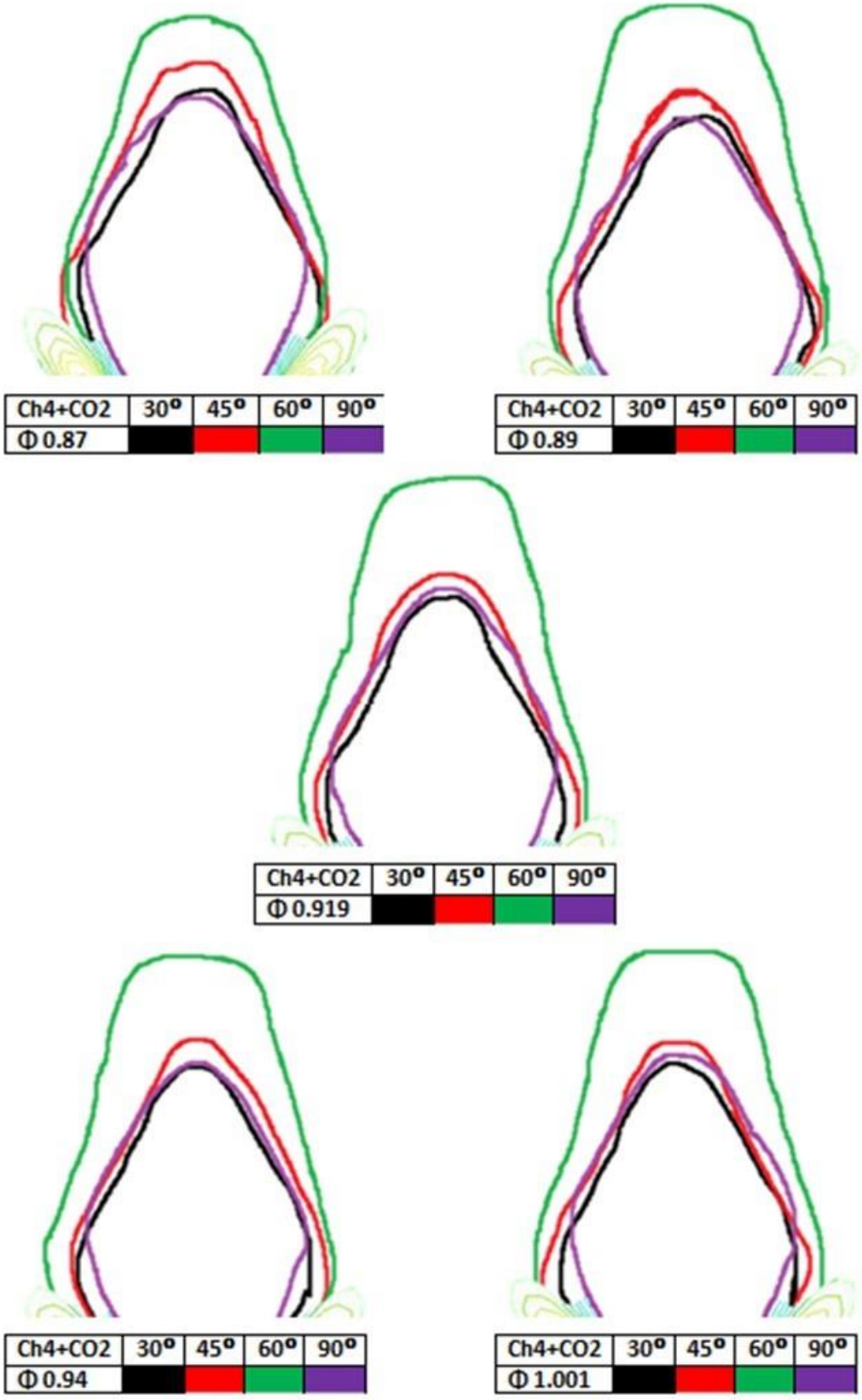

Figure 4-21: Comparison of the CRZ size for methane blends with CO_2

Figure 4.22 illustrates the axial velocity profiles generated when using pure methane and different nozzles at a constant mass flow rate. The smallest CRZ width was observed using the 90° geometry, as expected. Also the 90° nozzle produces higher outlet velocities than the 30°, 45° and 60° nozzles due to the slower expansion and direction of the shearing flow. This reduces the size of the central recirculation zone. The 45° nozzle generates axial velocities that are 60 % slower than the straight 90° geometry, thus allowing a better recovery of the CRZ. This causes an increase in size of CRZ, Figure 4.22.

The profiles measured using methane blended with carbon dioxide are shown in Figure 4.23. They demonstrate the negative axial velocities of the CRZ along the central axis of the burner at a position -0.3 < r/D < 0.3. The introduction of carbon dioxide produces incremental increases in the negative velocities of the recirculation zone, whilst reducing the velocity of the High Momentum Flow Region, thus confirming the effect of combustion in the process and change of the CRZ. For example, the maximum axial velocity of pure methane was obtained at 21 m/s using the 90° nozzle, compared with 12 m/s using methane blended with carbon dioxide and with the same nozzle.

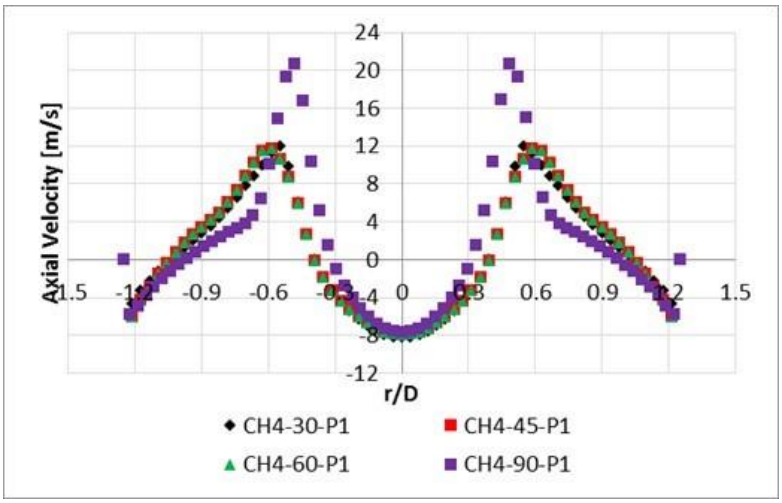

4-22: Comparison of Axial velocity with different angles at y/D=0.00 when using pure methane at φ = 0.83

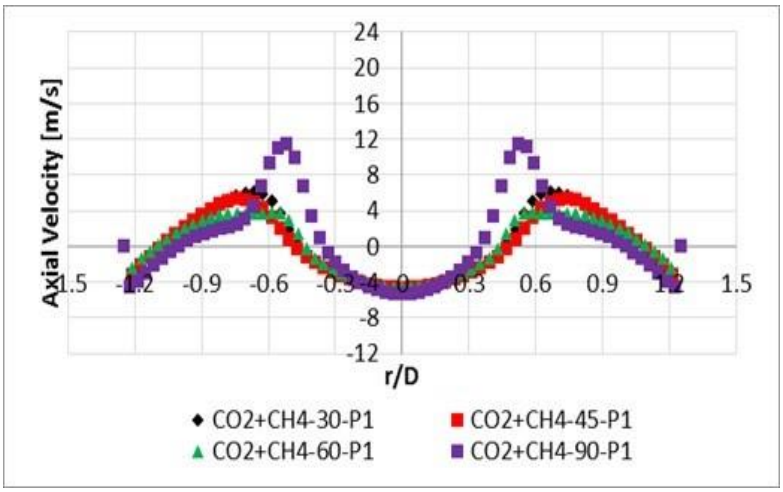

Figure 4-23: Comparison of Axial velocity with different nozzle angles at y/D = 0.00 using methane blended with CO_2, φ = 0.87.

4.4.4 Other Coherent Structures

The High Momentum Shearing Flow Region, illustrated in for both swirl numbers Figure 4.24, represents the divergence of the flow at the outlet of the nozzle. It is clear that an increase in swirl number will produce further expansion in the radial direction with a faster decay of velocity in the azimuthal direction, producing a wider CRZ for the 45° and 30° nozzles.

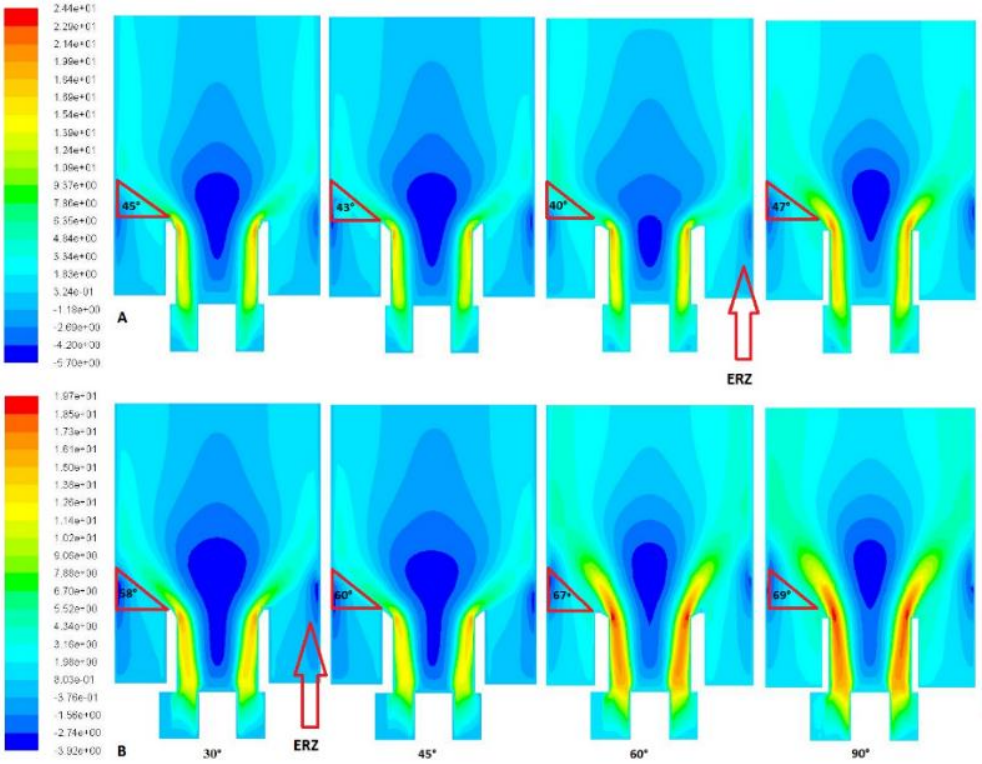

Figure 4-24: Combustion of methane for (A) S = 1.05 and (B) S = 1.50

Nonetheless there was no increase in the CRZ when using 60° and 90° nozzles associated with the geometrical swirl number and nozzle divergence at the same equivalence ratio and mass flow rate. This was due to the reduction of the axial velocity and the increased inlet area which leads to a reduced inlet tangential velocity.

Another structure that was measured and that also appears in these flows is the external recirculation zone (ERZ). Comparisons between cases were performed as shown in Table 4.11 and Figure 4.24. As the angle divergence of the HMFR increases, the size of the ERZ increases. The High Momentum Flow Region seems to become attached to and dragged by the ERZ, as observed elsewhere [136].

Table 4-11: Comparison of corner recirculation zones with both swirl numbers.

	30^0	45^0	60^0	90^0	S
WIDTH	0.22D	0.15D	0.13D	0.22D	1.05
HEIGHT	0.79D	0.94D	0.71D	0.75D	1.05
WIDTH	0.18D	0.22D	0.28D	0.3D	1.50
HEIGHT	0.53D	0.56D	0.79D	0.98D	1.50

4.5 Results and Discussions of confinement conditions

4.5.1 Effect of syngas composition on CRZ size.

Once the pure methane and methane blended with CO_2 had been studied, work progressed to the study of syngas blends. Comparison of CRZ boundaries for syngases 1, 2, 3 and 4 is given in Table 4.5 for 30°, 45°and 60° nozzles at 7.49kW. The velocity and momentum of the flow increased in localised regions of the burner through the High Momentum Flow Region (HMFR) [49]. The appearance of CRZs using different configurations and fuels has demonstrated that the shape and strength of the recirculation zone can change drastically depending on these alterations (Figure 4.25). Table 4.12 shows that the combustion of 4 syngases also produced different central recirculation zones for the different nozzles under the same power loads. Comparison of the CRZ size indicates that the use of a 60° nozzle produces the largest, narrowest structure, as expected.

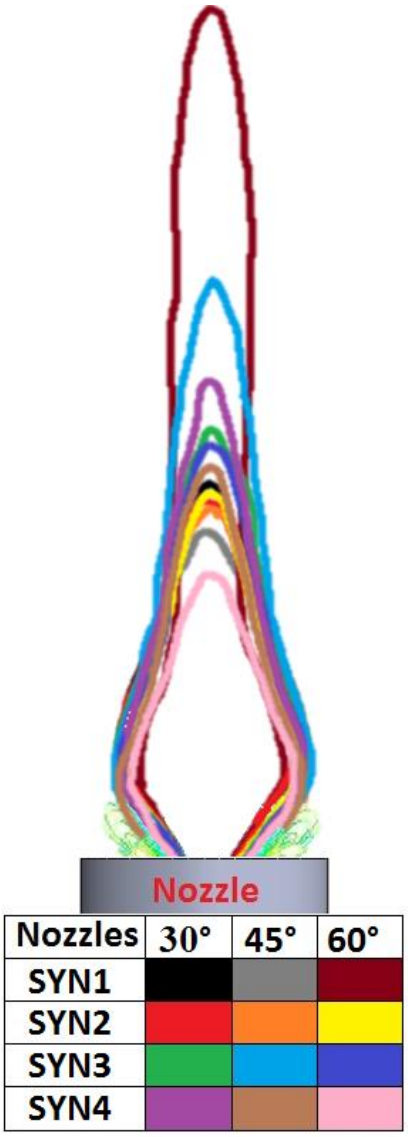

Figure 4-25: CRZ contours using different syngases.

Table 4-12: Comparison of the CRZ size for four syngases and three different angular nozzles

Gas Compositions	30°		45°		60°	
	Width	Length	Width	Length	Width	Length
Syn1(10%CH_4+45%H_2+45%CO)	1.85D	4.7D	1.9D	4.3D	1.4D	9.6D
Syn2(20%CH_4+40%H_2+40%CO)	1.8D	5.2D	1.85D	4.6D	1.8D	4.7D
Syn3(30%CH_4+35%H_2+35%CO)	1.9D	5.4D	1.9D	7.2D	1.8D	5.2D
Syn4(50%CH_4+25%H_2+25%CO)	1.9D	5.8D	1.9D	4.6D	1.7D	4D

When comparing the velocity profiles of all conditions (Figure 4.26) maximum velocities are measured where the shearing flow, i.e. the HMFR, is located. The point at which the flow becomes negatively diverged, where $-0.5 < r/D < 0.5$, indicates that the CRZ is increasing its width whilst the HMFR is getting slimmer and stronger. This

is because of the greater negativity of the recirculation structure, the reactivity of the blend, and the squeeze of the shearing flow. The maximum velocity in the profile was observed with syngas 2 using the 30° nozzle, whilst the lowest velocities were obtained using syngas 4 with a 60° nozzle.

Results also revealed the changes in Damköhler number equation (2.9) across these profiles. An increase of Da along the plenum (Figure 4.28) is observed due to a decrease in the turbulent intensity and an increase in the length scales of the flame (Figure 4.27). At the boundaries of the CRZ the length scales go to a minimum, thus increasing the turbulent intensity and decreasing Da, as is evident in Figures 4.27 and 4.28. The increase/decrease of chemical reaction time also affects Da and flame stretch (Figure 4.28c and Figure 4.29).

Turbulent flame speed equation (3.20) and stretch factors equation (3.25) (Figure 4.29) show different trends depending on the syngas used. For example there is an increase in turbulent flame speed and stretch factors as the hydrogen is increases, as expected. Usage of more hydrogen, i.e. Syngas-1, shows how a faster reactivity shortens the CRZ with 30° and 45°. While increasing in the height of CRZ using a 60° nozzle. Instead of allowing further reduction of the CRZ as progressively observed with the reduction of H_2. The most surprising aspect of the turbulent flame speed values is in the syngas-4 case, which consists of lower amounts of hydrogen. Nevertheless, for this composition it indicates that there is a higher thermal diffusivity, laminar flame speed and Reynolds number. This is because the CRZ had a wider size, which resulted in the increasing of stretch factor due to the excessive flame stretch. As observed in Table 4.13, turbulent flame speed is proportional to the stretch factor.

Table 4-13: Comparison of turbulent flame speed vs stretch factor for different nozzles

Mixture	30°		45°		60°	
	St	G	St	G	St	G
Syn1	1.2	0.8	1.19	0.8	1	0.8
Syn2	1	0.75	1.20	0.89	1.19	0.82
Syn3	0.7	0.59	0.8	0.7	0.99	0.75
Syn4	1.1	0.9	0.9	0.8	1.05	0.82

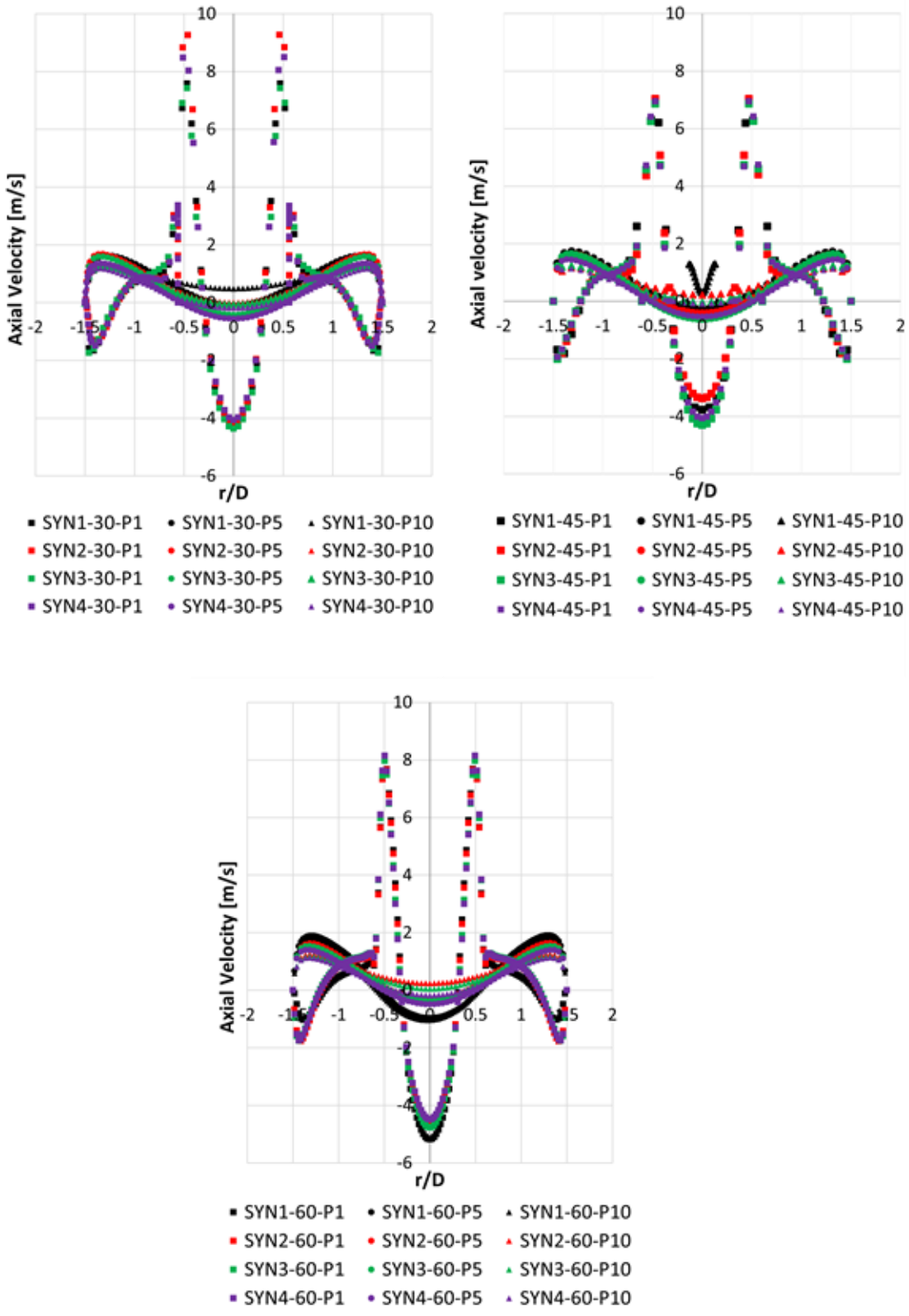

Figure 4-26: Axial velocity using (A) 30° nozzle, (B) 45° nozzle, and (C) 60° nozzle, at 3 different planes: P1, P5 and P10

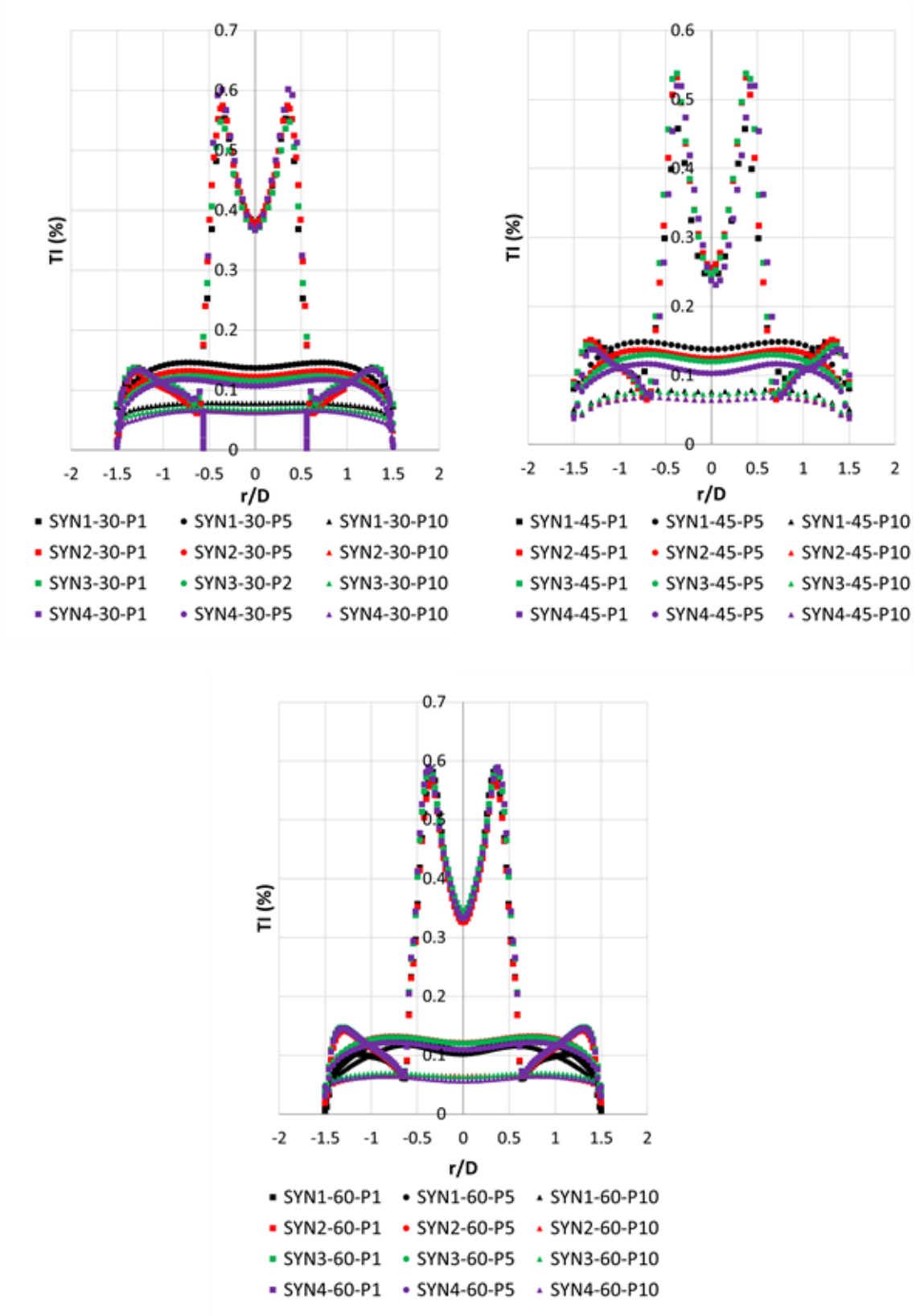

Figure 4-27: Turbulence intensity using (A) 30° nozzle, (B) 45° nozzle, and (C) 60° nozzle, at 3 different planes: P1, P5 and P10

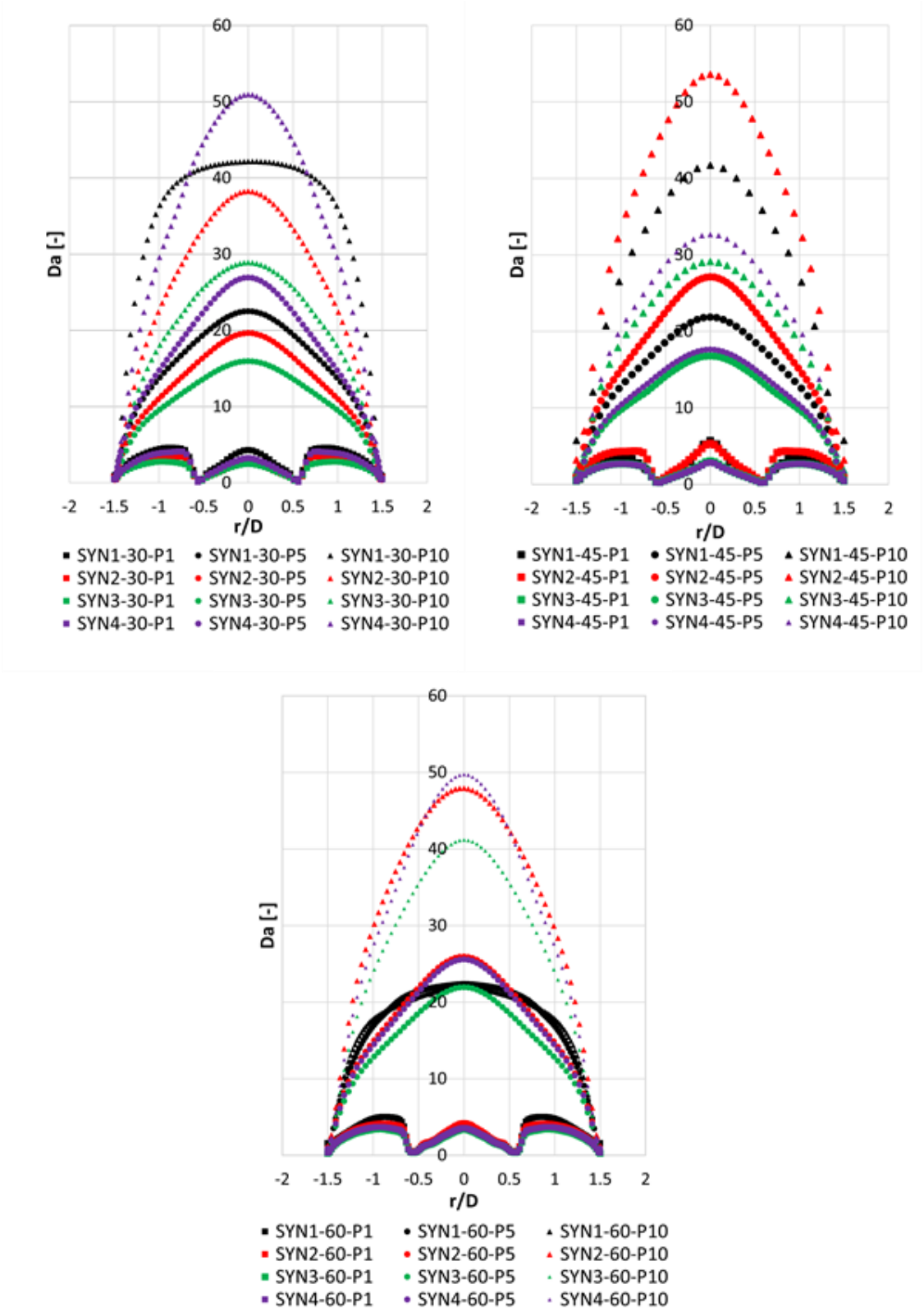

Figure 4-28:Damköhler Number using (A) 30° nozzle, (B) 45° nozzle, and (C) 60° nozzle, at 3 different planes: P1, P5 and P10

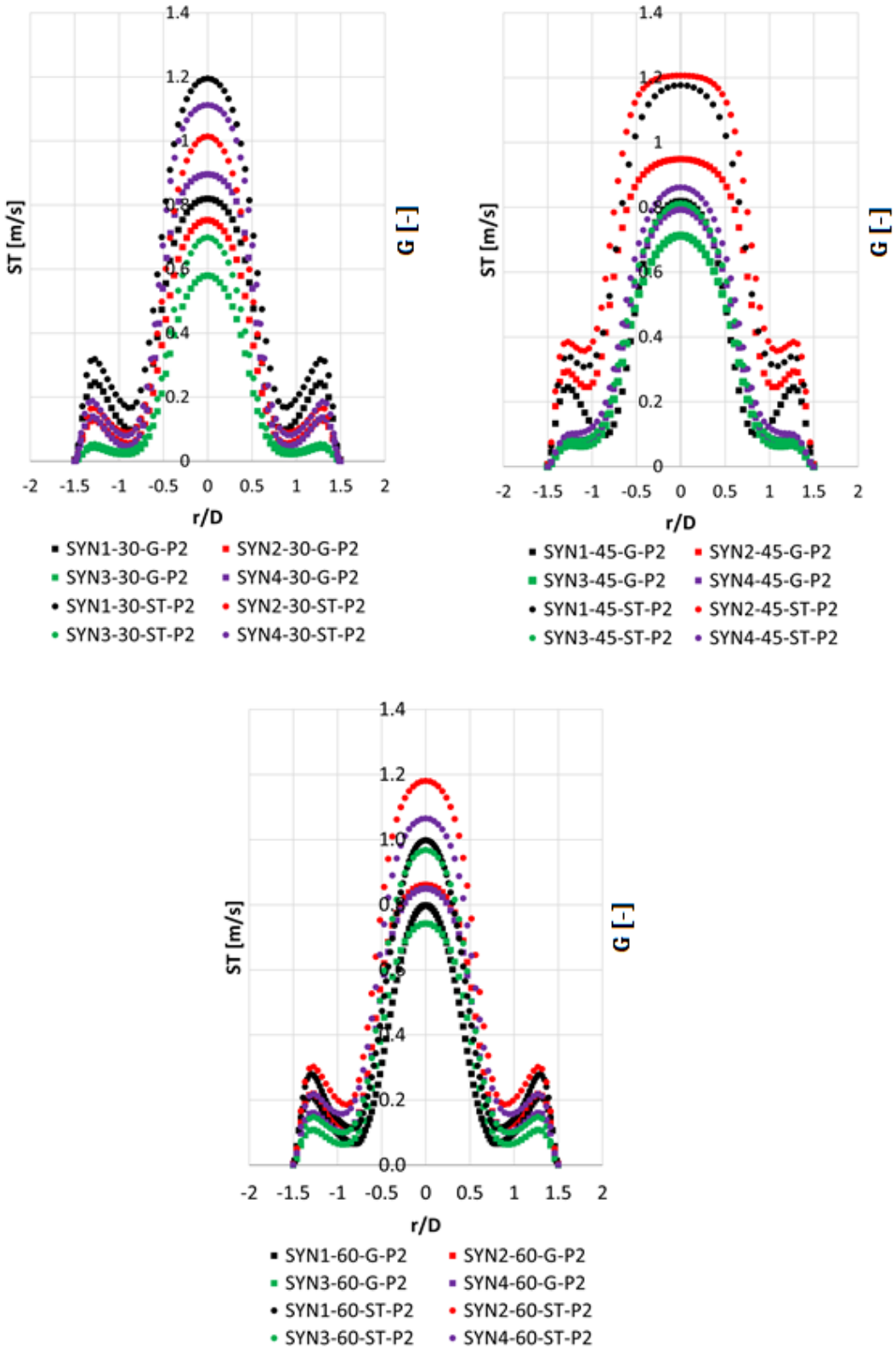

Figure 4-29: Comparison of Turbulent flame speed St with Stretch factor G [-] at plane y/D = 0.714

Figure 4.31 compares the results obtained from the preliminary analysis of the chemical time scale and the percentage of hydrogen in the mixture at the same power output using four syngases with three different nozzles.

Despite the reduction in hydrogen content in syngas 4,the 30° nozzle produced a shorter chemical time reaction (Figure 4.31a), which is due to the higher laminar flame speed and thermal diffusivity in that case. However, there is a quasi-linear reduction between syngas 4 and 3 using 45° and 60° nozzles, while syngas 1 and 2 give a significant reduction due to the higher percentage of hydrogen content in the mixture (Figure 4.31b and 4.31c). The changing divergence angles of the nozzle play an important role in the aerodynamic flow, which expansion through the nozzle causes axial decay of tangential velocity and hence radial pressure gradient. Thus, there is a change in the size of the central recirculation zone, which in turn alters the swirl number and equivalence ratio in the combustion regime.

Following the addition of hydrogen to the mixture, a significant decrease of Da number is observed. This is due to the faster chemical reaction correlated to another issue of changing the geometry for example nozzles angles. This effect will depend on the shape and strength of the CRZ, which affects Da and gives a different trend using different nozzles for the same gas (Figure 4.30).

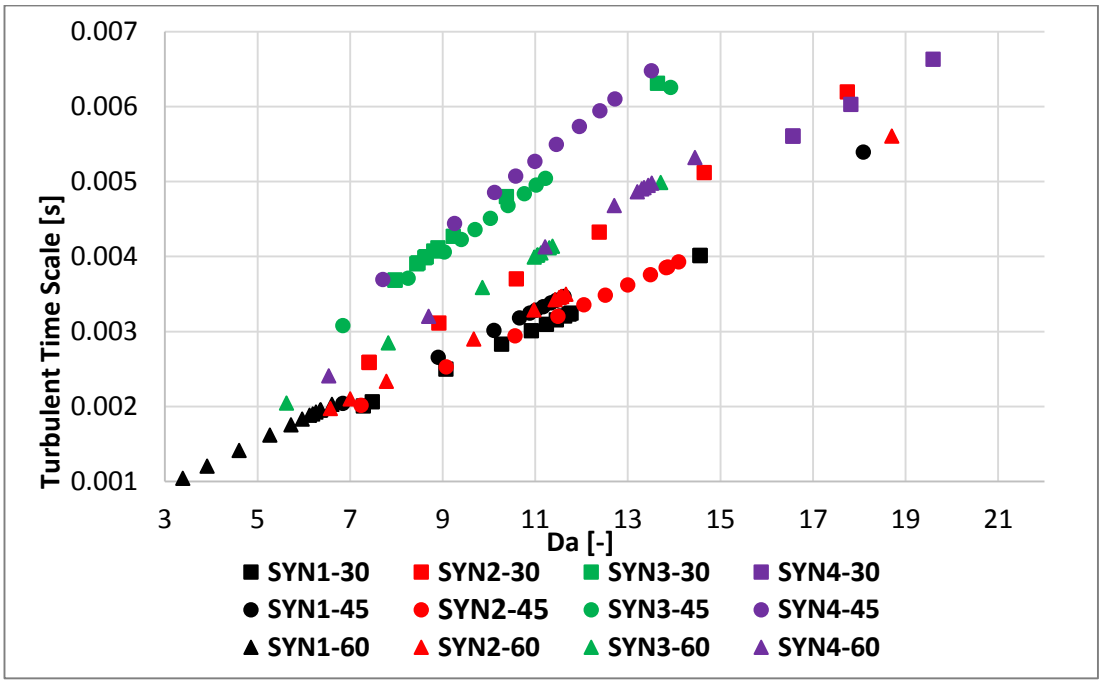

Figure 4-30: Turbulent timescale vs Damkohler number

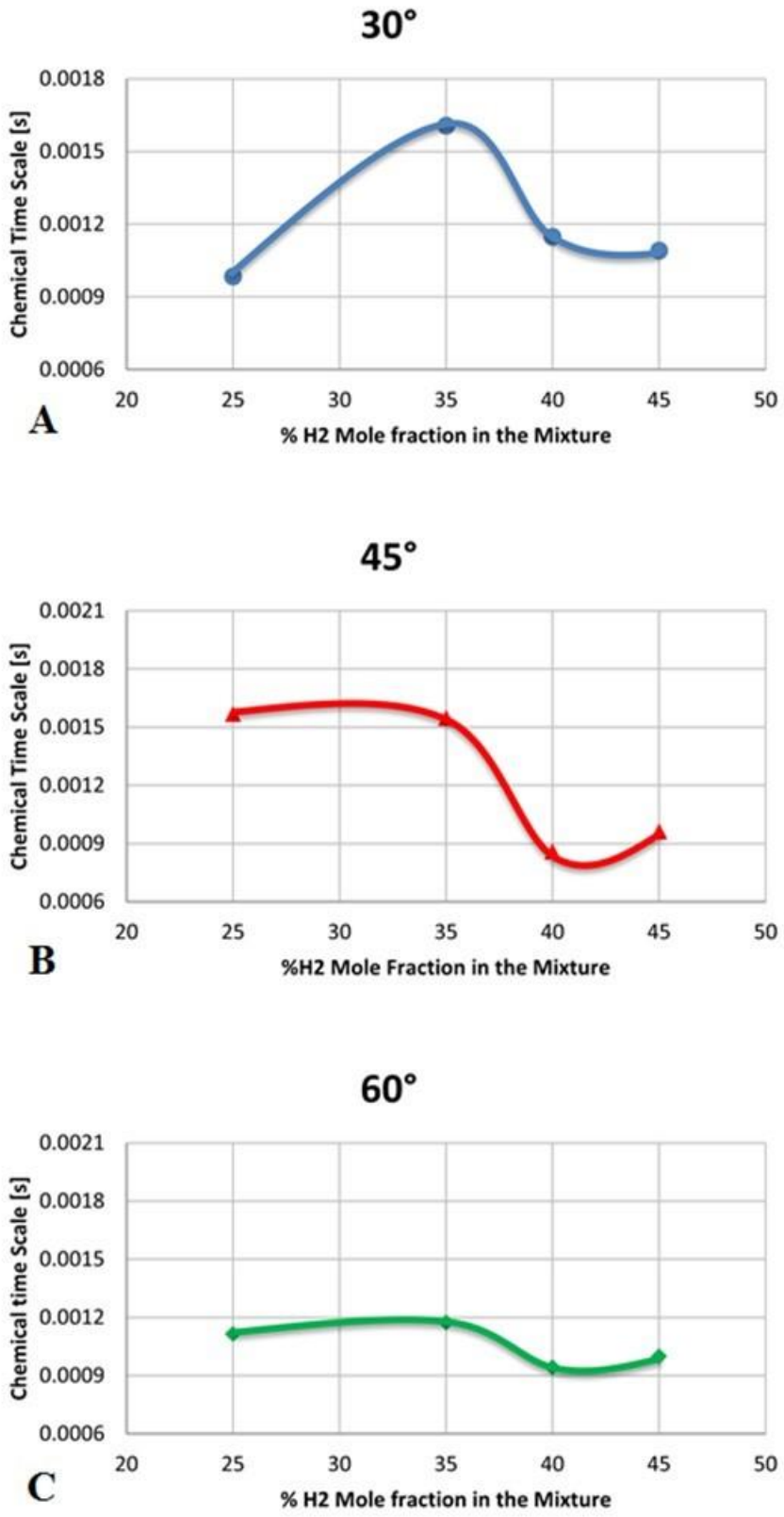

Figure 4-31: Chemical time scale vs H2 mole fraction in the mixture

4.6 Results and Discussions of open conditions

Different profiles of the CRZ for syngases 1, 2, 3 and 4 using 30°, 45° and 60° nozzles at 7.49kW were produced as a consequence of the different reactions and combustion swirl numbers (Figure 4.32). The velocity and momentum of the flow increases in localised regions of the burner through the High Momentum Flow Region [49].

The shape and strength of the CRZ can change dramatically depending on the use of different configurations and fuels (Figure 4.32; Table 4.15). Comparison of the CRZ size via CFD calculations and experimental results (Chapter 5), indicates that the use of the 60° nozzle produces the largest structure (Figure 4.32b; Table 4.14; Table 4.15). The worst predictions were obtained using the 30˚ nozzle with the slowest syngas (Syngas-4), and the 60° nozzle with the fastest syngas (Syngas-1). This lack of accuracy could be linked to 3-Dimensional large structures such as the PVC or HMFR that are not accurately predicted with this model and are not properly resolved as they are fast reaction phenomena.

Table 4-14: Comparison of CRZ size (experiment)

	30°		45°		60°	
	Width	length	Width	length	Width	length
SYN1	1.35D	1.92D	0.97D	1.73D	1.01D	1.43D
SYN2	1.50D	2.44D	1.28D	2.07D	1.13D	2.41D
SYN3	1.54D	1.95D	1.43D	2.86D	1.24D	2.41D
SYN4	2.11D	3.12D	1.43D	2.22D	1.24D	3.16D

Table 4-15: Comparison of CRZ size (CFD)

	30°		45°		60°	
	Width	length	Width	length	Width	length
SYN1	1.33D	2.00D	0.90D	1.94D	1.13D	1.80D
SYN2	1.47D	2.34D	1.27D	2.07D	1.20D	2.41D
SYN3	1.33D	1.74D	1.33D	2.67D	1.13D	2.41D
SYN4	1.60D	2.67D	1.34D	2.27D	1.14D	2.63D

It is evident from Table 4.16 that there is no significant difference between the experimental results and the CDF results. Accordingly, the CFD approach can predict the size of CRZ in the case of 3D confinement.

Table 4.12 and Figure 4.25, in the previous section, showed the numerical results in the case of confinement, illustrating the length and width of each gas, using three different nozzles.

Table 4-16: Comparison of numerical and experimental size of CRZ.

Gas mixture	30°		45°		60°	
	Width (%)	Length (%)	Width (%)	Length (%)	Width (%)	Length (%)
SYN1	1.48	4.17	7.2	12.1	11.8	25.8
SYN2	2	4.09	0.78	0	6.19	0
SYN3	13.6	10.7	6.9	6.6	8.87	0
SYN4	24	14	6.2	2.2	8	16

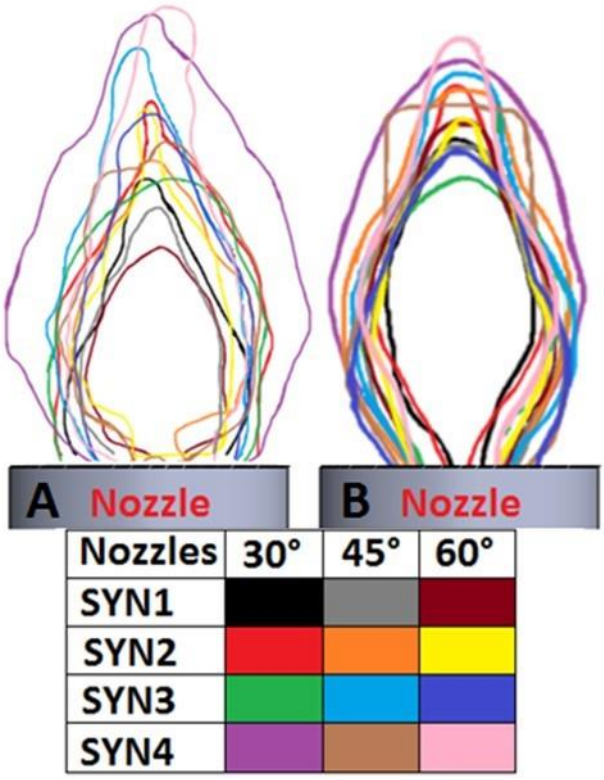

Figure 4-32: Comparison of CRZ size between (A) experiments and (B) CFD

The composition of syngas can vary widely depending on the source and processing technique. The change in fuel type and composition usually leads to significant changes in the characteristic time scale of chemical reactions in the combustion system, which consequently has a major impact on combustion operability including flashback, auto-ignition, lean blowout, and combustion dynamics.

Increasing the mole fraction of hydrogen in the mixture produces a faster chemical reaction (Figure 5.23) due to the higher thermal diffusivity of the hydrogen and the laminar flame speed. The syngas-1 mixture had a chemical time scale smaller than the other gases due to the large amount of hydrogen in the mixture. However, the there is a considerable reduction in chemical time scale of syngas 4, which has a small amount of hydrogen when using nozzle 30°. Regarding turbulence and reaction times, results were obtained using CFD to account for the 3 components of the velocity flow-field. Increasing the mole fraction of hydrogen in the mixture produces faster chemical reactions, Figure 5.23, and shorter turbulent time scales, Figure 4.30, due to the higher thermal diffusivity of hydrogen and laminar flame speed, as expected. However, two interesting phenomenon occur using a) Syngas-3 and nozzle 45˚, and b) Syngas-4 with a 30˚ nozzle, respectively. For the first case, the lowest chemical time scale is produced using 40% CO and an angle with moderate shear, a phenomenon previously hypothesized to occur as a consequence of the inhibiting nature of CO at these H_2 concentrations. On the other hand, the case with Syngas-4 using a 30˚ nozzle has been previously depicted as a condition where the CRZ-PVC interaction would show its highest impacts. However, as observed in Table 4.16, the assertions for this blend would need to be correlated with more advanced turbulence models.

4.7 Summary

Simulations were performed using all syngases with variable outlet configurations using under premixed conditions with FLUENT 14.5. All the CFD analyses were conducted using the same output power under both confined and unconfined conditions. The appearance of CRZs in the different configurations and difference fuel compositions has demonstrated that the shape and strength of the recirculation zone can change drastically depending on the fuel and configuration used.

CFD predictions of swirl burner aerodynamics show how variable outlet configurations and gas compositions change the CRZ patterns.

The addition of CO_2 in the blend with methane can be of great importance in changing or controlling the CRZ. It is clear that the size of the CRZ is affected by the use of CO_2, and the outlet nozzle angles. Changing the angle of the nozzle controls the direction of the shear flow. This in return could be beneficial for new blends by increasing the residence time of the products/reactants of these and other fuel/diluent compositions.

Carbon dioxide contained in the fuel leads to a lowering of the flame temperature, the effect of which is to reduce emissions of NO. However, it has been demonstrated that the increase of CO_2 can produce CRZs that can be detrimental to the flow, with some critical concentration of CO_2 leading to flame extinction.

It is clear that the increase in swirl number will produce further expansion in the radial direction, with a faster decay of velocity in the azimuthal direction, producing wider CRZs using 45° and 30° nozzles. Nonetheless there was no increase in the CRZ using 60° and 90° nozzles associated with the geometrical swirl number and nozzle divergence at the same equivalence ratio and mass flow rate. This was due to a reduction of the axial velocity and an increased inlet area of vanes which reduces the tangential velocity.

The addition of CO_2 produces longer recirculation zones that collapse suddenly and far away from the nozzle. The high turbulence of the CRZ when using CO_2 can also be an important parameter in the addition of other species that can improve the combustion process whilst recirculating CO_2 for other applications, e.g. carbon capture and storage.

When the swirl burner combustor is fired into a variable outlet configuration, with a variation of fuel types, swirl number, equivalence ratio and mass flow rate, significant changes of the recirculatory structures can be produced.

Combustor exit nozzles were of benefit in restricting the CRZ size and reducing the possibility of flame impingement on the fuel injectors. The angled nozzles produced compact CRZs associated with changes in pressure distribution, pressure decay and interaction with the shearing flow.

The results showed that for all nozzles the combustion of the 4 syngases produced different central recirculation zones under the same power loads. Measurements indicate that the 60° nozzle produced the largest, narrowest CRZ structure, while the syngas 4 with the 30° nozzle produced the widest CRZ.

The addition of hydrogen into the mixture caused a significant decrease of Da number as consequence of faster chemical reaction. This correlated with the effects of changing the geometry, for example nozzles angles, which affects the shape and strength of CRZ. This will alter the change of Da giving different trend using different nozzle at the same gas.

Increasing the hydrogen results in a faster reactivity and a shorter CRZ, even with a 60˚ nozzle. Instead of allowing further growth of the CRZ, as progressively observed with the reduction of H_2, the combustion process collapses the recirculation zone closer to the nozzle. On the other hand, the use of a 30˚ nozzle generates wider

structures. The reduction of hydrogen elongates the CRZ as a consequence of a delayed pressure decay. This occurs because of the lower reactivity of the blend. As the nozzle angle is increased to 45˚, more intense interaction between the CRZ and the shearing flow encourages the combustion reaction, thus reducing the size of the CRZ. This phenomenon could be linked to the shortening of the CRZ using Syngas-1 with the 60˚ nozzle.

Confinement can dramatically alter the size and shape of the CRZ and the External Recirculation Zones formed as the swirl burner flow expands. However, the use of different blends also considerably affects the size of the structure, impacting on the turbulence intensity and interactions between structures and shearing flows across the boundaries of the flame.

SST-k-ω turbulence models do not depict accurately the high reactivity and shearing phenomena of fast blends, whilst they under-predict the impacts produced by coherent structure interactions in slow blends. More advanced models need to be used for these conditions. However, the model shows high accuracy for the transitional conditions (medium speed blends), reducing computational costs and providing strong correlation.

CHAPTER5

CHAPTER 5

BLOWOFF EXPERIMENTS

5.1 Results and Discussions

5.1.1 Isothermal Experiments

The DI-2200 is an FFT (Fast Fourier Transform) analyser that is capable of measuring, processing, and displaying flow patterns. The first harmonic was found in all cases and permitted the characterisation of each flow. The presence of second and third harmonics allowed the selection of cases for more detailed analysis figure 5.1. During the experiments a regular periodic motion was observed, with frequencies which increased quazi-linearly with flowrate. The relationship of the Strouhal number with the Reynolds number is clearly evident, showing an independent relationship at high Re. It is clear that all harmonics are constant at high Re, as discussed by Syred [39].

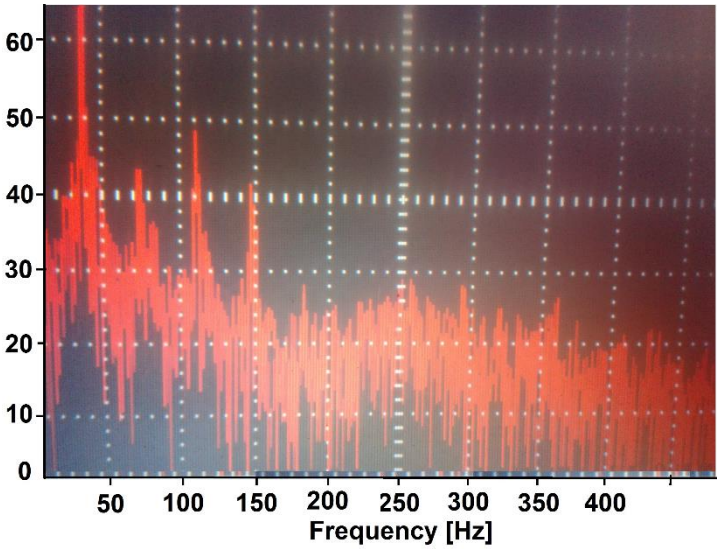

Figure 5-1: FFT Analysis, showing the presence of strong harmonics.

The Strouhal number showed a linear trend, as previously observed with other swirl burners[28,45].Thus, a clear appearance of the recirculation zone/precessing vortex core system was evident. This vortex system is created by the swirl motion as a consequence of the energy exchange between structures. It takes helical shape and is

defined by the CRZ when it has passed the burner nozzle. Figure 5.2 shows the precessing vortex core (PVC) and central recirculation zone (CRZ) produced by the sudden expansion of the flow as it leaves the burner nozzle as a consequence of the generated pressure gradients. A comparison of the Strouhal numbers was also performed between the unconfined and confined configurations. The dependency of Strouhal number on the frequency is evident, showing an approximately linear relationship at high frequency, coupled with Reynolds number because as the Re is increased the frequency increases. This phenomenon happens with three frequencies and it is clear that harmonics are constant at high frequency (high Re) for all cases (Figure 5.3).

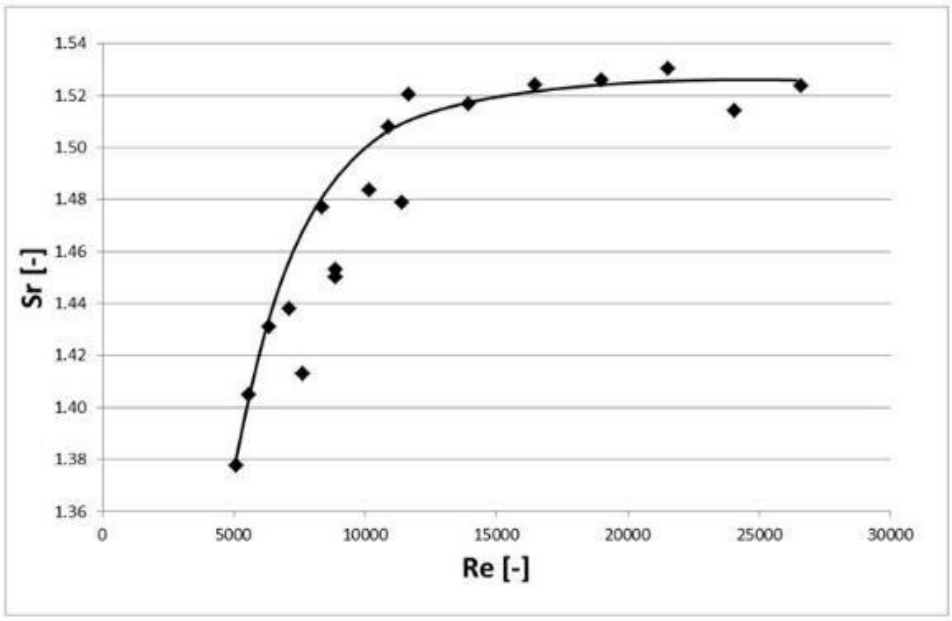

Figure 5-2: St vs Re, experimental analysis, isothermal conditions

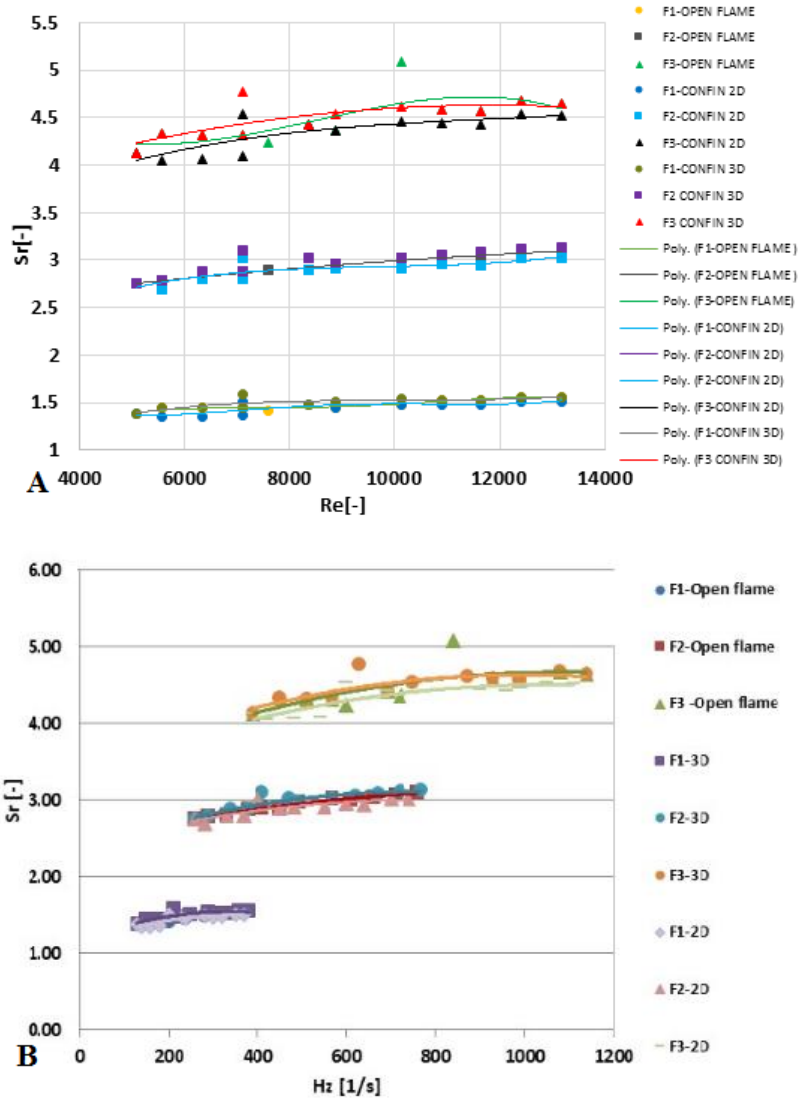

Figure 5-3: Comparison A (St vs Re) B (St vs Frequency) of isothermal experiments

5.2 Blowoff limits with different gases and geometries

According to Lefebvre [14] , the blowoff limit can be determined in two ways, either: (a) stable combustion is established at a fixed air mass flow rate and the fuel flow rate is varied until extinction occurs, or (b) the fuel flow rate is kept constant, and the air mass flow rate flow is increased to the point of extinction. In this work the second method was chosen. Once the flow was stable and the flame was stabilised, the air mass flow rate was increased gradually until blowoff occurred.

5.2.1 Blowoff limits of methane

Premixed combustion experiments using pure methane as a baseline were performed to determine the blowoff limits using 1 unconfined and 2 confined conditions. Confinement improved the blowoff limits due to the reduction of air interaction with the flame, as expected. Figure 5.4 shows the comparison of the three cases. The equivalence ratio of the open flame case was $\phi \approx 0.6$, while the blowoff equivalence ratio with confinement was reduced to 0.4. There is a slight difference between the two confined cases, with the 3D case being better, as shown in Figure 5.4D.

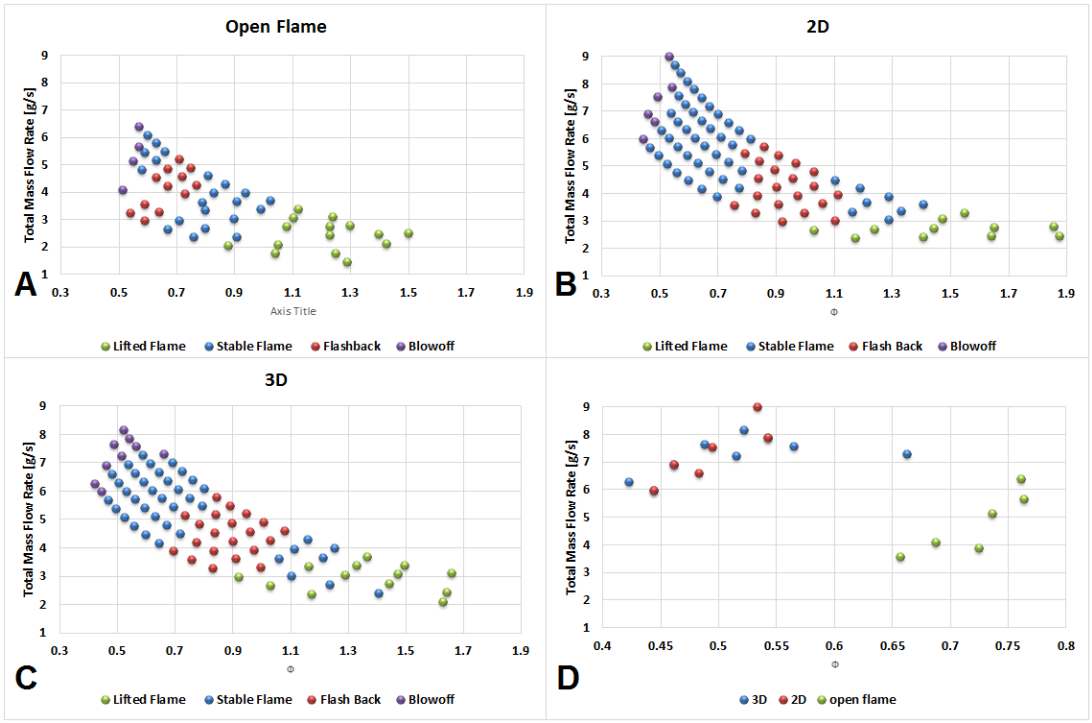

Figure 5-4: (A-C) Blowoff limits for different geometries; (D) Comparison between blowoff cases

5.2.2 Blow-off limits of methane blends with CO_2

Premixed combustion using pure methane blended with carbon dioxide was performed to determine the blowoff limits using open flame conditions for two different nozzle geometries. Measurements were obtained for pure methane and then for different concentrations of CO_2 (Table 5.1). CO_2 and CH_4 flow rates were set to constant. The

air was then gradually increased until blowoff was achieved. Due to the interest shown in lean combustion processes because of the reduced emissions [39] ,the chosen flow rates of methane were low enough to allow operation in the lean region of the mixture.

The injection of CO_2 and the variation in geometry seem to have a significant influence on the blowoff limit (Figure 5.5). The increase in carbon dioxide from 0.13 g/s to 0.89 g/s clearly shows the progression and movement of the limits of this instability, reducing the resistance of the flame as the diluent is augmented. The higher the CO_2 flow rate, the higher the equivalence ratio at which blowoff occurs. This fact indicates that operating in extra lean conditions may be impossible when CO_2 is added to the combustion mixture in an entirely premixed manner.

Table 5-1: Blowoff limits of CO_2 blended with pure methane

Angular nozzle										
Air g/s	**CH_4** g/s	Air g/s	**CH_4** g/s	Air g/s	**CH_4** g/s	Air g/s	**CH_4** g/s	Air g/s	**CH_4** g/s	**CO_2 (g/s)**
4.88	0.2	6.5	0.3	7.91	0.4	9.51	0.5	11	0.6	0.00
4.8	0.2	6.43	0.3	7.81	0.4	9.33	0.5	10.91	0.6	0.13
4.52	0.2	6.23	0.3	7.62	0.4	9.27	0.5	10.67	0.6	0.27
4.38	0.2	6.05	0.3	7.39	0.4	9.10	0.5	10.44	0.6	0.46
4.14	0.2	5.81	0.3	7.21	0.4	8.74	0.5	10.27	0.6	0.69
3.87	0.2	5.59	0.3	7.08	0.4	8.54	0.5	`9.96	0.6	0.89
Flat nozzle										
Air g/s	**CH_4** g/s	Air g/s	**CH_4** g/s	Air g/s	**CH_4** g/s	Air g/s	**CH_4** g/s	Air g/s	**CH_4** g/s	**CO_2 (g/s)**
4.96	0.2	6.71	0.3	8.17	0.4	9.54	0.5	11.21	0.6	0.00
4.82	0.2	6.5	0.3	8.13	0.4	9.48	0.5	10.07	0.6	0.13
4.65	0.2	6.29	0.3	7.9	0.4	9.36	0.5	10.87	0.6	0.27
4.42	0.2	6.02	0.3	7.58	0.4	9.15	0.5	10.69	0.6	0.46
4.25	0.2	5.91	0.3	7.44	0.4	9.02	0.5	10.51	0.6	0.69
4.16	0.2	5.72	0.3	7.07	0.4	8.77	0.5	10.34	0.6	0.89

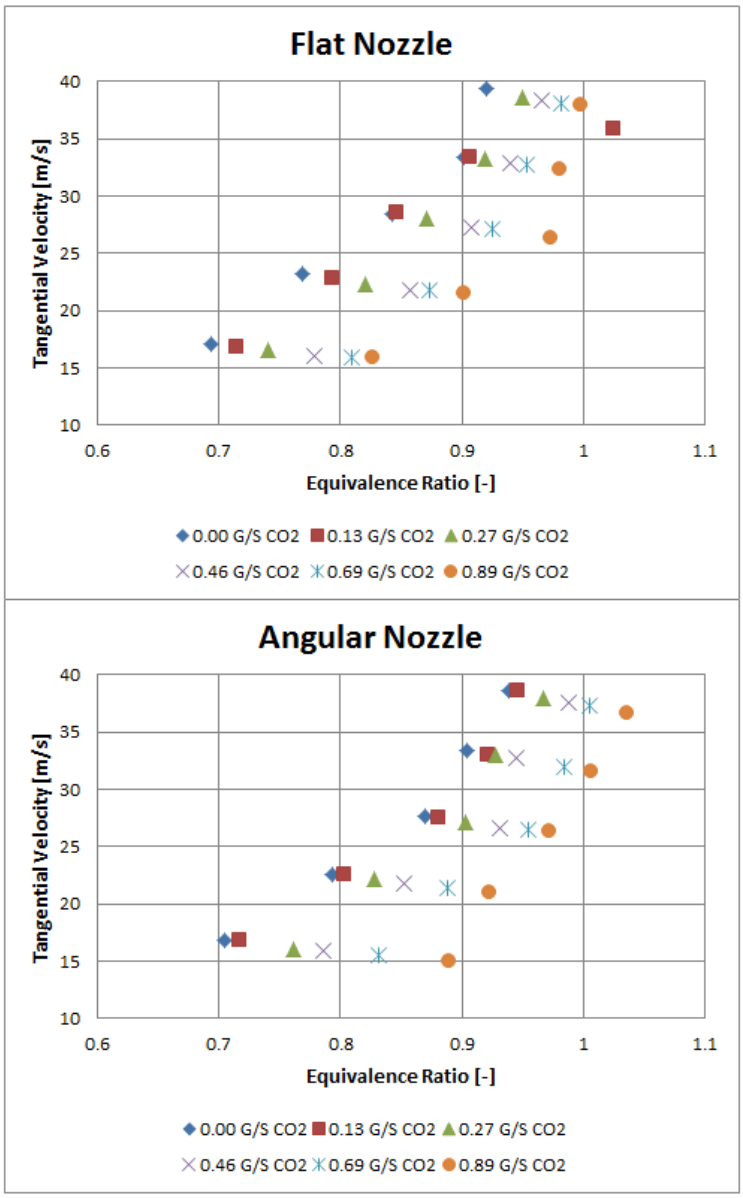

Figure 5-5: Experimental Comparison of CO_2 blended with pure methane for deferent geometries

5.3 Effect of changing gas composition upon blowoff mechanism

5.3.1 CO_2 Addition to methane flames

An increase in the flow rate of the mixture will augment the intensity of the shear layer, which will converge into a new structure known as the High Momentum Flow Region (HMFR), which is highly correlated with the CRZ [49]. Visualisation

experiments were carried out using Stereo PIV. Blends were set at the same powers outputs, adding the same quantity of CO_2 as is used for the real fuel. This increases the strength of the CRZ but reduces its dimensions (Figures 5.6 and 5.7). Table 5.2 shows the results of the Stereo PIV analysis. The total velocity in the system increases during the last experiments, being reduced in the first case due to the high negative velocity of the CRZ. The addition of CO_2 affects the velocity of the flow. It would be sensible to expect that the velocity of the flow would increase as a consequence of the combustion being closer to stoichiometric conditions. However, it was observed that the total velocity with pure methane provided faster profiles than with methane and carbon dioxide. Not only does the increase in temperature using pure methane account into this process, but the CRZ also has increases its strength and negativity. At the same time, it seems that the scale of the CRZ with CO_2 increases to a width of 1.14D and height of 1.78D (Test Point 2) compared to a width of 1.07D and a height of 1.50D for pure methane under similar equivalence ratios (Test Point 10, Figures 5.6 and 5.7).

Table 5-2: Turbulence intensity and CRZ size using the 45° nozzle

Test	Gas composition CH_4+CO_2	Field TI%	TI% CRZ	Φ [-]	Width of CRZ [m]	Height CRZ [m]	Width	Height
1	$0.13CH_4+0.13CO_2$+2.57 AIR	2.57	0.79	0.87	0.033	0.069	1.17D	2.4D
2	$0.156CH_4+0.156CO_2$+3.01AIR	2.25	0.77	0.89	0.032	0.050	1.14D	1.78D
3	$0.21CH_4+0.21CO_2$+3.93AIR	2.33	0.85	0.91	0.032	0.055	1.14D	1.96D
4	$0.24CH_4+0.24CO_2$+4.12AIR	2.53	0.81	1.00	0.033	0.046	1.17D	1.64D
5	$0.27CH_4+0.27CO_2$+4.94AIR	2.28	0.80	0.94	0.032	0.049	1.14D	1.75D
Test	**Gas composition CH_4**	**Field TI%**	**TI % CRZ**	**Φ [-]**	**Width of CRZ [m]**	**Height CRZ [m]**	**Width**	**Height**
6	$0.13CH_4$+3.2AIR	3.18	0.68	0.69	0.030	0.052	1.07D	1.85D
7	$0.156CH_4$+3.5AIR	2.38	0.68	0.76	0.030	0.045	1.07D	1.6D
8	$0.21CH_4$+4.69AIR	2.16	0.68	0.77	0.032	0.042	1.14D	1.5D
9	$0.24CH_4$+5.2AIR	3.22	0.67	0.79	0.032	0.042	1.14D	1.5D
10	$0.27CH_4$+5.58AIR	2.14	0.68	0.83	0.030	0.042	1.07D	1.5D

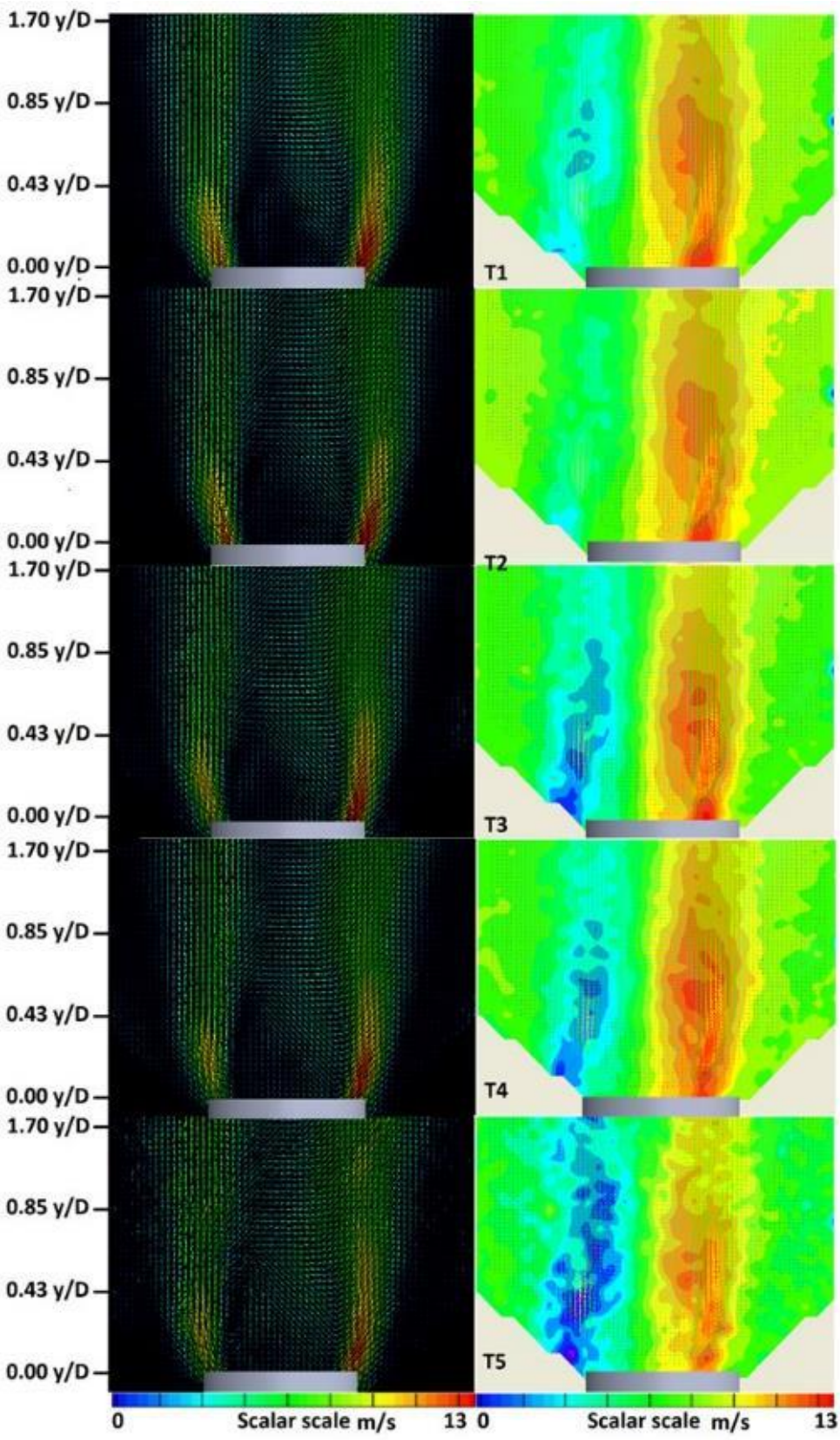

Figure 5-6: Vectors map and Stereo PIV results, respectively, using methane with a 45° nozzle. The PIV results show the tangential velocity in the colour scale

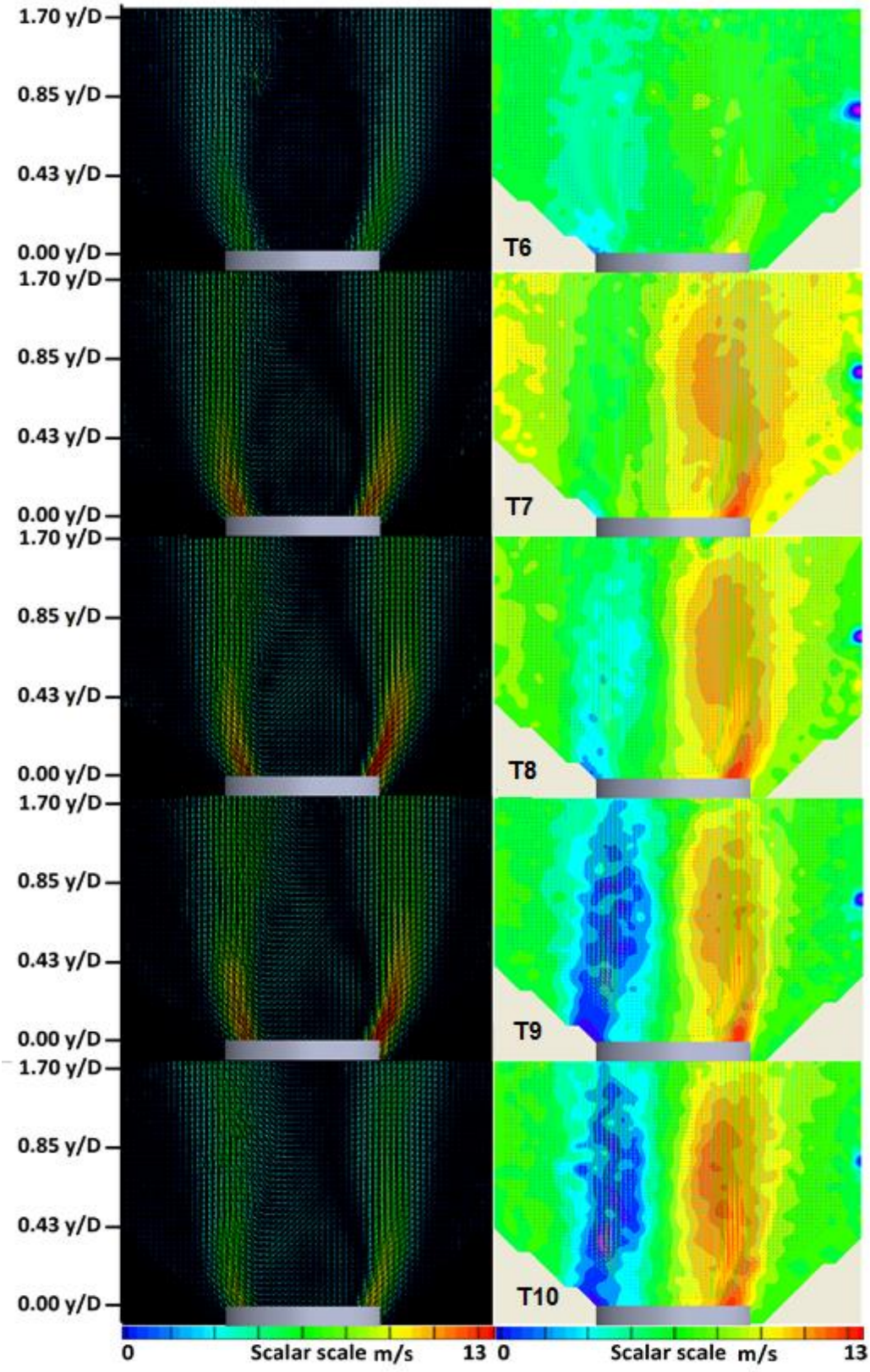

Figure 5-7: Vector maps and Stereo PIV results using methane and carbon dioxide with a 45° nozzle. The colour scale of the PIV data depicts the tangential velocity.

It is worth noting that, given the experimental conditions, the lowest achievable equivalence ratio of CO_2 (0.89 g/s) is almost equal to the highest equivalence ratio of methane/air combustion. This is encouraging, as the CO_2 could increase the strength of the CRZ whilst keeping maintaining the equivalence ratio required for blowoff. This could enhance the recirculation of other products in the field, augmenting their residence time whilst keeping the same power outputs. Moreover, the use of different geometries seems to give similar results (Figure 5.5), although the recirculation zones are different, as observed by Valera-Medina et al. [36]. It was expected that the different CRZs would provide different results as a consequence of the greater bending when using the 45^0 nozzle. Thus, it seems that the mechanism is influenced by Da, with a minimal influence from the radial moment of the flow. It would appear from the results in Figures 5.6 and 5.7 that the higher the density of CO_2 the higher the centrifugal forces (Equation 2.9), which in turn increases the CRZ. However, the size increment of the CRZ does not seem to be a major contributor to the blowoff limit under the conditions studied.

These assertions can also be seen in Table 5.2, where the turbulence intensity (TI) and CRZ size for the 45° nozzle can be compared. It is clear that the use of CO_2 increases by almost 20 % the turbulence of the structure (i.e. TI% CRZ), whilst augmenting its width and length by around 10%. The length of the recirculation zone increases due to the reduced reaction time of the blend and the higher turbulence inside of the structure. Figure 5.8 shows the progression of the CRZ and its boundaries, defined as a region of greater turbulence compared to the pure methane case. It is clear that the CRZ formed using CO_2 has increased in size whilst increasing the inner turbulence of the system at the same fuel flow rates.

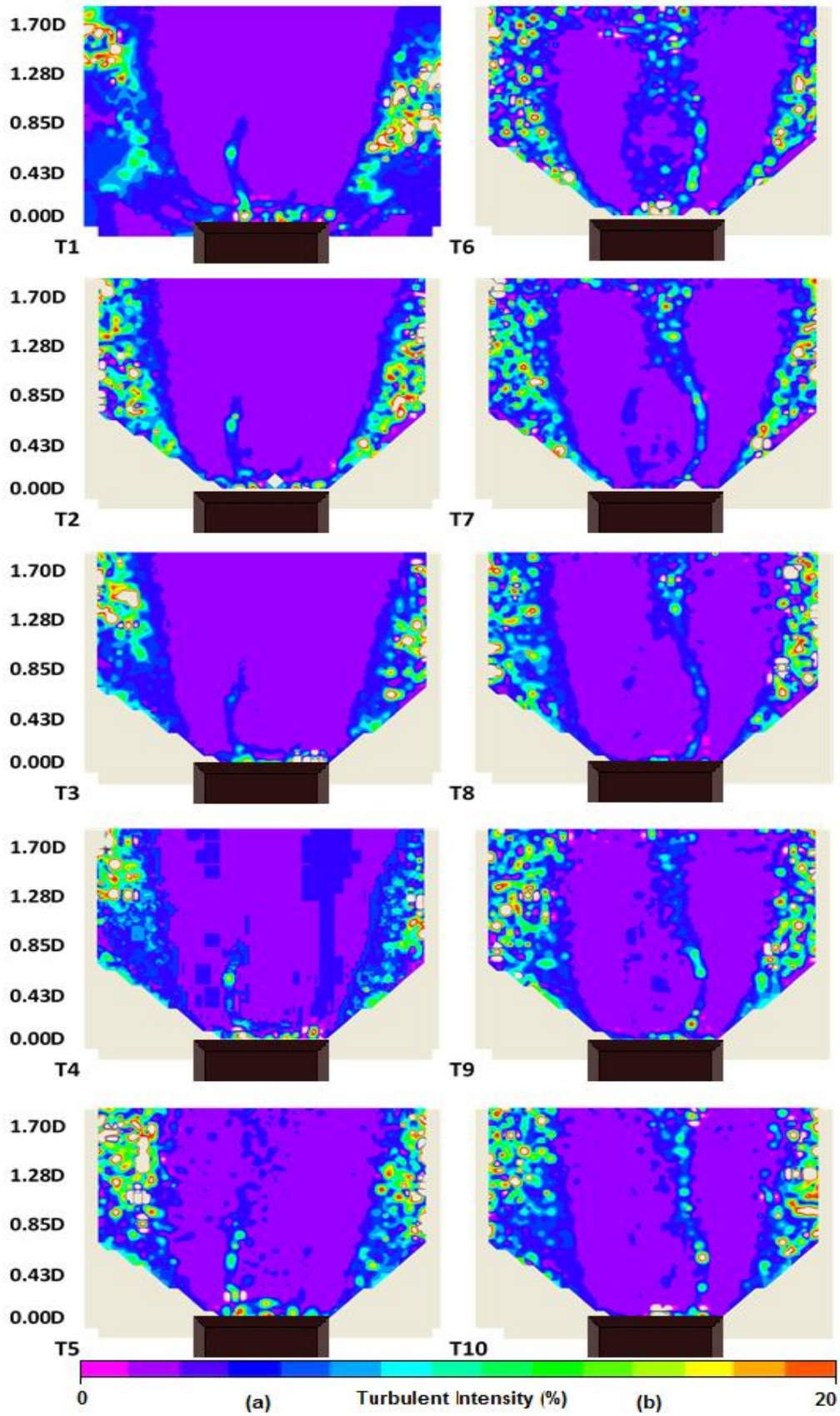

Figure 5-8: Comparison of turbulent intensity between (a) pure methane and (b) methane/CO2 flames. Tests as described in Tables 5.1 and 5.2. Colour axis spans from 0 to 20 %

The velocity profiles also seem to be affected to some extent (Figure 5.9). Both mixtures produce an initial smooth Rankine profile that decays slowly and gradually through the system. However, the use of CO_2 produces a profile that begins to collapse sooner. The high density of the CO_2 combined with the increased equivalence ratio provides more energy to the slow reacting CO_2 component of the High Momentum Flow Region. The energy of the system is partially used to heat up the CO_2. This, combined with the greater intensity of the CRZ distorts the profile even more than without CO_2. Nevertheless, the CRZ in these flows remains larger as a consequence of the increased energy and higher density of the CO_2 (Table 5.2). However, close to the nozzle the profiles are very similar due to the high reactivity of methane. Therefore, it would be expected that the profiles begin to show differences in behaviour further downstream of the burner nozzle.

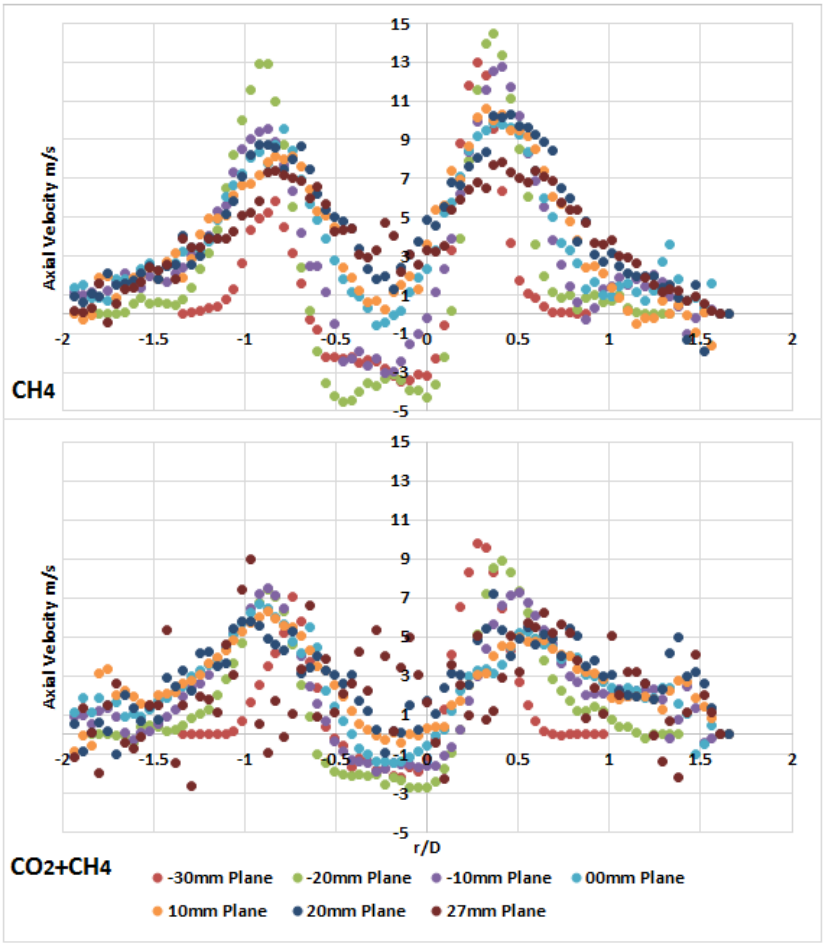

Figure 5-9: Axial velocity profiles in the combustion chamber burning pure methane and a blend of methane and carbon dioxide, respectively. Data corresponds to test 1 and 10 in Table 5.4 both of them ∅ =0.8

5.3.2 CO2 Pilot Injector

In order to investigate the fundamental changes in flame structure caused by the introduction of carbon dioxide to the flame, CO_2 diffusive injection was attempted close to blowoff conditions (Figure 5.10). Carbon dioxide was introduced through the pilot injector, and as such it had only an axial velocity component in the dumping plane.

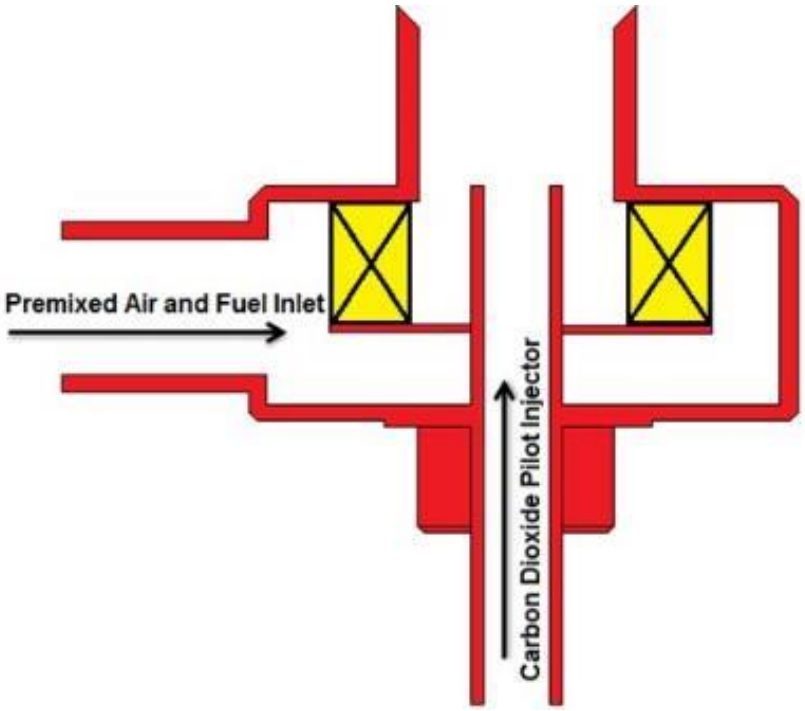

Figure 5-10: Schematic diagram of the generic burner

Between T1 and T6 (Table 5.3) the velocity within the HMFR increased as the total mass flow increased, as presented by [137]. Instead of suffering an increase in velocity resulting in a larger HMFR, the opposite occurred. The results showed that an increase in mass would reduce the size of the HMFR while producing an increase in intensity. Increasing the air flow rate would ultimately result in blowoff, but as the air is increased the intensity in the HMFR also increases, as shown previously by Dam et al.[138].

Table 5-3: Blowoff limits CO2 as Pilot injector Pure Methane

Tests	Mass flow rate [g/s] CH_4	Air	CO_2	Total mass	Φ	AFT [K]
T1	0.25	5.00	0.000	5.25	0.86	2083
T2	0.25	4.78	0.000	5.03	0.90	2134
T3	0.25	4.30	0.000	4.55	1.00	2226
T4	0.25	3.91	0.000	4.16	1.10	2211
T5	0.25	3.58	0.000	3.83	1.20	2137
T6	0.25	3.31	0.000	3.56	1.30	2057
T7	0.25	3.31	0.049	3.61	1.30	2038
T8	0.25	3.31	0.103	3.66	1.30	2017
T9	0.25	3.31	0.116	3.68	1.30	2012
T10	0.25	3.31	0.130	3.69	1.30	2007

Stereo PIV images [137] showed how the injection of differing amounts of carbon dioxide through the pilot of the generic burner could affect the velocity of the flame, significantly reducing the flame temperature.

Through T6 to T9 the introduction of CO_2 results in a continued decrease in the HMFR velocity. However, the velocity in the CRZ increases sharply as the high specific heat and density of the CO_2 increases the pressure differential that drives recirculation.

5.4 Effect of addition of H_2 and CO to Methane

Experiments were conducted to define the blowoff limits of different configurations using different gases. The gases used were a mixture of CH_4, H_2, CO_2 and CO (Table 5.4). The conditions were generally analysed at the same power output of 7.49 kW. The investigation of the effect of different nozzles was conducted using three different levels of power output: low power (3.499 kW), medium power (7.49 kW), and high power (11.477 kW), as presented in Table 5.5.

Table 5-4: Syngas compositions by Volume

Gas number	Gas compositions
Syngas 1	10% CH_4 + 45%H_2 + 45%CO
Syngas 2	20% CH_4 + 40%H_2 + 40%CO
Syngas 3	30% CH_4 + 35%H_2 + 35%CO
Syngas 4	50% CH_4 + 25%H_2 + 25%CO
Syngas 5	100% Methane
Syngas 6	50% CH_4+50% CO_2

Table 5-5: Experimental and all CFD conditions examined

Gas Number	Ṁ fuel [g/s]	Ṁ Air [g/s]	Nozzle angle	Total [g/s]	Φ	HHV Mj/kg	Power Output KW
Syn1	0.101	1.414	30°	1.515	0.425	73.941	7.49
Syn1	0.101	1.405	45°	1.507	0.428	73.941	7.49
Syn1	0.101	1.383	60°	1.485	0.453	73.941	7.49
Syn2	0.104	1.557	30°	1.661	0.485	71.892	7.49
Syn2	0.104	1.554	45°	1.658	0.486	71.892	7.49
Syn2	0.104	1.489	60°	1.593	0.508	71.892	7.49
Syn3	0.107	1.631	30°	1.738	0.563	69.843	7.49
Syn3	0.107	1.677	45°	1.784	0.548	69.843	7.49
Syn3	0.107	1.650	60°	1.757	0.557	69.843	7.49
Syn4	0.113	1.839	30°	1.953	0.689	65.745	7.49
Syn4	0.113	1.791	45°	1.905	0.707	65.745	7.49
Syn4	0.113	1.832	60°	1.946	0.692	65.745	7.49

5.4.1 Results and Discussions

Figure 5.11 shows the comparison between the 3 nozzles. Equivalence ratio reductions of around 20 % were observed with all nozzles using confinement while the system was still running under lean conditions. As the mole fraction of hydrogen increases, the equivalence ratio at which LBO occurs moves to leaner conditions, thus showing an improvement in blowoff limits (Figures 5.11 and 5.12). This has been proven elsewhere [116], however it can be seen that some trends follow linear progressions, especially during the experiments using the 45˚ nozzle and syngas-1. As the angle is decreased/increased, the results become less linear, implying a breakdown in the controlling phenomena due to more chaotic processes. This might be linked to the propagation of non-linear large coherent structures.

Similarly, the decrease in hydrogen produces less homogeneous results. This relates to the high reaction of hydrogen close to the burner outlet. The increase of H_2 decreases the Da number as a consequence of faster chemical reactions. Thus, convective processes and turbulence produced by the CRZ and shearing flows do not appear to be controlling the onset of LBO. However, the reduction in hydrogen produces conditions where the presence of these structures creates a less linear, more random behaviour towards the blowoff limit.

A comparison of blowoff limits (Figure 5.13) demonstrates the effects of the different fuels in addition to data recorded for pure methane and methane blended with carbon dioxide using a 45° nozzle [133]. Syngas-4, with 50 % methane, shows similar LBO values to pure methane. This demonstrates that although the Da values are different between the two gases, blowoff occurs at similar equivalence ratios as a consequence of mechanisms whose impact has greater effects on the blowoff process at slower reaction time scales.

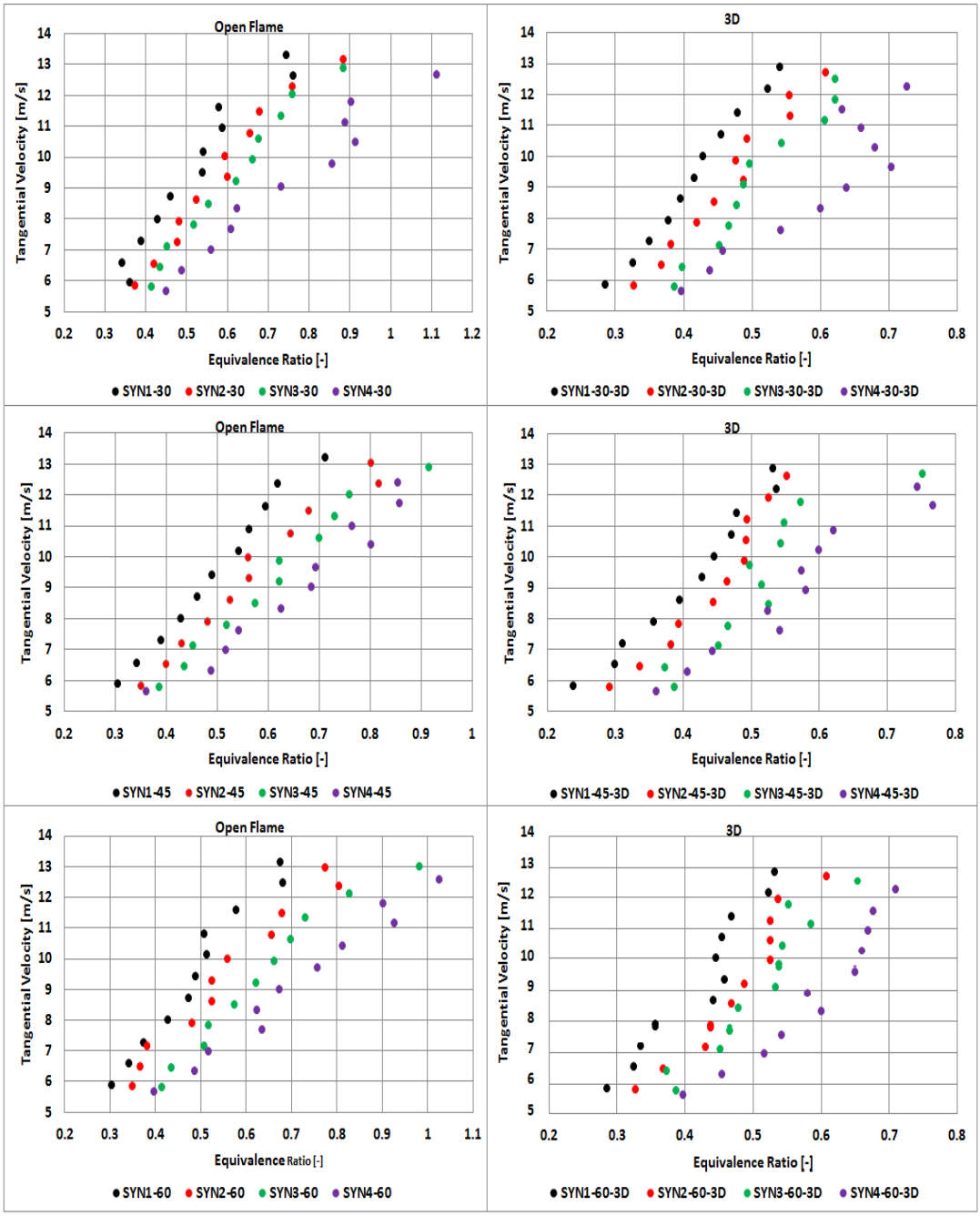

Figure 5-11: Comparison of blowoff limits with different nozzle geometries

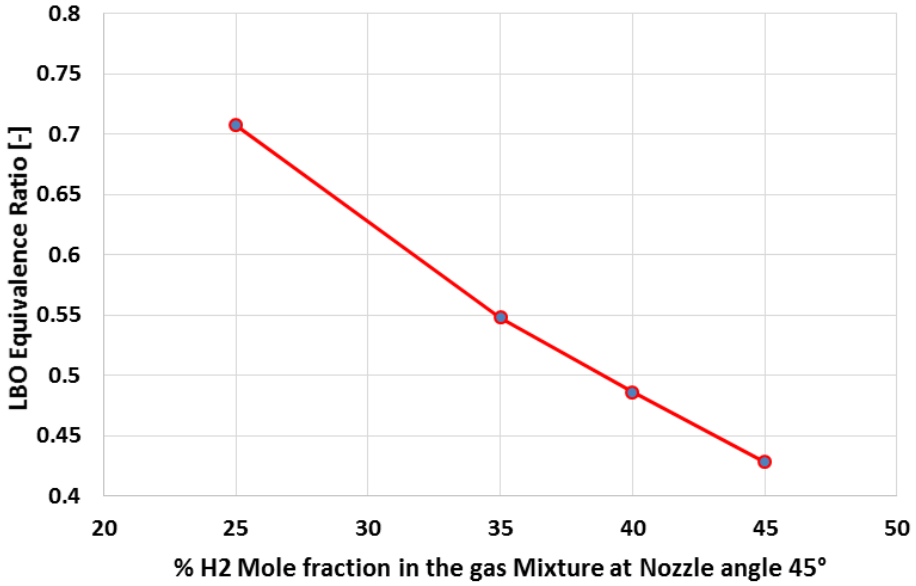

Figure 5-12: Effect of the H2 content on the LBO equivalence ratio

Transition to blowoff was observed to commence with the reduction of the flame size to a point of almost disappearance. Upon reaching this point, the flame begins to oscillate in the transverse direction, with the re-ignition of the blend at low frequencies as a consequence of the recirculation of gases. The stronger CRZ observed under isothermal conditions [32] pulls back some of the hot products that will find a point of high interaction with the reactants between the CRZ and the outgoing flow. It has been demonstrated that this region is where the CRZ and the Precessing Vortex Core co-exist, a region that shows the highest turbulence in the flow [35,33]. Since their interactions depend on the strength and shape of the CRZ, it was expected that the blowoff would depend more heavily of the on the geometry. However, at low flow rates just a slight dependency was observed (Figure 5.14a). Hydrogen content varies, thus causing a change in Da, which was more important to the phenomenon.

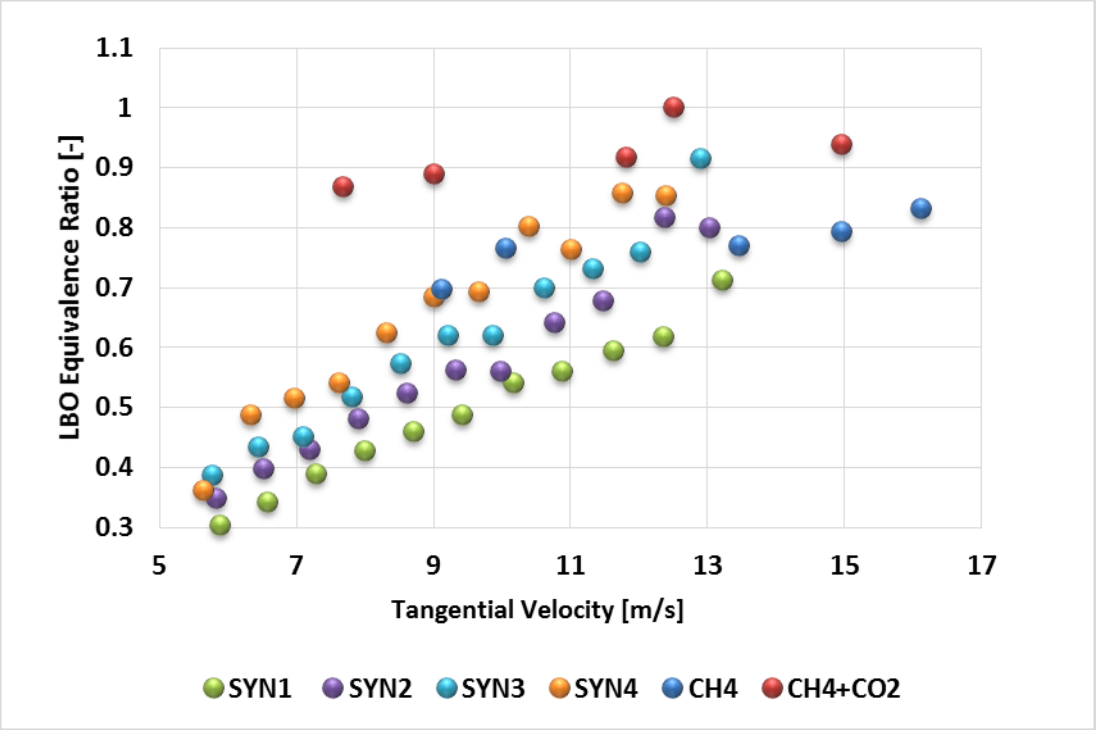

Figure 5-13: LBO equivalence ratios of different fuel mixtures at the same swirl numbers and for the same 45° nozzle

This is believed to be caused by the weaker CRZ-PVC interaction at these low Reynolds numbers. Moreover, being a localized phenomenon, the weaker CRZ-PVC interaction will allow the re-establishment of the flame in other regions. Thus, it is believed that the hydrodynamic interaction between the CRZ and PVC plays a minor role in the blowoff for these hydrogen enriched blends at the conditions examined. The influence of the nozzle causes a slight effect for all cases at low and medium flowrates. However, for syngas 4, as Re was increased there was a considerable shift in LBO equivalence ratios using all nozzles. This was a consequence of the reduction in H_2 and distortion of the CRZ, and thus the CRZ-PVC interaction. It is believed that at this stage the interaction is a critical part of the blowoff process due to the high flow rates and lower chemical reaction times (Figure 5.14B).

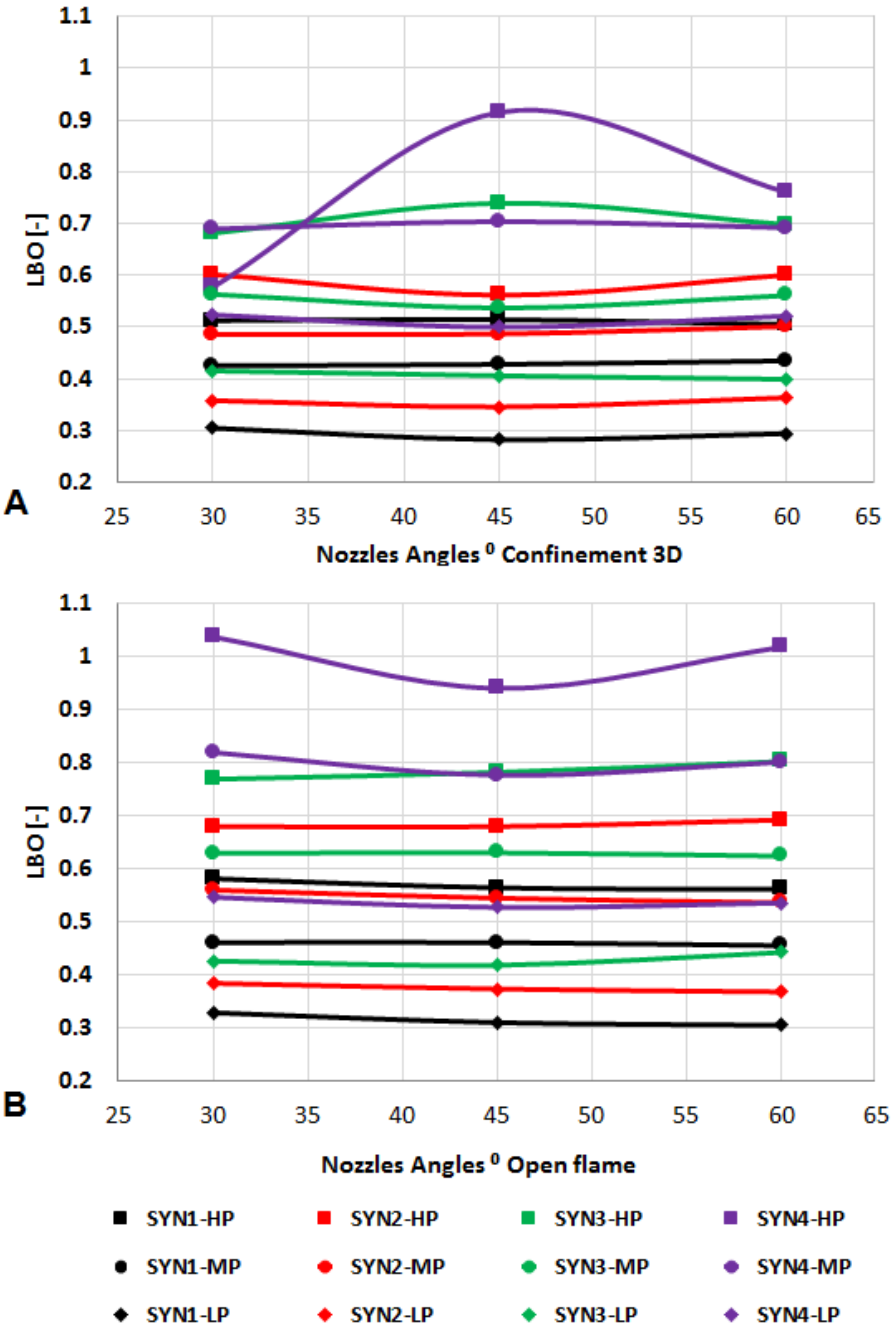

Figure 5-14: Comparison of the effect of outlet nozzle angle on LBO equivalence ratio for all syngases at LP, MP and LP [KW]

Final blowoff was produced after a longer flame appeared with an intermediate constriction at the centre (Figure 5.15). The flame showed a cycle of ignition, elongation and quenching just before increasing the flowrate for the final annihilation of the flame. The observed constriction seems to be formed by the reaction of the reactants around the CRZ and a secondary recirculation zone that forms further

downstream of the burner mouth. It is believed that this second recirculation zone, previously observed in other works [35,110] , can be defined by: (i) the baroclinic depression in the central region caused by the swirling motion, (ii) the strength of the main CRZ, (iii) the stratified reaction of different molecules, and (iv) the acoustics of a 3/4 wave. More research is required to investigate this phenomenon.

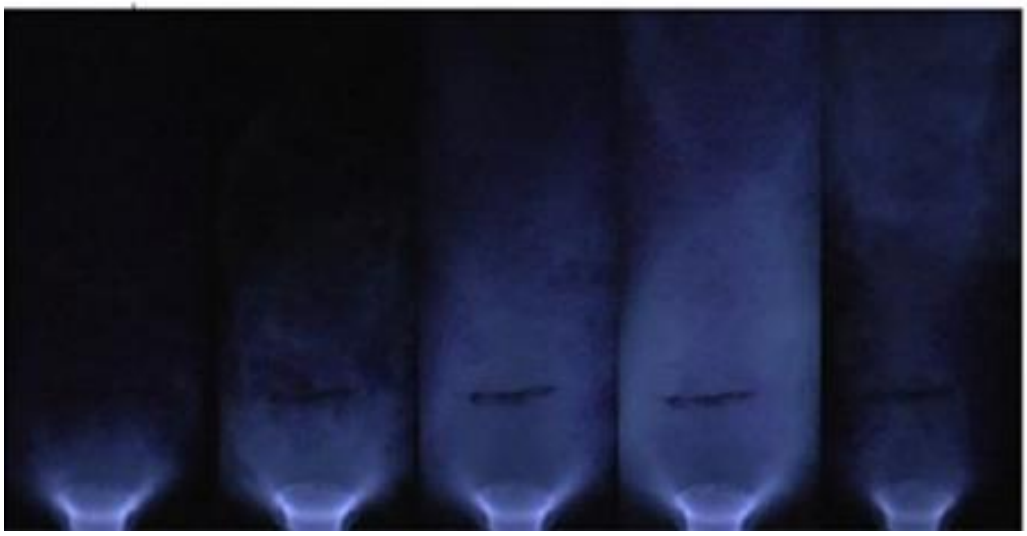

Figure 5-15: Pulsating flame. Progression of LBO seconds before final onset. S = 1.05, Φ = 0.525. Frequency = 10 Hz

PIV velocity contours and turbulence intensity maps were overlapped to clearly visualise the percentage of turbulence inside the CRZ (Figure 5.16). Turbulence intensity was set between 0-10 %, with a CRZ defined in a velocity range from -1.40 to 0.17 m/s. It is clear the CRZ distortion occurs for all cases (Table 5.5) and for all three nozzles. Therefore, a change in the interaction of the PVC-CRZ would be expected. Increased hydrogen content, i.e. Syngas-1, shows that a faster reactivity shortens the CRZ even with a 60˚ nozzle. Instead of allowing further growth of the CRZ, as progressively observed with the reduction of H_2, the combustion process collapses the recirculation zone closer to the nozzle. On the other hand, the use of a 30˚ nozzle shows wider structures, as expected. The reduction of hydrogen elongates the CRZ as a consequence of the lower reactivity of the blend giving a delayed pressure decay. As the nozzle angle is increased to 45˚, more intense interaction between the CRZ and the shearing flow encourages the combustion reaction, thus reducing the size of the CRZ. This phenomenon could be linked to the shortening of the CRZ using Syngas-1 with the 60˚ nozzle.

It is clear from this (Figure 5.16) that there is considerable contrast in the shape and size of the CRZ between the four syngases and the three different nozzles. The CRZ map of premixed combustion flames at lean equivalence ratios ≥ 0.5, using syngas 4, shows that the strength of the CRZ increased with an increase in the air flow rate. The variable formation and the shape of the CRZ provide strong evidence for the existence of a PVC, which enfolds and presses the CRZ (Figure 5.16) during the combustion of syngas 2, 3 and syngas 4 using 60° nozzles. This was also observed for syngas 3 using the 45° nozzle, and for syngas 2 using the 30° nozzle.

Figure 5.17 shows the normalised nozzle trends of the turbulence intensity to the negative velocities inside of the CRZ. Minimum and maximum turbulence values were expected from Syngas-4 and Syngas-1, respectively, as defined from the relation $S_T=S_L \bullet f(u')$. However, it is clear that maximum value using Syngas-1 is only obtained with a 60˚ nozzle, whilst minimum value overall is obtained with Syngas-3 using a 45˚ nozzle. Therefore, it is clear that the flow interaction affects the CRZ and thereby alters $f(u')$ through the impact between structures and shearing flow. Although bigger CRZs were observed for Syngas-4, and faster chemical times were expected using Syngas-1, this final interaction is an important parameter for the evolution towards blowoff, especially with low reactive blends.

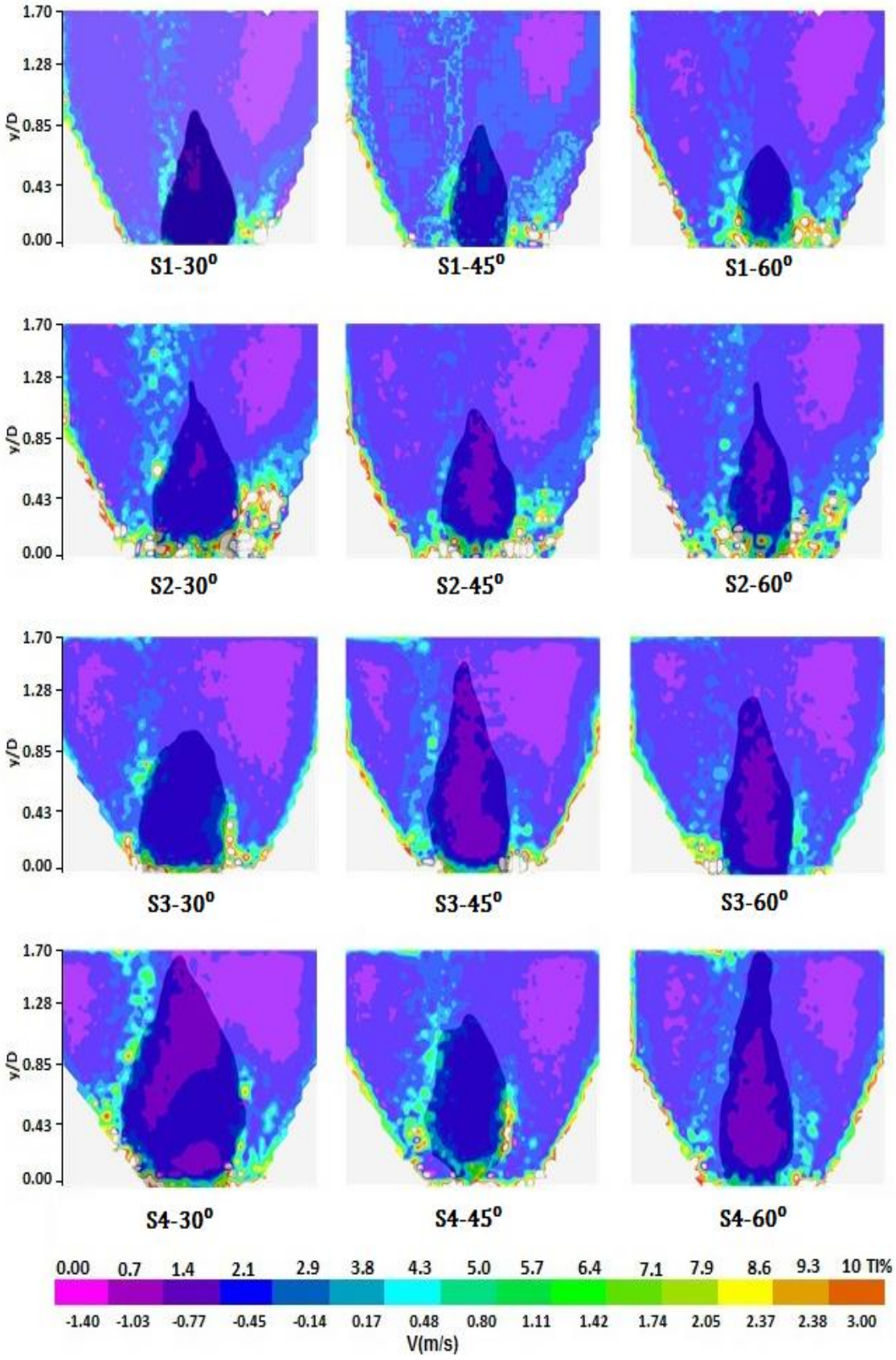

Figure 5-16: turbulent intensity matched with CRZ boundary (part shaded) using scale of turbulent intensity (0-10 %) and axial velocity range (-1.40 up to 0.17 m/s)

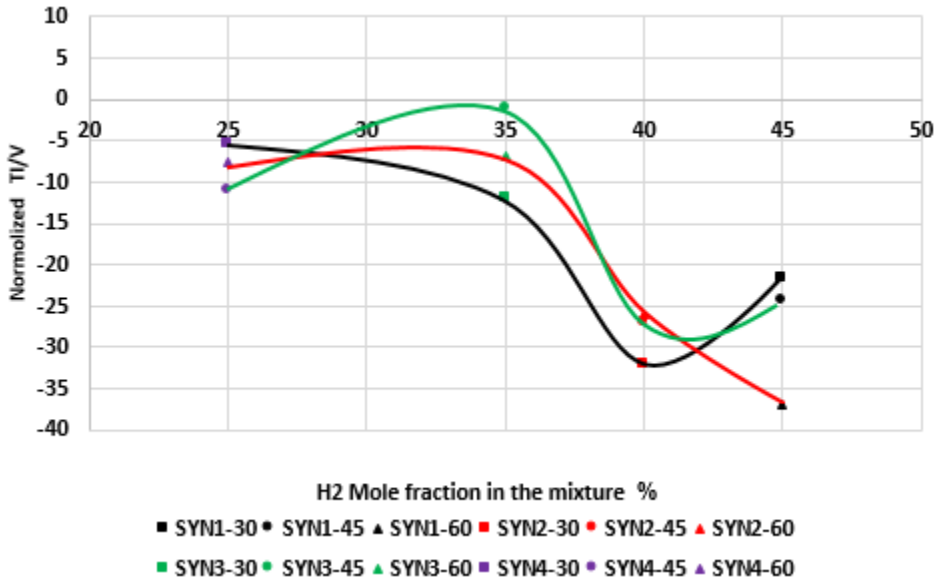

Figure 5-17: Normalising the turbulent intensity and axial velocity inside the CRZ.

Different profiles of the CRZ for all syngases and all nozzles were produced at 7.49 kW as a consequence of the different reactions and combustion processes (Figure 5.18). The velocity and momentum of the flow increase in localised regions of the burner through the High Momentum Flow Region (HMFR) [49]. The progressive introduction of hydrogen increases the strength of the recirculation zone, whilst reducing the velocity within the HMFR, i.e. it generates a highly 3-dimensional shearing flow. This is also observed from the point at which the curves cross the abscissas axis, indicating that the CRZ reduces in width with a hydrogen increase whilst the HMFR becomes stronger. Tangential velocities are also affected as a consequence of the increase of reactivity (Figure 5.19). This also affects the relationship between shearing flows and the formation of the CRZ.

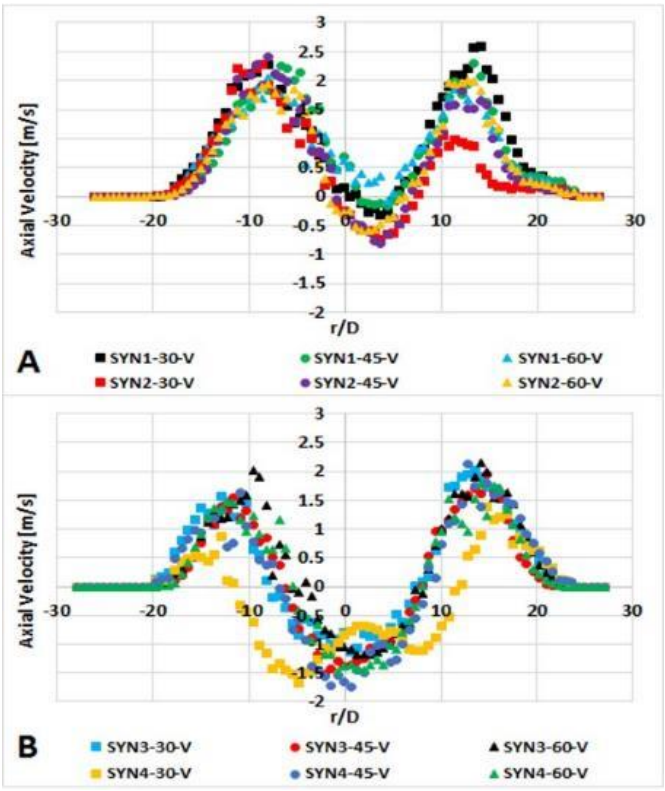

Figure 5-18: Axial velocity at y/D = 0.00 for (a) Syngases 1 and 2, and (b) Syngases 3 and4

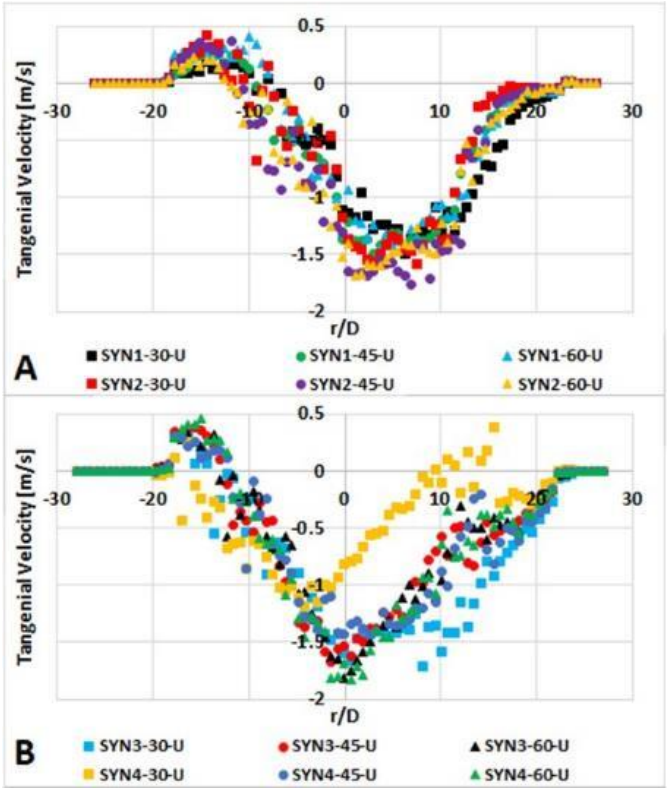

Figure 5-19: Tangential velocity at y/D = 0.00 for (a) Syngases 1 and 2 and (b) Syngases 3 and 4

PIV velocity contours were om btained to determine the boundaries of the CRZ, Figure 5.20. The CRZ boundaries were defined in a velocity range of -1.40 to 0.170 m/s. It is clear the CRZ distortion occurs for all cases, Table 5.5, using the three nozzles. Therefore, a change in the interaction of the PVC-CRZ would be expected. Usage of more hydrogen, i.e. Syngas-1, shows how a faster reactivity shortens the CRZ even with a 60˚ nozzle. Instead of allowing further growth of the CRZ as progressively observed with the reduction of H_2, the combustion process collapses the recirculation zone closer to the nozzle. On the other hand, the usage of a 30˚ nozzle shows wider structures, as expected. The reduction of hydrogen elongates the CRZ as a consequence of a delayed pressure decay consequence of the lower reactivity of the blend. As the nozzle angle is increased to 45˚, more intense interaction between the CRZ and the shearing flow encourages the combustion reaction thus reducing the size of the CRZ, a phenomenon that could be linked to the shortening of the CRZ using Syngas-1 with the 60˚ nozzle.

Comparisons between experimental results and CFD predictions for the CRZ size demonstrate that very good correlation can be achieved using the SST-k-ω model (Figures 5.21 and 5.22; Tables 5.6, 5.7 and 5.8). It is evident from Table 5.8 that there is no significant difference between experimental results and CFD calculations. The worst predictions were obtained using the 30˚ nozzle with the slowest Syngas-4, and the 60˚ nozzle with the fastest Syngas-1. This lack of accuracy could be linked to large 3-dimensional structures, such as the PVC, which is not accurately predicted with the model, or HMFR, which is not properly resolved due to it being a fast reaction phenomenon.

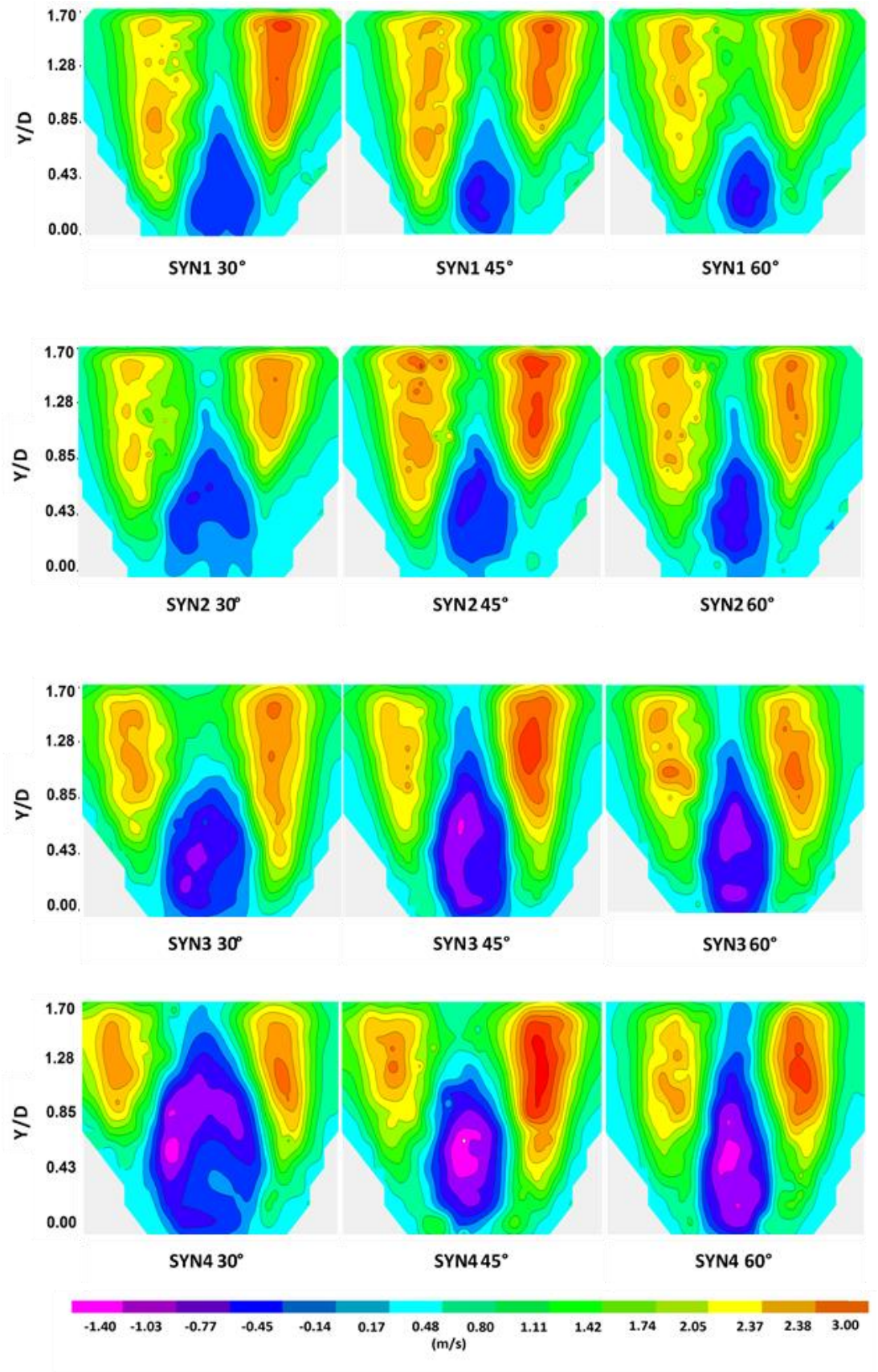

Figure 5-20: Axial velocity map of PIV results

Predictions using confinement were carried out to simulate more representative conditions to those used in industry. Table 5.9 shows the numerical results with confinement, illustrating the length and width of the CRZ with each gas, and with each nozzle. The confinement has an extremely important effect on the CRZ and its interaction with the PVC. As discussed by Syred [39] , confinement can dramatically alter the size and shape of the CRZ and the external recirculation zones formed as the swirl burner flow expands. It was found that the angle of 60° produces a larger CRZ with the narrowest profiles.

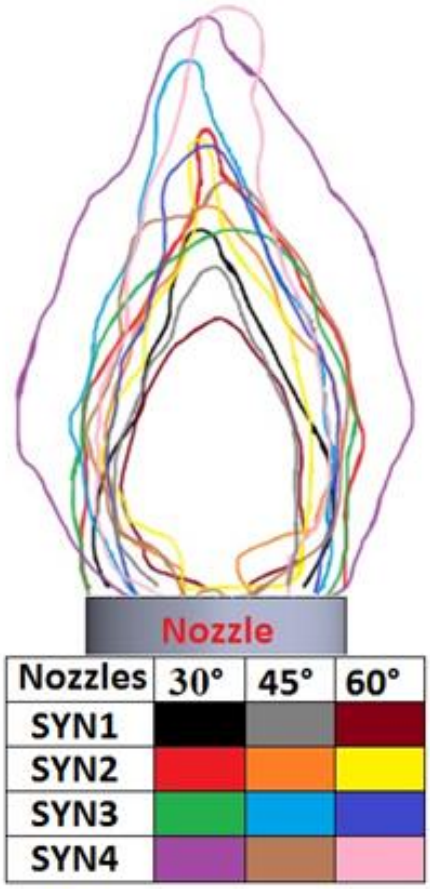

Figure 5-21: Experimental results of CRZ size

Table 5-6: Comparison of experimental of CRZ size

Gas mixture	30°		45°		60°	
	Width	length	Width	length	Width	length
SYN1	1.35D	1.92D	0.97D	1.73D	1.01D	1.43D
SYN2	1.50D	2.44D	1.28D	2.07D	1.13D	2.41D
SYN3	1.54D	1.95D	1.43D	2.86D	1.24D	2.41D
SYN4	2.11D	3.12D	1.43D	2.22D	1.24D	3.16D

Figure 5-22: CFD results of CRZ size

Table 5-7: Comparison of CFD results of CRZ size

Gas mixture	30°		45°		60°	
	Width	length	Width	length	Width	length
SYN1	1.33D	2.00D	0.90D	1.94D	1.13D	1.80D
SYN2	1.47D	2.34D	1.27D	2.07D	1.20D	2.41D
SYN3	1.33D	1.74D	1.33D	2.67D	1.13D	2.41D
SYN4	1.60D	2.67D	1.34D	2.27D	1.14D	2.63D

Table 5-8: Comparison of numerical and experimental CRZ size

Gas mixture	30°		45°		60°	
	Width [%]	Length [%]	Width [%]	Length [%]	Width [%]	Length [%]
SYN1	1.48	4.17	7.2	12.1	11.8	25.8
SYN2	2	4.09	0.78	0	6.19	0
SYN3	13.6	10.7	6.9	6.6	8.87	0
SYN4	24	14	6.2	2.2	8	16

Table 5-9: Prediction of CRZ size using confined conditions

	30°		45°		60°	
	Width	length	Width	length	Width	length
SYN1	1.85D	4.70D	1.90D	4.30D	1.40D	9.60D
SYN2	1.80D	5.20D	1.85D	4.60D	1.80D	4.70D
SYN3	1.90D	5.40D	1.90D	7.20D	1.80D	5.20D
SYN4	1.90D	5.80D	1.90D	4.60D	1.70D	4.00D

Interestingly, the largest profile is obtained using Syngas-1 and a 60˚ nozzle. This, as previously observed, could be an over-prediction, Table 5.8. The second largest profile is produced using a 45˚ nozzle with Syngas-3. This result shows a good correlation between experimental and numerical results. Although Syngas-3 has a large concentration of hydrogen, the high CO content seems to retard the reaction to allow the enlargement of the CRZ. The impacts of the PVC on this configuration would be considerable since the 45˚ nozzle reduces the shearing phenomena compared to the 60˚ configuration. However, the high reactivity would limit the response of the flame to the CRZ-PVC interaction, as previously stated. Therefore, these assertions lead to a Da phenomenon, where H_2 is inhibited by CO and CH_4, with insufficient hydrogen to drive the reaction. Therefore, it is at this point of 40 % CO that the injection of the latter can still control the reaction speed when using 40 % H_2.

Increasing the mole fraction of hydrogen in the mixture produces faster chemical reactions (Figure 5.23) and shorter turbulent time scales (Figure 4.30.) due to the higher thermal diffusivity of hydrogen and the laminar flame speed, as expected. However, two interesting phenomena occur using a) Syngas-3 with a 45˚ nozzle, and b) Syngas-4 with a 30˚ nozzle, respectively. For the first case, the lowest chemical time scale is produced using 40 % CO and an angle with moderate shear, a phenomenon previously hypothesized to occur as a consequence of the inhibiting nature of CO at these H_2 concentrations. On the other hand, the case with Syngas-4 using a 30˚ nozzle has been previously described as a condition where the CRZ-PVC interaction would show its highest impacts (Figure 5.14). However, as observed in Table 5.8, the assertions for this blend would need to be correlated with more advanced turbulence models.

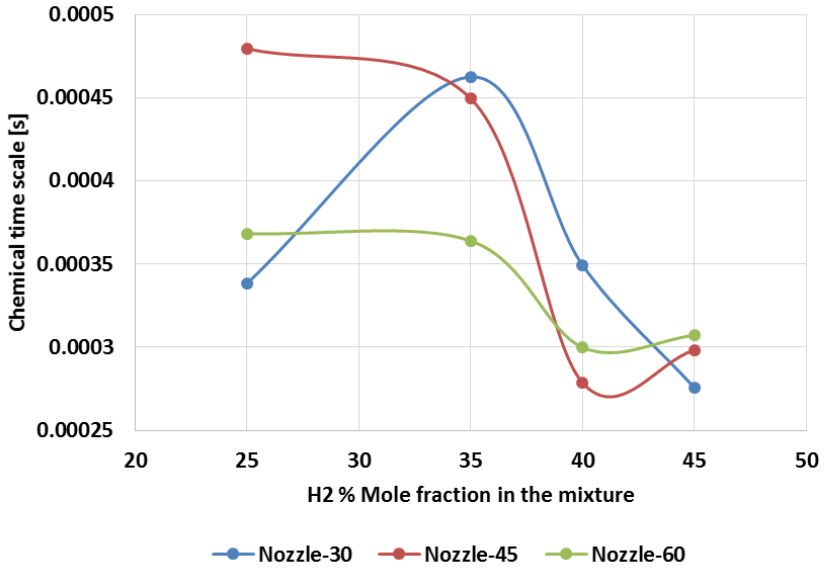

Figure 5-23: Chemical time scale vs the percentage of hydrogen in the mixture.

This is believed to be caused by a weak CRZ-PVC interaction, Figure 5.24. Moreover, being a localized phenomenon, this weak CRZ-PVC interaction will allow the re-establishment of the flame in other regions. This interaction has been previously studied elsewhere 26, 34], showing a considerable increase in turbulence where both structures collide. It is observed that the hydrodynamic interaction between the CRZ-PVC plays a minor role in the blowoff for these high hydrogen enriched blends at these conditions.

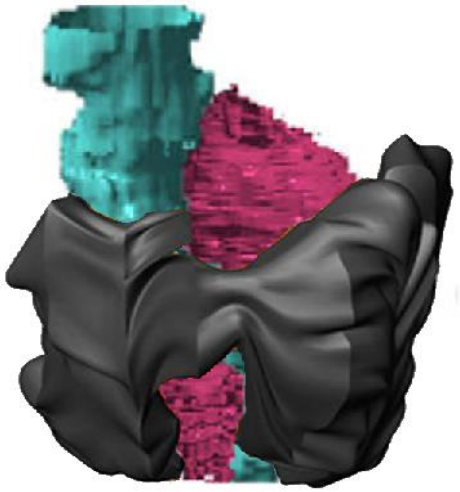

Figure 5-24: Schematic. CRZ-PVC interaction. The High Momentum Flow Region (HMFR; black) engulfs the CRZ (purple). The PVC (blue) evolves as a complex interaction between vortices, CRZ and HMFR.

5.5 Summary

Fuel flexibility will drive the energy demand in the near future. The use of different syngas compositions from various sources (i.e. coal, food, algae, etc.) will also play a major role in the global fuel mix. However, this contrasts with the experience of several global operators who have documented a vast number of problems with even minimal changes in fuel composition. Instabilities found can range from thermoacoustics, flashback, autoignition and blowoff. In terms of blowoff, the phenomenon is still not entirely understood. As the process occurs, theoretical limits do not match its measured behaviour. One possible explanation could link the stretch of the flame and its recovery with the transient nature of the Central Recirculation Zone (CRZ).

In the present chapter a series of experiments were described which aimed to determine the behaviour and impact on the blowoff process of using different geometries and gas compositions. The Central Recirculation Zone was measured and correlated with the blowoff phenomenon. A relationship was found between the CRZ size and strength, the different compositions of gases used (i.e. CO_2 and CH_4 content), and the burner nozzle geometry. The results show how the strength and size of the recirculation zones are highly influenced by all these parameters. However, it seems that the CRZ dimensions/strength do not play an important role in the blowoff phenomenon under the conditions studied, whilst the composition of the mixture shows a high correlation with blowoff parameters. Nevertheless, the intensity of the CRZ using these compositions can increase the residence time, which is important for improved combustion of other blends.

Although it is concluded that the size and shape of the CRZ seem to be minor factors in controlling the blowoff limit under the conditions analysed, it is clear that the CRZ can be increased by the use of CO_2. This could in turn be beneficial for new blends by increasing the residence time of the products/reactants of these and other fuel/diluent compositions. The addition of CO_2 produces longer recirculation zones that collapse suddenly and far away from the nozzle. Similar velocity profiles at the outlet are observed, with the same stability characteristics as those seen when pure methane is used. Similar stretch is expected, with lower resistance in the CO_2 blends as a

consequence of the reduced reaction rate. The high turbulence of the CRZ using CO_2 can also be an important parameter in the addition of other species that can improve the combustion process whilst recirculating CO_2 for other applications, ie. Carbon capture and storage.

The intensity of the HMFR, which was shown in previous work to be integral to the process of CIVB, was shown to increase as air flow reduced the equivalence ratio of the flame, squeezing the CRZ. The introduction of CO_2 increased the intensity of the CRZ whilst reducing that of the HMFR, effectively leading to scenarios more prone to blowoff.

Experimental tests and numerical simulations have been conducted in an atmospheric, premixed swirl burner to investigate the LBO limit of various syngas mixtures at a moderate swirl number and at the same power output using three types of outlet nozzles. Increasing the mole fraction of H_2 from 25 % to 45 % extended the LBO limit of a given fuel mixture. This has been previously observed in other experiments and studies. A consequence of increasing the mole fraction of hydrogen in the mixture is that a faster chemical reaction is produced, with a shorter turbulent time scale due to the higher thermal diffusivity of the hydrogen and laminar flame speed. Another characteristic of hydrogen addition to the mixture is a significant change in the flame structure, indicated by a shorter and more robust flame.

The nozzle angle has a small effect on the LBO at low flow rates using all mixtures. However, there is a pronounced effect at higher flowrates with blends of low hydrogen content. This is believed to be a consequence of the effect of the CRZ-PVC on the flame as a result of a slower chemical reaction. It has been assumed for a long time that this interaction does not influence the blowoff process; however this work shows that the process is influenced if a slower reacting mixture is used. As the H_2 is increased, the fast reaction of the molecule reduces any perceptible dependency on the hydrodynamics close to the nozzle. It was observed that different CRZs were formed under a variety of conditions at the same power output, a consequence of squeezing caused from PVC formation. Also, the size of the CRZ is highly affected by the blend. The appearance of the reaction zone depends heavily on the governing turbulent

structures and the chemical properties of the flow. Thus, fuel compositions produced from a potentially variable composition of syngas will result in a multitude of chemical properties in terms of thermal diffusivity, density, laminar flame speed, and heating value. The use of confinement altered both the size and shape of CRZ. However, the use of different blends also considerably affected the size of the structure, impacting on the turbulence intensity and the stretch across the boundaries of this region.

CHAPTER6

CHAPTER 6

HYDRODYNAMIC EFFECTS COANDA EFFECTS

6.1 Results and discussion

6.1.1 Combustion Experiments

Experiments with combustion using the Stereo PIV system showed a clear distribution of the flame. It was observed that the flame behaved similarly to other Open Jet Flow-Medium Swirl (OJF-MS) conical flames at ΔY/D=0.145 and 0.107 with α=45.Careful ignition of the flow was attempted, as it was observed that a sudden uncontrolled reaction would lift the flow not allowing the visualization of the Coanda effect. This was denoted by a Rankine tangential velocity profiles, a CRZ and HMFR characteristic of such flows, Figure 6.1, 6.3. However, based on the observations of Sidhu et al[55], the system would present a shift in patterns as the flat base plate approaches to the nozzle lip .Thereafter, the base plate was moved towards the nozzle and positioned at ΔY/D=0.072. This change in geometry produced a Coanda Jet Flow (CoJF). ΔY/D was then changed to 0.036 and 0.000, and the same flat distribution was observed, Figure, 6.2, 6.4 In the Coanda Jet (CoJ) flow the flat profile allows greater quantities of air entrainment, whilst producing series of vortical structures between the incoming air and the flow attached to the base plate [54,59].

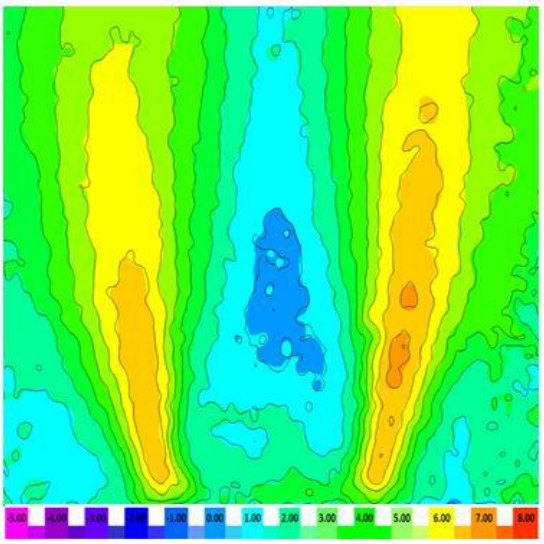

Figure 6-1: OJF-MS shape. Re~15,500, ΔY/D=0.145, equivalence ratio 0.58, α=45°. U velocity in [m/s].

Stereo PIV results of the Coanda effect showed that strong flow interaction occurs only close to the nozzle and up to 1D downstream, Figure 6.4. The flat profile allows greater quantities of air entrainment, whilst producing series of vortical structures between the incoming air and the flow attached to the base plate. This has been previously modelled and experimentally analysed with the recognition of a trapped vortex (TV) observed by Henri Coanda between the shearing flow and the base plate wall [54,70].

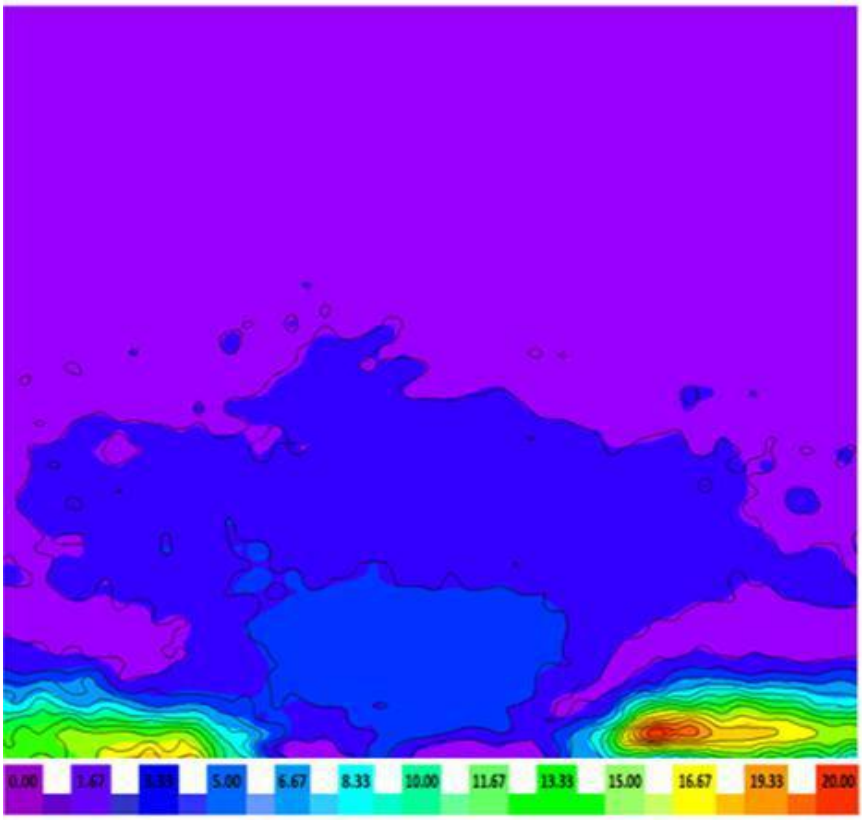

Figure 6-2: Experimental CoJF shape. Re~15,500, ΔY/D=0.000, equivalence ratio 0.58, α=45°. Total velocity in [m/s].

A closer look at the stereo PIV results and visual inspection showed how a trapped vortex interacts with the flame, Figs.6.5 and 6.6. Due to the high circulation caused by the flow, the latter bends towards the base plate trapping the vortex, which otherwise would have become an External Recirculation Zone (ERZ) with a conical profile. The high velocity exhaust flow bends towards the exhaust plate trapping the vortex. This can be observed at 0.193D from the base plate, Fig.6.5, where a high positive peak appears in the axial velocity component U. The vortex seems to be very strong only on one side of the system. Results also show that the tangential velocity component

rapidly becomes irregular and intermittent radially as r becomes greater than the external diameter.

All experiments using α=90° showed only a conical OJF-MS flame. Therefore, it was concluded that no Coanda jet could be produced with that particular geometry at S=1.05 and the Re numbers studied. This matches the results of Singh and Ramamurthi [71].

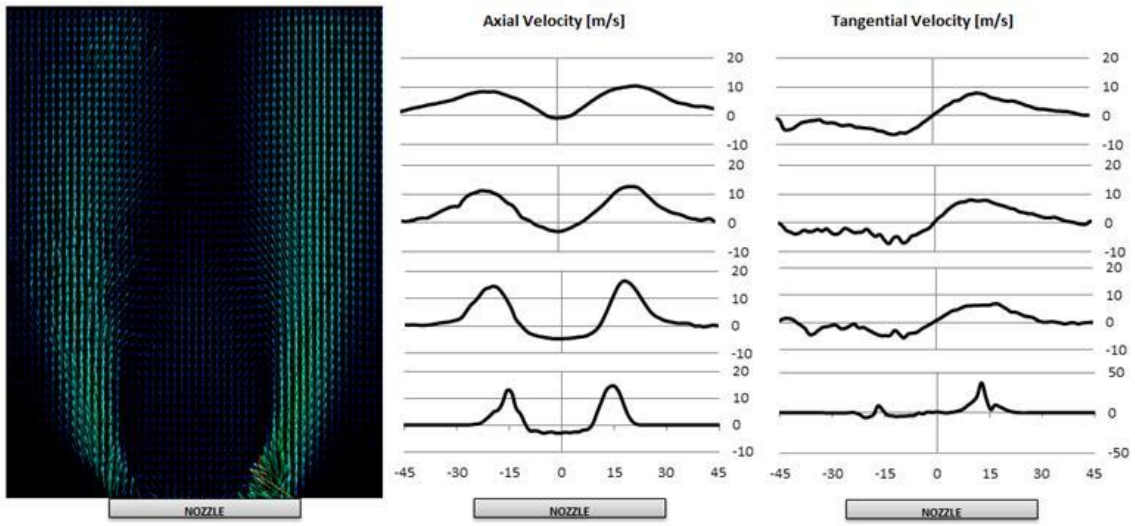

Figure 6-3: OJF-MS shape. Re~15,500, ΔY/D=0.107 and α=45°.

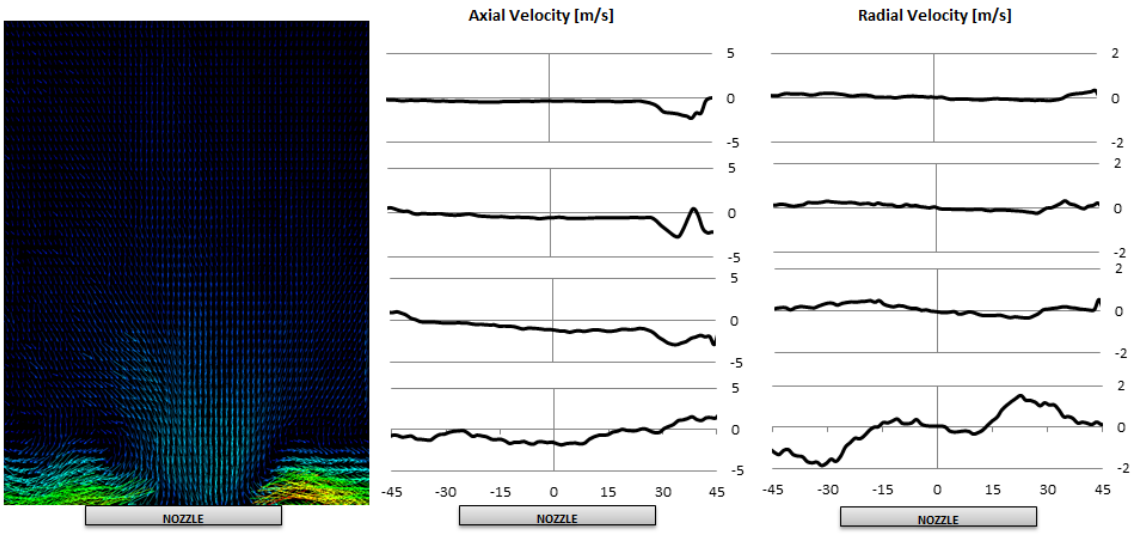

Figure 6-4: CoJF shape. Re~15,500, ΔY/D=0.000 and α=45°.

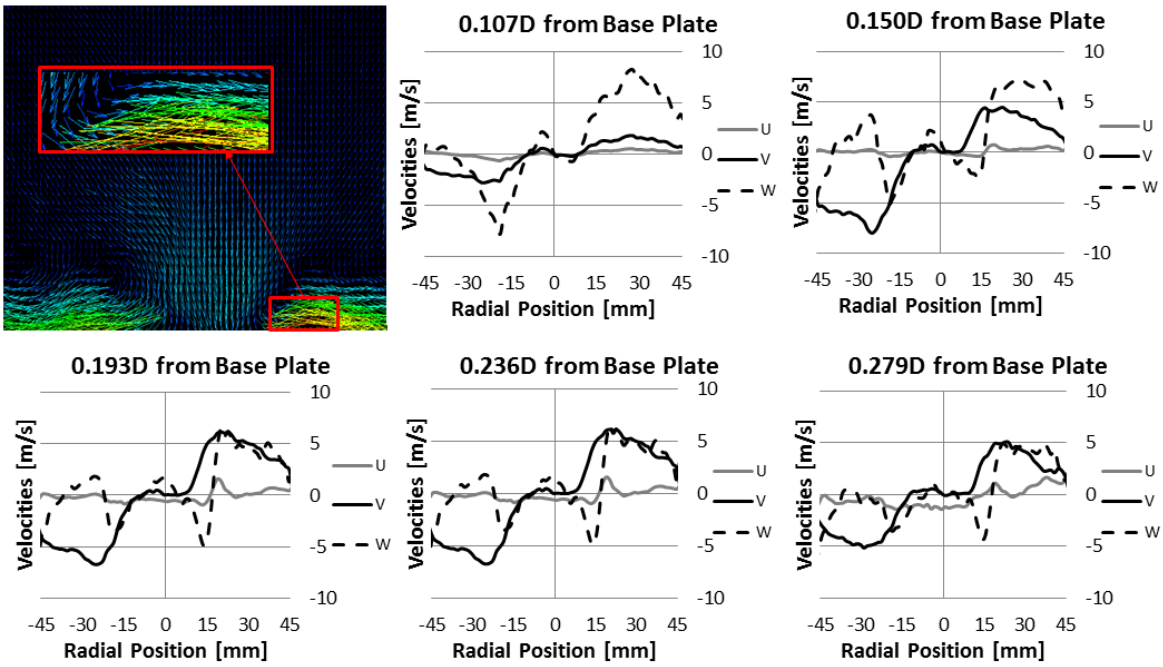

Figure 6-5: CoJF shape. Re~15,500, ΔY/D=0.000, equivalence ratio 0.58, α=45°. X coordinate going upwards, Y to the sides and Z outwards. Trapped vortex zoomed.

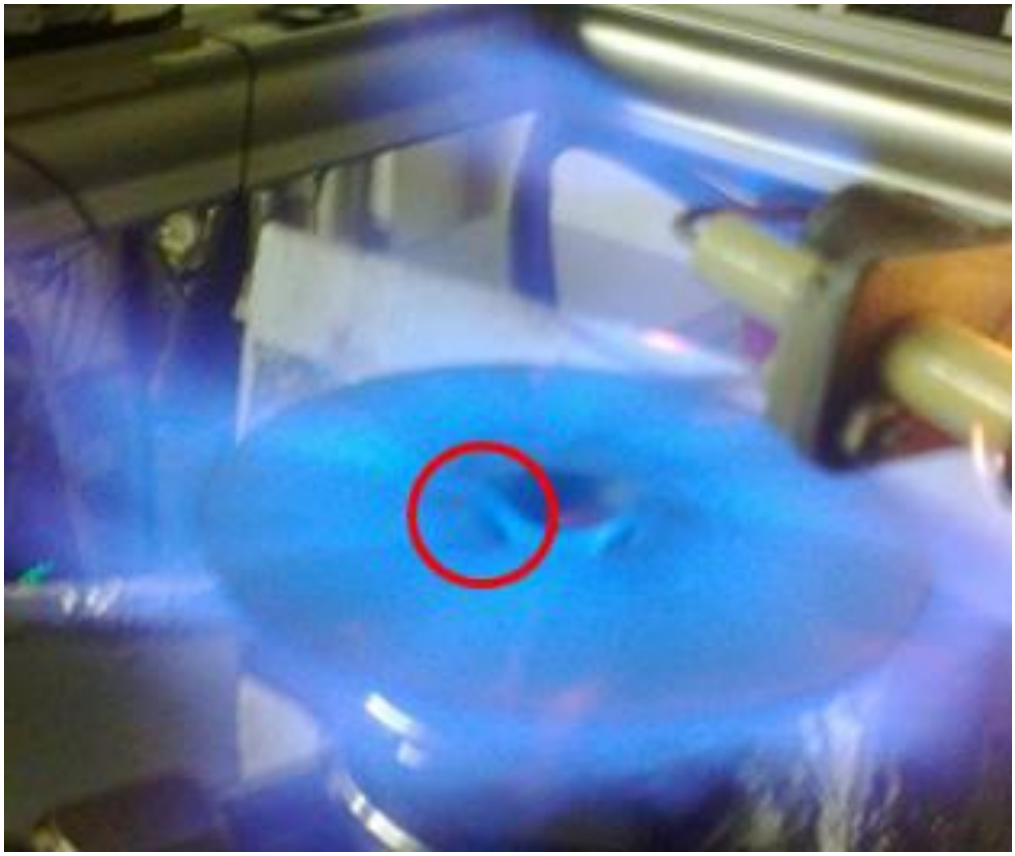

Figure 6-6: CoJF shape. Re~25,000, ΔY=0.0023, α=45°. Trapped vortex encircled.

Transition between the two flow states was observed in the range between ΔY/D=0.072 and 0.089. Experiments in this range were conducted with increments of Δ (ΔY)/D=0.004 to correctly determine the crucial position for transition. It was observed that the jet had a comparatively randomised pattern at ΔY/D=0.082. The experiments were run at different Re and all experiments showed that it was at this ΔY/D when the system changed suddenly from a CoJF flow to a conical OJF-MS flame and vice versa. This shift in behaviour occurred with the reduction of Strouhal number, Figure 6.7. Evidently this was associated to the transition of the flow as the TV/ERZ structure transitioned from one state to the other under these conditions.

The TV/ERZ is also transient and moves with the High Momentum Flow Region (HMFR). Although part of the flow moves towards the base plate all around the nozzle on both systems producing a toroidal minor structure, it is where the HMFR increases its velocity where the TV/ERZ becomes stronger. This transient nature of the TV/ERZ is a product of the self-stabilization mechanism of the system, which otherwise could be annihilated due to the strong shear stress in the HMFR.

In order to recognise any shift in the system, the second mode of the acoustic signal was monitored. Figure. 6.7 shows the results using α=45°. Almost all the experiments produced a similar trend close to St~1.50. It was notorious that the only different trend was the one obtained at ΔY/D=0.082, with St~1.38. Although the phenomenon is not entirely understood, the frequency shift could be related to the transition of the flow, as the TV structure could be damping some of the strength of the PVC and HMFR in an effort to regain stability. Moreover, as the PVC and HMFR have been affected by the Coanda Effect, Figure . 6.13, it is possible that this change in frequency is directly impacting on the precessing motion of the PVC-HMFR system, reducing its frequency in ~20-30 Hz. As the CRZ is in transition as well, the PVC seems to be only dragged by the TV. Due to the transient nature of the TV at ΔY/D=0.082, it is possible that the strength of the TV has also been affected, being unable to drag the PVC-HMFR system at its original frequency, thus reducing the St number.

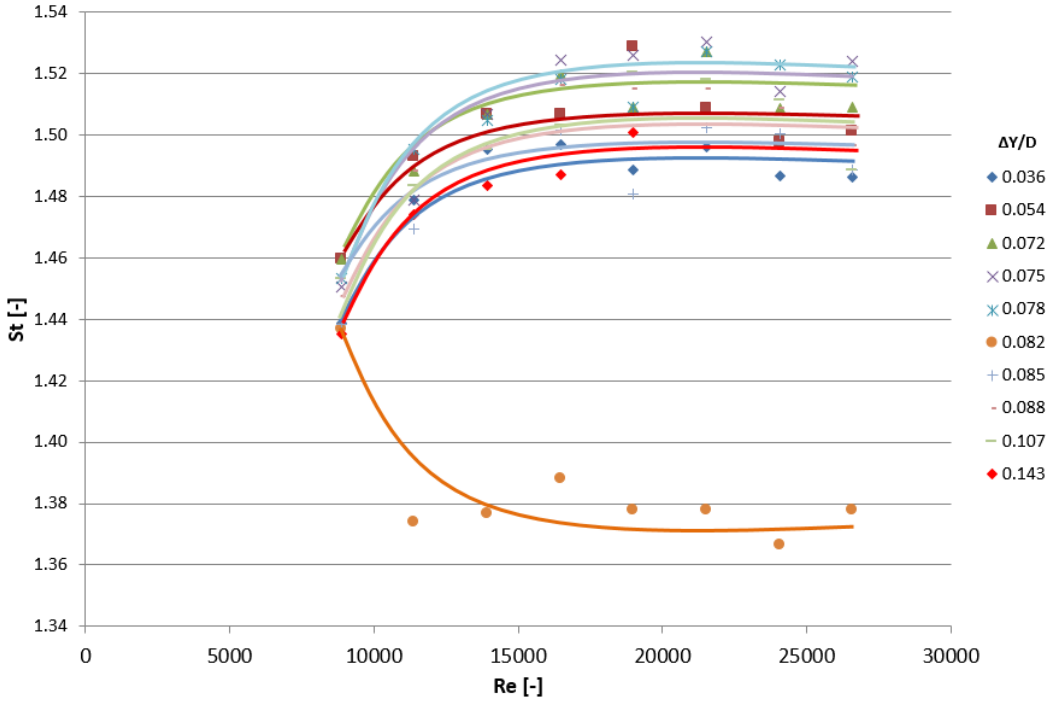

Figure 6-7: St v Re for all the experiments. Note Shift in frequencies for ΔY/D=0.082.

High Speed Photography experiments showed the transition of the trapped vortex and how this is destroyed when the flow recovers its OJF-MS pattern, Figures 6.8 and 6.9. First moments of the transition show an attached flow that is bending at a constant frequency as a product of the trapped vortex. When the system loses its stability, the vortex is unable to keep the flame attached, t=0.000 s. The flame starts lifting whilst the trapped vortex moves around the burner from t=0.001 s. Figure 6.8 at t=0.001 s shows the movement of the TV behind the flame. As the trapped vortex keeps moving around the nozzle, the flame detaches causing series of waves across the profile from 0.001s< t <0.007s, Figure 6.9a. The TV seems to be responsible for the detachment. At t=0.007 s the TV is in front of the flame, after completing a cycle around the nozzle.

The trapped vortex disappears when it reaches the first point of detachment of the flame at t=0.008 s. A moment of extreme chaotic behaviour follows from t=0.009 s, with an undefined shape of the flame at t=0.010 s, Figure 6.9b. Suddenly, a PVC appears opposite to the place where the trapped vortex would be if it was still present in the field, t=0.012 s, grapping around the flame after that, Figure 6.9c.

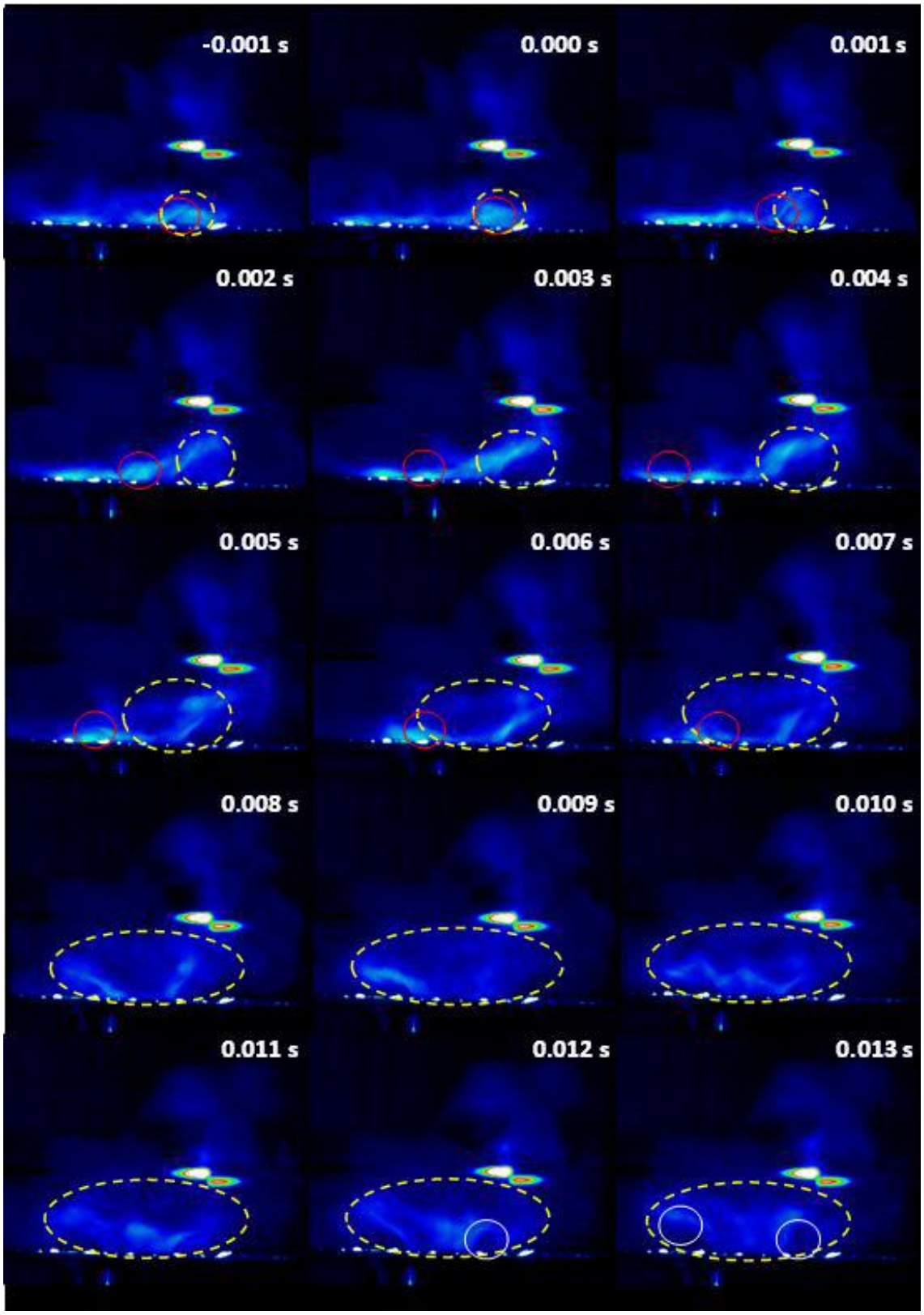

Figure 6-8: High Speed Photography of the transition event. Detachment (yellow dotted line), Trapped Vortex (red line) and PVC (white line) can be observed at different times. Flame lifting is slower than TV.

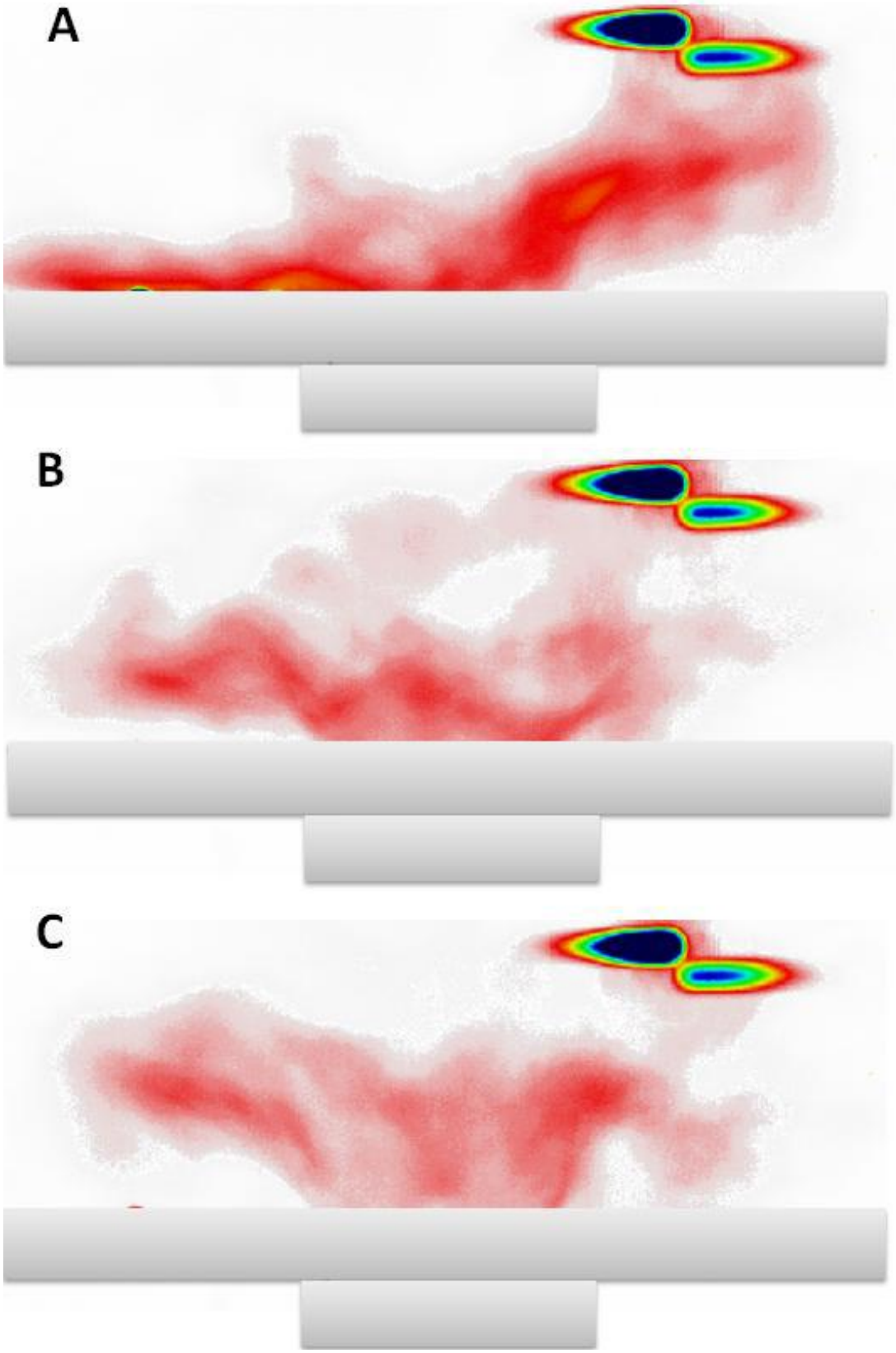

Figure 6-9: High Speed Photography of the transition event, details of 3 stages using inverted colouring. a) Trapped Vortex moving around nozzle; b) Chaotic behaviour; c) PVC around the flame.

From these results it seems that the trapped vortex has progressed into an External Recirculation Zone, with the TV being completely independent towards the appearance of the PVC. It is only the remnants of the vortices across the flame during the chaotic behaviour that started to gather to form the PVC.

6.1.2 Isothermal Experiments

Isothermal experiments were carried out and similar patterns to the ones detected during combustion were observed. Although the decrease in density that occurred as the consequence of higher temperature affected the swirl number [39], it was noticed that the same transition happened at $\Delta Y/D=0.082$ with $\alpha=45°$ at the same Re numbers Figure 6.10. This phenomenon of superimposition was previously observed by Vanoverberghe [54]. Careful ignition was attempted to avoid a sudden reaction that would produce an OJF-MS. As the high temperatures of the Coanda flame posed a threat to the Stereo PIV cameras and the flowrates were going to be kept at the same values, it was decided to shift experiments to isothermal conditions.

To give some understanding of 3-D effects in the system, the frequency of the fluctuating pressure precessional signal was monitored, Figure .6.7, 6.10 and 6.11 the data being plotted as Strouhal number. There is some scatter generally in the results with Strouhal number variations less than 3%, with typical Strouhal numbers being around 1.5. The only exception is for $\Delta Y/D=0.082$ with St~1.38, the point where there is change between the two flow regimes. Clearly this is associated with the transition of the flow, as the TV/ERZ structure radically changes between the two flow states, giving frequency drops of ~20 to 30Hz. The phenomenon seems like a rupture point where the system losses its stability, regaining it by decreasing the St number to ~1.38. This could be related to the oscillatory nature of secondary flows due to the bending of the flow. Due to the unstable nature of the flow at the critical step, the oscillation could result in energy dissipation. More research is required on this point.

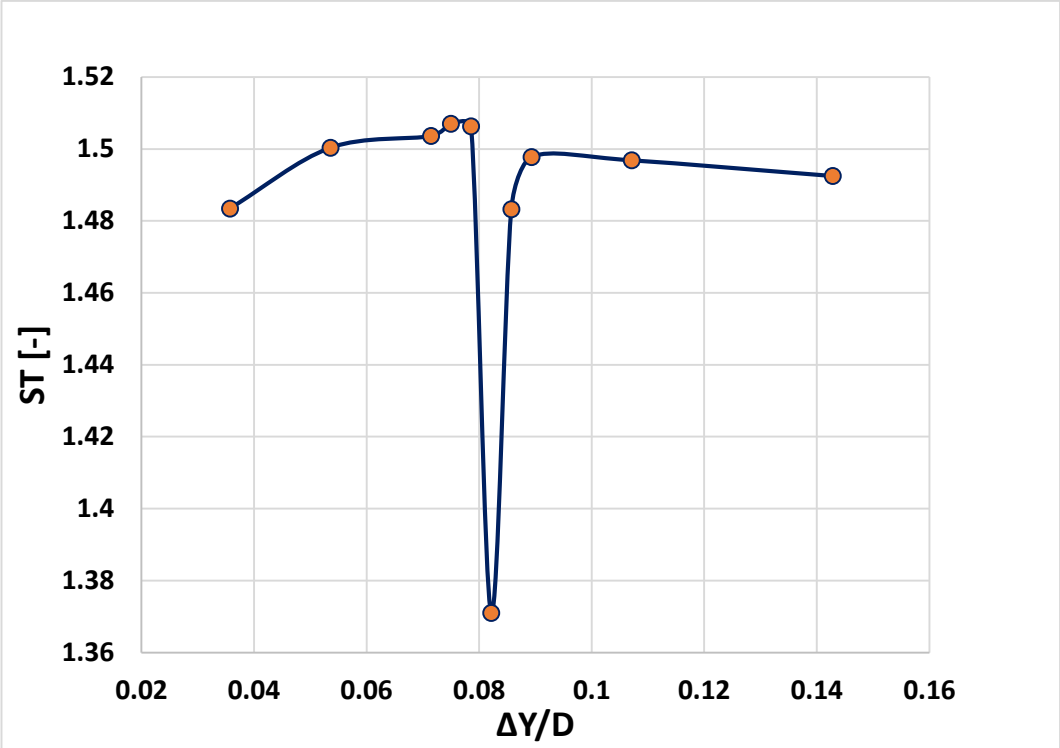

Figure 6-10: Average St v step size ΔY/D. Loss of stability at critical point of ΔY/D=0.082.

Different nozzles were used with various α. The frequencies of the fluctuating precessional signal were monitored, the data being plotted as Strouhal number. Average values of the Strouhal number were obtained after repeating the experiments 10 times to ensure consistency in the results.

Comparison between all the cases was performed against the step size, Figure 6.11. At α=30°, the burner experiences a very abrupt sudden change of frequency during transition that last for several steps. Before recovering stability at 1.52 St, there is a considerable jump in frequency in the system at ΔY/D=0.081, Figure10. A similar effect happens at α=45°, being first stable with a CoJ pattern that is followed by an OJF-MS. However, the transition is not as abrupt and the recovery is smoother. When the geometry is changed to α=60° there is a minimal change in frequency that is barely noticeable. Finally, α=90° does not show any change in frequency since the flow never experiences any transition to CoJ, always staying as a OJFMS.

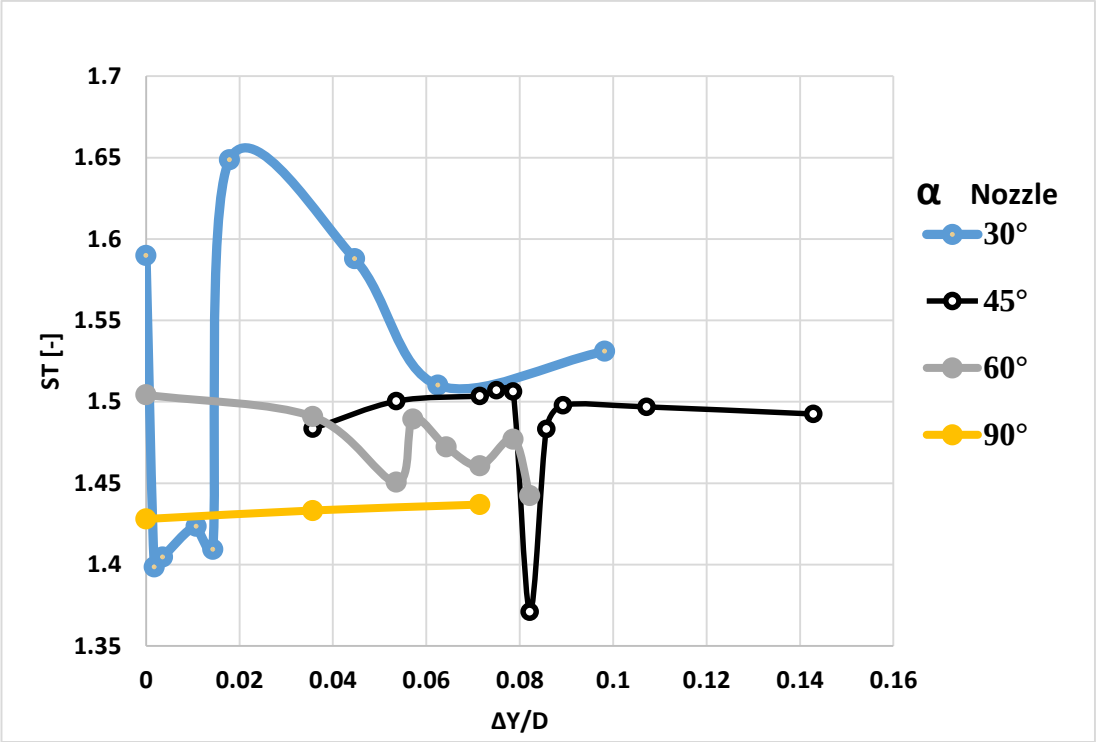

Figure 6-11: Comparison between different geometries. St v ΔY/D. Abrupt and longer transition for geometries close to α=°0.

Thus, the geometry creates different transitions going from abrupt to very smooth as the geometry is closer to α=90°. Moreover, transition at α=30° takes place with almost no resistance to the step size and a longer transition, whilst at 45° and 60° the phenomenon occurs at a similar step size of ΔY/D=0.082 with a quick progression to stability. It is clear that once that stability is regained, the OJF-MS flow has a lower frequency than the CoJF.

Radial-Tangential velocity measurements were carried out to complement the experimental study. The results showed the transient and complex nature of the TV/ERZ, shown in Figures 6.12and 6.13. It is clear that on both systems a very strong TV/ERZ has formed at the right hand corner of the nozzle outlet. This matches the axial radial maps Figure 6.5, with the strong signal arising from highest velocity peak produced by the structures on the right-hand side. The negative values denote a flow that is moving towards the exhaust plate, whilst the positive velocities emphasize the strong outgoing flow produced by the rotation of the TV/ERZ. The surrounding air moves towards the ERZ, being soaked in by the structure.

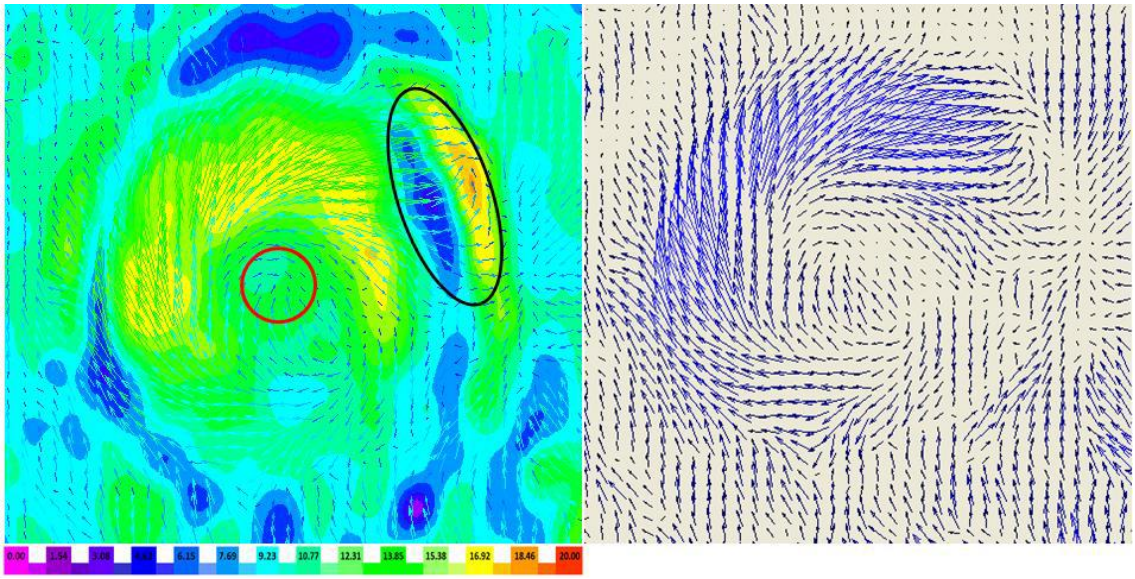

Figure 6-12: OJF-MS axial velocity contours and V-W velocity vectors exactly at the outlet of the nozzle, respectively. Re~19,000, ΔY/D=0.082 and α=45°. PVC (red) and ERZ (black) encircled. Velocity in [m/s].

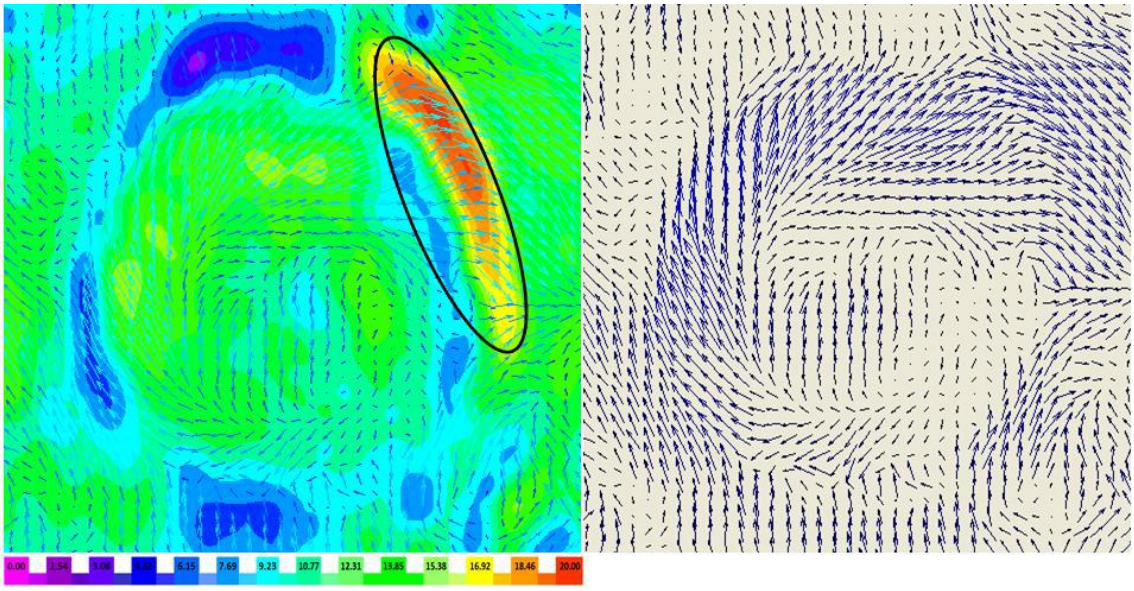

Figure 6-13: COVB axial velocity contours and V-W velocity vectors exactly at the outlet of the nozzle, respectively. Re~19,000, ΔY/D=0.082 and α=45°. TV (black) encircled. Velocity in [m/s].

6.2 Discussion

An important point arising from the OJF-MS case is that the frequency comes from the PVC structure. However, for the CoJF case the PVC and HMFR have been suppressed as a consequence of the interaction between the TV and the shearing flow, Figures 6.4 and 6.13. Then, the triggering signal for the phase locking arises from the TV rather than the PVC as it changes from the OJF-MS to a CoJF case. In all the experiments, the CoJF has a St Number slightly higher than the OJF-MS, confirming that the structure that triggers the system is different and faster. Moreover, the TV shows a very strong pressure signal for phase locking. Compared to the OJF-MS flow, the region has increased by around 150% of its original dimensions, with a significant increase in velocity vector levels. These changes in the structures could be explained as follows,

Coanda stabilization: The only way that the trapped vortex can resist the attachment of the flow and the compression of the shearing flow is through an increase in strength, increasing its velocity. The trapped vortex increases the interaction with the surrounding flow, increasing recirculation and anchoring the flame, behaving in the same way as a Central Recirculation Zone. Therefore, the structure seems to be passing through a similar phenomenon of Vortex Breakdown as the one observed in the CRZ. Therefore, a Coanda Vortex Breakdown (COVB) is taking place. This COVB will increase the velocity and strength of the flow close to the flat plate through the change from supercritical to subcritical conditions, as observed in the stretch of the flow and further expansion downstream, Figure 6.5 These results show how the TV pulls more resources from its surrounding increasing its velocity. This alters the flow in a similar way as a cavity profile will lead to the impingement of the shear layer in the opposite side of such a cavity [139][140]. In terms of the ERZ/TV, the high velocity flow leaving the exhaust nozzle tries to entrain ambient air but entrains it from parts of the downstream jet, creating an ERZ, which pulls the jet due to pressure difference onto the exhaust plate forming a TV whose strength anchors the flow and produces a COVB.

Transition: During transition, the trapped vortex loses its strength which leads to reduction of the frequency of the structure. Being capable only to sustain itself, the structure cannot move at the same speed, reducing St. However, the structure is still

strong enough to rotate at elevated revolutions. The TV, as any other vortex, will increase the stretch of the flame as it moves around the system [92]. This phenomenon will be accompanied by the extra air intake produced by the critical geometry at which the system is in transition. This extra air combined with the stretch of the flame will reduce the local equivalence ratio of the flame, thus reducing its velocity. Once that the TV has passed, the flame will be slower, being unable to reattach as a CoJF, regaining the flame stability but at the price of making the transition to an OJF-MS. Once that the stability has been regained as an OJF-MS the structure reduces its suctioning characteristics, as observed in the PIV results, Figure 6.12.

Therefore, the frequency of the system should be different and lower, as observed during the experiments.

The nozzle angle is another parameter that plays an important role in the transition of the flow. Figure 6.11 shows how the St number changes and decreases with the increase of α. Moreover, the abrupt transition observed at low angles is barely noticeable at α=60°. This phenomenon is due to the position of the TV and its radial movement through the nozzle. Since the TV has been trapped by the flow producing a COVB, the bigger α is, the greater its interaction with the axial flow. Thus, at low α the COVB is partially protected by the geometry, being stabilized by the pressure differences and incoming air. When α is increased, the axial flow pushes the TV out of its position of stability, annihilating the structure faster. A similar phenomenon was observed by Najm and Ghoniem [140], who reported the convection of recirculating flow regions in cavities. A similar phenomenon occurs here due to the high momentum of the shearing flow under OJF-MS profiles. Therefore, convection of the TV occurs due to the lack of strength and cover from the geometry, producing the OJF-MS pattern. However, the recovery of the COJF happens as the pressure close to the nozzle is still low enough to pull back the flow to the plate.

Open Jet stabilization: As soon as this process stops due to changes in geometry, density or sudden combustion, the flow will recover its OJF-MS features, allowing the appearance of the Central Vortex Breakdown with its CRZ and the appearance of the PVC, ERZ and HMFR. At larger step sizes, the flow is incapable of bending enough to avoid the incoming air to increase the pressure, thus ensuring that the COVB will disappear.

6.3 Summary

Swirl stabilized flows are the most widely deployed technology used to stabilize gas turbine combustion systems. However, there are some coherent structures that form in these swirling flows close to the nozzle whose occurrence during transition. The external recirculation zone and the Precessing Vortex Core to/from the Coanda effect are some of them. Thus, in this chapter the transition of an Open Jet Flow-Medium Swirl flow pattern to/from a Coanda jet flow is studied using various geometries nozzles 30°,45°,60°and 90° at a fixed Swirl number 1.05 . Phase Locked Stereo Particle Image Velocimetry and High Speed Photography experiments were conducted.

Experimental where carried out to observe and understand the transition of a CoJF to/from a OJF-MS. Special emphasis was done on the progression of different coherent structures across the profile. It was found that the process occurs at a particular geometry and step size, with a shift in frequency produced by the leading structure due to the entrainment of air and strength of the latter. The formation of a CoJF occurs after a Coanda Vortex Breakdown has occurred, a process similar to the one observed in the central region of the flow under an OJF-MS. This will lead to the formation of a Trapped Vortex that will be highly 3- dimensional in nature. This Trapped Vortex will be the structure that will trigger the system, contrary to the OJFMS system where the PVC/HMFR are the leading, triggering structures. The stability of this Trapped Vortex will depend on its position in the field relative to the shearing flow, with a protected vortex being more difficult to convect downstream. This TV will experience a decay of frequency if it is going through transition, as the structure will have just momentum to try to stabilize itself, reducing its impinging effect on the opposite and surrounding flows. During transition, the Trapped Vortex will still be present and its movement around the nozzle will lift the flame due to both local stretch and reduction of equivalence ratio, allowing the flame to re-stabilize but at lower velocities, reducing the suctioning stretch of the structure. Once that the TV reaches the first point of detachment it will be convected by the shearing flow forming an External Recirculation Zone. This process will occur with a very chaotic behaviour, probably as a consequence of the appearance of the Central Vortex Breakdown

phenomenon, leading to the destruction of the coherent patterns and vortical structures in the system. The remaining vortices, located all around the field, will start to gather due to the presence of the newly formed Central Recirculation Zone, creating a structure named Precessing Vortex Core.

CHAPTER7

CHAPTER 7

DISCUSSION

The suite of experiments and numerical simulations in this research has confirmed that the central recirculation zone (CRZ), external recirculation zones, precessing vortex core (PVC), and high momentum flow region can coexist under a variety of conditions. This was demonstrated under several different fuel compositions, outlet configurations and swirl numbers at the same power output using Particle image velocimetry (PIV), high speed photography and computational fluid dynamics (CFD). It was found that the interaction between the coherent structures CRZ and PVC generated a considerable increase in turbulence where the structures meet. It was observed that the hydrodynamic interaction between the CRZ and PVC plays a minor role in the blowoff for high hydrogen-enriched blends under these conditions. Moreover, the Coanda Effect also showed traces of the formation and initial interactions between structures, phenomena that can be used to unravel barely understood relations between large coherent structures. This chapter will describe how experiments and numerical simulations were conducted, and will be divided into three sections based on the experimental conditions:

7.1 Isothermal conditions

During the experiments, a regular periodic motion was observed with frequencies which increased quazi-linearly with flowrate. A relationship between the Strouhal number (St) and the Reynolds number (Re) (see Figure 5.2) was evident, showing an independent relationship at high Re. It is clear that all harmonics are constant at high Re.

The Strouhal number showed a linear trend, as has been observed previously with other swirl burners [39]. Thus, the appearance of the recirculation zone/precessing vortex core system was clearly evident. This is created by the swirl motion as a consequence of the energy exchange between structures, and takes a helical shape controlled by the CRZ passing the burner nozzle. The PVC and CRZ are produced by

the pressure gradients resulting from the sudden expansion of the flow as it leaves the burner nozzle**.**

A comparison of the Strouhal numbers was also performed between the unconfined and confined configurations (Figure 5.3). Here the dependency of the Strouhal number on the frequency was evident, showing an approximately linear relationship at high frequency. The frequency was also coupled with Re number, increasing as the Re increased. This phenomenon occurs with three frequencies, and it is clear that the harmonics are constant at high frequency for all cases.

To determine the flow pattern changes between the two swirl numbers analysed, a comparison was made between different geometries under isothermal conditions. Specifically the aim was to investigate the effect of swirl on the recirculation zone sizes (Figures 4.13 and 4.14). The results indicated that the CRZ increased in length with higher Swirl numbers using 30° and 45° nozzle, while the 60°, and 90° nozzles produced a smaller CRZ (in terms of both length and width) as shown in Table 4.8.

Isothermal experiments were conducted in order to examine the Coanda effect. The experiments were run at different Re and all experiments showed that it was at this ΔY/D when the system changed suddenly from a CoJF flow to a conical OJF-MS flame, and vice versa. This shift in behaviour occurred with the reduction of Strouhal number (Figure 6.7). Evidently this was associated with the transition of the flow as the TV/ERZ structure changed from one state to the other under these conditions. The TV/ERZ is also transient and moves with the HMFR.

Part of the flow moves towards the base plate around the nozzle on both systems producing a toroidal minor structure, the TV/ERZ becomes strongest where the HMFR increases the velocity. This transient nature of the TV/ERZ is a product of the self-stabilization mechanism of the system, which could otherwise be annihilated by the strong shear stress in the HMFR. To detect any shift in the system, the second mode of the acoustic signal was monitored. For α=45° (Figure 6.7), all but one of the

experiments showed a Strouhal number around 1.50. It was noted that the only difference occurred at $\Delta Y/D = 0.082$, which gave a Strouhal number of around 1.38. Although the phenomenon is not entirely understood, the frequency shift could be related to the transition of the flow, as the TV structure may be damping some of the strength of the PVC and HMFR in an effort to regain stability. Moreover, as the PVC and HMFR are affected by the Coanda Effect (Figure. 6.13) it is possible that this change in frequency impacts directly on the precessing motion of the PVC-HMFR system, reducing its frequency by 20-30 Hz. As the CRZ is in transition as well, the PVC seems to be only dragged by the TV. Due to the transient nature of the TV at $\Delta Y/D=0.082$, it is possible that the strength of the TV has also been affected, being unable to drag the PVC-HMFR system at its original frequency, thus reducing the Strouhal number.

An important point arising from the OJF-MS case is that the frequency is controlled by the PVC structure. However, for the CoJF case, it has been shown for the first time that the PVC and HMFR are suppressed as a consequence of the interaction between the TV and the shearing flow (Figures 6.4 and 6.13). The triggering signal for the phase locking arises from the TV rather than the PVC as it changes from the OJF-MS to a COJF case. In all the experiments, the CoJF had a Strouhal Number slightly higher than that of the OJF-MS, confirming that the structure that triggers the system is different and faster. Moreover, the TV shows a very strong pressure signal for phase locking. Compared to the OJF-MS flow, the region has increased by around 150 % of its original dimensions, with a significant increase in velocity vector levels. These changes in the structures can be explained according to the following processes and parameters:

Coanda stabilisation: The only way that the trapped vortex can resist the attachment of the flow and the compression of the shearing flow is through an increase in strength, increasing its velocity. The trapped vortex increases the interaction with the surrounding flow, increasing recirculation and anchoring the flame in the same way as a Central Recirculation Zone. Therefore, the structure seems to be passing through a similar phenomenon of Vortex Breakdown as the one observed in the CRZ. This

shows for the first time that a Coanda Vortex Breakdown (COVB) is taking place. This COVB will increase the velocity and strength of the flow close to the flat plate through the change from supercritical to subcritical conditions, as observed in the stretch of the flow and further expansion downstream (Figure 6.5). These results show that the TV pulls more resources from its surroundings, increasing its velocity. This alters the flow in a similar way that a cavity profile leads to the impingement of the shear layer in the opposite side of such a cavity [138,139]. In terms of the ERZ/TV, the high velocity flow leaving the exhaust nozzle tends to entrain ambient air, but entrains it from parts of the downstream jet, creating an ERZ. This ERZ pulls the jet onto the exhaust plate due to the pressure difference, forming a TV whose strength anchors the flow and produces a COVB.

Transition: During transition, the trapped vortex loses its strength, leading to a reduction in the frequency of the structure. Being capable only of sustaining itself, the structure cannot move at the same speed, reducing St. However, the structure is still strong enough to rotate at elevated revolutions. The TV, like any other vortex, will increase the stretch of the flame as it moves around the system [92]. This phenomenon is accompanied by the extra air intake produced by the critical geometry at which the system is in transition. This extra air combined with the stretch of the flame reduces the local equivalence ratio of the flame, thus reducing its velocity. Once the TV has passed, the flame is slower and unable to reattach as a COJF. It regains flame stability, but at the price of making the transition to an OJF-MS. Once the stability has been regained as an OJF-MS the structure reduces its suctioning characteristics, as shown in the PIV results (Figure 6.12). This suggests the frequency of the system should be lower, and this was confirmed by the experiments.

Nozzle angle: The nozzle angle, α, is an additional parameter that plays an important role in the transition of the flow. The Strouhal number decreases with an increase in α (Figure 6.11). Moreover, the abrupt transition observed at low angles is minimally noticeable at $\alpha = 60°$. This phenomenon is due to the position of the TV and its radial movement through the nozzle. The TV is trapped by the flow, producing a COVB. Therefore, the bigger α is, the greater its interaction with the axial flow. Thus, at low

α the COVB is partially protected by the geometry, being stabilised by the pressure differences and incoming air. When α is increased, the axial flow pushes the TV out of its position of stability, annihilating the structure faster. A similar phenomenon was observed by Najm and Ghoniem [140], who reported the convection of recirculating flow regions in cavities. The phenomenon occurs here due to the high momentum of the shearing flow under OJF-MS profiles. Therefore, convection of the TV occurs due to the lack of strength and cover from the geometry, producing the OJF-MS pattern. However, the recovery of the COJF occurs as the pressure close to the nozzle is still low enough to pull the flow back onto the plate.

Open jet stabilisation: As soon as this process stops, due to changes in geometry, density or sudden combustion, the flow recovers its OJF-MS features. This allows the Central Vortex Breakdown to occur with its CRZ, and the appearance of the PVC, ERZ and HMFR. At larger step sizes, the flow is incapable of deflecting enough to avoid the incoming air to increase the pressure, thus ensuring that the COVB will disappear.

7.2 Combustion of Methane Blended With CO_2

Due to the interest shown in lean combustion processes because of their reduced emissions, the chosen flow rates of methane were low enough to allow operation in the lean region of the mixture. Premixed combustion using pure methane blended with carbon dioxide was performed to determine blowoff limits using open flame conditions with two different nozzle geometries. Measurements were obtained for pure methane and then for mixtures with different fractions of CO_2. The CO_2 counted as a part of the air and considered as inert gas, which produced the AFR stoichiometric of the mixture the same that obtained from the pure methane. The injection of CO_2 and change of geometry has a significant influence on the blowoff limit (Figure 5.5).

The increase of carbon dioxide changes the limits of the instability, reducing the resistance of the flame as the diluent is augmented. The higher the CO_2 flow rate, the higher the equivalence ratio at which blowoff occurs. This fact indicates that operating in extra lean conditions may be impossible when CO_2 is added to the combustion

mixture in an entirely premixed manner. It is worth mentioning that, given the experimental conditions, the lowest achievable equivalence ratio for high amounts of CO_2 is almost equal to the highest equivalence ratio for methane/air combustion (Figure 5.5). This is encouraging, as the CO_2 could increase the strength of the CRZ whilst maintaining almost the same equivalence ratio before blowoff. This could enhance the recirculation of other products in the field, augmenting their residence time whilst keeping the same power outputs.

It was observed that an increase in the flow rate can augment the intensity of the shear layer, causing a convergence into a new structure known as the High Momentum Flow Region (HMFR), which is highly correlated to the CRZ. Different blends were set to the same power, adding the same quantity of CO_2 as was used for the CH_4. This increases the strength of the CRZ but reduces its dimensions. The addition of CO_2 affects the velocity of the flow. One might expect that the velocity of the flow would increase as a consequence of the combustion being closer to stoichiometric conditions. However, it was observed that the total velocity with pure methane provided faster profiles than with methane and carbon dioxide, and a CRZ with increased strength and negativity.

The higher the density of the CO_2, the stronger the centrifugal forces (Figures 5.6 and 5.7). This in turn increases the size of the CRZ. However, the size increment of the CRZ does not significantly affect the blowoff limit under the conditions studied. These assertions were verified by the data in Table 5.2, which showed the turbulence intensity and CRZ size for the 45° nozzle. The use of CO_2 increases the turbulence of the structure by almost 20% (i.e. TI% CRZ), whilst augmenting its width and length by around 10%. The length of the recirculation zone increases due to the reduced reaction time of the blend and the higher turbulence levels inside the structure. The CRZ using CO_2 is increased in size whilst increasing the inner turbulence of the system at same fuel flow rates (Figure 5.8).

Good correlation was obtained from the CFD results (Figure 4.17; Table 4.10), for example for the profiles measured using methane blended with carbon dioxide. They

demonstrate the negative axial velocities of the CRZ along the central axis of the burner at a positions in the range -0.3 < r/D < 0.3. The progressive introduction of carbon dioxide produces incremental increases in the negative velocities of the recirculation zone, whilst reducing the velocity of the High Momentum Flow Region, thus confirming the effect of combustion on the CRZ. For example, the maximum axial velocity of pure methane and the 90° nozzle was found to be 21 m/s, compared with 12 m/s using methane blended with carbon dioxide. Thus, the results of CFD validated the results of experiments in terms of the both size and length of the CRZ. This supports the use of CFD for the blends using confined conditions.

7.3 Combustion of syngas

Experiments were conducted to compare the lean blowoff limit for 3 different nozzle configurations (Figure 3.3, Figure 5.11) using different equivalence ratios. As the mole fraction of hydrogen was increased, the equivalence ratio at which lean blowoff (LBO) occurs moves to leaner conditions, thus showing an improvement in blowoff limits (Figures 5.11 and 5.12). This has also been demonstrated previously [103]. It was found that some trends follow linear progressions, especially during the experiments with a 45˚nozzle and Syngas-1. As the angle is decreased/increased, the results become less linear. This implies a breakdown in the controlling phenomena due to a more chaotic process. The breakdown could be linked to the propagation of non-linear phenomena related to coherent structures such as the CRZ and PVC.

The results have shown that a change in the combustor nozzle can produce different central recirculation zones under the same injection conditions. Stronger recirculation has been observed using different angled nozzles. Normalised CRZ velocities were calculated from PIV measurements and it was found that the use of a 45° angled nozzle produced a negative velocity around 80 % stronger than the one observed using a 90° nozzle. This velocity increment was accompanied by a reduction in size of around 11 %, and the CRZ was compressed by an increased pressure as a consequence of the sudden expansion at the nozzle exit.

It has been demonstrated in previous research and also this research figure (4.27) that the region of interaction between the CRZ and the Precessing Vortex Core (PVC) has

the highest turbulence in the flow [35,33]. Since this interaction depends on the strength and shape of the CRZ, a greater dependency of the blowoff on the geometry was expected. However, at low flow rates, only a slight dependency was observed (Figure 5.14). The variation in hydrogen content, and the resulting change in Da, was more important to the phenomenon under these conditions. This is believed to be caused by a weak CRZ-PVC interaction (Figure 4.30). Moreover, being a localised phenomenon, this weak CRZ-PVC interaction allows the re-establishment of the flame in other regions. This interaction has been studied previously [35,33], and showed a considerable increase in turbulence where the two structures collide. It is observed that the hydrodynamic interaction between the CRZ and PVC plays a minor role in the blowoff for high hydrogen enriched blends under these conditions.

The influence of the nozzle has a slight effect on LBO equivalence ratios for all cases at low and medium flowrates (Figure 5.14). However, with Syngas-4, as the power was increased there was a considerable shift in the LBO equivalence ratios using all nozzles. This is believed to be a consequence of the reduction in H_2 and a stronger CRZ-PVC interaction. It is believed that at this condition the interaction is a critical part of the blowoff process due to the high flow rates and lower chemical reaction times (Figure 5.14b).

Different profiles of the CRZ for all syngases using the 30°, 45° and 60° nozzles at 7.49 kW were produced as a consequence of the different reactions and combustion processes (Figure 5.19). The velocity and momentum of the flow increases in localised regions of the burner through the High Momentum Flow Region (HMFR) [49].The progressive introduction of hydrogen increases the strength of the recirculation zone, whilst reducing the velocity within the HMFR, i.e. a highly 3-Dimensional shearing flow. This is also observed from the point at which the curves cross the abscissas axis (figure 5.19), indicating that the CRZ reduces its width whilst the HMFR is getting stronger with a hydrogen increase. Tangential velocities are also affected as a consequence of the increase in reactivity (Figure 5.19). This also affects the relationship between the shearing flow and the formation of the CRZ.

Similarly, the decrease in hydrogen produces less homogeneous results. This relates to the high reaction of hydrogen close to the dumping plane. The increase in H2 decreases the Da number as a consequence of faster chemical reactions. Thus, convective processes and turbulence produced by the CRZ do not appear to be controlling the onset of LBO. However, the reduction in hydrogen produces conditions where the presence of these structures might generate less linear, more random behaviour towards the blowoff limit.

Experimental results have demonstrated that the shape and strength of the CRZ can change dramatically depending on the alterations imposed in both fuel composition and flow. CFD analyses using the SST-k-ω model were carried out to observe the change in size of the CRZ. Simulations were calibrates and it was recognised that the CFD slightly under-predicts the location of the shearing flow. However, further comparison between experimental results and CFD predictions for the CRZ size demonstrate that very good correlation was achieved between both techniques (Figure 5.21; Figure 5.22; Tables 5.6, 5.7 and 5.9). Measurements were obtained at the widest and highest point of the structures. It is evident that there is no significant difference between experimental results and CFD calculations in most cases (Table 5.8). Therefore, predictions using confinement were carried out to simulate conditions more representative of those used in industry. Table 5.9 shows numerical results with confinement, illustrating the length and width of the CRZ for each gas (Table 5.5) and all nozzles. The confinement has an extremely important effect upon the CRZ and its interaction with the PVC. As discussed by Syred [39], confinement can dramatically alter the size and shape of the CRZ and External Recirculation zones formed as the swirl burner flow expands. Figure 4.25 showed the numerical results for the CRZ, where it was found that an angle of 60° produces larger CRZ with the narrowest profiles.

CHAPTER8

CHAPTER 8

CONCLUSIONS AND FUTURE WORK

8.1 CONCLUSIONS

Specific conclusions will be given here with respect to the original objectives of the study:

To study the upper limit problem of lean premixed combustion that is recognised as flame blowoff.

This study has developed both an experimental apparatus and a CFD methodology. In the experimental tests, a generic swirl burner with radial swirl vanes was used and the flow field was analysed under both atmospheric and confinement conditions. Confinement was achieved using a pair of quartz cylinders with diameters of *2D* and *3D*, respectively, where *D* is the external nozzle diameter of 0.028m. The shear flow and high momentum flow regions were controlled by four nozzles with angles of 30°, 45°, 60° and 90°. Frequency measurements were made using a PCB Piezotronics 378B02 condenser microphone located in the centre of the nozzle outlet. Particle image velocimetry (PIV) was used to quantify the velocity behaviour of the flow field. Photron high speed cameras were used to visualise the flows.

To determine the potential of CFD and its limitations in studying the upper limit for various fuel blends.

CFD has been presented as an important tool for designing combustion systems in gas turbines. The main function of CFD is to analyse fluid flows, heat transfer and combustion. Fluent ANSYS was used to analyse both the combustion and flow regimes. The CFD work was based on the Zimont model [132], using a shear-stress

transport (SST) *k-ω* model as it is suitable for complex 3D flows with strong swirl. A lean premixed combustion model was used for all the experimental and numerical work in this thesis.

SST-k-ω turbulence models do not depict accurately the high reactivity and shearing phenomena of fast blends, whilst they under-predict the impacts produced by coherent structure interactions in slow blends. More advanced models need to be used for these conditions. However, the model shows high accuracy for the transitional conditions (medium speed blends), reducing computational costs and providing strong correlation.

To define the stability limits of various syngas and CO_2 fuels. These limits are identified by defining the normal combustion and blowoff limits with respect to the mixture mass flow rates at various equivalence ratios.
And,

To determine the behaviour and impact of nozzle geometries and gas compositions on the blowoff process at various swirl numbers.

Experimental tests and numerical simulations have been conducted in an atmospheric, premixed swirl burner to investigate the LBO limit of four syngas mixtures at a moderate swirl number and at the same power output using three types of outlet nozzles.

Simulations were performed using four premixed syngases with variable amounts of hydrogen and with various outlet configurations. All the CFD analyses were conducted using an output power of 7.49 kW, under confined and unconfined conditions. The results showed that for all nozzles the combustion of the four syngases produced different central recirculation zones under the same power loads. Measurements indicate that the 60° nozzle produced the largest, narrowest CRZ structure, while the syngas 4 with the 30° nozzle produced the widest CRZ.

The addition of hydrogen into the mixture caused a significant decrease of Da number as a consequence of a faster chemical reaction. This correlated with the effects of

changing the geometry, for example the nozzle angle, which affects the shape and strength of CRZ. This will alter the change of Da, giving a different trend using different nozzles with the same gas.

Increasing the hydrogen results in a faster reactivity and a shorter CRZ, even with a 60˚ nozzle. Instead of allowing further growth of the CRZ, as progressively observed with the reduction of H_2, the combustion process collapses the recirculation zone closer to the nozzle. On the other hand, the use of a 30˚ nozzle generates wider structures. The reduction in hydrogen elongates the CRZ as a consequence of a delayed pressure decay. This occurs because of the lower reactivity of the blend. As the nozzle angle is increased to 45˚, more intense interaction between the CRZ and the shearing flow encourages the combustion reaction, thus reducing the size of the CRZ. This phenomenon could be linked to the shortening of the CRZ using Syngas-1 with the 60˚ nozzle.

Increasing the mole fraction of H_2 from 25 % to 45 % extended the LBO limit of a given fuel mixture. This has been previously observed in other studies. A consequence of increasing the mole fraction of hydrogen in the mixture is that a faster chemical reaction is produced, with a shorter turbulent time scale due to the higher thermal diffusivity of the hydrogen and laminar flame speed. Another characteristic of hydrogen addition to the mixture is a significant change in the flame structure, indicated by a shorter and more robust flame.

Confinement can dramatically alter the size and shape of the CRZ and the External Recirculation Zones formed as the swirl burner flow expands. However, the use of different blends also considerably affects the size of the structure, impacting on the turbulence intensity and interactions between structures and shearing flows across the boundaries of the flame.

A series of experiments was performed to validate and supplement the results of the aforementioned numerical simulations. The aim of the experiments was to determine

the impact on the blowoff process of using different geometries and gas compositions. The Central Recirculation Zone was measured and correlated with the blowoff phenomenon. A relationship was found between the CRZ size and strength, the different compositions of gases used (i.e. CO_2 and CH_4 content), and the burner nozzle geometry. The results show how the strength and size of the recirculation zones are highly influenced by all these parameters. However, it seems that the CRZ dimensions/strength do not play an important role in the blowoff phenomenon under the conditions studied, whilst the composition of the mixture shows a high correlation with blowoff parameters. Nevertheless, the intensity of the CRZ using these compositions can increase the residence time, which is important for improved combustion of other blends.

It was found that the nozzle angle has a small effect on the LBO at low flow rates using all mixtures. However, there is a pronounced effect at higher flowrates with blends of low hydrogen content. This is believed to be a consequence of the effect of the CRZ-PVC on the flame as a result of a slower chemical reaction. It has been assumed for a long time that this interaction does not influence the blowoff process, however this work shows that the process is influenced if a slower reacting mixture is used. As the H_2 is increased, the fast reaction of the molecule reduces any perceptible dependency on the hydrodynamics close to the nozzle. It was observed that different CRZs were formed under a variety of conditions at the same power output, a consequence of squeezing caused from PVC formation. Furthermore, the size of the CRZ is strongly affected by the blend. The appearance of the reaction zone depends heavily on the governing turbulent structures and the chemical properties of the flow. Thus, fuel compositions produced from a potentially variable composition of syngas will result in a multitude of chemical properties in terms of thermal diffusivity, density, laminar flame speed, and heating value. The use of confinement altered both the size and shape of CRZ. However, the use of different blends also considerably affected the size of the structure, impacting on the turbulence intensity and the stretch across the boundaries of this region.

To determine the impacts of a variety of CRZs and various turbine gases on blowoff, and to determine how the strength and size of the recirculation zones are highly influenced by these parameters.

Although it is concluded that the size and shape of the CRZ seem to be minor factors in controlling the blowoff limit under the conditions analysed, it is clear that the CRZ can be increased by the use of CO_2. This could in turn be beneficial for new blends by increasing the residence time of the products/reactants of these and other fuel/diluent compositions. The addition of CO_2 produces longer recirculation zones that collapse suddenly and far away from the nozzle. Similar velocity profiles at the outlet are observed, with the same stability characteristics as those seen when pure methane is used. Similar stretch is expected, with lower resistance in the CO_2 blends as a consequence of the reduced reaction rate. The high turbulence of the CRZ using CO_2 can also be an important parameter in the addition of other species that can improve the combustion process whilst recirculating CO_2 for other applications, i.e. carbon capture and storage. The intensity of the HMFR, which was shown in previous work to be integral to the process of CIVB, was shown to increase as air flow reduced the equivalence ratio of the flame, squeezing the CRZ. The introduction of CO_2 increased the intensity of the CRZ whilst reducing that of the HMFR, effectively leading to scenarios more prone to blowoff.

CFD predictions of swirl burner aerodynamics show how variable outlet configurations and gas compositions can change the CRZ patterns. The addition of CO_2 in a blend with methane can be of great significance in changing or controlling the CRZ. It is clear that the size of the CRZ is affected by the use of CO_2, and the outlet nozzle angles. Changing the angle of the nozzle controls the direction of the shear flow. This in turn could be beneficial for new blends by increasing the residence time of the products and reactants of these and other fuel/diluent compositions.

Carbon dioxide contained in the fuel leads to a lowering of the flame temperature, the effect of which is to reduce emissions of NO. However, it has been demonstrated that the increase of CO_2 can produce CRZs that can be detrimental to the flow, with some critical concentration of CO_2 leading to flame extinction.

It is clear that an increase in swirl number produces further expansion in the radial direction, with a faster decay of velocity in the azimuthal direction, producing wider CRZs using 45° and 30° nozzles. Nonetheless there was no increase in the CRZ using 60° and 90° nozzles associated with the geometrical swirl number and nozzle divergence at the same equivalence ratio and mass flow rate. This was due to a reduction in the axial velocity and an increased inlet area of vanes which reduces the tangential velocity.

When the swirl burner combustor is fired into a variable outlet configuration, with a variation of fuel types, swirl number, equivalence ratio and mass flow rate, significant changes of the recirculatory structures can be produced. Combustor exit nozzles were of benefit in restricting the CRZ size and reducing the possibility of flame impingement on the fuel injectors. The angled nozzles produced compact CRZs associated with changes in pressure distribution, pressure decay and interaction with the shearing flow.

To study various hydrodynamic effects using swirling flows and the way that these affect the flame. Some of the studied effects and interactions include the effect of Coanda flow upon the High Momentum Flow Region, the Precessing Vortex Core and the External Recirculation Zones.

Swirl stabilized flows are the most widely deployed technology used to stabilize gas turbine combustion systems. However, coherent structures can form in these swirling flows close to the nozzle during transition. The external recirculation zone and the Precessing Vortex Core to/from the Coanda effect are some of them. Thus, the transition of an Open Jet Flow-Medium Swirl flow pattern to/from a Coanda jet flow is studied using various nozzle geometries (30°, 45°, 60° and 90°) at a fixed Swirl number of 1.05. Phase Locked Stereo Particle Image Velocimetry and High Speed Photography experiments were conducted.

Experiments were carried out to observe and understand the transition of a Coanda open jet flow (COJF) to/from an open jet-flow with medium swirl (OJF-MS). Special

emphasis was given to the progression of different coherent structures across the profile. It was found that the process occurs at a particular geometry and step size, with a shift in frequency produced by the leading structure due to the entrainment of air and strength of the latter. The formation of a COJF occurs after a Coanda Vortex Breakdown has occurred, a process similar to the one observed in the central region of the flow under an OJF-MS. This leads to the formation of a Trapped Vortex that will be highly 3-dimensional in nature. This Trapped Vortex (TV) triggers the system, contrary to the OJFMS system where the PVC/HMFR are the leading, triggering structures. The stability of this Trapped Vortex depends on its position in the field relative to the shearing flow, with a protected vortex being more difficult to convect downstream. The TV experiences a decay in frequency as it goes through transition, as the structure has just enough momentum to try to stabilize itself, reducing its impinging effect on the opposite and surrounding flows. During transition, the Trapped Vortex is still present and its movement around the nozzle lifts the flame due to both local stretch and reduction of equivalence ratio, allowing the flame to re-stabilise at lower velocities, reducing the suctioning stretch of the structure. Once the TV reaches the first point of detachment it is convected by the shearing flow, forming an External Recirculation Zone. This process occur with a very chaotic behavior, probably as a consequence of the appearance of the Central Vortex Breakdown phenomenon, leading to the destruction of the coherent patterns and vortical structures in the system. The remaining vortices, located all around the field, start to gather due to the presence of the newly formed Central Recirculation Zone, creating a structure named a Precessing Vortex Core.

8.2 FUTURE WORK

Due to the great importance of thermal energy and its wide applications it is required to design new combustors that are able to burn different types of fuels. Furthermore, the previous research needs of further research to be conducted in the future to enhance combustion technologies. The present research could be extended based on the following recommendations:

8.2.1 Modelling:

- More advanced turbulence models are needed for these conditions in order to reveal the complex coherent structure(s) produced by swirling flow. Large eddy simulation should provide better visualisation of the processing vortex core (PVC) and their interaction with central recalculation zone (CRZ) to give clearer picture of the flame behaviour and aerodynamic flow motions especially in the shear layer region. Another benefit of this models could be to obtain the velocity profile of three dimensions at any planes even inside the nozzle.
- The effects of different combustion models should be compared, for example the previous work was based on the Zimont model which could be compared with Peters model.
- CFD flow dynamic prediction could help to redesign the nozzle shape and angle to obtain the biggest size of CRZ and recognise the best swirl number case in terms of velocity profile.
- More broadly, research is also needed to determine the mechanism of the velocity position and correlation between the CFD and PIV data which faced in this research difficulty to calibrate the values between cases to ensure correct comparison.

8.2.2 Combustion:

- The chosen experimental techniques have somewhat limited capabilities, in that only a 3D PIV results allowed a very shallow field of view in the tangential direction, while the flow structure of the swirling combustor is inherently highly

three dimensional. More advanced solutions need to include the third velocity component, for example LDV or tomographic PIV techniques.

- More research is required to determine a Borghi diagram of the flame and linked to important engineering issues such as NOx emissions, instabilities and stabilities. Thus the Borghi diagram can represent a designing tool for applied applications.
- Further work needs to be done to establish whether the integral length scale with the three nozzles is different across fuels at different planes. This will help to understand the average of the vortex in the flame regime and Kolmogorov length scale and Damköhler number interactions.
- It is recommended that further research is undertaken in the following areas regarding the transition from Open Jet Flow-Medium Swirl (OJF-MS) to Coanda Jet Flow (COJF),
    - In particular, the critical transition point should be identified to determine the transitions occurring at a critical ΔY/D step with new fuel blends, and revealed the interactions between the Coanda flow, the High Momentum Flow Region, the Precessing Vortex Core and the External Recirculation zones using four syngas.
- It would be interesting to assess the effects of new nozzle angles at the same diameter, for example 25°, 35°, 45°, 55°,65°, 75° and compare with previous works especially for Coanda effects.
- Further experimental investigations are needed to estimate the effect of swirl number on the combustion regime at the same conditions that were use.

REFERENCES

REFERENCES

[1] A. A. Bazmi and G. Zahedi, "Sustainable energy systems: Role of optimization modeling techniques in power generation and supply - A review," *Renew. Sustain. Energy Rev.*, vol. 15, no. 8, pp. 3480–3500, 2011.

[2] LLC, "Glassman Wealth Services." [Online]. Available: http://glassmanwealth.com/is-an-energy-crisis-next-on-the-horizon-2/.

[3] "Climate change." [Online]. Available: http://www.sciencemuseum.org.uk/ClimateChanging/ClimateScienceInfoZone/ExploringEarthsclimate/1point5/1point5point2.aspx.

[4] IPCC, "Climate change Caused by Human Activity." [Online]. Available: http://www.paristechreview.com/2010/10/15/climate-change-caused-human-activity/.

[5] "Intergovernmental panel on climate change 2007." [Online]. Available: http://www.ipcc.ch/publications_and_data/ar4/syr/en/mains2-4.html.

[6] I. E. Agency, "Carbon Capture and Storage and the London Protocol," 2011.

[7] "Global Warming, greenhouse gases and their harmful effects – Urgent reduction of these are essential to save our environment." [Online]. Available: http://saferenvironment.wordpress.com/2008/10/31/global-warming-greenhouse-gases-and-their-harmful-effects-%E2%80%93-urgent-reduction-of-these-are-essential-to-save-our-environment/.

[8] O. Of and a I. R. Quality, "United states environmental protection agency," *EAP*, 2009. [Online]. Available: http://www.epa.gov/climatechange/ghgemissions/gases.html.

[9] "The Energy Information Administration (EIA).and Annual Energy Outlook 2011," 2011. [Online]. Available: http://www.instituteforenergyresearch.org/2010/12/30/eia-releases-new-energy-forecast-fossil-fuels-still-reign-in-2035/#_edn1.

[10] "Ministerial Conference on Global Environment and Energy in Transport."

[11] "World Energy Trilemma 2015." [Online]. Available: https://www.worldenergy.org/publications/2015/world-energy-trilemma-2015-priority-actions-on-climate-change-and-how-to-balance-the-trilemma/.

[12] Prof BW Ang & Assoc Prof TSA Ng, "Department of Industrial and Systems Engineering)." [Online]. Available: http://www.eng.nus.edu.sg/EResnews/062014/sf3.html.

[13] "Wikipedia, the free encyclopedia GAS TURBINE." [Online]. Available: http://en.wikipedia.org/wiki/Gas_turbine.

[14] A. . Lefebvre, *Gas Turbine Combustion.*, Second Edi. USA, 1999.

[15] "How does a Gas Turbine Power Plant Work," 2009. [Online]. Available: http://www.brighthubengineering.com/power-plants/25424-how-does-a-gas-turbine-power-plant-work-the-auxiliary-systems/.

[16] “Tikalon Innovation Service Model,” 2012. [Online]. Available: http://tikalon.com/blog/blog.php?article=2012/detonation_engine.

[17] “Combustion chamber of a gas turbine.” [Online]. Available: http://www.google.co.uk/patents/US6192669.

[18] “Can-annular combustor with premixed tangential fuel-air nozzles for use on gas turbine engines.” [Online]. Available: https://www.google.co.uk/patents/WO2013028169A1?cl=en&dq=can+annular+combustor&hl=en&sa=X&ved=0ahUKEwjEkJ_tuKTKAhVL0xoKHURSArQQ6AEIKDAB.

[19] “Thermoacoustic Oscillations in an Annular Combustion Chamber with Swirl Stabilized Premix Burners.” [Online]. Available: http://129.187.45.233/tumtd/de/forschung/themen/thermo_osci_annular.

[20] “combuster - burner.” [Online]. Available: http://www.pilotfriend.com/training/flight_training/tech/turbo/burner.htm.

[21] “Power Engineering.” [Online]. Available: http://www.power-eng.com/articles/print/volume-118/issue-5/features/fuels-combustion-environmental-considerations-in-industrial-gas-turbines.html.

[22] M. Konter and M. Thumann, “Materials and manufacturing of advanced industrial gas turbine components,” *J. Mater. Process. Technol.*, vol. 117, no. 3, pp. 386–390, 2001.

[23] H. Oskarsson, “Material Challenges in Industrial Gas Turbines,” *J. Iron Steel Res. Int.*, vol. 14, no. 5 SUPPL. 1, pp. 11–14, 2007.

[24] I. G. Wright and T. B. Gibbons, “Recent developments in gas turbine materials and technology and their implications for syngas firing,” *Int. J. Hydrogen Energy*, vol. 32, no. 16, pp. 3610–3621, 2007.

[25] “Department for Environment, food and Rural Affairs.” [Online]. Available: http://www.defra.gov.uk/industrial-emissions/eu-international/lcpd/.

[26] “Large Combustion Plant Directive.” [Online]. Available: http://en.wikipedia.org/wiki/Large_Combustion_Plant_Directive.

[27] N. . M. B. Syred, “Combustion in swirling flows,” *A Rev. Combust. flame*, vol. 23, pp. 143–201, 1974.

[28] N. Beer, J. M. and Chigier, “Combustion Aerodynamics,” *Appl. Sci. Publ. LTD*, 1972.

[29] M. O. Vigueras-Zuñiga, a. Valera-Medina, and N. Syred, “Studies of the precessing vortex core in swirling flows,” *J. Appl. Res. Technol.*, vol. 10, no. 5, pp. 755–765, 2012.

[30] Y. Bouremel, Y. Bouremel, M. Yianneskis, M. Yianneskis, A. Ducci, and A. Ducci, “Vorticity and Strain Dynamics for Vortex Ring Mixing Process,” *Ltces.Dem.Ist.Utl.Pt*, no. 1271, pp. 07–10, 2008.

[31] S. Qi, “Effect of Swirl on Combustion Characteristics in Premixed Flames,” vol. 120, no. July 1998, pp. 488–494, 2015.

[32] A. Valera-medina, N. Syred, and A. Griffiths, “Characterization of Large Coherent Structures in a Swirl Burner under Combustion Conditions,” *47th AIAA Aerosp. Sci. Meet. 5 - 8 January 2009, Orlando, Florida*, no. January, pp. 1–19, 2008.

[33] S. Roux, G. Lartigue, T. Poinsot, U. Meier, and C. Bérat, “Studies of mean and unsteady flow in a swirled combustor using experiments, acoustic analysis, and large eddy simulations,” *Combust. Flame*, vol. 141, no. 1–2, pp. 40–54, 2005.

[34] a. Valera-Medina, N. Syred, and a. Griffiths, “Visualisation of isothermal large coherent structures in a swirl burner,” *Combust. Flame*, vol. 156, no. 9, pp. 1723–1734, 2009.

[35] T. C. Claypole and N. Syred, “The effect of swirl burner aerodynamics on NOx formation,” *Symp. Combust.*, vol. 18, no. 1, pp. 81–89, 1981.

[36] B. P. Valera-Medina A, Syred N, “Central Recirculation Zone Analysis using a Confined Swirl Burner for Terrestrial Energy,” *J AIAA Propuls. Power*, vol. 29, no. 1, pp. 195–204, 2013.

[37] K. McManus, F. Han, W. Dunstan, C. Barbu, and M. Shah, “Modeling and Control of Combustion Dynamics in Industrial Gas Turbines,” *Vol. 1 Turbo Expo 2004*, pp. 567–575, 2004.

[38] S. Hong, S. J. Shanbhogue, and A. F. Ghoniem, “Impact of fuel composition on the recirculation zone structure and its role in lean premixed flame anchoring,” *Proc. Combust. Inst.*, vol. 35, no. 2, pp. 1493–1500, 2014.

[39] N. Syred, “A review of oscillation mechanisms and the role of the precessing vortex core (PVC) in swirl combustion systems,” *Prog. Energy Combust. Sci.*, vol. 32, no. 2, pp. 93–161, 2006.

[40] C. S. S, *flow induced vibration of circular cylindrical structures*. Hemisphere, 1990.

[41] H. T. Falvey, “Observations of unsteady f l o after vortex breakdown,” 1970.

[42] R. . Blevins, *Flow Induced Vibration*, 2nd ed. 1990.

[43] A. N. Lupas and R. B. Russell, “The structure of vortex breakdown. Annu Rev,” *J. Struct. Biol.*, vol. 179, no. 3, p. 251, 2012.

[44] a. Valera-Medina, N. Syred, P. Kay, and a. Griffiths, “Central recirculation zone analysis in an unconfined tangential swirl burner with varying degrees of premixing,” *Exp. Fluids*, vol. 50, no. 6, pp. 1611–1623, 2011.

[45] M. K. Kim, J. Yoon, S. Park, M. C. Lee, and Y. Yoon, “Effects of unstable flame structure and recirculation zones in a swirl-stabilized dump combustor,” *Appl. Therm. Eng.*, vol. 58, no. 1–2, pp. 125–135, 2013.

[46] O. Lucca-Negro and T. O’Doherty, “Vortex breakdown: A review,” *Prog.*

Energy Combust. Sci., vol. 27, no. 4, pp. 431–481, 2001.

[47] A. Coghe, G. Solero, and G. Scribano, "Recirculation phenomena in a natural gas swirl combustor," *Exp. Therm. Fluid Sci.*, vol. 28, no. 7, pp. 709–714, 2004.

[48] S. M. Bulat G, Stopford P , Turrell M, Frach D, Buchanan E, "Predictions of aerodynamic Frequencies in a Gas Turbine Combustor using transient CFD," *ASME Turbo Expo*, vol. 2, pp. 585–594, 2009.

[49] M. O. Vigueras-zuniga, A. Valera-medina, N. Syred, and P. Bowen, "High Momentum Flow Region and Central Recirculation Zone Interaction in Swirling Flows," pp. 195–204, 2014.

[50] K. U. Leuven, F. Ingenieurswetenschappen, D. Werktuigkunde, A. T. Mechanica, and E. N. Energieconversie, *Fluid Mechanics and Control of Annular Jets With and Without*. 2007.

[51] D. Froud, "Phase averaging of the precessing vortex core in a swirl burner under piloted and premixed combustion conditions," *Combust. Flame*, vol. 100, no. 3, pp. 407–410, 1995.

[52] W. Hovercraft, "DiscoverHover CURRICULUM GUIDE BERNOULLI'S PRINCIPLE AND THE COANDA EFFECT," 2004. [Online]. Available: http://www.discoverhover.org/infoinstructors/guide8.htm.

[53] "The Bernoulli equation Work and energy." [Online]. Available: http://www.efm.leeds.ac.uk/CIVE/CIVE1400/Section3/bernoulli.htm.

[54] K. Vanoverberghe, *Flow, turbulence and combustion of premixed swirling jet flames*, no. January. 2004.

[55] A. C. Sidhu, B. S.; Syred, N.; Styles, "Flow and General Characteristics of High Performance Diodes," *ASME WINTER METT*, pp. 113–122.

[56] O. T. Dawson J.R., Rodriquez-Martinez V.M., Syred N., "The effect of combustion instability on the structure of recirculation zones in con fined swirling flames," *Combust Sci Technol*, vol. 177, pp. 1–22, 2005.

[57] V. M. R.-M. J. R. D. T. O. N. Syred, "Low frequency combustion oscillations in a swirl burner furnace," *AIAAA*, vol. 22, no. 1, pp. 217–221, 2006.

[58] S. Yamaguchi, N. Ohiwa, and T. Hasegawa, "Structure and blow-off mechanism of rod-stabilized premixed flame," *Combust. Flame*, vol. 62, no. 1, pp. 31–41, 1985.

[59] C. P. Lubert, "On some recent applications of the Coanda effect to acoustics.," *J. Acoust. Soc. Am.*, vol. 128, no. 4, pp. 2286–2286, Oct. 2010.

[60] C. Lubert and R. J. Shafer, "Shock Associated Noise Generation in Curved Turbulent Coanda Wall Jets," vol. 14, p. 040002, 2011.

[61] D. J. Wing, "Static investigation of two fluidic thrust-vectoring concepts on a two-dimensional convergent-divergent nozzle," no. December 1994, 1994.

[62] S. Kniesburges, C. Hesselmann, S. Becker, E. Schlücker, and M. Döllinger, "Influence of vortical flow structures on the glottal jet location in the supraglottal region," *J. Voice*, vol. 27, no. 5, pp. 531–544, 2013.

[63] C. Lubert, "Application of Turbulent Mixing Noise Theory to Flows over Coanda Surfaces," vol. 13, no. 1, p. 22807, 2008.

[64] S. V. Alekseenko, P. a. Kuibin, V. L. Okulov, and S. I. Shtork, "Helical vortices in swirl flow," *J. Fluid Mech.*, vol. 382, pp. 195–243, 1999.

[65] Y. V Lieuwen T, "Combustion Instabilities in Gas Turbine Engines, Prog. In Astronautics Aeronautics," *AIAA, U.S.A.*, vol. 210, pp. 213–276, 2005.

[66] N. Mirkov, B. Rasuo, U. A. Vehicle, and C. F. Dynamics, "Maneuverability of an Uav With Coanda Effect," pp. 1–6.

[67] C. L. Rumsey and T. Nishino, "Numerical study comparing RANS and LES approaches on a circulation control airfoil," *Int. J. Heat Fluid Flow*, vol. 32, no. 5, pp. 847–864, 2011.

[68] V. Dragan and V. Stanciu, "Contributions regarding a fluid barrier super circulation technique," *UPB Sci. Bull. Ser. D Mech. Eng.*, vol. 75, no. 2, pp. 17–30, 2013.

[69] E. Tavakoli and R. Hosseini, "Large eddy simulation of turbulent flow and mass transfer in far-field of swirl diffusers," *Energy Build.*, vol. 59, pp. 194–202, 2013.

[70] N. K. Singh and K. Ramamurthi, "Formation of Coanda jet from sharp-edged swirl nozzle with base plate," *Exp. Therm. Fluid Sci.*, vol. 33, no. 4, pp. 675–682, 2009.

[71] T. Nishino and K. Shariff, "Effect of Jet Nozzle Lip Momentum Loss on Circulation Control Airfoil Performance," *AIAA J.*, vol. 50, no. 3, pp. 551–558, 2012.

[72] M. D. Turrell, P. J. Stopford, P. O. Box, and L. L. N. Uk, "GT2004-53112 CFD Simulation of the Flow Within and Downstream of a High- Swirl Lean Premixed Gas Turbine Combustor," pp. 1–8, 2004.

[73] S. Candel, D. Durox, T. Schuller, J.-F. Bourgouin, and J. P. Moeck, "Dynamics of swirling flames," *Annu. Rev. Fluid Mech.*, vol. 46, pp. 147–173, 2014.

[74] N. Peters, *Turbulent combustion*. Cambridge University Press, 2000.

[75] I. Glassman, *Combustion*. San Diego, CA : Academic Press, 1996.

[76] "finite volume method." [Online]. Available: http://www.cfd-online.com/Wiki/Finite_volume.

[77] H. J.O, *Turbulence*. McGraw-Hill Inc, 1975.

[78] D. C. . Wilcox, *Turbulence Modelling for CFD*. DCW Industries, Inc. La Canada, California, 1993.

[79] H. K. V. W. Malalasekera, *An Introduction to Computational Fluid Dynamics-The Finite Volume Method*, no. Second Edition. Longman Group Ltd, 2007.

[80] "Ansys fluent 12.0 Theory Guide." [Online]. Available: https://www.google.co.uk/webhp?sourceid=chrome-instant&ion=1&espv=2&ie=UTF-8#q=ansys fluent 12.0 theory guide pdf.

[81] A. P. Dowling and Y. Mahmoudi, "Combustion noise," *Proc. Combust. Inst.*, vol. 35, no. 1, pp. 65–100, 2015.

[82] F. a. Williams, *Combustion theory: the fundamental theory of chemically reacting flow systems*, vol. 54. 1985.

[83] D. Laera, G. Campa, S. M. Camporeale, E. Bertolotto, S. Rizzo, F. Bonzani, A. Ferrante, and A. Saponaro, "Modelling of thermoacoustic combustion instabilities phenomena: Application to an experimental test rig," *Energy Procedia*, vol. 45, pp. 1392–1401, 2014.

[84] A. Lefebvre, D. Ballal, and D. Bahr, *Gas turbine combustion: alternative fuels and emissions*. 2010.

[85] J. Lewis, "The behavior of swirling flames under variable fuel composition.," CARDIFF UNIVERSITY, 2014.

[86] N. Shelil, P. Said, A. J. Griffiths, N. Syred, L. Assistant, and P. Said, "Numerical Study of Stability Limits of Premixed-Swirl Flames," no. August, pp. 1–15, 2009.

[87] D. D. R. Noble, Q. Zhang, A. Shareef, J. Tootle, A. Meyers, and T. Lieuwen, "Syngas mixture composition effects upon flashback and blowout," *ASME Conf. Proc.*, vol. 2006, no. 42363, pp. 357–368, 2006.

[88] P. Sayad, A. Schönborn, M. Li, and J. Klingmann, "Visualization of Different Flashback Mechanisms for H\n 2\n /CH\n 4\n Mixtures in a Variable-Swirl Burner," *J. Eng. Gas Turbines Power*, vol. 137, no. March, p. 031507, 2014.

[89] N. Syred, a. Giles, J. Lewis, M. Abdulsada, a. Valera Medina, R. Marsh, P. J. Bowen, and a. J. Griffiths, "Effect of inlet and outlet configurations on blow-off and flashback with premixed combustion for methane and a high hydrogen content fuel in a generic swirl burner," *Appl. Energy*, vol. 116, pp. 288–296, 2014.

[90] K. Umemura, A. and Tomita, "Rapid flame propagation in a vortex tube in perspective of vortex breakdown phenomena," *Combust. Flame*, vol. 125, pp. 820–838, 2001.

[91] F. Nicoud and T. Poinsot, "Thermoacoustic instabilities: Should the Rayleigh criterion be extended to include entropy changes?," *Combust. Flame*, vol. 142, no. 1–2, pp. 153–159, 2005.

[92] T. Lieuwen, *Unsteady Combustor Physics*. USA: Cambridge Press, 2012.

[93] S. G. Tuttle, S. Chaudhuri, S. Kostka, K. M. Kopp-Vaughan, T. R. Jensen, B.

M. Cetegen, and M. W. Renfro, “Time-resolved blowoff transition measurements for two-dimensional bluff body-stabilized flames in vitiated flow,” *Combust. Flame*, vol. 159, no. 1, pp. 291–305, 2012.

[94] Cohen M 7F Users Group, “preventing blowout trips,” *Comb cycle J,3.*, 2011.

[95] S. J. Shanbhogue, S. Husain, and T. Lieuwen, “Lean blowoff of bluff body stabilized flames: Scaling and dynamics,” *Prog. Energy Combust. Sci.*, vol. 35, no. 1, pp. 98–120, 2009.

[96] J. P. Longwell, E. E. Frost, and M. a. Weiss, “Flame Stability in Bluff Body Recirculation Zones,” *Ind. Eng. Chem.*, vol. 45, no. 8, pp. 1629–1633, 1953.

[97] J. F. Driscoll, “Turbulent premixed combustion: Flamelet structure and its effect on turbulent burning velocities,” *Prog. Energy Combust. Sci.*, vol. 34, no. 1, pp. 91–134, 2008.

[98] R. A. Kenneth Kuan-Yun Kuo, *Applications of Turbulent and Multi-Phase Combustion*. 2012.

[99] V. D. Poinsot T, *Theoretical and Numerical Combustion*. USA, 2005.

[100] DeZubay EA, “Characteristics of Disk-Controlled Flames,” *Aero Dig.*, vol. 61 (1), pp. 54–56, 1951.

[101] DE Cavaliere, “Blowoff in Gas Turbine Combustors,” Cambridge, England, UK, 2013.

[102] L. A. Ballal DR, “Weak Extinction Limits of Turbulent Heterogeneous Fuel/Air Mixtures,” vol. 102, no. 2, pp. 416–421, 1980.

[103] K. Radhakrishnan, J. B. Heywood, and R. J. Tabaczynski, “Premixed turbulent flame blowoff velocity correlation based on coherent structures in turbulent flows,” *Combust. Flame*, vol. 42, pp. 19–33, Jan. 1981.

[104] E. E. Zukoski and F. E. Marble, *The role of wake transition in the process of flame stabilization on bluff bodies*. 1955, pp. 205–210.

[105] Valera-Medina A, “Coherent Structures and their Effects on Processes occurring in Swirl Combustors,” Cardiff University ,Wales, UK, 2009.

[106] J. Kariuki, J. R. Dawson, and E. Mastorakos, “Measurements in turbulent premixed bluff body flames close to blow-off,” *Combust. Flame*, vol. 159, no. 8, pp. 2589–2607, 2012.

[107] D. E. Cavaliere, J. Kariuki, and E. Mastorakos, “A comparison of the blow-off behaviour of swirl-stabilized premixed, non-premixed and spray flames,” *Flow, Turbul. Combust.*, vol. 91, no. 2, pp. 347–372, 2013.

[108] S. I. Shtork, N. F. Vieira, and E. C. Fernandes, “On the identification of helical instabilities in a reacting swirling flow,” *Fuel*, vol. 87, no. 10–11, pp. 2314–2321, 2008.

[109] M. Karalus, “An Investigation of Lean Blowout of Gaseous Fuel Alternatives

to Natural Gas," University of Washington, 2013.

[110] J. Hwang, N. Bouvet, K. Sohn, and Y. Yoon, "Stability characteristics of non-premixed turbulent jet flames of hydrogen and syngas blends with coaxial air," *Int. J. Hydrogen Energy*, vol. 38, no. 12, pp. 5139–5149, 2013.

[111] K. K. J. Ranga Dinesh, K. H. Luo, M. P. Kirkpatrick, and W. Malalasekera, "Burning syngas in a high swirl burner: Effects of fuel composition," *Int. J. Hydrogen Energy*, vol. 38, no. 21, pp. 9028–9042, 2013.

[112] G. E. Ballachey and M. R. Johnson, "Prediction of blowoff in a fully controllable low-swirl burner burning alternative fuels: Effects of burner geometry, swirl, and fuel composition," *Proc. Combust. Inst.*, vol. 34, no. 2, pp. 3193–3201, 2013.

[113] J. Lewis, A. Valera-medina, R. Marsh, and S. Morris, "Augmenting the Structures in a Swirling Flame via Diffusive Injection," vol. 2014, 2014.

[114] T. Lieuwen, V. McDonell, E. Petersen, and D. Santavicca, "Fuel Flexibility Influences on Premixed Combustor Blowout, Flashback, Autoignition, and Stability," *J. Eng. Gas Turbines Power*, vol. 130, no. 1, p. 011506, 2008.

[115] M. C. Lee, S. Bin Seo, J. Yoon, M. Kim, and Y. Yoon, "Experimental study on the effect of N2, CO2, and steam dilution on the combustion performance of H2 and CO synthetic gas in an industrial gas turbine," *Fuel*, vol. 102, pp. 431–438, 2012.

[116] P. Strakey, T. Sidwell, and J. Ontko, "Investigation of the effects of hydrogen addition on lean extinction in a swirl stabilized combustor," *Proc. Combust. Inst.*, vol. 31 II, pp. 3173–3180, 2007.

[117] R. W. Schefer, D. M. Wicksall, and A. K. Agrawal, "Combustion of hydrogen-enriched methane in a lean premixed swirl-stabilized burner," *Proc. Combust. Inst.*, vol. 29, no. 1, pp. 843–851, Jan. 2002.

[118] P. Sayad, A. Schönborn, and J. Klingmann, "Experimental investigations of the lean blowout limit of different syngas mixtures in an atmospheric, premixed, variable-swirl burner," *Energy and Fuels*, vol. 27, no. 5, pp. 2783–2793, 2013.

[119] A. Jairaman and S. Hsu, "T He B Ehavior of E Ndothelial C Ells in 3D B Iomaterials for T Issue E Ngineering," *Biomaterials*, p. 60021, 2007.

[120] J. Raffel, M., Willert, C., Wereley, S., Kompenhans, *Particle image velocimetry. A practical guide, Springer, Berlin.* Tokio: Springer, 1998.

[121] "Laser Optical Measurement Systems and Sensors," *DANTEC DYNAMICS*. [Online]. Available: http://www.dantecdynamics.com/measurement-principles-of-piv.

[122] A. S. C. E., *Particle Image Velocimetry:* 1965.

[123] S. Anderson, D. J., Greated, C. A., Jones, J. D. C., Nimmo, G., and Wiseall, *Fibre optic PIV studies in an industrial combustor.* 1996.

[124] “Stereo PIV.” [Online]. Available: http://velocimetry.net/stereo_principles.htm.

[125] “High-speed photography.” [Online]. Available: https://en.wikipedia.org/wiki/High-speed_photography.

[126] “High speed cameras.” [Online]. Available: http://www.photron.com/?gclid=CK_cwZfPzcUCFeLLtAodiBAArQ.

[127] A. Sayma, *Computational Fluid Dynamics*. Ventus Publishing, 2009.

[128] S. B. Pope, *Turbulent Flows*, vol. 12, no. 11. Cambridge University Press, Cambridge, UK, 2001.

[129] Nasser Shelil, “Flashback Studies with Premixed Swirl Combustion,” Cardiff University, 2010.

[130] F. R. Menter, “Two-equation eddy-viscosity turbulence models for engineering applications,” *AIAA J.*, vol. 32, no. 3, pp. 1598–1605, 1994.

[131] FLUENT 6.1, *User’s Guide*. 2006.

[132] V. Zimont, W. Polifke, M. Bettelini, and W. Weisenstein, “An Efficient Computational Model for Premixed Turbulent Combustion at High Reynolds Numbers Based on a Turbulent Flame Speed Closure,” *J. Eng. Gas Turbines Power*, vol. 120, no. 3, p. 526, 1998.

[133] H. Baej, A. Valera-Medina, P. Bowen, N. Syred, T. O’Doherty, and R. Marsh, “Impacts on Blowoff by a Variety of CRZs Using Various Gases for Gas Turbines,” *Energy Procedia*, vol. 61, pp. 1606–1609, 2014.

[134] K. G. H.Schlichting, *Boundary layer theory*, 8th ed. Springer, 2000.

[135] I. ANSYS, “Ansys ICEM CFD Tutorial Manual,” 2011. [Online]. Available: https://support.ansys.com/portal/site/AnsysCustomerPortal.

[136] S. N. Gupta A.K., Lilley D.J., *Swirl flows*. 1984.

[137] M. S. and B. H. Lewis J , Marsh R, Valera-Medina A, “The Use of CO2 to Improve Stability and Emissions of an IGCC Combustor,” *ASME Turbo Expo*, vol. 4, p. 11, 2014.

[138] B. Dam, G. Corona, M. Hayder, and A. Choudhuri, “Effects of syngas composition on combustion induced vortex breakdown (CIVB) flashback in a swirl stabilized combustor,” *Fuel*, vol. 90, no. 11, pp. 3274–3284, 2011.

[139] M. Stöhr, C. M. Arndt, and W. Meier, “Effects of Damköhler number on vortex-flame interaction in a gas turbine model combustor,” *Proc. Combust. Inst.*, vol. 34, no. 2, pp. 3107–3115, 2013.

[140] H. N. N. and A. F. GHONIEM, “Numerical simulation of the convective instability in a dump combustor,” *AIAA Journal*, vol. 29, no. 6, pp. 911–919, 1991.